DISS. ETH NO. 27370

Locomotion of Spiders - What Robotics can Learn from Spiders and vice versa

A thesis submitted to attain the degree of

DOCTOR OF SCIENCES of ETH ZURICH

(Dr. sc. ETH Zurich)

presented by

Chantal Göttler

M.Sc., University of Stuttgart

born on 12.10.1993
citizen of Germany

accepted on the recommendation of

Prof. Dr. Roland Siegwart, Examiner
Prof. Dr. Metin Sitti, Co-examiner
Prof. Dr. Marco Hutter, Co-examiner
Prof. Dr. Guillermo Amador, Co-examiner

2021

Abstract

The locomotion of spiders has been fascinating researchers and engineers for over a century. Different to insects and humans, spiders use muscles to flex, but hydraulic pressure to extend their legs. Fluidic actuation, known for fast and high-power outputs, are receiving a rising interest in the last decade for soft, lightweight and compliant robotic implementations. These robots have application fields in safe-human-robotic interactions, actuation through narrow inaccessible terrain for rescue purposes or adaptable manipulation of complex and delicate shapes for manufacturing and production facilities, but also medical applications.

In this thesis, the detailed joint structure, functioning and material properties of the femur-patella joint of jumping spiders (*Phidippus regius*) was analyzed. Unlike humans and insects, spiders use a combination of muscles and blood pressure to move their limbs. In this process, flexion is produced by a large number of muscles, while extension is produced by the hydraulic pressure of the body fluid (hemolymph). The focus of this work was to gain a better understanding of morphological components in order to translate them into a technical application, more specifically a fluidic actuator. The properties of the articular membrane, which plays an essential role in hydraulic stretching, were given special attention. Various optical methods, such as light, scanning and laser microscopy, were used to visualize the functioning of the joint membrane as well as surface properties. Micro structures were discovered, which are distributed in alternating sections on the membrane and could play a role in communication, self-cleaning and friction reduction. The disappearance of these micro structures after deproteinization of the exoskeleton indicates that the microstructures are likely formed by proteins in the outermost layer of the exoskeleton, the epicuticle. UV light analysis further indicates that differences in protein incorporation exist between the two alternate domains, possibly incorporating the elastic protein, resilin. Material properties, such as stiffness and hardness of the articular membrane, were analyzed by nanoindentation and a significant difference between the alternating micro structural parts was found. Histological sections and X-ray images suggest that thickness and density differences between the alternating parts is another cause for their different material properties. The results confirm the hypothesis of a so-called anisotropic articular membrane. It can be suggested that the stiffened segments or half-rings allow controlled and guided folding of the membrane during flexion of the joint and prevent unintentional inflation of the

membrane when large pressures are applied during extension. The translation of the hinge membrane folding mechanism, as well as the stiffened elements, into a flexible 3D-printed prototype have shown, that the absence of stiffening elements would not allow a controlled folding, but rather result in tip-induced wrinkling. This ultimately leads to material failure and thus prevents longevity of the membrane.

In general, the fabrication and implementation of the spider-inspired actuator took today's requirements for soft, fluidic actuators into account. These include high flexibility and compliance, a lightweight and modular design, and durability and environmental sustainability. As the demand for small implementations increases, the fabrication and materials were chosen in such a way to allow smaller actuators to be manufactured in the future. The presented prototype was fabricated using filament-based 3D printing technology from flexible and robust themoplastic polyurethane (TPU) and sealed internally with latex. Water was used for hydraulic extension and wires for flexion to simulate the interaction of muscles and hydraulic stretching. The spider-inspired principle achieved working angles of 125°, which far exceeds previous implementations (60-90°) and approaches the capabilities of spiders (140°). Analysis of the pressure and force relationships have shown that the actuator motion can be accomplished via linear relationships. The results further showed that a single 6-10 g articulated segment was able to lift weight elements of 600 - 1kg against gravity at a hydraulic pressure of 200-300 kPa. The rapid, radial deployment of the articulated segment also enabled high torque transmission, which was demonstrated by jumps. The 120g platform was able to achieve jumps of up to 10 cm in height and 10 cm in width. The analyses showed that when the joint is opened quickly, there is an immediate drop in pressure, which may be explained by the inertia of the fluid. Such a pressure drop could generate losses in force and torque transmission and also lead to material damage.

Therefore, to understand whether this phenomena would also appear in spiders, the fluid This included the fluid speed, shear rates and viscosity property of the hemolymph under different pressures and the flow behavior inside the femur-patella joint. The exact fluid flow was visualized and a non-Newtonian (shear-thinning) behavior of the hemolymph was detected. Such a property could explain why rapid volume displacement is possible during spider leg extension. This would avoid cavitation when the leg springs open during jumping. For hydraulic applications, such a fluid could increase mechanical efficiency at high pressures while keeping the volumetric efficiency (transfer rate of the fluid) constant over a wide range.

Finally, the successful, functional implementation of the spider-inspired actuator thus not only enables its application in the field of prostheses or robots in the future, but also yields new questions and insights into the behavior and functioning of spider motion.

Zusammenfassung

Die vorliegende Doktorarbeit handelt von der detaillierten Analyse des Gelenkaufbaus, der Funktionsweise und der Materialeigenschaften des Femur-Patella Gelenks von Springspinnen der Gattung *Phidippus regius*. Im Gegensatz zu Menschen und Insekten benutzen Spinnen eine Kombination aus Muskeln und Blutdruck für die Bewegung ihrer Gliedmaßen. Dabei erfolgt die Beugung über eine große Anzahl an Muskeln, während die Streckung über den hydraulischen Druck der Körperflüssigkeit (Hämolymphe) erzeugt wird. Der Fokus dieser Arbeit bestand darin, ein besseres Verständnis von morphologischen Komponenten zu bekommen, um diese in eine technische Anwendung, genauer gesagt einen fluidischen Aktor, umzusetzen. Die Eigenschaften der Gelenkmembran, welche bei der hydraulischen Streckung eine essentielle Rolle spielt, wurden hierbei besonders beachtet. Verschiedene optische Methoden, wie Licht-, Raster- und Lasermirkoskopie wurden eingesetzt um die Funktionsweise der Gelenkmembran sowie Oberflächeneigenschaften darzustellen. Dabei wurden Mikrostrukturen entdeckt, welcher in alternierenden Abschnitten auf der Membran verteilt sind und eine Rolle in der Kommunikation, Selbstreinigung und Reibungsreduzierung spielen könnten. Das Verschwinden dieser Mirkostrukturen nach einer Deproteinierung des Exoskeletts weist darauf hin, dass die Mikrostrukturen wahrscheinlich von Proteinen in der äußersten Schicht des Exoskeletts, der Epikutikula, gebildet werden. UV-Licht Analysen zeigen weiterhin, dass Unterschiede in der Proteineinlagerung zwischen den zwei alternierenden Bereichen bestehen und möglicherweise das elastische Protein, Resilin, eingelagert ist. Materialeigenschaften, wie die Steifigkeit und Härte der Gelenkmembran wurden mittels Nanoindentation analysiert und es konnte ein signifikanter Unterschied zwischen den alternierenden Mikrostrukturbereichen festgestellt werden. Histologische Schnitte und Röntgenstrahl Aufnahmen lassen vermuten, dass Dicke und Dichtigkeitsunterschiede zwischen den alternierenden Bereichen eine weitere Ursache für deren unterschiedliche Materialeigenschaften ist. Die Ergebnisse bestätigen die Hypothese einer sog. anisotropen Gelenkmembran. Es lässt sich vermuten, dass die versteiften Segmente bzw. Halb-Ringe eine kontrollierte und geführte Faltung der Membran während der Beugung des Gelenks ermöglicht und ein ungewolltes Aufblasen der Membran bei großen Druckeinwirkung während der Streckung verhindert. Die Übersetzung des Faltmechanismus der Gelenkmembran, sowie der versteiften Elemente in einen flexiblen, 3D-gedruckten Prototypen haben gezeigt, dass das Fehlen von Versteifungselementen eine kontrol-

lierte Faltung nicht ermöglichen würden und es zu spitzzuflaufenden Knitterungen kommt, welche letztenendes zu Materialversagen führen und somit eine Langlebigkeit der Membran verhindert. Im Allgemeinen wurde für die Fabrikation und Umsetzung des spinnen-inspirierten Aktors die heutigen Anforderungen für soft, fluidische Aktoren beachtet. Dazu gehören eine hohe Flexibilität und Nachgiebigkeit, ein leichter und modularer Aufbau sowie Langlebigkeit und Umweltverträchlichkeit. Da die Nachfrage nach immer kleineren Implementierungen steigt, wurde auch versucht die Fabrikation und das Material so zu wählen, dass in Zukunft kleinere Aktoren hergestellt werden können. Der vorgestellte Prototyp wurde mittels Filament basierter 3D Druck Technologie aus flexiblen und robusten themoplastischem Polyurethan (TPU) hergestellt und mit Latex innenseitig abgedichtet. Wasser wurde zur hydraulischen Kraftübertragung und Fäden zur Beugung benutzt, um das Zusammenspiel von Muskeln und hydraulischer Streckung zu simulieren. Das spinnen-inspirierte Prinzip ermöglicht einen Arbeitswinkel von 125°, welches vorherige Umsetzungen (60-90°) weit übertrifft und der Spinnenfähigkeiten (140°) näher kommt. Die Analyse der Druck und Kraft Verhältnisse haben gezeigt, dass sich die Bewegung des Aktors über lineare Verhältnisse bewerkstelligen lässt. Es konnte gezeigt werden, dass ein einzelnes 6-10 g schweres Gelenksegment Gewichtelemente von 600 - 1kg bei einem hydraulischen Druck von 200-300 kPa gegen die Schwerkraft anheben kann. Das schnelle, radiäre Aufschnellen des Gelenksegments ermöglicht zudem eine hohe Übertragung des Drehmoments, welches mittels Sprüngen demonstriert werden konnte. Die 120g schwere Plattform konnte dabei Sprünge von bis zu 10 cm Höhe und 10 cm Weite erzielen. Die Analysen ergaben, dass bei einem schnellen Aufschnellen des Gelenks, es zu einem sofortigen Druckabfall kommt, welches sich möglicherweise durch die Trägheit der Flüssigkeit erklären lässt. Ein solcher Druckverlust könnte zu Verlusten bei der Kraft und Drehmomentübertragung erzeugen und auch zu Materialschäden führen. Um das Flüssigkeitsverhalten in der Spinne zu verstehen wurden deswegen die Viskositätseigenschaft der Hämolymphe unter verschiedenen Drücken und das Flussverhalten im Bein untersucht. Es konnte der genaue Flüssigkeitsstrom im Gelenk dargestellt und ein nicht-newtonisches bzw. ein scherverdünnendes Verhalten der Hämolymphe festgestellt werden. Eine solche Eigenschaft könnte erklären, weshalb eine schnelle Volumenverschiebung während der Streckung der Spinnenbeine möglich ist und es nicht zu einer Kavitation beim Aufschnellen während des Sprungs bzw. zur Sauerstoffunterversorgung der Muskeln und Organe bei hoher Aktivität kommt. Für hydraulische Anwendungen könnte eine solche Flüssigkeit die mechanische Effizienz bei hohen Drücken erhöhen, wobei die volumetrische Effizienz, also die Übertragungrate der Flüssigkeit über einen großen Bereich konstant gehalten werden kann. Die erfolgreiche, funktionelle Umsetzung des spinnen-inspirierten Aktors ermöglicht somit nicht nur die Anwendung im Bereich von Prothesen oder Robotern in Zukunft, aber ergibt auch neue Fragestellungen und

Einsichten in das Verhalten und die Funktionsweise der Bewegung von Spinnen.

Acknowledgements

I would like to thank Prof. Dr. Metin Sitti for the opportunity to work on this very interdisciplinary and interesting topic, the financial support and for the scientific discussions and feedback on my research.

I would like to express my very great appreciation to Prof. Dr. Roland Siegwart for the great opportunity to work at the Autonomous Systems Lab, ETH Zurich, for his interesting questions and ideas, for the financial and networking support, the opportunity to attend World.minds and the wonderful time in Zurich.

I am particularly grateful for the scientific support by Prof. Dr. Guillermo Amador, for the great and fruitful discussions on my research, the support in my scientific career and for being part of my committee.

My special thanks to Prof. Dr. Marco Hutter for being part of my committee and taking the time to read about my research.

I would like to thank Prof. Dr. Bernhard Schölkopf and Prof. Dr. Thomas Hofman for financial support and creating the Center for Learning systems.

I am very thankful for the constant emotional and scientific support during my PhD by Dr. Karin Elflein, for all the insights on spider dissection and histology methods and for the late night discussions about spiders and life.

I would like to acknowledge Prof. Dr. Abdon Pena-Francesch for his great support on the fabrication of microstructured surfaces, his constant excite on this topic and being a great support during my PhD thesis.

I would like to express my gratitude to Dr. Thomas van de Kamp for 3D scanning the spider legs at KIT, introduction into Amira and Biomedisa, invitation to the Graduiertenforum Morphologie and to the Westdeutscher Entomologentag and for all the great and interesting conversations about insects, especially ants.

I would like to thank Prof. Dr. Joachim Spatz and Ioanis Grigoridis for the

introduction and use of the SEM.

I appreciate the feedback offered by Dr. Lionel Ott and his support on my papers, always having an open ear and being a great roommate.

I have greatly benefited from Dr. Juan Nieto and Dr. Nicholas Lawrance as my go-to-persons at the ETH, providing me with feedback on my papers, always being supportive, being fast responders and always in for fun ideas.

I am deeply grateful to Dr. Jen Jen Chung for being super supportive, for detailed feedback on my paper and talks about career and future.

I received generous support from Achim Diem in assistance and analysis of the nano-indentation experiments.

I would like to thank Nagaraj Krishna-Subbaiah and Anitha Shiva for their help in the fabrication of micro channels and micro structures.

I would like to offer my special thanks to Lisa Böhler for her work as my HiWi, her support in care-taking my spiders, for assisting me during high speed and OCT recordings.

I would like to thank Prof. Dr. Stelian Coros for giving me the advise to use TPU as printing material.

I am very grateful for the support by Prof. Dr. Zoey Davidson, on discussing the role of microstructures and his general advice.

I would like to thank Prof. Dr. Kirstin Petersen and Dr. Alexander Spröwitz for their initial support on my PhD topic and the ICRA publication.

I am thankful for the support and encouragement by Prof. Dr. Guozhan Lum, for giving great advice about research and showing us the great world of Singapore.

I appreciate the feedback and help offered by Dr. Marcus Zuber and for assistance in CT scans of the spiders.

I would like to express my gratitude to Janes Odar for support in Amira, emotional support and fun times during scanning in Karlsruhe.

I have greatly benefited from Philipp Lösel, who introduced me to Biomedisa.

Special thanks to Dr. Abel Gawel for welcoming me in Zurich, for his support, for the great time in Singapore and being a great friend!

I am grateful for insights provided by Dr. Bekim Berisha and Philipp Wilhelm about tensile tests and FEM analysis.

I would like to offer my special thanks to Dr. Thomas Braun for providing insights into contact angle measurements with nanodroplets on peltier elements.

I have greatly benefited from Dr. Nino Läubli and Dr. Jan Burri as assistance in handling the Femto tool.

I would like to offer my special thanks to Michael Riener for his help and support and just being a great Swiss guy!

I am really thankful for the support by Muhammad Yunusa, for being the second PhD suffering with me from the beginning! Thanks for being supportive through out all the time!

I received generous support from Prof. Dr. Martin Adams, his wife and family and would like to thank them for giving me a great time and very nice memories in Zurich.

I would like to generally thank my roommates, accepting me and my chaos.

Furthermore, I would like to thank the whole PI, ASL and CLS including the staff members for their constant support and a great time. Especially, Lucy, Cornelia, Janina, Patricia, Jutta, Sarah, Sara, Leila and Magdalena for their great support in making my life easier. I would also like to thank my BOGY and Bachelor students for the great time and remembering me about the fun side of science.

I am more than thankful for all my close colleagues and friends; Berk, Varun, Donghoon, Sukho, Yunwoo, Amir, Hamed, Ville, Josh, Wendong, Xiaoguang, Matthew, Dirk, Onder, Oncay, Ceren and Victoria for being a great emotional support during my time in Stuttgart, the fun discussions during lunch and dinner, Chinese Restaurant at Schwaben Galerie, Bowling, (Korean) BBQ, soccer tournaments, ping pong, Singapore and karaoke nights!

My deepest appreciation goes also to Julian, Ken, Michel, Hermann, Vivian, Teja,

Fadri, TJ, Helen, Rene, Gianluca, Lukas, Rik, Weixuan, Matthias, Karen and Margarita for being a great emotional support during my time in Zurich, the fun board game nights, ping pong, dance nights, the street food festival, sushi!, the snoring nights during the Skitrip, the great Avengers countdown and the fun Christmas Video making!

I would like to show my greatest appreciation to Mehdi, Partha, Anurag, Alex, Shoubik, Kamil and Timmy for the fun fun discussions during the retreat, the memorable and epic board game nights in Tübingen and many more unforgettable events that reinforced our friendship!

Also, special thanks to Wolf, Carola, Fabienne, Simone, Damir, Tobias, Ann-Catrin and Patrick for being good friends, staying interested on my research and my life although we were all busy as always.

I am particularly grateful for the support by Dr. Herbert Ammann, who was the best landlord one can only wish for and organized memorable wine-evenings above the Zurich lake.

I am very thankful for the support by Vanessa Oehmig, who was my "spider dealer" and provided me with advice for breeding and keeping jumping spiders.

I owe a very important debt to all the spiders, who supported my research.

I would like to express my sincere thanks to my grandparents for caring about me and asking me now and then whether I am still alive, also to my mother-in law, Annette, for being understanding and supportive!

I am very thankful for my siblings, Annique, Henry, Richard, who were always supporting me, helping me with 3D printing maintenance, image editing, discussion about my research and being my personal crew. Don't know what I would do without you.

I am deeply thankful for my parents for always believing in and pushing me to achieve my dreams and goals, for supporting me in every stage of my life, so that I could concentrate on my research. Thank you for everything. I love you.

And finally, without my husband Thorsten, his emotional support, his late night assistance, being taxi driver, dinner cook, food supplier, spider daddy, and his patience for discussion, more discussions, endless discussions about my research and life this

thesis would not have been possible. I love you and I cannot thank you enough.

Thanks to everybody and everyone I forgot.

August 26, 2021 *Chantal Göttler*

Financial Support

The research leading to these results has received funding from the Max Planck Society, ETH Zurich and the Max Planck ETH Center of Learning Systems.

Contents

List of Figures

List of Tables

Preface

To my friends, my husband and family
to the spiders with two legs too many
to my little six-legged creature
for the good and the better in future
I wonder, if things are how they should be?
But isn't that the real mystery.
Not knowing what life will bring.
Doesn't this drive us to do a thing?
Ten years ago, I had no idea
that my life will end up, being here
Still, I have settled the fundament
So probably it was no accident
Building up, brick by brick
another step in my life, so quick
Where has time gone so fast?
Will anything ever last?
What comes next? You may ask-
I can tell you, it's a difficult task!
Swimming in the lake of academy?
struggeling to found my own family?
So listener, I'll thank you a lot
for reading my entire plot
of research I have done hitherto
I hope it was a joy to you!

The Beginning

It all began with the idea of building a small jumping leg inspired by spiders. It was summer and the nearby forest was full with spiders, especially the harmless wolf spiders, known to be fast runners and jumpers. Luckily they were easy to find and catch and became the first inspiration of this project. Using highspeed cameras and simple Stereomicroscopes, the movement of the joints were observed. It turned out pretty soon, that the joint behaviour of the spiders was not fully mirrored by the biological literature or the previous published spider-inspired actuators and the locomotion mechanism was still not fully uncovered. While working on the first prototype, many more questions arose, which had to be answered to understand the principle behind the locomotion of spiders and how these aspects could be implemented into a robotic device.

The questions were either of biological nature leading to the need of biological samples and their preparation and dissection or were asking about design, fabrication and material aspects which needed to fullfil modern robotic challenges, while still able to answer and test hypothesis and principles.

Spiders

To dig down deeper into the biological understanding of spider legs with focus on the mechanical aspects, jumping spiders (Salticae) with their versatility in gait pattern seemed to be interesting candidates. As gender, age and species play an important role when studying biological systems, the availability of samples should not be dependend on the outside season and therefore the keeping and breeding of the animals should be practicable. *Phidippus regius*, which has been studied in some literature before, belongs to the largest jumping spiders in the world, is a calm spider species, easy to keep and breed, with a large breeder community (in Germany) behind it. Furthermore the size of adult spiders was ideal, as it was right at the corner of being too large to fit in the field of view of most microscopes and on the other hand being too small turning preparation and dissection as well as highspeed recordings into another challenge.

Breeding *Phidippus regius* had to be done carefully as female spiders tend to be aggressive towards males when they are not ready. Armed with a tweezer and a water spray bottle, to intervene in case of an aggressive attack by the female, the largest male (Jimmy) was placed into the box of the female (Big Berta). The male approached the female slowly while constantly shaking his forarms. Luckily the first trial was immediately successful. The female spider prepared a huge and dense sleeping bag like net, where she laid hundred of eggs inside. She stayed inside the net protecting her offsprings and closing the entry, when a mealworm or cricket tried to move inside. During this time she barely ate food, but waited until the small spiders hatched, before she went out herself

to catch prey. The little juvenile spiders stayed in place for a couple of days before they start wandering around searching for small animals as e.g. aphids. Juvenile *Phidippus regius* have to be fed continously when not kept individually as they would start hunting their siblings when reaching a specific age and size. While started with a population of 100 spiders, predatory siblings, death through dryness, too large water droplets, fights with larger prey or molding problems have occured until around 50 spiders reached adulthood after 8-10 month.

Actuator fabrication

The fabrication of a functional actuator was another main field of questions. While letting prototypes be fabricated by other companies would save work time for sure, it often comes with the cost of limiting understanding of the fabrication problems, limiting parameters to tune, limiting materials, high cost and large waiting time until a prototype is finished. Therefore only a small number of prototypes and materials could be tested. As the design of the actuator was still in early stage and should be adapted in parallel to new biological findings, the decision of in-house, self-fabricated prototypes was made early. During that time, additive manufacturing was a rising star in prototype technology and 3D printing became the technology of choice. Beside its popularity, 3D printing brings many advantages for fast prototyping. In theory, any conceivable shape could be designed and fabricated, while casting processes or screwing objects together are limited in avaible shapes, need special tools and often result in long finishing hours. But although 3D printing seemed to be the way to go, it still took many cycles, testing and trying until the most suitable material for prototyping was found and the desired shape designed.

Chapter 1

Introduction

Bioinspired robotics has risen in popularity since the early 2010's. New materials and fabrication methods on the robotic side in combination with advanced recording and analytic methods to study the locomotion, behavior and material of the biological counterpart has pushed this research field into focus, enough to even found a new journal, Science Robotics, in 2016. Interestingly, most ideas have been formulated already in the 1980s by the father of "Bionik", Werner Nachtigall, but not all were implemented successfully as there was either still a large lack in understanding the biological inspiration or technology was far behind the requirements needed. New developments in artifical intelligence, gene-editing tools as CRISPR (Clustered Regularly Interspaced Short Palindromic Repeats), the rise of soft robotics for safe human-robot interactions and extraordinary jumps in microscopy resolution as well as high speed technology in combination with the human desire to still stay close to nature while technology is becoming more and more part of our everyday life, have been pushing the field of bioinspiration into the spotlight. Needless to say, expectations are high, but there is still a lot to learn for biologists and engineers to allow successful communication and implementation of these two different fields, so that both sides could benefit during this evolution.

This work covers one special subject of the wide range of bioinspiration, the locomotion of spiders. Scientists have been fascinated by these creature of nightmares for centuries as they are equipped with many tools and behaviors to survive and hunt preys including their venomous claws, their sticky silk wired nets, their hairy feet allowing crawling on glass or - a very recent discovery - the feeding of juvenile spiders with a mother milk like substance [27]. Jumping spiders, the spotlight animal in this thesis, are furthermore equipped with well developed eyes, which are constantly tracking their prey, before they catch it with a well-planned and precise jump. This specialization in active hunting

preys makes jumping spiders an interesting model for studying locomotion.

To give the reader a detailed look into both parts of the research project, the work is divided into three main chapters. The first part focuses on the biological aspects of the locomotion study. The reader will be introduced into the relevant biological terms, along with new research results and discoveries made during this PhD. The second part covers the robotic implementation. An overview of spider-inspired actuators and robots will be given together with the newest approach based on the biological findings from the chapter before. The last part provides a detailed discussion of approaches, open questions, how biology and engineering can benefit from each other and where the future of this field lies.

1.1 Motivation and Objectives

- Understanding and presentation of joint membrane folding involved in fast and large working angle movements
- Analyzing material properties of joint membrane for proving reinforcement hypothesis
- Understandig the 3D construct and hydraulic extension mechanism
- Analyzing the body fluid properties and its advantage as hydraulic fluid
- Implementation of joint mechanism into robotic fluidic actuator
- Understandig the benefits of such a design

1.2 Approach

To accomplish the objectives, I grouped this thesis into two parts. The first part was mainly conducted at the Max Planck Institute and focuses on biological aspects. To get a deeper insight into the morphological and geometrical set-up of the spider leg, different microscopical methods (Stereo-, Laser-, and Scanning Electrion Microscopy), high speed recording, histological sections and 3D X-ray reconstruction have been used. These studies gave new insights about the folding principle of the joint, about the surface roughness, and about the inner structure of the leg. Material properties were then analyzed with nanoindentation methods and the refabrication of certain aspects (e.g. microstructures). The findings of these studies resulted in a recently accepted journal publication [43]. Hemolymph velocity inside the leg was further detected

with optical coherent tomography and the physical properties (viscosity) were analyzed by collecting hemolymph and studying its velocity under different pressures inside a microchannel. The results of the hemolymph study are in preparation for publication.

The second part of this thesis focuses on the design and fabrication of a spider-inspired fluidic actuator. A first early prototype was published in the beginning of my PhD [120], which bases on stiff shell element sliding and only a superficial understanding of the working principle of the spider joint and its benefits. A constant development of the prototype was carried out along side new findings on the biological side. The robotic implementation was finalized at the ETH Zurich. The implementation of the spider-inspired folding and design principle was also published in [43]. The fabrication and analysis of the developed actuator gave better understanding of the advantage of several design aspects (e.g. reinforcement hoops) and also about challenges the spider might be exposed to when using hydraulic actuation in biological systems.

1.3 Contribution

While the results and methods of this thesis will be presented and discussed in the scope of this work arranged around all influences on the locomotion of spiders and spider-inspired robots, I would like to give the reader a first insight into the focus of my work, its contribution to the community and the major findings and developed methods without further discussion at this point. The reader can then find the linked chapter and sections to read about each point in detail and find an in-depth discussion about it in the final discussion chapter.

1.3.1 Findings and Developments

In this work,

- I have reviewed locomotion-related literature and pointed out problems and hypotheses from each of these fields including respiratory system, gait pattern, body motion and jumping behavior. Although outside of the focus of my thesis, I have conducted high speed recordings which support some the brought up arguments and hypotheses.

- I have successfully developed a new SEM (scanning election microscopy) preparation method for inflated biological soft structures to allow high resolution imaging of the femur-patella joint and its articular membrane. The SEM images led to the discovery of alternating microstructures on the surface.

- I have discussed the function of the microstructures on the articular membrane for communication, self-cleaning and low friction as well as adhesion motion and I have proposed and developed experiments to study their influence in future.
- I have conducted experimental studies on the mechanical properties of the articular membrane covering the femur-patella joint to prove reinforcement structures which are essential for the folding of the articular membrane.
- I have provided the first detailed microscopy video recordings to complete schematic drawings from elder literature and to give a better understanding on the folding characteristics of the articular membrane in living jumping spiders. I showed, that the 3D folding of the membrane does not resemble a traditional bellow, but is arranged like a stroller sun shade, where the reinforced parts of the membrane slide into each other like in an ice-cream-scooper.
- I have modified traditional histolocial methods to allow the thin film microtome cutting of samples with high stiffness gradients. This method showed the inner composition of the femur-patella joint and the articular membrane.
- I have used high resolution X-ray scans to visualize the 3D set-up of the unfolded femur-patella joint, showing the articular membrane in detail and to give information about geometry and fluid flow. Proposed arterial valve systems from elder literature were not discovered, however I have proposed an alternative mechanism for pressure control involving the arcuate sclerite.
- I have used optical coherent tomography to conduct a non-invasive study on the body fluid flow of the femur-patella joint on living animals. This method works without any addition of chemical substances to enhance the imaging. I was able to show fluid flow direction and velocity and found an interesting spiral flow inside the femur-patella joint, which have not been reported before.
- I have experimentally studied the fluid behavior of the inner body fluid, hemolymph, using microchannels at different pressures mimicking the fluid environments inside the spider arteria. I derived the relationships of pressure and velocity to determine the viscosity from the experimental data and showed that the hemolymph exhibits a non-Newtonian behavior. I have discussed the influence of viscosity and shear-changing behavior on hydraulic systems.

- I have designed a folding mechanism inspired by the articular membrane of spiders for rotatory motion. The design allows one degree of freedom (DoF) rotation with working angles of 125° along a given hinge joint. The working angle exceeds previous spider-inspired designs by 30-80° without additional material or overextension of the material.

- I have evaluated materials and methods for the fabrication and sealing of a flexible rotatory actuator. I have modified FDM (fused deposition modeling) printing parameters for the printing of thermoplastic polyurethane and defined curing protocols of Latex milk for sealing purposes of the final fabrication of a lightweight, flexible, chemical resistant, modular, low-cost and environment-friendly fluidic actuator.

- I have shown that the reinforcement design of the folding membrane not only allow a guided motion to avoid undesired wrinkles and damages, but can also contribute to the storage of elastic energy.

- I have designed a flexing mechanism, which allow the coupling of flexing and fluid collection, furthermore I have proposed a magnetic flexing design, which allows to switch between locomotion modes (walking and jumping) and reduce the number of motors in the system for future integration.

- I have characterized the prototype and showed that at pressures of 200 kPa, forces of 10 N (torque: 0.3 Nm) can be generated. The operating pressure is thereby 10-1000 times smaller than in other proposed fluidic spider-inspired designs. The stable positions and the use of water instead of air further reduces the "wobbeling" motion, which can be often observed in soft pneumatic systems due to the compressibility of air. While the control of soft actuators could be complex and non-linear due to e.g. the hyperelasticity of the material, the characterized pressure-angle-force behaviour of the prototype shows a simple linear to quadradic behavior.

- I have demonstrated complete lifting and jumping abilites. A single actuator of 6 g is thereby able to completely lift 600 g against gravity. For jumping demonstration, I have constructed a jumping platform and achieved similar jumping capabilities as derived from the simulations.

- I have discussed, the advantages of the rotary fluidic prototype and why spiders might use this mechanism rather than muscles or elastic proteins to create precise and strong motions.

1.4 Contribution

While the results and methods of this thesis will be presented and discussed in the scope of this work arranged around all influences on the locomotion of spiders and spider-inspired robots, I would like to give the reader a first insight into the focus of my work, its contribution to the community and the major findings and developed methods without further discussion at this point. The reader can then find the linked chapter and sections to read about each point in detail and find an in-depth discussion about it in the final discussion chapter.

1.4.1 Findings and Developments

In this work,

- I have reviewed locomotion-related literature and pointed out problems and hypotheses from each of these fields including respiratory system, gait pattern, body motion and jumping behavior. Although outside of the focus of my thesis, I have conducted high speed recordings which support some the brought up arguments and hypotheses.

- I have successfully developed a new SEM (scanning election microscopy) preparation method for inflated biological soft structures to allow high resolution imaging of the femur-patella joint and its articular membrane. The SEM images led to the discovery of alternating microstructures on the surface.

- I have discussed the function of the microstructures on the articular membrane for communication, self-cleaning and low friction as well as adhesion motion and I have proposed and developed experiments to study their influence in future.

- I have conducted experimental studies on the mechanical properties of the articular membrane covering the femur-patella joint to prove reinforcement structures which are essential for the folding of the articular membrane.

- I have provided the first detailed microscopy video recordings to complete schematic drawings from elder literature and to give a better understanding on the folding characteristics of the articular membrane in living jumping spiders. I showed, that the 3D folding of the membrane does not resemble a traditional bellow, but is arranged like a stroller sun shade, where the reinforced parts of the membrane slide into each other like in an ice-cream-scooper.

- I have modified traditional histolocial methods to allow the thin film microtome cutting of samples with high stiffness gradients. This method showed the inner composition of the femur-patella joint and the articular membrane.
- I have used high resolution X-ray scans to visualize the 3D set-up of the unfolded femur-patella joint, showing the articular membrane in detail and to give information about geometry and fluid flow. Proposed arterial valve systems from elder literature were not discovered, however I have proposed an alternative mechanism for pressure control involving the arcuate sclerite.
- I have used optical coherent tomography to conduct a non-invasive study on the body fluid flow of the femur-patella joint on living animals. This method works without any addition of chemical substances to enhance the imaging. I was able to show fluid flow direction and velocity and found an interesting spiral flow inside the femur-patella joint, which have not been reported before.
- I have experimentally studied the fluid behavior of the inner body fluid, hemolymph, using microchannels at different pressures mimicking the fluid environments inside the spider arteria. I derived the relationships of pressure and velocity to determine the viscosity from the experimental data and showed that the hemolymph exhibits a non-Newtonian behavior. I have discussed the influence of viscosity and shear-changing behavior on hydraulic systems.
- I have designed a folding mechanism inspired by the articular membrane of spiders for rotatory motion. The design allows one degree of freedom (DoF) rotation with working angles of 125° along a given hinge joint. The working angle exceeds previous spider-inspired designs by 30-80° without additional material or overextension of the material.
- I have evaluated materials and methods for the fabrication and sealing of a flexible rotatory actuator. I have modified FDM (fused deposition modeling) printing parameters for the printing of thermoplastic polyurethane and defined curing protocols of Latex milk for sealing purposes of the final fabrication of a lightweight, flexible, chemical resistant, modular, low-cost and environment-friendly fluidic actuator.
- I have shown that the reinforcement design of the folding membrane not only allow a guided motion to avoid undesired wrinkles and damages, but can also contribute to the storage of elastic energy.

- I have designed a flexing mechanism, which allow the coupling of flexing and fluid collection, furthermore I have proposed a magnetic flexing design, which allows to switch between locomotion modes (walking and jumping) and reduce the number of motors in the system for future integration.

- I have characterized the prototype and showed that at pressures of 200 kPa, forces of 10 N (torque: 0.3 Nm) can be generated. The operating pressure is thereby 10-1000 times smaller than in other proposed fluidic spider-inspired designs. The stable positions and the use of water instead of air further reduces the "wobbeling" motion, which can be often observed in soft pneumatic systems due to the compressibility of air. While the control of soft actuators could be complex and non-linear due to e.g. the hyperelasticity of the material, the characterized pressure-angle-force behaviour of the prototype shows a simple linear to quadradic behavior.

- I have demonstrated complete lifting and jumping abilites. A single actuator of 6 g is thereby able to completely lift 600 g against gravity. For jumping demonstration, I have constructed a jumping platform and achieved similar jumping capabilities as derived from the simulations.

- I have discussed, the advantages of the rotary fluidic prototype and why spiders might use this mechanism rather than muscles or elastic proteins to create precise and strong motions.

1.5 Thesis Outline

In the following chapters, the contributions of this thesis will be presented. The thesis is divided into five major parts: Biology of Spiders, Locomotion of Spiders, Robotic Implementation, Discussion, Material and Methods.

The first chapter (Biology of Spiders) introduces the reader into important terms from the outer and inner morphology as well as the "gadgets" of spiders. Especially for readers outside the field, this chapter could help to get a better understanding of the functioning and behavior of spiders. Aspects, which need special caution when reading, where extended by a comment section to explain difficulties.

The second chapter (Locomotion of Spiders) could be divided into two parts. The first part (Locomotion Behavior and Jumping Kinematic Modeling) give an overview about behavioral studies as e.g. gait patterns or body motions.

This part provides the reader with background information of previous research on the locomotion of spiders and my additional insights.

The second part of this chapter (Spider Leg and Hydraulics) forms the heart of this work. It provides information about the design and functioning of the semi-hydraulic femur-patella joint. New experimental results on the three dimensional (3D) geometrical set-up, the material properties, the folding behavior and micro structures of this joint are presented. Furthermore, the fluid flow, speed, shear rate and viscosity of the hemolymph of spiders is presented. These result provide new insights into the advantage of hemolymph as hydraulic fluid.

Leading to the third chapter (Robotic Implementation), which is divided into three main parts. The first part gives a short introduction for the symbiosis of biology and technology, hydraulic actuation and existing spider-inspired work. The second part provides the design criteria for a spider-inspired fluidic actuator and a short summary on all fabrication methods tested in this work. Finally, the characterization of the prototype shows the performance including torque, working angle, pressure resistance, durability and jumping performance.

The forth chapter provides an overall discussion about the biological and robotic aspects covered in this work. Here, insights gathered from biological and robotic experiments are discussed and placed into previous work. The performance of the here presented prototype is finally compared to previous works spider-inspired actuators.

The last chapter provides additional information on material and methods used in this thesis. As many experimental set-ups had to be developed or modified to be able to measure the small samples of spiders and to fabricate the prototype, this part does not only supplement the thesis, but can be seen as additional important results. Researchers who would like to perform similar experiments could benefit on these details.

Chapter 2

Biology of Spiders

Arthropods as insects, arachnids and crustacean have been around for over 550 million years and share a lot of similarities in morphology and behavior. While many arthropods are herbivores, specialized in feeding on plants, crops or nectar, some others ended up on the predator side of the scale, hunting for living. Spiders, forming the largest order among the arachnid class, are hunters par excellence. With a small number of exceptions, all spiders feed on arthropods, some even on small vertebrates, by catching their preys with phenomenal techniques. Common spiders are known for their beautiful sticky silk webs in house corners, causing shivers running down people's spine when doing the mission impossible abseil while attacked by a scream and a broom. However, this is not the only technique mother nature has equipped spiders with to keep the number of flies in balance. Net casting, luring by mimicking behavior or mating pheromones of preys, building trap doors or directly hunting with their claws on water or on land are just a small list out of their bag of tricks.

The studied jumping spiders (fig. 2.1) belong to one of the most agile and well-equipped species among spiders [37]. Sensor hairs on the legs notice any vibration in their surroundings. Once the source of vibration is recognized, two large eyes keep following it, never losing track even when it shortly moves outside the field of view. These sensory information are constantly sent and evaluated by a fast processing nervous system. When identified as a prey, jumping spiders slowly approach it. Their hairy feet even allow them to walk upside down on leaves or glass. Finding the perfect position, they anchor a safety wire into the ground and prepare their legs to allow precise targeting not only in horizontal jumps, but also from horizontal into vertical position or from upside down. The safety wire keeps the spider body in position during the jump and prevents somersaults at landing. During the jumping flight phase,

Figure 2.1: Jumping spider *Phiddipus regius*. From left to right: 1. Big Bertha (adult female), waiting for food. 2. Big Bertha and Flycatcher Jim (largest adult male), after mating, in Bertha's home "cuddling". Bertha did not attack Jim before or during mating, but kicked him out after a while. 3. Isabella (female adult), with a very large abdomen after mating with Jim. Unfortunately died before laying eggs (got eaten by crickets and meal worms) during pregnancy. 4. R3 (female adult), "red form", origin unknown, not from Florida as the other three, presumably Cuba, was therefore not used for breeding or experiments.

the front legs form a "catching basket" which hug around the prey, before the spiders ram their venomous claws into it, to dissolve the prey's innards. The day-active, sun loving jumping spiders are also quite communicative. When meeting a conspecific, their front legs are often waving in lifted position as they would say "hello" or "goodbye", but actually try to protect themselves from attacking each other. Similar behaviors can be observed when males approach females during mating seasons. The peacock jumping spider shows even a complete dance pattern to impress the females. While jumping spiders do not build catching webs, they do use their silk to create sleeping bags, where they hide to rest at night, during molting and mating, for birth and protecting the newborns and when they just want to slurp their meal worm cocktail in peace. As a little anecdote, during my PhD, latter behavior of the kept spiders (*Phiddipus regius*), often ended up in a pile of empty or half empty corpses lying on the ground below the sleeping bag, which was sometimes even revisited by the spiders to have another sip, when hungry, but lazy.

Although non-biologists often count spiders as insects, the eight-legged spiders (*Araneae*) differ very strongly in their morphology on the inside and outside from their six-legged cousins. This is important to know, as not all preparation methods widely used in entomology for insects can be directly transferred to spiders. Furthermore the comparison between data gathered from insects and spiders should always be carefully conducted as small differences in morphology can already have great impacts on their properties and therefore change usage

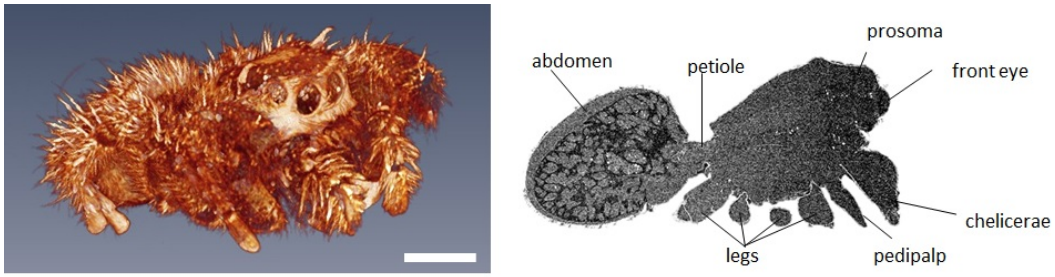

Figure 2.2: Body parts of the Jumping Spider *Phiddipus regius*.. Left: Spiders are covered with hair, which can have a sensory, protection or adhesion function. The characteristics of jumping spiders (*Salticidae*) are their large front eyes and short thick legs. The image shows a CT (computer tomography) scan of a *Phidippus regius* male recorded at KIT, Karlsruhe with Marcus Zuber. Scale bar: 0.5 cm. Right: Spiders consist of two body parts (prosoma and abdomen), which are connected via the petiole. The soft, sack-like abdomen contains the heart, a dense digestive network, reproductive and respiratory organs and the "silk factory". The front body part consists of two shells (carapace and sternum), with eight legs and the fangs (chelicerae) fitted in between. The prosoma holds a large nervous system, necessary to process all the visual signals. Furthermore it is packed with muscles for locomotion and the suction stomach. Image shows a cross-section through the CT scan.

purposes, behavior and locomotion patterns of the animals To dig a little deeper into the functioning of spider bodies and to understand how spiders do, what they do, the following section will give a closer introduction into the morphology of spiders. Knowing how spiders are built up is essential to design preparation methods, dissect specific parts and interpret dissections and 3D scans. Furthermore it gives information about its functioning, which is of great importance for abstracting the (bio-inspired) working principle to implement it into a e.g. robotic device.

2.1 Outside Morphology (Eidonomy)

Different to insects, spiders do not consist of three, but only two body parts (prosoma and abdomen), which are connected via a thin tube-like shaft (petiole, also called pedicel) (fig. 2.2). The front body part (prosoma, also called cephalothorax) is divided into an upper (dorsal) and lower (ventral) shell. The legs and other appendages as the fangs (chelicerae) are attached between these two shells (carapace and sternum). The orientation of spider fangs are important to characterize spiders. The so called jackknife fangs can be divided

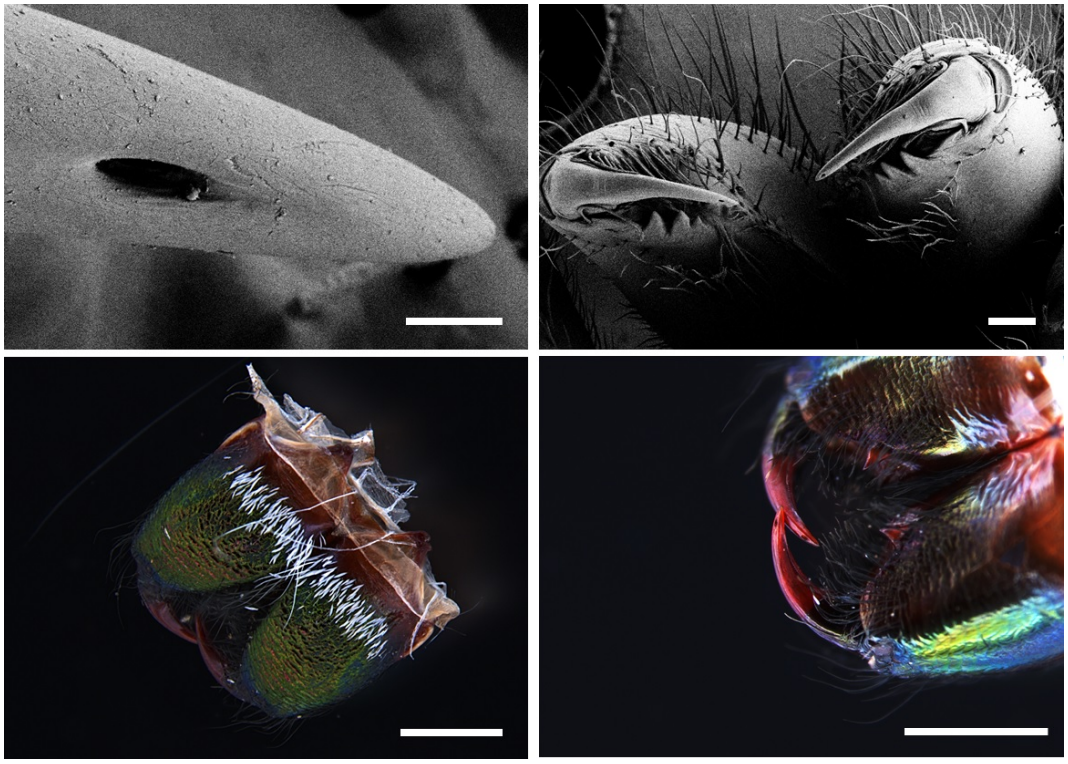

Figure 2.3: Chelicerae - Fangs of *Phidippus regius*. Top left: Opening of the venom channel. Scale bar: 10μm ; Top right: Jackknife fangs of Labidognathous close vertically into serrated mounting (paturon). Opening of the venom channel. Scale bar: 100 μm ; Bottom Left: Iridescent coloration of fangs and bright white scale-hair. Scale bar: 1 mm ; Bottom right: Red smooth injection fangs. Coloration might be a result of metal embedded into the tip of the chitin injection needle [94]. Scale bar: 1 mm; Images were taken at the MPI-IS Stuttgart. The upper images are scanning electron microscopy (SEM) shots, the lower images are taken with a Leica Stereo microscope.

into two types, the orthognathous and labidognathous fangs. Orthognathous fangs are closing in parallel to the body orientation and can be found in *Mygalomorphae*, which are mainly tarantulas. Labidognathous fangs are closing vertically like a pliers and can be found in *Araneomorphae*, which includes the common web-spinning, wolf and jumping spiders (fig. 2.3). Spiders, do not have antennas, but have trichobothria, which are elongated, flexible and movable hairs (setae), distributed on their legs to sense vibration and air flow. Pedipapls, another leg-like pair of appendages close to the fangs in the front of the spiders are equipped with taste and smell detectors, supporting the leg hair sensing. In adult male spiders, the tip of pedipapls are often enlarged

into boxer glove like structures (palpal bulb), which serve as sexual organ to transfer sperm into the female during mating.

The upper shell (carapace) resembles a helmet-like shell, with a characteristic furrow on the top. The carapace is often detached from the prosoma in molts, revealing the sternum and holes of the appendages on the inside. Furthermore, this helmet holds up to eight eyes, which are not divided into compounds as in insects, but are single lens eyes (fig. 2.6). Jumping spiders have very-well developed and significantly enlarged front (anterior median) eyes, giving them a "cute" characteristic.

The second body part (abdomen, also called opisthosoma) resembles an inflated, soft bag, carrying most of the organs. On the under (ventral) side, two spiracle openings of the book lungs can be found. The female genital (epigyne) lies in between these two openings. Close to the anus at the end (posterior) of the abdomen, lies the spinneret, consisting of two to four pairs of telescopic, movable structures, extruding, like the nozzle of 3D printers, thin fibers with different material properties, which are then combined and interwoven to produce various types of silk for different purposes.

2.1.1 Exoskeleton

Invertebrates do not have an inner skeleton in their body and limbs, allowing many invertebrates as octopus, snails and worms to deform and squeeze their body into various shapes. To protect their body and interact with the environment, many invertebrates have hard and stiff parts in addition. Examples are tools for ingestion and locomotion (teeth of snails, bristle hair in earth worms) or shells for protection (housing of snails or sea shells). The largest group among invertebrates, the arthropods, have an exoskeleton (cuticle) made out of layers of chitin microfibers "glued" together by proteins. This exoskeleton covers the skin (epidermis) and protects the inner organs from damage. It does not grow, therefore arthropods have to constantly molt and produce new cuticle during their development. By variation of the hierarchical structure and material composition of the chitin-protein construct, the exoskeleton can have a various number of characteristics as soft and compliant (maggots, caterpillars), flexible but robust (wings of beetles and dragonflies) or stiff and tough (shrimp shell or beetle elytra).

The exoskeleton can be divided into three distinct parts: the epi-, exo- and endocuticle (fig. 2.4). The epicuticle is a thin waxy layer on the outside, protecting arthropods from dehydration. The exocuticle is often highly sclerotized (stiffened due to cross-linking of proteins). The endocuticle forms the innermost part of the exoskeleton, containing non-sclerotized soft microfiber-chitin-protein-layers. It plays an important role in the growth of arthropods

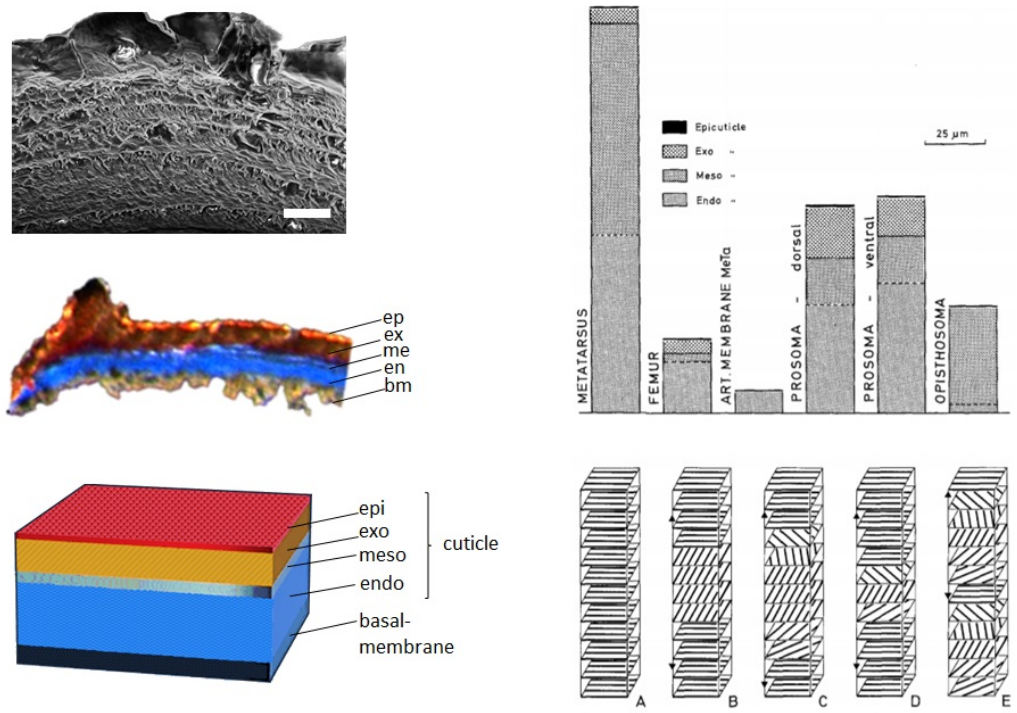

Figure 2.4: Layout of spider exoskeleton. Left side, top to the bottom: 1. Cross section through tibia-metatarsus articular membrane, showing the fabric like set-up of the exoskeleton, taken under the SEM. Scale bar: 10μm. 2. Stained histological section through the patella leg segment, showing the different layers of the exoskeleton. 3. Schematic drawing of the cuticle layers above the basal membrane (epidermis). Right side: schematic drawings by Barth [10]. Top: Average layer thickness of different body parts in spiders. Stiff body parts or elements show thick layers of exocuticle, which are lacking in soft body parts as the opisthosoma or the articular membrane. Bottom: Cuticle is build up by chitin-microfiber layers which are stuck together by different proteins. the layer orientation can be uni- to multi-directional (A-E) and can therefore differ in their material properties as stiffness and friction toughness.

during the formation of a new exoskeleton for molding. The three parts can be distinguished by histological coloration and often show a difference in their fiber orientation. Depending on the coloration methods, another differently colored section could appear between the exo- and endocuticle, the mesocuticle. This intermediate part normally does not show a distinct fiber orientation as the endocuticle. In spiders, the exoskeleton of the prosoma and legs are normally reinforced showing a stiff, sclerotized exocuticle. The abdomen, however, is lacking this layer of exocuticle, but consists mostly of mesocuticle and

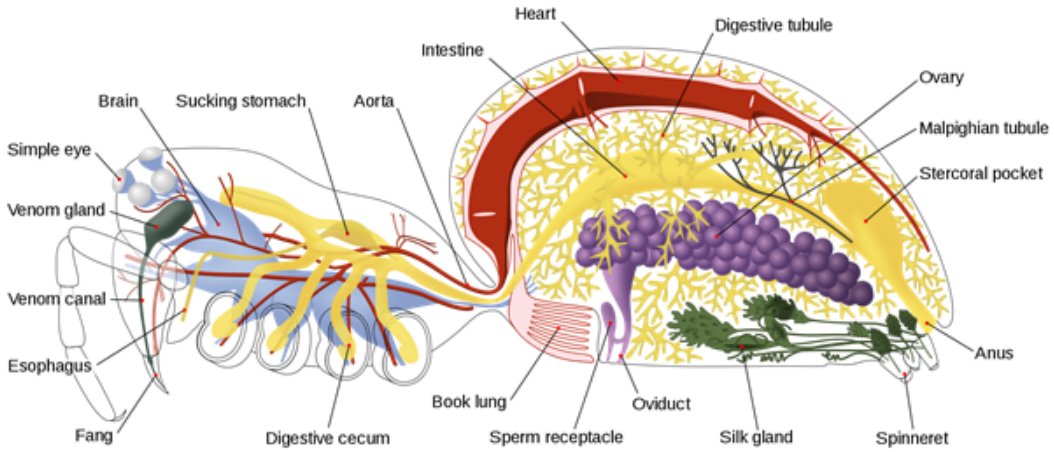

Figure 2.5: Schematic drawing of inner morphology. Spider consists of two body parts which are densely filled with organs. Drawing[1] originally from John Henry Comstock and description according to [37].)

endocuticle. The absence of the stiff exocuticle gives the abdomen a softer characteristic and enables it to expand, when the spider has a large food intake or during pregnancy. The material properties of the exoskeleton are important to understand as the functional purposes of body segments as it could have an impact on energy storage, flexibility and behavior. The material properties of the joint membrane will be of special interest in latter sections.

2.2 Inside Morphology (Anatomy)

The spider body is filled with multiple organs (fig. 2.5[1]). Especially the heart and digestive system are often reflected by the color patterns of spiders, making them essential for species identification. The tubular heart on the upper (dorsal) side of the abdomen, pumps the inner body fluid (hemolymph) through a net of arteries into the body. Beneath the heart lies the intestine, which splits into several thinner structures, forming a spongy like mass for effective digestion. The intestines are connected to a fecal reservoir (stercoral pocket) directly ending into the anus. Malphagian tubules support the excretion as they have a similar role as the human kidney, collecting waste products and forming urine. The abdomen also holds up to several hundreds of silk glands producing different types of "raw material" for silk wire manufacture. Muscles control the movement of the spinneret. Muscles for leg steering and locomotion can be

[1] https://en.wikipedia.org/wiki/Spider; last accessed on: 19th Dec. 2020

found in the prosoma. A fan-shaped muscle connects the sucking stomach to the furrow (fovea) of the carapace. Venom glands close to the fangs, produce the spider's venom, which is injected through venom channels into the prey for external digestion. The liquefied meal is then sucked into the body where it is internally digested by the stomach, which further branches into structures inside the legs (digestive cecum) and the intestine organs in the abdomen.

The sucking stomach is important to create the fluid flow from the mouth, through the food pipe (esophagus) into the digestive organs. The esophagus is encircled by the nervous system of the spiders. While insects have a nervous system which is prolonged through the body ("Strickleiternervensystem"), spiders in contrast have a brain centralized completely in the prosoma. Depending on the behavior, the brain parts for touch sensitivity or visual processing could be enlarged [37].

2.3 Visual System

As the studied jumping spiders show a well-developed visual system, this will also be shortly covered. The neural part taking care of the visual input (optical ganglia) is taking over 30% in space of the jumping spiders brain. Spider eyes are separated into two types, the two front eyes (principal or anterior eyes) and the smaller secondary eyes. In jumping spiders, the enlarged principal eyes (fig. 2.6) allow them to observe and track their preys, while the secondary eyes are mostly used as motion detectors.

The structure of spider eyes differs significantly from insect or mammal eyes. The compound eyes of insects are divided into hundreds to thousands of smaller hexagonal units (ommatidia), providing single images as pixels on a photo or single dots on an impressionistic painting to the brain. Some insects as wasps have three tiny, "simple eyes" (dorsal ocelli) on their forehead for motion detection. Spider eyes are also "simple eyes" (ocelli) but differ highly in form and function and are very well adapted to their behavior. Studies on the optics of jumping spiders (*Portia* spec.) have shown that their eyes have two lenses and a tubular shape, resembling binoculars [46]. This forms a telephoto system, which allows the jumping spiders to even observe and track distant objects. The retina ("image sensor") consists of several stacked layers of photo receptors allowing color vision (green, blue, ultra-violet) and enables jumping spiders to distinguish two objects with a distance of 0.12 mm from 20 cm apart. Their resolution (0.04°) is therefore ten times higher than the resolution of the best performing dragonflies (0.4°) with similar eye size and only five times lower, when compared to humans (0.007°). Latter finding is astonishing when considering that human eyes are not only larger in size but consist of more

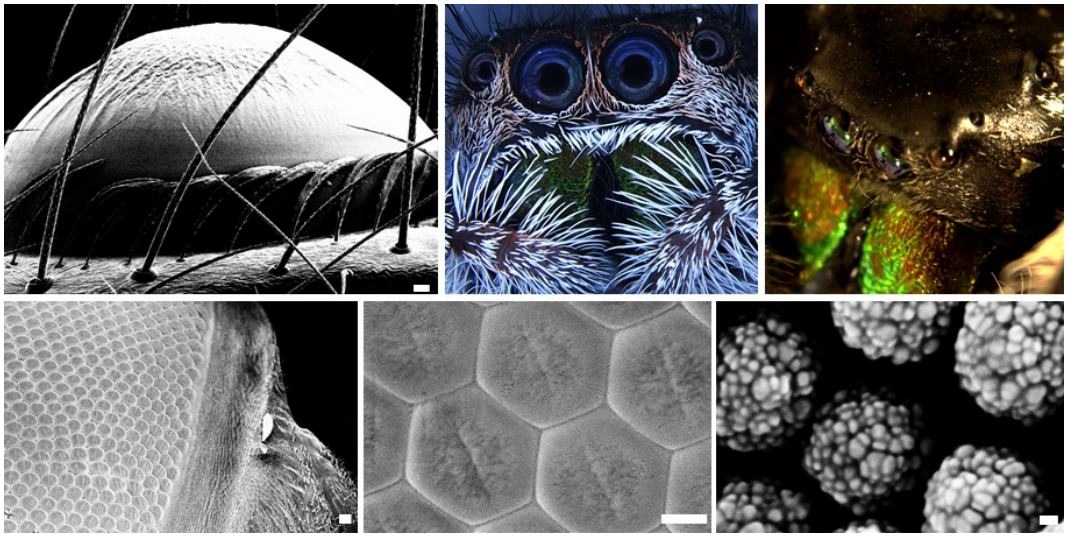

Figure 2.6: Visual system of Arthropods. Upper row: Spider, *Phiddipus regius*; Left: Large anterior eye of juvenile jumping spider under the SEM taken together with BoGY students in 2017. The image shows that the eye is not divided into compounds. Scale bar: 10 μm. Middle: Photography of male, alive, juvenile jumping spider taken under the Leica Stereo microscope together with my student Lisa Böhler in 2018. The two front eyes are significantly enlarged in comparison to the side eyes, which is very common for jumping spiders. Right: Photography of "Flycatcher Jim", large adult male spider, father of the second generation of lab spiders, taken under the Leica Stereo microscope after his natural death in 2018. Photography shows secondary eyes on the side, which are mostly used for motion detection. Lower row: Butterfly, *Nessaea aglaura*; Left: The butterfly eye is divided into thousands of compounds. Scale bar: 20 μm. Middle: The compounds are shaped in regular hexagons. Scale bar: 10 μm. Each compound is covered by thousands of pillars, which are again nano-structured. Scale bar: 20 nm. All three SEM images of the butterfly were taken in 2015 together with my colleague Nikolai Rosenthal.

than 150 million photo receptor cells while in jumping spiders this number lies in thousands. Although the focused area (fovea centralis) is rather small in jumping spiders, eye muscles can move the tubular eyes around to observe large objects or track prey. Another fascinating aspect of jumping spider vision is their ability to precisely estimate distances to catch their prey.

Although equipped with two main eyes as humans, spiders cannot use the information to construct a 3D image (stereopsis). While birds (with eyes on the sides) move their eyes up and down and overlay these images for 3D reconstruction, spiders have developed their own technique called "blurry vision"

for depth perception. Thereby green light and their stacked retina structure play a special role. While green light hits the first layer of photo receptors in focus, it is blurred on the second layer. Interestingly, the level of blur depends on the distance of the object, the closer, the fuzzier the image on the second layer [79]. While tests show that jumping spiders fail judging distance under only red light, an adaption on short green light makes sense when considering that in dense forests, where jumping spider lives, most red light is absorbed by the plants.

2.4 Respiratory System

As jumping spiders are very agile and active spiders, their muscles and nerves have to be provided with enough oxygen. While insects highly depend on oxygen diffusion through trachea (silvery shimmering fine tubes running through the body), large tarantulas use two pair of book lungs for breathing (fig. 2.7). Book lungs are leaf-like constructs (lamellae) which are stacked like the pages of a book. Air enters through a spiracle opening into a chamber (atrium) and fills up the lamellae with air. The spider "blood" (hemolymph) flows between the book lung constructs, gaining oxygen by diffusion.

Interestingly, common spiders (most *Araneomorphae*) as web-spinning, wolf and jumping spiders use a combination of book lungs and trachea (bi-modal breathing) [107]. Trachea are postulated to prevent water loss and support oxygen intake at areas of high oxygen demands [105]. Web-spinning spiders, needing long leg activities to envelop their prey, show trachea directly entering the legs, which are however lacking in jumping and wolf spiders, although they are known for running and jumping behaviors in hunting. Instead, jumping spiders show trachea entering their nervous system, which could support the visual processing of their large eyes. Wolf spiders show less trachea compared to jumping spiders [108], but also a less developed visual system. Crab spiders, which lurk on preys by camouflaging plants and often do not use any silk wires, have a very dense tracheal system [105] in the abdomen, which might support an effective digestion as the behavior of crab spiders can lead to long waiting and starving periods. Interestingly, the water spider *Argyroneta aquatica* body is fully covered with trachea additionally to their book lungs. Considering its way of life under water, mostly breathing from a silk web caught air bubble (diving bell) or by lifting the abdomen into the water surface, air diffusion through many trachea into the body might provide a better oxygen support than only two spiral holes from the book lungs under limited air supply condition.

Interpretation of the advantages and disadvantages of book lungs, trachea or the bi-modal breathing are in general challenging as many parameters e.g.

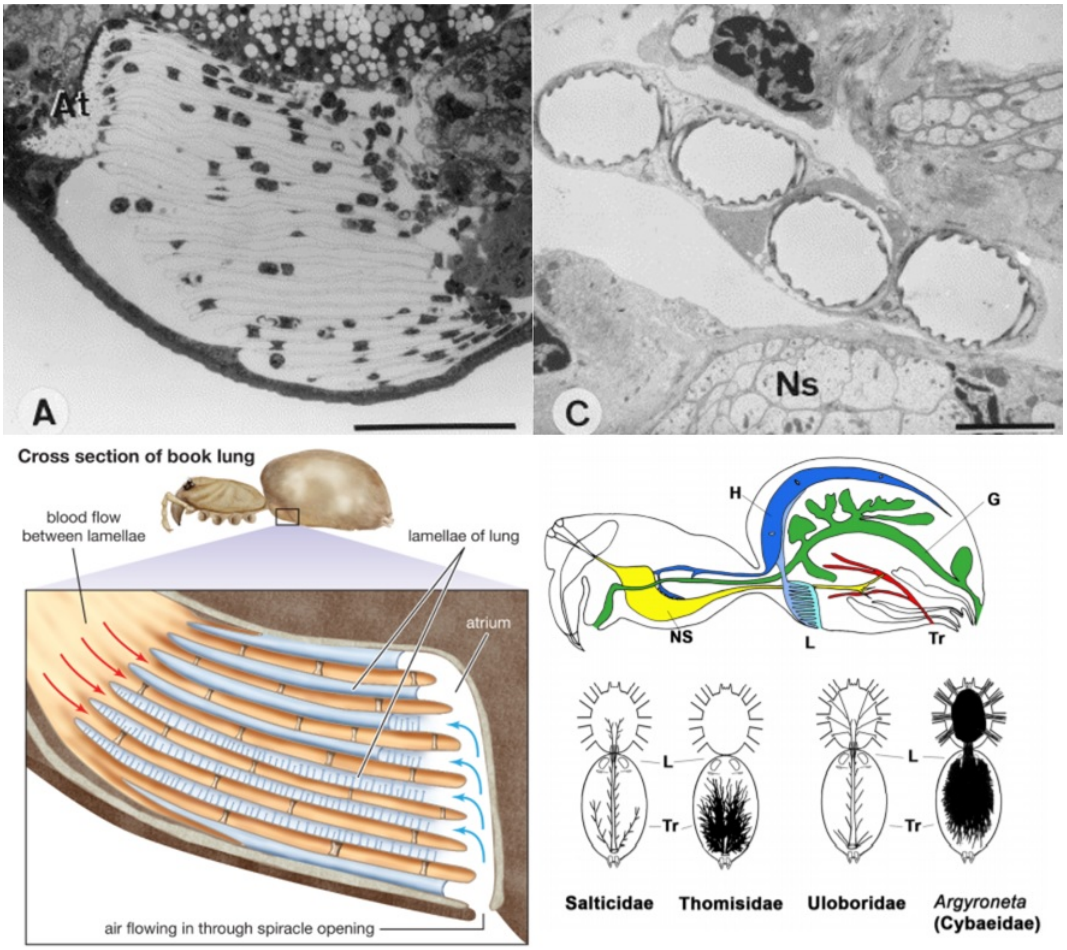

Figure 2.7: Respiratory system of spiders. Top Left: Cross section through book lung, showing the atrium and lamellae. Scale bar: 100μm. Photography taken from [106]; Top Right: Cross section through group of trachea (secondary) close to the central nervous system (NS). Scale bar: 5μm. Photography taken from [106]; Bottom Left: Schematic drawing of blood flow through the book lung (L) to gain oxygen. Drawing taken from [30]. Bottom Right: Schematic drawing of trachea (Tr) distribution in different spider family. In jumping spiders (*Salticidae*), the book lungs (L) and heart (H) are supported by trachea directly supplying the nervous system (NS), which are hypothesized to need large amount of oxygen to process the visual input. In other spider families (e.g. crab spiders *Thomisidae*), the dense digestive system and the gut (G) in the abdomen needs a large amount of oxygen, which might explain the dense network of trachea. Drawing taken from [105].

molting, sex, size, body mass, behavior as well as oxygen and prey availability have an influence on the respiratory system [105]. Direct comparison of running spiders [104] are challenging as behavior can vary among tested animals during an experiment depending on starvation, size and "desire". Therefore measured oxygen intake and recovery time can vary largely. Furthermore, the circulatory system could have an influence on the respiratory need. Interestingly, spiders with trachea in the front body part (prosoma), show lower heart rates in comparison to those with trachea only limited to the abdomen [105].

Detailed information about the circulatory system of many species are still lacking as 3D analysis was only possible with performance improvements of computer tomography technologies and therefore have been performed in the last decades. Systematic analysis in combination with behavioral, morphological and anatomical studies might provide a detailed answer why spiders have book lungs or still have book lungs.

Authors comment on respiratory system literature

Careful reading is necessary when going through spider literature. Confusion can be caused by the naming of species. The German "Tarantel" actually describes larger wolf spiders (*Lycosa tarantula*) belonging to the "modern" spiders (*Araneomorphae*). The meaning of "tarantula" has, however, changed in the English speaking community, now describing *Theraphosidae*, so "Vogelspinnen". While wolf spiders have trachea to support their book lungs, tarantula do not have any trachea. This could lead to confusions, when wolf spiders are described as (mainly) lung-breathing spiders [103].

Furthermore, researchers have hypothesized that a "less-well developed" circulatory system might be the reason for the development of trachea [103]. However, with a lack in a definition what "less-well developed" means and in biological data about the circulatory system, this conclusion has to be handled with caution, as physical effects due to size differences (e.g. regarding the air diffusion) may also play a role.

Due to the size of tarantula (in German "Vogelspinne") the analysis of anatomical structure as the circulatory or respiratory system is comparably easier when only classical histology and microscopy methods were available and are still today when resolution is limited on devices. While many data is available about tarantula, their often slow behavior and lack of trachea has to be kept in mind when "getting inspired" by spider research. Using all biological studies on spiders without distinguishing species and behavior could lead to wrong assumptions or problematic interpretations.

Tarantula are often referred as the more "basal and older" type of spiders, especially in older literature. Therefore, features of tarantula are often inter-

preted as less adapted and disadvantaged, when compared to "modern" smaller spiders, the *Araneomorphae*. As evolutionary studies have majorly improved due to new molecular biological techniques, the classification keeps changing, making the interpretation of "better" or "more adapted" features based on evolution challenging. In contrast to the tarantulas, representatives of the often smaller, "modern" type as jumping spiders have only one pair of book lungs and additional trachea. As insects are also using trachea, most interpretation are in favor of trachea [38], keeping the question open, why book lungs are still present in agile and well adapted spiders.

When reading through literature, the following evolutionary interpretation came to my mind: Spiders and insects both have evolved around 300 million years ago during Carboniferous period, when oxygen level covered 35% of the atmospheric volume. The higher oxygen level compared to today (21%) is one of the main arguments, why insects were larger in size, when oxygen intake is just dependent on diffusion through trachea. Insects have probably evolved from water living crustacean. The internal gills of crustacean where then reused and modified into trachea. For early insects (as large dragon flies), covering the body with many air filled tracheal tubes could reduce weight and support oxygen intake at energy consuming areas during flight, but also under water for the aquatic larval stages, without relying on the circulatory system. Early spiders, which did not fly or swim, but hunt large prey on land, have developed book lungs which are assumed to have evolved from outside lying book gills of water living ancestors. As the inner body is not filled with tracheal tubes, the body could be filled with other gadgets as a dense digestion network or silk and venom glands. Furthermore, the walls of trachea are limited in mechanical stability and therefore cannot withstand high hydrostatic pressures [53].

A lack of trachea in spider bodies might have allowed the evolution of hydraulic leg extension to lift heavy prey and strong flexing muscles for grasping. With decrease in oxygen level, oxygen intake through book lungs might become insufficient for smaller spiders, when large energy consumption is needed, explaining the development of trachea in spiders. This idea matches with the fact, that many generally small representatives of arachnids as mites and harvestmen developed trachea, while larger species as scorpions still have book lungs. One larger exception are camel spiders (*Solifugae*, do not belong to the "real" spiders!), with a well-developed tracheal system [38] and no book lungs. An explanation might again be the way of living, as camel spiders live in the desert (water loss) and are speed runners (oxygen support). Research has also reported air sacs, which might lower the weight of the claws (chelicerae) and provide extra oxygen supply for the large muscles inside [38].

Figure 2.8: Circulatory system of spiders. Top: Network of arteries spreading out from the heart (h). The abdomen is filled with a dense network supplying the digestive system. The prosoma shows defined arteries for each appendage. 3D reconstruction of μ-CT scan taken from [50]. Bottom: The hemolymph flows along defined arteries to the organs and along empty spaces between the muscles and organs (lacunae), through the book lungs back to the heart. The flow through the hydraulic leg joint was estimated by histological cuts showing several channels filling the joint. Drawing taken from [14].

2.5 Circulatory System

As the circulatory system will play an important part in later sections, a detailed introduction into currently available data is given and will be expanded in given sections (cf. section 3.4.3).

In closed circulatory systems as in humans, blood is pumped through very well-defined vessels and capillaries, supplying organs with oxygen. A second network, the lymphatic circulatory system, fills up spaces (lacunae) between vessels and cells with the interstitial fluid (lymph), allow further nutrient and waste exchange. In contrast, arthropods as spiders have an open-circulatory system with no difference in blood and interstitial fluid. The tubular heart in the abdomen pumps the body fluid (hemolymph) through arteries (vascular

system) into the cavities (lacunar system) of the body. The heart is not divided into valve-separated chambers as in insects or humans, but has openings (ostia) to let fluid flow inside and close during contraction. One main artery (anterior aorta) connects hemolymph flow from the heart into the front body part, where it splits into smaller channels entering into the legs and organs (fig. 2.8). The abdomen is provided with hemolymph by another aorta (posterior aorta), which splits further and further into a dense network supplying the intestine, reproductive glands (gonads) and the silk glands. Interestingly, although one-way fluid flow should be guaranteed to avoid a mixture in oxygen-rich and oxygen-poor hemolymph (as the human blood by defined arteries, veins, the heart valves and venous valves), arterial valves have been postulated but not verified. When the heart relaxes, oxygen-poor hemolymph travels back passing the lamellae (leaf-likes pages) of the book lungs to gain oxygen and reenter the heart through the ostia.

In those spiders that have been studied so far (mostly tarantula), hemolymph volume fills up around 20% of the body [122] and the heart rate ranges from 30 to 200 beats per minute depending on activity level and species [37, 91]. In tarantula, a hemolymph volume of 50 μl is pushed out with every heart beat [37]. The pressure inside the body was shown to vary from 6 kPa during resting to 60 kPa during activity [7, 89, 123]. Observations from 1989 [91] further showed that in resting spiders, the heart seems to change the pumping direction occasionally. During activity however, the hemolymph flows from heart to prosoma seems to be reduced or even stopped, while the backwards flow into the opisthosoma seems to be increased.

Freshly collected hemolymph appears slightly bluish. This color is given by the respiratory pigment hemocyanin, which, unlike the red hemoglobin, uses copper rather than iron to bind oxygen. Instead of blood cells, hemocytes are free floating inside the hemolymph, beside many nutrients as sugar, salt, amino acids and proteins. These hemocytes are part of the immune system and reported to prevent stronger bleeding, when spiders drop off a leg (autotomy), induce coagulation and support wound healing. There are four different types of hemocytes: plasmatocytes, granulocytes, cyanocytes and prohemocytes (fig. 2.9) [2, 60]. Plasmatocytes have an oval or spindle shape with a length of 17 μm and play an important role in the blood-clotting (coagulation) of hemolymph. The round granulocytes are with a diameter of 15 μm, help to stop hemolymph loss and produce antimicrobial peptide. Cyanocytes are large circular cells with diameters of 20 - 30 μm. They do not appear in high frequencies, but are important in the hemocyanin (pigment) fabrication. Proemocytes are the smallest cells with a size a diameter of 8 μm. They are released by the cell wall, act like stem cells and can develop into any of the other three cell types.

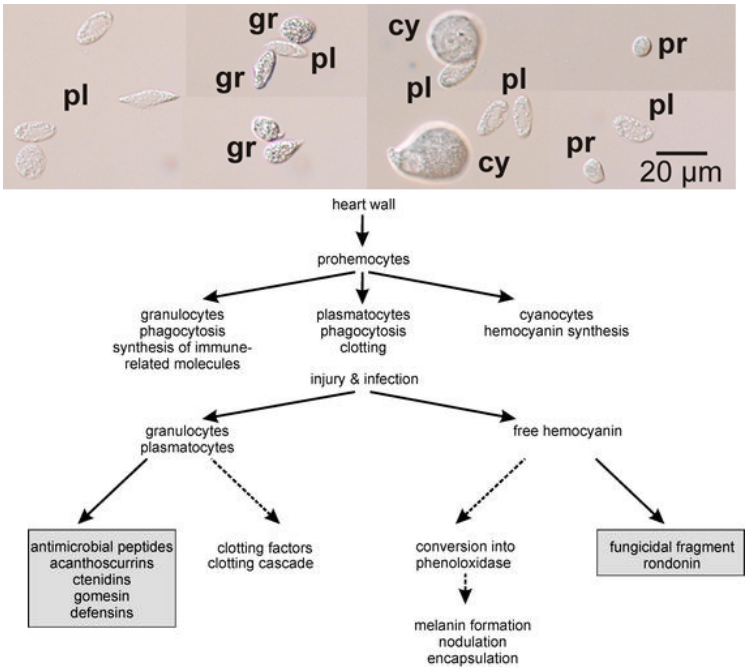

Figure 2.9: Hemocytes inside the hemolymph. Top: Different type of hemocytes including plasmatocytes (pl), granulocytes (gr), cyanocytes (cy) and prohemocytes (pr). Image taken from [2]. Bottom: Functional roles of hemocytes in the immune system of spiders. Image taken from [60].

Chapter 3

Locomotion of Spiders

There are many aspects to investigate when looking into the locomotion of spiders. Gait patterns, body movement, as well as speed and jump kinematics, foot adhesion and material and design. The most stunning fact is that spiders use hydraulics for leg extension, highly in contrast to their six-legged cousins, the insects. While insects use muscles to flex and extend their limbs, the eight legs of spiders show a large amount of flexor muscles, but lack in extensor muscles in two of their joints. The next section will give a short overview about studies in locomotion and jumping behavior including my own observations and open questions. Then I will dive deeper into the functional morphology of spider legs and the hydraulic mechanism, including major findings made in this thesis. Finally, I will present new insights into the body fluid (hemolymph) flow and physical properties and theoretically discuss how these properties could have an effect on hydraulic systems.

3.1 Locomotion Behavior

Behavioral studies are important to get a feeling of what spiders are capable of and what techniques they use to achieve e.g. hunting, escaping or digging movements. They also provide information on how well the biological system performs under different circumstances, which is important to interpret data and the bio-inspired implementation purposes. To abstract a principle and transfer it to a (technological) system for a similar or even totally different purpose, the deep understanding of the inspired principle is necessary to know which parameters are of importance, so that desired parameters can be thoughtfully changed.

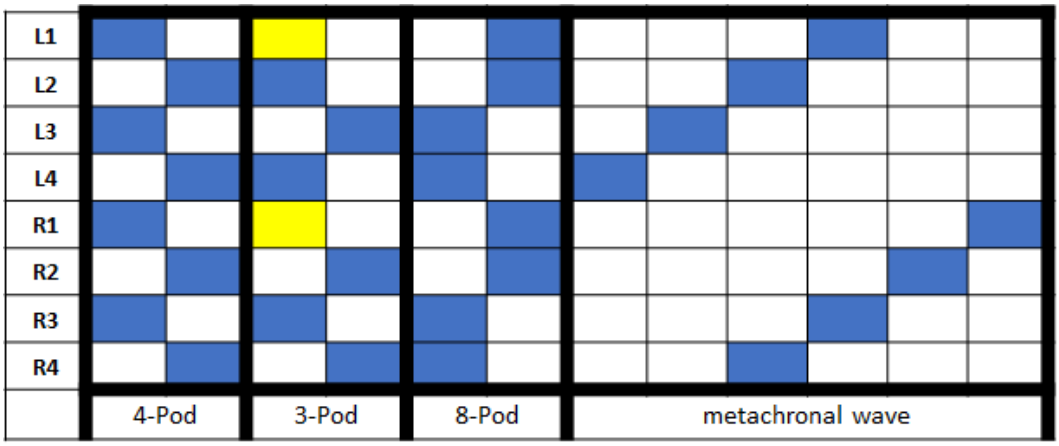

Figure 3.1: Example of schematic representation of different step patterns. Spiders usually walk in tetrapod (4-pod) and double quadropod (8-pod) step patterns. The description on the left describe the legs (L1 = front left leg). Blue marks in a column are marking those legs that are touching the ground at the same time. Ant-like spiders have been proposed to walk as ants in tripod patterns with the two front legs lifted (yellow). However, this hypothesis has been dismissed. Speed running cockroaches appear to have metachronal wave gait pattern (here shown for eight instead of six legs).

3.1.1 Gait Pattern

Traditional gait pattern analysis was done by letting insects and spiders run through carbon black powder and follow the foot steps of the animals on a white paper. With new high speed technologies in the 1980s, locomotion of animals were studied intensively, but there is still a large lack of knowledge about many species. Many studies on arthropods have only appeared recently, as high speed recording and 3D tracking technologies have improved and bio-inspired locomotion became a popular field not only for robotics, but also to understand animal behavior.

One of the most iconic locomotion pattern is the one from the desert wheel spider (*Cebrennus rechenbergi*), which does fast "flic flac" rolls, probably to reduce foot contact with the hot desert sand. Discovered in 2006 by Ingo Rechenberg, another big name in the founding of bio-inspired principles and optimization algorithms, the combination of rolling and crawling has inspired engineers at Festo and other groups [125] to imitate the locomotion ten years later.

Different gait patterns can allow arthropods to dig into soil, run fast, traverse over various terrain or even mimic other animals. The jumping spider

(*Myrmarachne formicaria*), for example, imitates body shape and behavior of ants to hide from predators (Batesian mimic). Although it was long believed that these jumping spiders would mimic the gait of ants as the spider lifts its front pair of legs to imitate the antennas, recent studies have shown that they walk like other jumping spiders, but when stopped the front legs move around similarly to antennas [113]. Furthermore they mimic the several other motion components of ants as in their single movement distances and turns while moving [82]. Latter behavior is very uncommon in non-ant like spiders, which normally turn in stationary position.

Insects and spiders usually walk with left and right alternating legs in sync, resulting in tripod and tetrapod gait during normal walking [111, 136]. During running, cockroaches and some arachnids show a change into a wave (metachronal) gait [136]. This pattern resembles a dolphin swimmer, where all left side and right side legs form a wave from front to back and it can also be found in spiders walking on the water surface [115].

Interestingly, locomotion studies on six-legged robots have shown that a bipod locomotion, where each leg pair goes in sync from front to back, would actually be faster as the usual tripod locomotion, but as many insects have adhesion pads for climbing, tripod locomotion might be the better solution [97].

Studies on tarantulas have shown that beside the tetrapod stepping pattern, they can also use a double-quadruped gate pattern (octopod) (fig. 3.1). Thereby the front two leg pairs and the last two leg pairs, each form a quadruped, which are swinging in phase, meaning the first and third pair are synchronized as well as the other two pairs [13]. Recent research on different grounds showed that tarantulas tend to have even more legs (up to six) on the ground at the same time to stabilize the body [45].

Fast running have been reported to lead to irregular gait patterns especially in large spiders and have been explained by leg length differences in some of the studied spider species. However, the eight legs of tarantulas have similar length and therefore the causes of this irregular patterns are still unknown, but is postulated as an effect of an insufficient hydraulic mechanism [133]. Latter effect was also postulated to be the main cause of the speed limitation in tarantula [18].

Authors comment on gait studies

(High speed) video recordings demonstrating the locomotion behavior of spiders and giving the reader an easier access into how spiders are running and what are meant with irregular patterns are lacking. Although current literature is based on high speed recording analysis [134], the results only provide schematic drawings of step patterns, but joint angles and detailed (visual) information

about which joints are mostly involved and what behavior the animals have are missing.

Although hydraulic effects have been determined to reduce speed performance and cause irregularities, the underlying principles which lead to this conclusion have to be read carefully. Speed limitations in tarantula are affiliated with lack of oxygen as the animals need to recover after runs. The researchers argument that during fast movements, the hydraulic mechanism hinders body fluid (hemolymph) transfer, which leads to a lack of oxygen and therefore limit speeds and cause irregular motion [135]. However, the cause of a lack of oxygen could also be a result of the respiratory system, instead. While tarantulas only depend on book lungs, large huntsman spiders and wolf spiders are known to run much faster speeds, but have developed trachae to support oxygen intake. Web spiders, which are not known for their running abilities but for quick, fast and constant leg movements to wrap their prey are even known to have trachae directly entering their leg muscles to support oxygen transport. Furthermore, information about the circulatory system is lacking, which could also have a great influence on the oxygen transport. Irregular gait patterns in fast runs could also be a result of adhesion pads, which might be avoided during runs or cause problems due to their stickiness.

It is important to know, that the interpretation of "recovery or resting" behavior is also problem as experimental animals are often triggered with food and can just lose interest. As fast running can be caused by "scaring" the spider to trigger escape runs, this might also result in uncoordinated movement as if the spider would "stumble away". Therefore the motion behavior could differ largely to controlled hunting runs.

3.1.2 Body Movement

There are several models describing the center of mass (COM) movement during animal movement: the *inverted pendulum*, *bouncing ball*, and the *pendulum* model (fig. 3.2)[87].

Human bipedal locomotion can be described by the inverted pendulum model where the center of mass is lifted by kinetic energy acting on a stiffened leg. The created potential energy can then be recovered into kinetic energy resulting in a constant up and down of the center of mass.

The bouncing ball model or spring-loaded inverted pendulum model shows similar up and down movement of the center of mass. However, the leg acts like a spring, which gets compressed by gravity. The elastic energy propels the center of mass then back up again. This type of movement can be observed in running vertebrates and has been reported for insects and daddy-long-legs.

The regular pendulum model describes the usage of potential energy to create

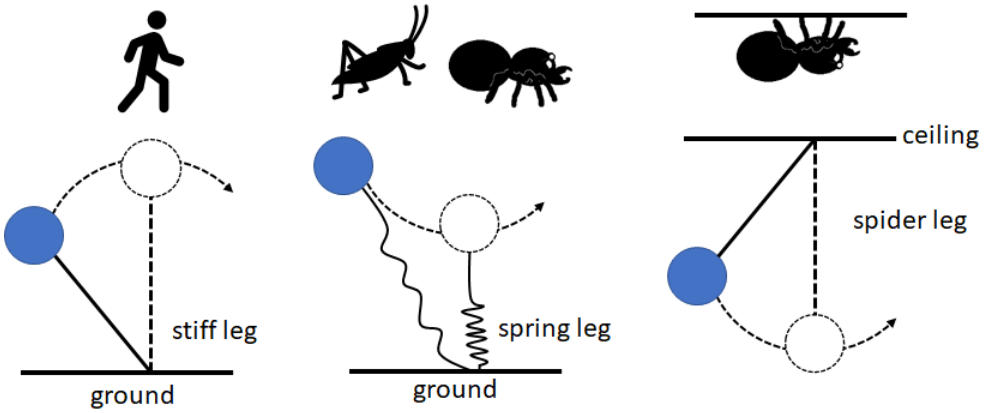

Figure 3.2: Schematic description of center of mass (COM) movement. Left: In humans, the bipedal motion can be described by the inverted pendulum motion. The stiff legs lift the COM against gravitation creating potential energy. Middle: Insects and daddy-long legs show legs that act as springs and store elastic energy for forward movement, resembling a bouncing ball motion. Interestingly, when observing spiders walking on the ground their COM motion rather resembles a "wheel-like" motion, as the body shows almost no vertical bouncing. Right: Spiders walking on the ceiling are assumed to follow a regular pendulum motion. The energy conversion of potential energy to kinetic energy can thereby be compared to brachiation of monkeys or children. Drawing was made according to [87].

kinetic energy and swing into the next position. It is similar to the inverted pendulum model despite the fact that the leg position lies higher than the center of mass. The locomotion of hanging web spiders has been postulated to fit this model [76], but experimental data are lacking.

When observing ground spiders moving, the first thing that stands out is that the center of mass seems to almost not move in vertical direction. Their movement reminds more of a 'wheel like' motion, making spider toys with movable legs, but wheels to move horizontal quite "convincing". Studies on large (ground) spiders as tarantulas, but also the large wander spider (*Cupiennius salei*) have shown that they do not show any flight phase even during running [13]. The locomotion model was first postulated to fit best to the inverted pendulum model. However, the vertical motion of the COM is so small resulting in a very low estimated energy recovery of only 8 - 12% [133], which contradicts the large horizontal movement and ballistic behavior of the COM. As there is no characteristic bouncing of the COM and no elastic structures in

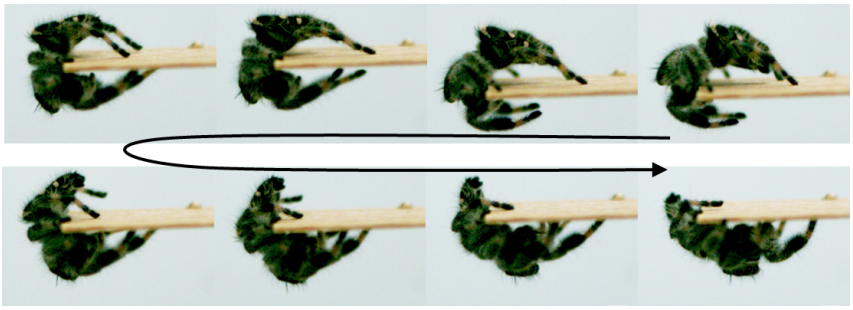

Figure 3.3: Turnaround of *Phidippus regius*. This image sequence shows a *Phidippus regius* climbing around an edge from the upright to upside down position. A safety wire might be attached, but could not be observed in the video. Leg pairs 2 and 3 are holding on the edge, pivoting the spider around while the leg pairs 1 loses contact in the beginning and pair 4 at the end when flipping around.

the legs have been reported to store and release elastic energy, the researches also excluded the spring-loaded model for large spiders. However the structures and mechanism to create the horizontal movement are not clear.

Authors comment on body motion

Although no elastic structures have been reported for spiders at the time of body motion studies, it has to be said that other arthropods show cuticle (exoskeleton) to support their hydraulic extension [112, 116, 117]. Furthermore the hydraulic joint itself could be seen as a spring, when assuming that the fluid is not compressible and therefore volume decrease by muscles or gravity could lead to pressure increase and, or a deformation of body parts which might not directly lie at the legs. The joints are covered with a thin membrane which folds and unfolds during movement. Elastic energy storage could also be partially provided by this membrane.

Studies on body motion of jumping spiders during running, climbing and walking are lacking. An interesting behavior can be observed when jumping spiders are tracking a prey by their eyes and need to turn their body to keep the prey in sight. By quickly moving the legs around the body, the body seems to spin around one single axis. Further studies on this behavior could provide more information about the body movement model and maybe even inspire quick turns or edge crawling (fig. 3.3) for legged-robots.

3.1.3 Dancing on a String

The spider's net is one of its most iconic gadgets and could not be missing in any spider(man)'s movie. Spiders produce a various number of different silk threads for different purposes. Ballooning spiders (*Linyphiidae*) shoot silk into the air to "fly", ogre-faced spiders (*Deinopidae*) form a square shaped catching basket with their front legs and everyone knows the beautiful spider webs. These silk wires however bring some trickiness with it. They can be sticky. Orb-weaving spiders usually avoid the sticky area of their net by only traveling on non-sticky areas. Nevertheless, they do get in touch with sticky silk when weaving the sticky catching area. Researchers showed that spiders use careful movements, dense hair, constant grooming and non-sticky coatings on their tarsus to prevent any adhesion [21, 52]. The stickiness of the spider silk could thereby be caused by glue-like droplets [121], van der Waals and hygroscopic forces under high humidity condition [47]. Some spiders (*Uloborus plumipes*) even comb their hair creating extremely sticky, electrically charged puffy nano wires [58].

Jumping spiders use their silk strings mostly as a safety wire to abseil from heights and crawl back to their original position, while collecting the wire at the same time [48]. This behavior has even inspired researchers to create an abseiling robot [131]. Jumping spiders further need this drag line for very controlled jumps, as the wire helps keep the body in position and to prevent somersaults [26]. When keeping jumping spiders in transparent, smooth boxes one can observe many "sticking marks" especially on the lid or around their sleeping bag. It can be assumed that the wires also help in orientation and traversing gaps. The sleeping bags are densely woven and serve as hiding place during night or when molting. It repels water to some extent, but usually does not stick. Even denser bags are formed by pregnant female spiders, to form a almost tight, strong, white bag where hundreds of juvenile jumping spiders grow up. In my case, when Big Berta was pregnant, she built this dense net underneath her sleeping bag, and sat above this egg-cocoon to protect her offspring. She further actively closed her sleeping bag "door" with her front legs when getting disturbed. This protective behavior could also be observed for wolf spiders, who attach their round cocoon to their abdomen when traveling and protect it underneath their body when attacked. The cocoon is also made of silk but has an almost paper-like characteristic.

In order to approach the question, how spiders traverse on thin wires, I have filmed juvenile jumping spiders running on a Nylon wire (0.45 mm) using high speed recording (fig. 3.4). A challenge was to keep the spider in position and in focus, while magnifying the wire and feet. As this was done during a student visit, it was not further investigated, but the video findings are still interesting.

Figure 3.4: Jumping spider walks on a nylon wire. Although the nylon wire (0.45 mm) is over 100 times thicker than the spiders silk wire, the observed high speed recorded walking behavior still turned out to be interesting. The juvenile jumping spiders do not use their front claws but the adhesive pads on their feet to grip to the wire. The spider walked with a tetrapod gait and secured itself with a safety wire on the nylon wire (barely visible on this image, but abdomen is "stretched".)

The recordings revealed that spiders use their tarsus tip to walk on the Nylon wire. Interestingly the close-up images showed that the adhesive hairs of the hind leg tarsus grip around the surface and not the hooks.

3.1.4 Jumping Behavior

Several spiders are known for their jumping abilities. Wolf spiders and wandering spiders [134] show unprepared and prepared jumps. During escapes, the spider catapults itself away, whereby the legs often fly around in an uncoordinated way and the landing phase could result in somersaults. Studies of wandering spiders showed that these unprepared jumps could happen for-, side- and backwards. Prepared jumps, instead, play an important role when trying to overcome obstacles or for hunting and happen in the field of view of the spider. Thereby all legs are extended in the flight phase allowing to grip on the target during landing. Funnily, these two type of jumps resembles the human uncoordinated fun jump into a swimming pool, in comparison to a controlled dive start, where the swimmer pushes himself off and extends his arms to enter the water.

Figure 3.5: Jumping of *Phidippus regius*. Jumping spider secures itself by attaching a safety wire on the substrate. This safety wire also prevents the spider from somersaults during landing. Before jumping, the spider lifts the first two pairs of legs. The third pair acts as pivot point, while the last pair of legs extends for jumping. During jumping the spider forms a catching basket to fully cover the prey or landing place.

Jumping spiders (*Salticidae*) form one of the most diverse family of spiders equipped with big eyes and the ability to catch their prey with very precise jumps (fig. 3.5). Studies have even showed that jumping spiders (salticids) are able to adapt their jumping performance under low gravity condition in space [49].

The salticid's jump starts with the attaching of a safety wire onto the substrate and the extension of the front four legs (fig. 3.6). It then launches itself onto a ballistic trajectory. The eight legs extend and form a "catching basket" around the prey. The drag line does not only serve as safety wire, but prevents the jumping spider from doing uncontrolled somersaults during landing [26] and seem to also be used as a brake to decelerate the body. Latter observation is supported by the fact that the silk of jumping spider drag lines have a higher yield stress than web-spinning spiders silk due to increased crystallization. This allows the drag line to absorb more energy. Studies showed that the silk converts over 65% of kinetic energy into heat rather than elastic recoil [98]. As the jumping spiders seem to constantly extend the silk wire during jumps and actively apply a friction brake, jumping spider do not bounce like a bungee jumper when landing in air.

Jumping spiders, also called, salticids, are able to vary their jumping speed and direction relative to the target position, so that they can end in precise jumps even from a ceiling upside down to a prey on the ground. Interestingly, unlike most insects capable of jumping, salticids do not show any obvious specialization in their legs [90]. Insects often have developed an elastic protein, resilin, or strong extension muscles in hind legs to create jumping. Recent studies suggested that the jumping performances resemble more the jumps insects with muscle created jumps, rather than insects with resilin [77]. They concluded that muscles are the driving force behind the jumping principle,

rather than hydraulics, although previous researchers reported erected leg spines, which are probably resulting from an increase in pressure.

While the front two pairs of legs are extended right before the jump in jumping spiders and therefore not involved in the propulsion process, the studies on wandering spiders, suggested that the second pair of legs seem to be involved in the jumping procedure [134]. However, they could play a similar role as the third pair of legs of jumping spiders, which are proposed to serve as a pivot point against the ground.

Authors comment on jumping literature

Improved high speed recording techniques in recent years allowed simplified studies and detailed observations of jumping spiders. However this tend to result in quick assumptions taken from video data. David E. Hill, who has constantly worked on the jumping principles of salticids since the early 2000s, has reviewed the jumping studies of salticids many times over the years. In his last review, in 2018, he pointed out that the research published in the same year about the comparison of insect and salticid jumping shows a major problem. Although the jumping performances seem to be similar to insects which use muscle-generated extension for jumps rather than those using resilin, concluding that jumping spiders use muscles rather than hydraulics is a huge problem. First of all, comparing the controlled jumps of spiders with insects which only use their jumps for escapes is already an issue.

As jumping spiders control their ballistic trajectory by a drag line, the jumps can be much lower or less wide as in insects, which just try to catapult themselves away as far as possible. Moreover, the main joints involved in jumping (femur-patella and tibia-metatarsus) are not equipped with any extensor muscles. Even if the body-leg joint is somehow involved, which was postulated by Weihmann et al., concluding that hydraulics might not be the only mechanism to allow jumps in large spiders, hydraulics is still the main mechanism to allow leg extension. When looking carefully into the mentioned study from 2018, one can quickly see that all jumping analysis were only based on one spider as the researchers failed to let the other three spiders jump. Furthermore, the researchers themselves also pointed out that due to *"time constraints on the experimental work [...], it was only possible to obtain a single example jump for a given jumping task (15 tasks/jumps in total)"*[77].

From a statistical point of view, the results actually have no significant statement. In public press, this work was widely sold as "researchers successfully trained spiders to jump", as the researchers claimed, they have not use any stimulation as prey or air blow to enforce jumping. However, it has to be said, that jumping spiders do jump from edge to edge when forced over the plank,

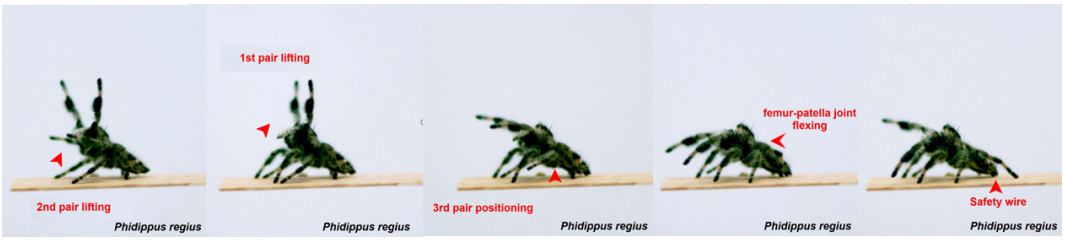

Figure 3.6: Initial preparation before jumping. From right to left: First the spider attaches its safety wire on the substrate. Then it flexes the femur-patella joint of its hind legs. The third leg pair is then positioned into place, forming a pivot point. Afterwards the first and second leg pair is lifted into the air, which also lifts up the front body part.

but also do it quite frequently without other stimulation. Furthermore, light itself is a jumping trigger as jumping spiders like to move towards warm and shiny places. Regardless of these two other triggers, the researchers have only managed to let one out of four spider to jump. This brings me to another problematic of this study. Not breeding the spiders themselves brings the disadvantage of not knowing the age, stage of development and history of the spiders. The spiders could be injured or not healthy due to natural diseases, or they could be in molting phase or even pregnant. All of these could lead to different behavior. Before this research was released in early 2018, I have examined several jumping experiments to study the jump of juvenile spiders in the beginning of 2017 and adult jumping spiders by the end of 2017. Juvenile spiders are quite active and jump frequently, but run away when scared. Larger spiders tend to be much lazier, especially when they are fed with a cricket a week as mentioned in the publication above. Animal experiments bring much patience and understanding of the animal to not frighten it or trigger other behaviors. "Time constraints" are therefore generally very problematic in biological studies as weather, humidity and other external factors could also influence the study.

3.2 Jumping Kinematic Modeling

3.2.1 Model by Parry and Brown

In 1959, Parry and Brown studied the jumping motion of jumping spiders and analyzed the torques and pressures inside the leg. The results were based on torques calculated from take-off velocities observed in high speed recordings and the geometry of the legs. Parry and Brown estimated that the torques would

be the same for both semi-hydraulic joints (femur-patella and tibia-metatarsus) at around 0.5 - 1 μNm. Given the relationship of $P = F/A$ (pressure P, force F, area A), they followed that the estimated pressures are then higher in the smaller joint (tibia-metatarsus) than in the femur-patella joint. However, assuming that the pressure should be the same along a pipe, they explained this pressure difference by flexor muscle tension [90], if viscosity does not show any effects. Due to many lacking information, most of their calculations based on assumptions. They studied the angular velocity of 50 radian/sec and the needed equivalent volume change of 15 mm^3/ sec [89]. Using the Hagen-Poiseuille equation, describing the volume flow Q,

$$Q = \frac{\pi \cdot r^4}{8 \cdot \mu \cdot L} \cdot \Delta P \tag{3.1}$$

and estimating a length L of 1 cm and a viscosity μ of 5 cP (human blood), they found that

$$r^4 \cdot \Delta P = \frac{8Q\mu L}{\pi} = \frac{8 \cdot 15mm^3/sec \cdot 5cP \cdot 10mm}{\pi} \approx 2Pa \cdot mm^4 \tag{3.2}$$

and although the radius r was not known, they argued that the pressure gradient is negligible. Given that they measured 6 kPa - 60 kPa for inactive and active spiders and an aorta radius of 200 μm [89], the pressure drop from prosoma to the first hinge joint would only be 1 kPa, which can be neglected for active spiders. However, for the second joint (tibia-metatarsus), which has a much smaller diameter, the equation shows clearly that with smaller radius, the pressure drop increases drastically. This again contradicts with the pressure and torque estimation Parry and Brown made, showing higher pressure in the tibia-metatarsus joint. In later studies, experiments have qualitatively shown a pressure drop along the leg [7, 18]. This means, that the torque generated by the second joint is either smaller as it was experimentally shown for tarantula [112] or valves are separating the two joints from each other, which however have only been proposed but never discovered.

3.2.2 Model by Blickhan and Zentner

Thirty years later, researchers around Blickhan studied the jumping kinematics of the wandering spider *Cupiennius salei* for technical applications. Lena Zentner (born Bohmann) numerically modeled the hydraulic behavior of spider locomotion to get new insights into the kinematics and dynamics of spiders [143]. She simplified the channel structure (aorta and lacunae) inside the femur leg segment with length L_0 and radius r_1 into three lacunae with fixed radius a_1

(same to inital radius a_0) in the middle of the leg and calculated the pressure drop again via Hagen-Poiseuille equation:

$$P_0 - P_1 = \frac{8\mu}{\pi a_0^4} L_0 \dot{V} \tag{3.3}$$

whereby the volume flow changes with angle ϕ (and ϕ as inital angle):

$$\dot{V} = (\pi r_1^2) r_1 \dot{\phi} \tag{3.4}$$

Using differential motion equations, she modeled the joint behavior:

$$J\ddot{\phi} = -mgL_s \sin\phi + A \cdot P_1 r_1 \sqrt{2} - k\dot{\phi} - M_c \tag{3.5}$$
$$M_c = c \cdot (\phi - \phi_0) \tag{3.6}$$
$$A = 3\pi a_1^2 \tag{3.7}$$

for a leg with the mass m, lacunae cross area A, a mass moment of inertia J and a distance of the mass center from the rotation center of L_s. The muscle behavior were integrated by a spring-damper construct, given through the damping coefficient k and the spring element M_c through the spring stiffness c.

Citing Parry and Brown [90], she used the viscosity of human blood and later the viscosity of water for the simulation. Although many parameters were still missing, she was able to give qualitative information about the jumping behavior. She showed that a linear increasing cross-section area to opening angle behavior would increase the take-off velocity. She further investigated the initial position needed to achieve the highest take-off velocities and vertical jumps. She concluded that with given parameters, a spider weighing above 3 g should not be able to jump if it is only using hydraulics due to "segment oscillation" and muscle "damping".

Authors comment on jumping modeling The simulation and conclusions taken from the simulations are based on many assumptions and are lacking major influences. That is why conclusions taken out from these should be carefully elaborated.

In general, spiders lift their front body part for jumping, which could shift their center of mass, influencing the jumping behavior, the influence of "silk braking" was also not known and also often ignored in later jumping studies. Viscosity effects were not taken into account, as there were no data available, but viscosity could have large impact on volume shifts, temperature dependent behavior and performance. Furthermore, the flow inside the leg and joint was not known and cross sectional area as well as volume shifts were estimated by

the empty space "lacunae" inside the leg and "artificial" experiments, where cut off leg were extended by filling them with fluid via a syringe. All these parameters could have a great impact on the Hagen-Poiseuille equation, the resulting pressure drop and torque. Looking into the modeling by Zentner, the seven-jointed-leg locomotion were reduced to the three main joints (hip, femur-patella and tibia-metatarsus) and leg segment lengths were determined from a tarantula for simulation purpose. However, it is not clear whether or not the foot (tarsus) was integrated or not integrated into the leg segment length. The studies assumed that the force is acting via the tip of the foot (tarsus) on the ground.

Video recordings show that the studied wandering spiders *C. salei* barely touch the ground with the rest of the tarsus, however the metatarsus-tarsus is not straight, but bent in a specific angle, which is not considered in the simulation. The model shows three parts with almost similar length, but it can be assumed that the third part, the part touching the ground is actually smaller as the tarsus is bent around. This might also explain, why the initial position of the simulated spiders shows highly flexed tibia-metatarsus joints and almost open femur-patella joints, which is the opposite in real spiders. Experimental studies by Weihmann and Karner showed this much steeper flexing angle for coordinated, prepared jumps.

The modeling parameters introduced by Zentner are based on leg parameters of tarantulas. At this point, I need to say, that tarantulas, wandering, wolf or jumping spiders show completely different weight distributions, leg length and hunting behavior. Using conclusions interchangeably are therefore not necessarily useful. It is not clear, why Zentner used tarantula legs, but it might be as due to their size, they were easier to study. However, tarantulas are not optimized for jumping, as it is not in their frequent behavioral repertoire. And still, tarantulas with a weight over 120 g (much larger the 3 g limit set by Zentner) were able to be triggered into "jumps" of 2-3 cm [135]. Weihmann and Sens however assume that these jumps might be supported by the muscles from the hip joint, questioning the advantage of hydraulics [111, 135]. I hypothesize that not muscles but the elastic properties of the joint membrane might support the hydraulic jumping and that tarantulas neither have enough muscle power to withstand the pressure needed for lifting their weight, nor the right leg geometry. Humans and Kangaroos both have muscles. Still kangaroos can jump much more impressive than humans, concluding that muscles are the problem in this equation would therefore probably not be the first choice, however somehow spider research continuously does this.

While Parry and Brown [90] assumed that the jump of spiders is scalable from smaller to larger spiders, Weihmann [135] hypothesized that viscosity

could cause delays in volume shifts in larger spiders, reducing its performance. I assume that non-Newtonian fluid behavior might resolve this problem.

Zentner introduced the term of "segment oscillation" and the "necessary muscle damping" would also increase with animal size according to simulations and therefore reduce the jumping ability [15, 135]. However it is not clear how the "segment oscillation" occur on real spiders and I was not able to find any detailed information about this term.

With the insights provided in this thesis, a much more detailed simulation with better computational tools should be conducted in future to shine light into the real jumping kinematics of jumping spiders.

3.3 Spider Legs

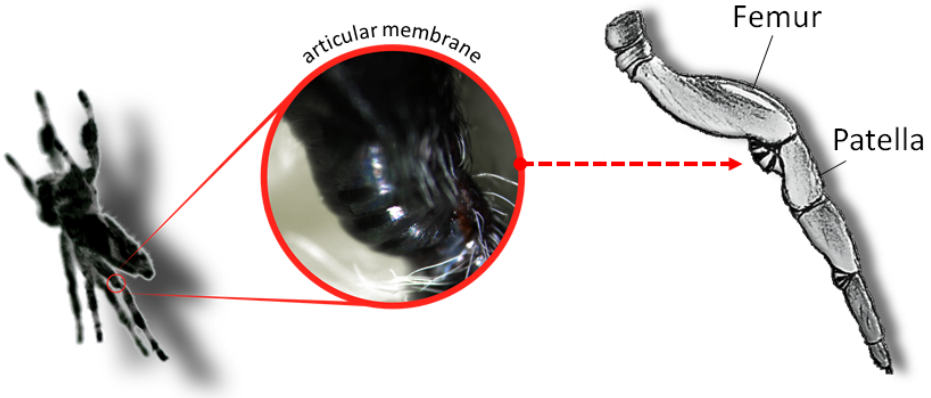

Figure 3.7: Femur-patella joint of jumping spider. This work focuses on the mechanism of the femur-patella joint. This joint is mainly involved in walking and jumping. The pit is covered by a thin articular membrane, which folds and unfolds during movement and forms a chamber for pressure-dependent extension. The articular membrane shows a zebra-pattern like coloration. The three black appearing hoops seem to be stiffer than the rest of the membrane. The color is given by pigments embedded inside the basal membrane. The articular membrane itself is therefore actually transparent. Published in [43].

One of the main contributions of this thesis is a better understanding of the spider leg joint (femur-patella joint) working principle. A first step is to look into the "design", so morphology, of the spider leg. The following subsection will give an overview of what a spider leg is equipped with and what we can expect when looking into the leg. The main focus of this thesis will be presented in detailed afterwards, covering a close look into the largest joint (femur-patella) and the thin membrane (articular membrane) covering this joint's pit (fig. 3.7). Using new imaging, preparation and measurement technologies, I was able to provide detailed information about the functional morphology of the femur-patella joint and was thus able to shed light on aspects that were previously either undiscovered or difficult to access using traditional methods.

3.3.1 Morphology of Spider Legs

The linguistic origin of Arthropods lies in the Greek words "*arthron pous*", which means "jointed" or "segmented foot". The Arthropod's body is divided into segments and so are their legs.

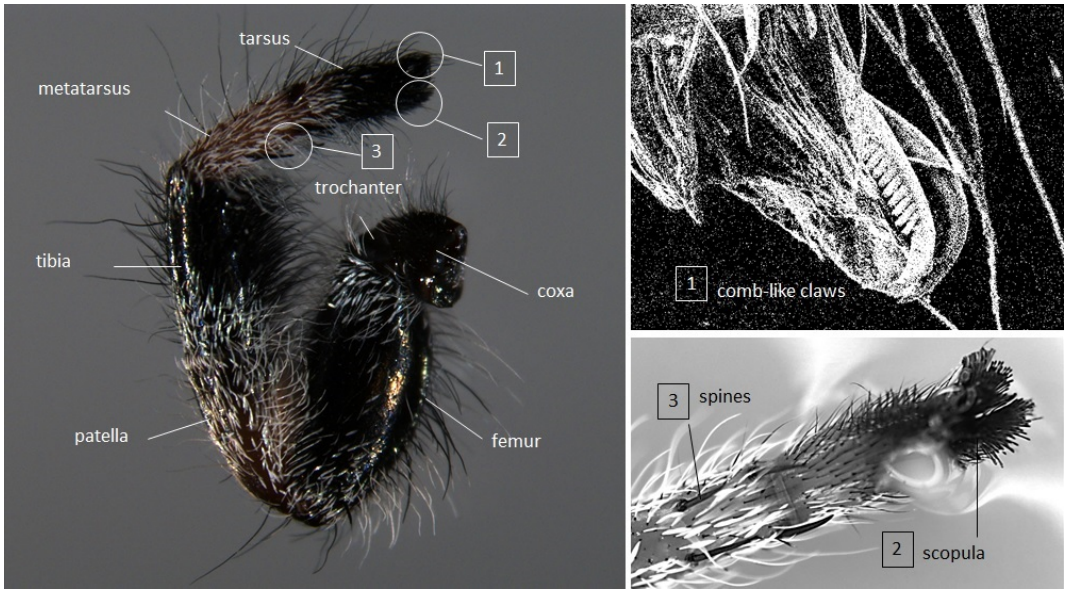

Figure 3.8: Morphology of the jumping spider *Phiddipus regius* leg. Left: The hairy leg of spiders is divided into seven segments. The leg naturally folds into fully flexed position, when it is disconnected from the body or when the spider is dead. Two of the joints (femur-patella and tibia-metatarsus) use hydraulics for extension and are highly involved in jumping, walking or gripping motions. The foot (tarsus) is covered with adhesive hairs (scopula (2)) allowing spiders two climb upside down on smooth surfaces. Furthermore comb-like claws (1) give additional support on rough terrain and allow the spider to comb the silk wire in order to change its properties. It is also hypothesized that the comb is necessary to allow efficient climbing up a silk string. Spines on the metatarsus could either function as sensors or give support during jumping or landing.

Regardless of the spider species, spiders have eight legs, which are divided into seven segments (coxa, trochanter, femur, patella, tibia, metatarsus, tarsus) (fig. 3.8). Thereby, four joints are mainly guiding the locomotion of the spiders: the muscle-driven joints at the hip (body-coxa-trochanter joint construct) and the foot (metatarsus-tarsus) and the two hydraulically extending joints (femur-patella, tibia-metatarsus). The hip joint enables stance and pan movement [64]. The foot joint allows interaction with the substrate. For spiders with adhesive pads, the foot joint is essential during attachment to and detachment from the surface. The semi-hydraulic joints are lacking in extensor muscles, but are filled with flexor muscles and are highly involved in running, jumping and grasping. While orb-weaver spiders are known for their long and delicate

legs, which spin the silk wires around their prey, jumping spiders and tarantula tend to have short and thick legs in contrast. All spiders have in common that their legs will never appear in advertisements to promote smooth skin. Their hairiness and spikiness is rather a common cause to trigger arachnophobia.

Many of these hairs are actually tactile hairs reacting to objects in their surroundings. Some tactile hairs and inner sensory cells close to the leg joints even provide information about the joint position and receive feedback about speed and direction when the joint position changes. Beside hairs, spider legs are equipped with another interesting sensor, the slit sensor. This slit sensor is a slit-shaped dent on the exoskeleton, which gives information about mechanical deformation of the surrounded exocuticle. While single slits can appear all over the body, these slit sensors are often arranged in parallel groups (lyriform organs) close to the leg joints, providing information about the joint movement during walking and about distance and orientation. Furthermore, lyriform organs are shown to react to vibrations in specific frequencies, allowing spiders to distinguish prey from leaves caught in their net and to communicate during mating [37].

In general, spider legs are densely packed with muscles (fig. 3.9). Over thirty muscles can be counted inside the spider's leg [37]. This number is significantly higher than in other arthropods (insects: 10; scorpions and crustacea: 16 leg muscles [37]). While insects have antagonistic working muscles, spider legs are filled with flexor muscles. Researchers therefore assume that the main reason for a hydraulic extension is a larger space for these flexor muscles to allow fast, strong and precise grasping movement [37]. Beside the muscles, three main (peripheral) nerves run through the spider legs. The purely sensory nerve is the largest among these three, which intercepts the signals of the many sensors a spider leg is equipped with. In addition, there is the slightly smaller purely motor nerve, which sends signals to the muscles and the third fine, thin mixed-type (sensory and motor) nerve.

The muscles and nerves divide the tightly packed spider legs into different sections through which the body fluid (hemolymph) flows. Cross-sections show a main artery, which provides the muscle and nerve cells with oxygen and nutrients. Other spaces between the muscles have been assigned as the so-called lacunae, which are filled with hemolymph and allow the hemolymph to flow back to the heart. Unlike humans, the spiders have no defined veins to collect the oxygen-deficient "blood".

The focus of this work will lie on the femur-patella segment, which is the main contributor to jumping in the studied spiders and shows the largest working

Figure 3.9: 3D-reconstruction of femur-patella joint. The femur (f) and patella (p) leg segments are covered by the articular membrane (am), which is attached to the arcuate sclerite (as) and forms a chamber. A short part of the articular membrane is spanned between the arcuate sclerite and the patella segment. This membrane does not show any microstructures under the SEM and is not inflated during extension. However, it might protect the ripping of the functional articular membrane when external forces cause "over-bending". The leg segments are densely packed with muscles (m) and two nerves (n) are running in between the muscles.

angle of 120-160°.

3.3.2 Femur-Patella Joint

The femur-patella joint is the largest hinge-joint in spider legs and covers rotational movements of 120-160°. During resting position, the femur-patella joint is usually flexed at a 80-100° position. Complete extension can be observed during jumping, running and when communicating with conspecifics. Full flexing occurs right before jumps and during prey capture. Several muscles, running down the femur segment, are attached to the arcuate sclerite [88], a very stiff arc shaped part of the patella segment (fig. 3.9, 3.10). When the muscles pull on this arcuate sclerite, the joint flexes, folding the articular membrane, which covers the joint pit. The femur and patella segments are both beveled, allowing a folding into the femur-segment, explaining this large working angle. The muscles and the articular membrane are forming a chamber where the hydraulic fluid flows in and causes leg extension when pressure increases inside.

When spiders die, their legs tend to fully flex, bringing them into the "mummy" position, which can be often observed in dead arthropods. This flexing is caused by death-induced muscle-shortening (rigor mortis) and the deflation of the joint due to evaporation of the body fluid (hemolymph).

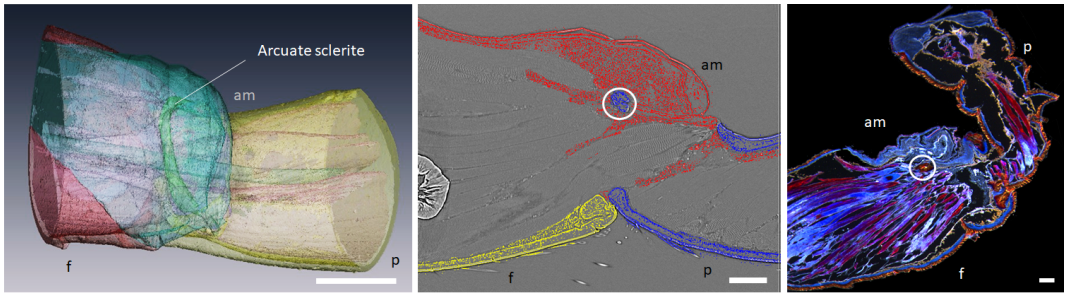

Figure 3.10: The arcuate sclerite of the femur-patella joint. Left: Serving as an attachment point for the muscles and the articular membrane (am), the bow shaped, stiff arcuate sclerite plays an important role in the joint actuation. The 3D reconstruction shows the arrangement of this arcuate sclerite underneath the articular membrane of the femur (f) and patella (p) segments. The muscles are not shown. Scale bar: 0.5 cm. Middle: This single projection of the 3D scan shows a longitudinal section through the femur (yellow) and patella (blue) segments. The articular membrane (red) and the muscles (grey, background) are attached to the arcuate sclerite (white circle). Scale bar: 100 μm. Right: The histological section shows the arcuate sclerite (white circle) underneath the layered articular membrane. Muscles are stained in blue and purple. Scale bar: 100 μm. Published in [43].

3.3.3 Arcuate Sclerite

The word "arcuate sclerite" does not appear in newer literature anymore. The reason might be that the arcuate sclerite does not appear on the surface, but is hidden underneath the articular membrane and can only be observed by histological sections or CT (computer tomography) scan. Latter has been done by several research group, but only Landkammer [64] shortly mention this "patella sclerite" as the muscle attachment point and claims in his thesis, that it reduces the area where pressure is acting on. However, Manton [72] already described that this arcuate sclerite is significantly involved in allowing the muscles to create this large working angle by pulling on the arcuate sclerite. The arcuate sclerite rotates inside the leg when flexed, continuously reducing the pulling distance with the flexing angle. Histological cuts also show that the articular membrane is wrapped around this arcuate sclerite (fig. 3.10, right) forming the chamber together with the attached muscles. The joint extension movement is thereby restricted by the inflation of this chamber and the full unfolding of the articular membrane, since the hydraulic mechanism can only act until both segments are in line.

However over-extension can happen, when e.g. external forces bend the

leg extremely or during jumping the leg is excelled in high speed and opens rapidly. I hypothesize that the fold of the articular membrane created by the arcuate sclerite and the membrane stretched between the arcuate sclerite and the patella segment, separate when the leg is overextended to help absorb external energy, preventing the chamber from ripping, which would be fatal for the hydraulic actuation. Interestingly the membrane between patella segment and arcuate sclerite does not show any microstructures when observed under the SEM. Further studies on this particular segment and the role of the arcuate sclerite are needed to completely understand its functioning.

3.3.4 Articular Membrane

There are several different definitions of the word membrane, which are important to know when communicating between scientists and engineers to avoid misunderstanding. In chemistry, thin boundary layers such as filters are usually called membranes, which separate structures from each other and often allow limited permeability of certain substances. Such structures can be found at cellular level, including the cell membrane or basal membrane. They often play an important role in the transmission of signal and information as in nerve cells or energy (ATP) generation. Such membranes can also be found in battery technology, where they are often referred to as separators. In physics, one also finds the so-called oscillating membranes, which oscillate when external force is applied. The eardrum or membrane of a speaker belong to this type of membranes. For a similar reason, the wing skin of bats are also called flight membranes. In measurement technology, pressure membranes describe a thin, impermeable sealing layer that deforms when pressure is applied. In construction technology, on the other hand, thin, foil-like materials are called membranes, which are slightly plastically deformable and often used for wide-span roofs.

In the following sections, I would like to provide detailed images of the articular membrane to give the reader a feeling about what type of membrane we are talking about. I would like to show the reader why the articular membrane is of importance for the locomotion of spiders and show them how it supports the movement of the joint by its mechanical properties. Finally, I have looked into several more interesting aspects, which have popped up during the analysis of the articular membrane.

3.3.4.1 Morphology of articular membrane

The articular membrane is neither permeable nor does it have a swinging function. It actually is part of the exoskeleton (cuticle) of spiders and describes

a thin cling film-like sheet spanning between the femur-patella joint pit. Many arthropods have similar joint membranes, which flexibly connect limb segments. However, Blickhan and Barth [14] discovered that the articular membrane of spiders seem to play a special function in spider legs, as, in contrast to other arthropods, spiders use hydraulics for extension.

The articular membrane appears white-transparent in most studied spiders as tarantula, wandering spiders and wolf spiders. I assume the reason why elder literature tends to have schematic drawings of the articular membrane is that due to its transparency, the membrane can barely be seen on images in elder literature as the image technology was not developed enough back then. A first close-up optical microscopy picture and a scanning electron microscopy image appeared during my PhD in the review in 2016 by Landkammer [64] and in his doctoral thesis [61] three years later. However, these images are taken from tarantula and therefore differ to jumping spiders and further lack in some important details, which I would like to provide in the following.

The articular membrane of the studied jumping spider *Phidippus regius* seems to have three black hoops. However this coloration is provided by pigment corns embedded in the basal membrane underneath the articular membrane. The cuticle assigned to the articular membrane is as in other spider species transparent. Under light, this transparent sheet shows rainbow reflections (iridescent). Iridescence is an important method used for communication especially in jumping spiders [33].

As *Phidippus regius* tend to lift and wave their front arms fully when seeing another conspecific and males show their front arms to the females during mating approaches [37], the coloration of the articular membrane might therefore play an important role in spider behavior.

The iridescence could be an effect of microstructures on the membrane. Scanning electron microscopy (SEM) can be used to provide a closer look onto the membrane. However, it only allows imaging of dead animals. When spiders die, they flex their legs, which lead to deflation of the articular membrane and even when manually "reopening" the joint, the articular membrane does not appear in its natural inflated shape (fig. 6.1). Traditional preparation and fixation methods do not consider this problem. Therefore, I have developed a reliable and quick preparation method, which not only allows the observation of the native shape of extended spider legs under the SEM, but also allows high magnification images as charging effects are reduced by this method. Biological material is often not conductive enough and are therefore coated with a couple of nanometer (10-20 nm) thin sheet of gold or graphite (sputter coating), to avoid charging of the samples. Charging effects can however still appear, when

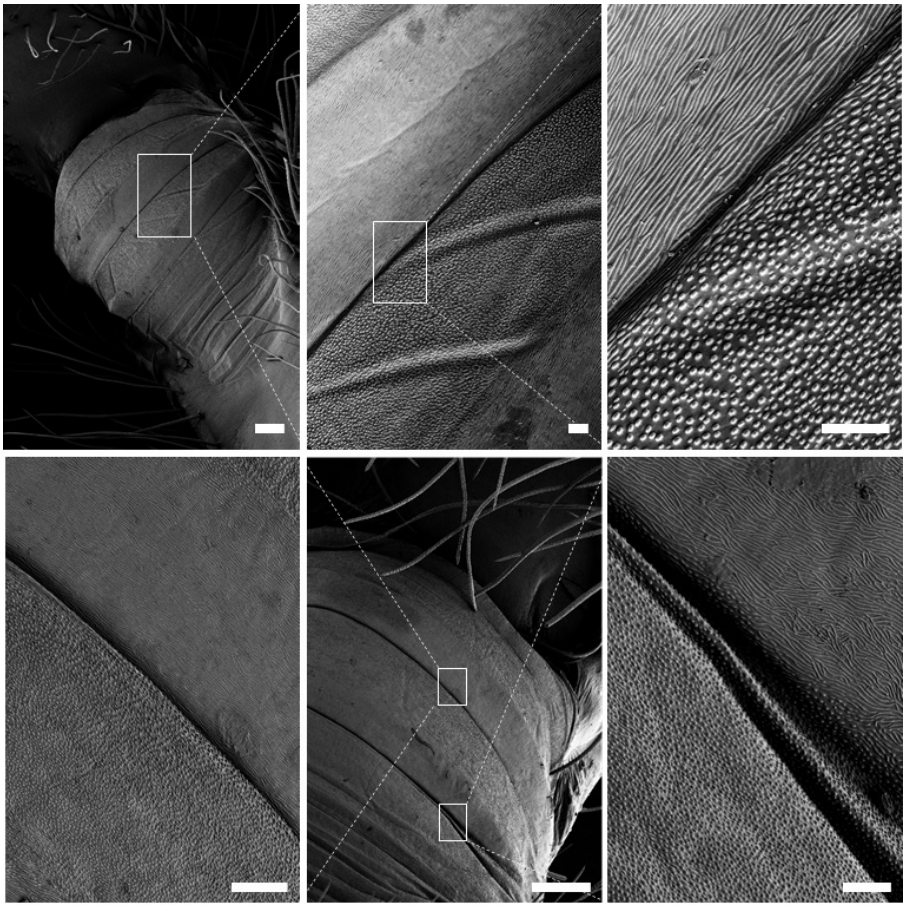

Figure 3.11: Scanning electron microscopy of articular membrane. Top Left: Inflated fabric like articular membrane of the front femur-patella leg joint showing the hoops structure. Scale bar: 100 μm. Published in [43]. Top Middle: Magnification of marked white square from the image on its left focusing on the intersection between the different areas. Scale bar: 10 μm. Top Right: Magnification of the marked square from the image on its left showing microstructures. The stiffer appearing hoop show fingerprint like line structures while the area between the hoops show bumpy dot structures. Scale bar: 10 μm. Bottom Left: Magnification of upper white square from the middle image showing the transition between the two regions. Scale bar: 20 μm. Bottom Middle: Overview of the femur-patella joint from the hind leg, showing the same alternating structure on the articular membrane. Scale bar: 100 μm. Bottom Right: Magnification of wrinkle shown in the middle image showing the fingerprint-like lines and the dotted areas. Scale bar: 10 μm.

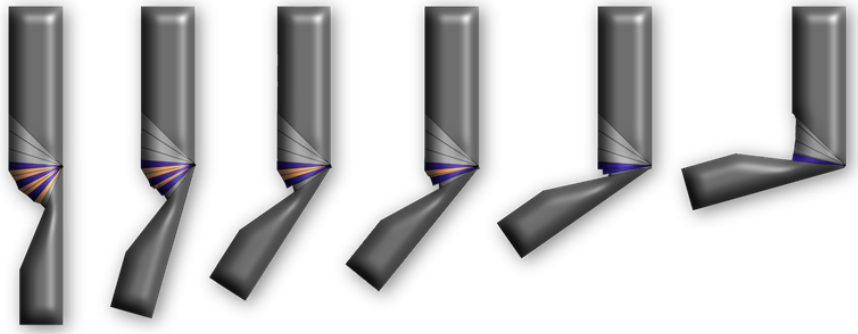

Figure 3.12: Animation of articular membrane folding behavior. The femur-patella joint of jumping spiders shows a zebra-stripe like pattern. Thereby the black hoops (here marked in purple) seem to show a stiffer behavior than the membrane part in between (marked in orange). The three-dimensional structure is reminiscent of a stroller-umbrella. During motion, the stiffer hoops slide into each other like a ice-scream scooper, allowing large working angles of 120 to 160°. Published in [43]

the objects are not planar enough during sputter coating and their surface could therefore not be evenly coated. This reduces the resolution under the microscope and often lead to white stripes on the images. A detailed description on how I solved the preparation problem can be found in the Material and Methods section of this thesis (cf. section 6.2.2). The SEM images reveal an interesting aspect, which has not been reported in literature so far. The articular membrane is covered with alternating microstructures. While the black appearing hoops have fingerprint-like, line-shaped microstructures, the rest of the membrane shows dotty micro bumps. The dimensions of these microstructures increase with spider growth, which might be another hint for age-differentiating features during conspecific communication [33]. A more detailed look on the microstructures and possible functions are given in a later section (cf. section 3.3.4.5).

3.3.4.2 Folding of articular membrane

The rather interesting part is that the black appearing hoops with the line-shaped microstructures, seem to have a stiffer characteristic. This observation matches with the assumption made by Blickhan and Barth [14]. They described the articular membrane as an anisotropic membrane, which inflates during extension and folds in a "bellow-like" manner, when the joint is flexed. Although the "bellow-like" folding has become an established term and is often cited in

"spider-inspired" studies, I would like to use a different way to describe the folding mechanism. The reason is, that the term "bellow" is set to a defined shape in the (soft) engineering context, which does not fully reflect the joint folding of spiders and lead to confusion in spider-inspired work. I would rather introduce an old description from 1958 by Manton [72], which unfortunately fell into oblivion. She described the articular (arthrodial) membrane as a construct which is "stiffened by five hoops of more fully sclerotized cuticle", which "are so arranged that they shuffle over one another when the joint flexes, the limper arthrodial membrane folding between them" [72].

At this point, I would like to mention that all of these descriptions are mainly done by words and drawings. For a reader who has never seen how a spider folds its leg, it is rather difficult to imagine the working principle. Therefore, I provide video-sequences in combination with a simple schematic drawing to show how the folding works (fig.3.12).

The folding is induced by muscles pulling at the arcuate sclerite, where the membrane is attached to. Similar to Manton's description [72], the three (and not five) hoops slide under each other like the inner ring of an ice-cream scoop. The folding resembles the sun-shade of a stroller, with the difference that the diameter of each ring slightly decreases, to allow the sliding into each other. Landkammer [64] described the sliding as a Z-shaped fold. However, he assumed only one large Z-fold which rolls out during extension, although he has assigned the three presumably reinforced (stiff) structures on the membrane. This description is only based on observation and Landkammer did not provide any detailed video sequences of the folding mechanism nor did he experimentally proof the actual reinforcement of the membrane.

3.3.4.3 Stiffness and hardness characterization of articular membrane

As the stiffness difference and anisotropy of the membrane seems to play a key role in a controlled folding and unfolding of the articular membrane and maybe also energy storage. I have conducted different indentation measurements to look into the mechanical properties of the different parts.

Nanoindentation results (fig. 3.13) support the hypothesis of a difference in the mechanical properties between the dot and line areas, showing a mean Young's modulus E of 3.8 GPa for the dot and 5.0 GPa for the line area. Furthermore, the hardness H appears to be more than twice as high for the line area than the dot area, with means of 0.12 GPa for the dot and 0.29 GPa for the line area.

The mechanical properties of spider exoskeleton has been examined in the late 80s by Blickhan and Barth [14], who showed that the stiff leg segments

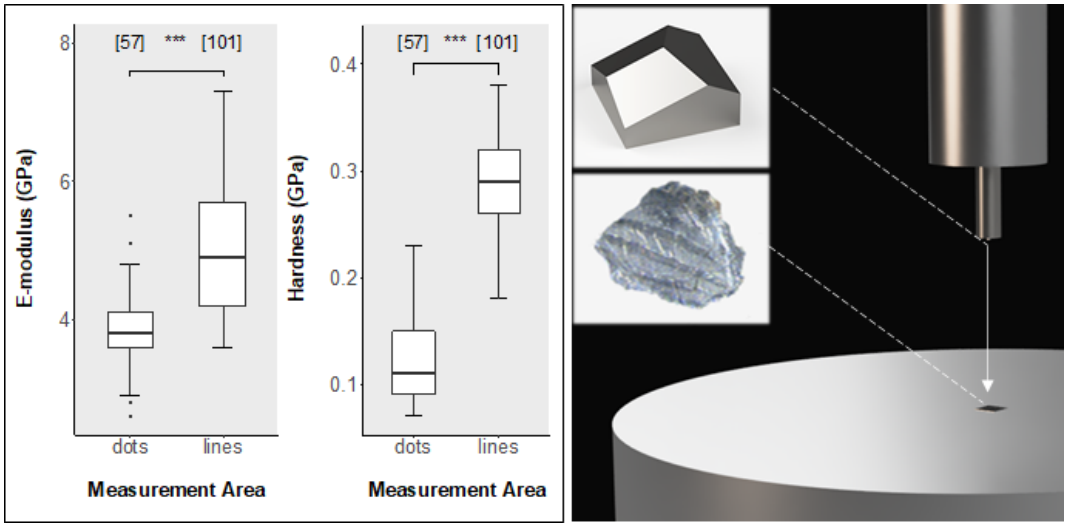

Figure 3.13: Material property characterization of articular membrane. The mechanical properties stiffness and hardness of the articular membrane were measured via nanoindentation. Therefore, the membrane ($\sim$ 1 mm^2) was dissected, flatten on an aluminium block and displaced by a Berkovich tip. The results show that the stiffness and hardness show significant (asterisk) between the area with dotted microstructures (n = 57) and with line structures (n = 101). Published in [43]

could have a stiffness of 18 GPa. Barth showed that the composition of the exoskeleton has a large influence on the mechanical properties [10]. Legs, which have a thick exocuticle are rather stiff in comparison to the abdomen or articular membrane which are lacking this exocuticle, but have a rather laminar arranged thick layer of endocuticle. Barth estimated according to the layer structure of the articular membrane [10], that its stiffness lies between 3-5 GPa and is therefore close to the stiffness measured for dragonfly wings [119].

The histological cuts through the femur-patella joint revealed that the articular membrane lacks in the stiff exocuticle explaining the lower stiffness of the articular membrane in comparison to the leg segment (e.g. femur).

While the traditional nanoindentation measurements are conducted on dry sample material, which may have an influence on the mechanical properties, I have later found a method to measure the hydrated mechanical properties of the spiders articular membrane.

Using the femto tool[1] developed by the ETH group around Brad Nelson, I was able to measure the mechanical properties of hydrated sample (fig. 3.14),

[1] https://www.femtotools.com/; last accessed on 19th Dec. 2020

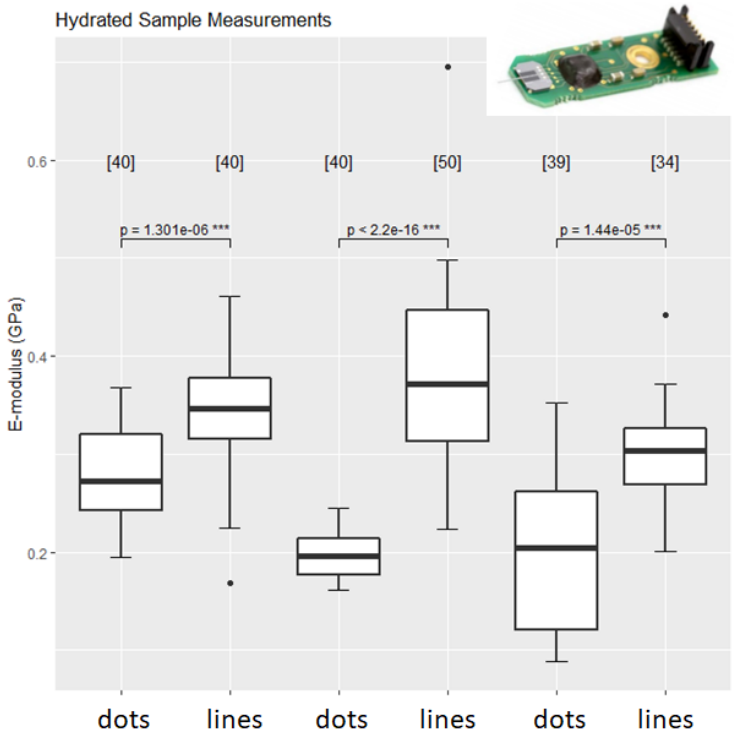

Figure 3.14: Stiffness characterization of hydrated samples. The femto tool was used to measure the stiffness of soft hydrated articular membranes. The dot and line areas of three different membranes were characterized. All three measurements showed a significant difference between the dot and the line area. The measured stiffness (0.2 - 0.4 GPa) is in general 10 times lower than in dry samples.

showing that the mechanical properties are in general significantly lower, but still show a difference between the two areas. As known from previous literature, fresh biological samples tend to show ten times lower mechanical properties [3, 57]. When hydrating the material, the cells, proteins and chitin layers take the water in and start to slightly swell giving it a softer characteristics. This property is often used in butterfly preparation to enable the movement of the feet and wings and fix them into the desired position. Therefore the lower mechanical properties under hydrated condition is not surprising.

3.3.4.4 Interesting aspects of the articular membrane

During the sample preparation, the flexibility and slight elasticity of the thin articular membrane stand out. The folding resembles folded cloth. When

dissected out of the joint, the articular membrane reveals a cling-film like characteristic, whereby the membrane unfolds completely and any wrinkles disappear when transferred onto a water surface. The membrane appears to be quite robust and the question arose whether the elastic protein resilin is incorporated into the membrane. Resilin can be found in the articular membranes of insects [74, 75] and in the joints of many jumping insects as in locusts [22] or frog hopper insects [23] and is also speculated to be in click beetles [23].

The literature does not provide any information about resilin in spiders, so I decided to quickly run the indirect resilin test to see whether or not resilin might be added into the membrane to support the jump of spiders and store elastic energy. Resilin shows strong blue fluorescence under UV light [23]. The quick test revealed that the membrane does show light blue fluorescence, but only in the line region and not in the dotted (fig. 3.15). However, resilin might not be the source of the observed very light blue fluorescence (fig. 3.15, middle), but rather a result of high nitrogen-content (e.g. nitrogen rich proteins) in that area [138]. While resilin has not been reported in arachnid studies, researchers have observed blue fluorescence in scorpion exoskeleton [39]. Similar to the coloration and patterning, this fluorescence might be involved in communication and recognition with conspecifics [39]. I assume that not resilin, but the nitrogen-rich proteins in the epicuticle are responsible for the two different mechanical characteristics of the articular membrane. Furthermore, the thickness can emphasize the mechanical difference between the dot and the line area. Histological sections lead to the assumption that the articular membrane shows a higher number of layers in the line area compared to the dot area (fig. 3.16). This hypothesis is supported by the fact that the line area appears much denser and clearer under X-ray scanning.

3.3.4.5 Microstructures on different regions of the articular membrane

Although the main work of this thesis focuses on the jumping spider *Phidippus regius*, I have also taken images of the running and jumping wolf spiders in the beginning of my PhD (fig. 3.17). The joint pit of wolf spiders does not show a zebra stripe coloration pattern, but the microstructures do alternate along the membrane. While the folding region still similar bumps, the stiffened area does not show finger print like lines, but rather Mercedes stars to dog bone arranged structures. It can be assumed that the spider species have structures adapted to their behavior to allow their preferred type of motion.

Microstructures have been reported to cover a wide range of functions. They can reduce wettability for water collecting self-cleaning purposes. Microstructures can also reduce the reflection of light, creating highly transparent wings

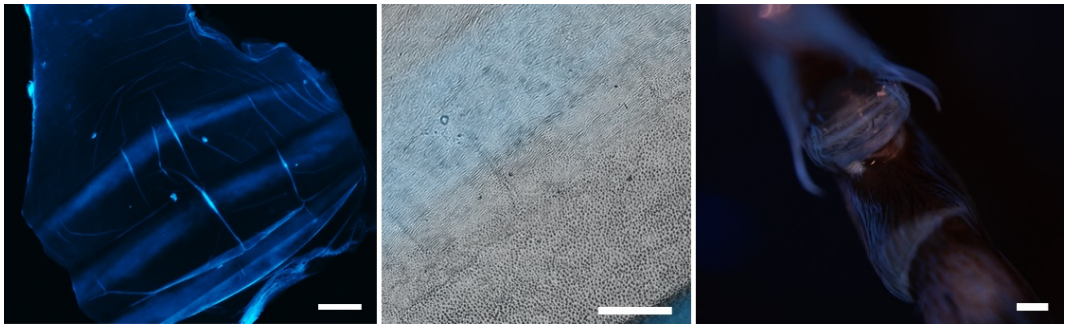

Figure 3.15: Autofluorescence respond of articular membrane under UV light. Left: The stiffer appearing "hoops" show blue coloration under UV-light. Scale bar: 50 μm. Published in [43]. Middle: The original not emphasized autofluorescence color is bright blue and only appears on the part with the "line" microstructures. Scale bar: 50 μm. Published in [43]. Right: Hair and other parts of the leg also show white to bright blue responses under UV light. Scale bar: 100 μm.

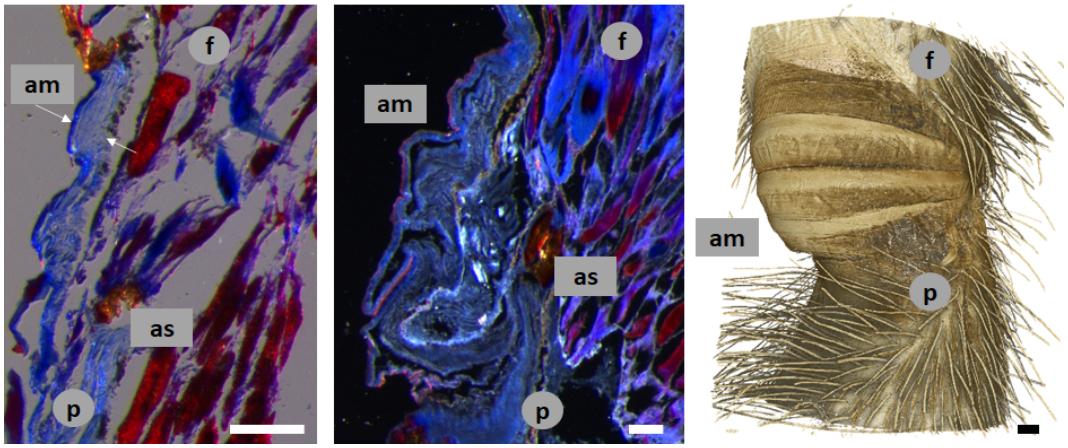

Figure 3.16: Thickness and density variance along the articular membrane. Left: Histological section through the femur (f)- patella (p) joint. The articular membrane (am) shows thicker elements (60 μ m, corresponding to the stiff hoops and thinner (30 μm) parts. Scale bar: 100 μm. Published in [43]. Middle: The articular membrane is lacking the stiff epicuticle and moslty built up by "loose" - wavy laminar layers giving it a soft characteristic. The articular membrane is covered by a thin waxy layer (light red), the epicuticle and connected to the arcuate sclerite (as). Scale bar: 50 μm. Published in [43]. Right: The stiff appearing hoops show a higher density under the X-ray scan. Scale bar: 100 μm.

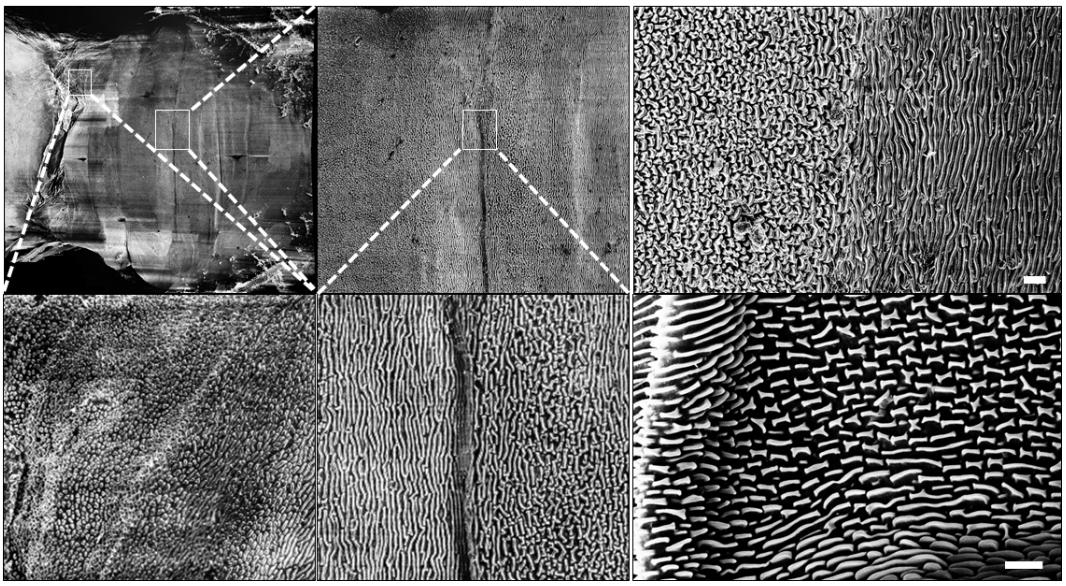

Figure 3.17: Microstructures on articular membrane of wolf spiders. Left: The first successful SEM image was taken from wolf spider joints. The image shows a x-y stacking of 500 high resolution images allowing a large digital zoom into the areas. Right: original single SEM images. Scale bars: 2 μm.

for camouflage or anti-reflective eyes for better vision. Additionally, they cause iridescence coloring, which give arthropods their often shimmery structural coloration and which are used for recognition and communication purposes. Furthermore the composition and arrangement of microstructures are known to be involved in friction reduction, abrasive wear and adhesion reduction.

To analyze the geometry of the jumping spider membrane, I used laser microscopy in addition to the scanning electron microscope images to get the actual height of the structures. It turned out, that the dots are 10 times higher than the line microstructure (fig. 3.18). The dots seem to be randomly distributed along the surface and do not show any obvious pattern, however the distances of the dots lie in the range of 10-20 μm. The microstructures could be the explanation of the iridescence shimmering of the articular membrane [124]. I further assumed that the bumpy structures which are folded in and out during movement might be useful to keep the membrane clean as it shows similarities to the self-cleaning abilities of lotus leaves [28].

In a first attempt to study whether or not such microstructures could support self-cleaning abilities, I tried to re-fabricate the exoskeleton using Chitosan and the silk protein (fibroin) as the membrane size appeared to be too small to measure adhesion with the available instruments. Different fabrication

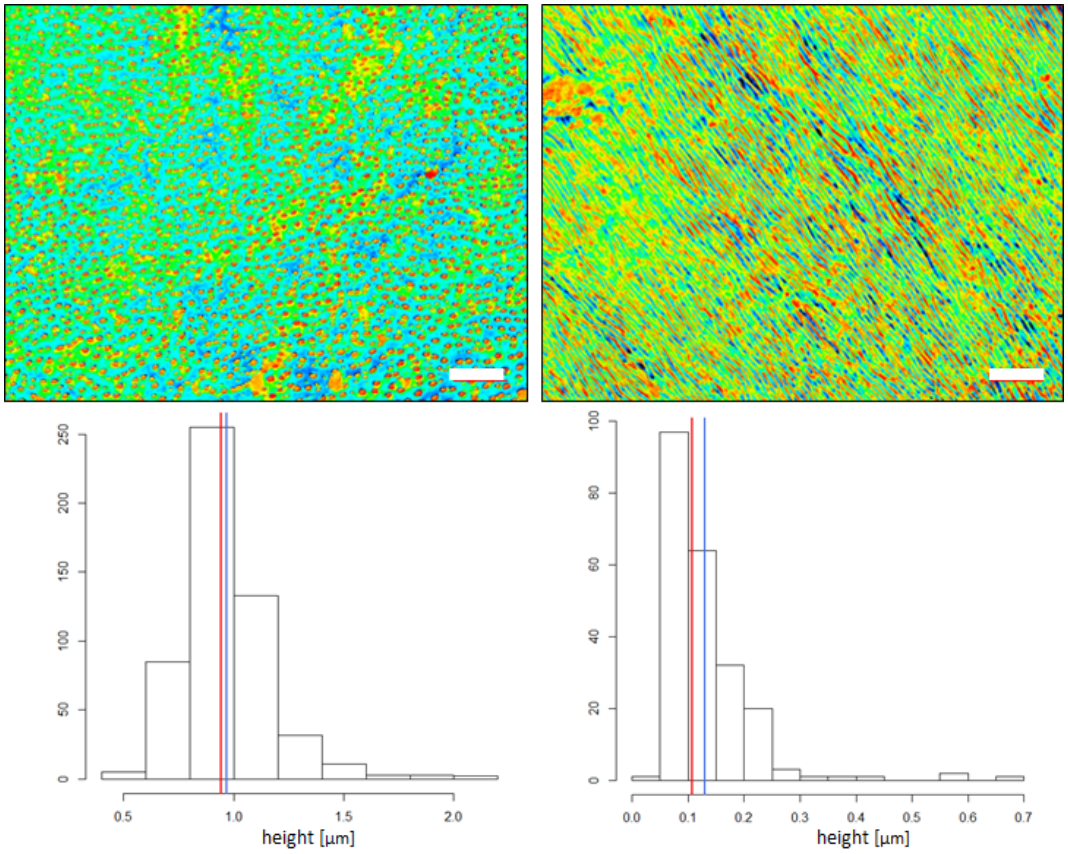

Figure 3.18: Height characterization of microstructures. Top: Lasermicroscopy image of dot and line area. Scale bars: 10 μm. Bottom: Histogramm of height distribution. The dot microstructures show a height average of 0.97 μm (median: 0.94, std.: 0.21, n = 529) while the line microstructures are only 0.13 μm (median: 0.11, std.: 0.08, n = 223) high.

methods were tried to replicate the microstructures of spiders. 3D printing with Nanoscribe allows to directly replicate images of laser microscopy images. However the structures were at the resolution limit and too close and therefore stuck together. Furthermore the printing of large surface area (1mm^2) would be too time intense. Using photolitography large molds with defined shapes could be produced with microstructures in the range of 5 μm to 100 μm. By casting the silk fibroin extracted from the pupae of the silk moth, microstructured protein thinfilms could be fabricated.

The extraction of silk needed to be optimized as the published protocol did not work out well in the first attempts. Another challenge was the filling process of the protein solution into the microstructure mold, without leakage

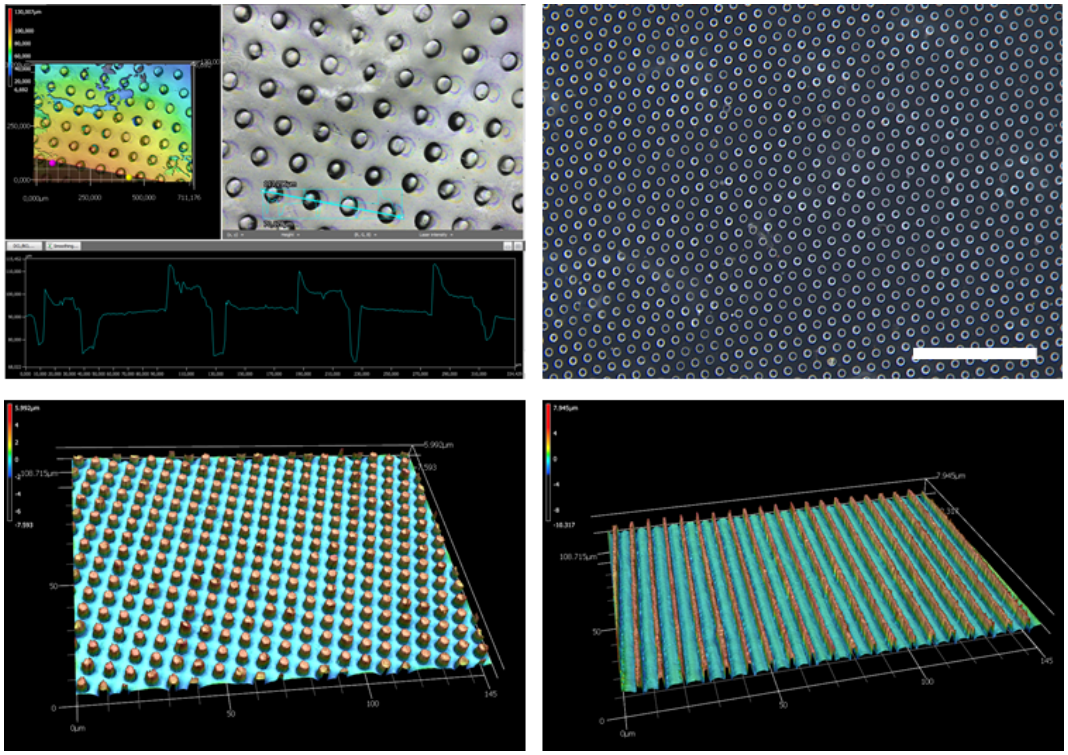

Figure 3.19: Artificial microstructured surfaces. Top: Microstructured Chitosan thin film with bump structures (10 μm). Scale bar: 250 μm. Bottom: Lasermicroscope image of successful microstructured silk fibroin sheets with dot (5 μm) and line (5 μm) microstructures.

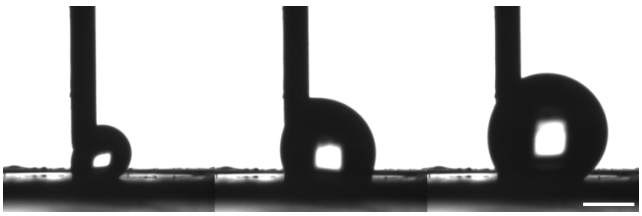

Figure 3.20: Contact angle measurement of water on artificial microstructured membrane. Water droplet on microstructured parylene coated artificial membrane (5 μm). Preliminary analysis showed contact angles of 100 - 115°. Scale bar: 0.5 mm.

and without trapping air bubbles. After several trials and errors to optimize the fabrication process, the fabrication of microstructured transparent sheets were successful (fig. 3.19). To mimic the waxy epicuticle, these sheets were covered with a thin parylene coating.

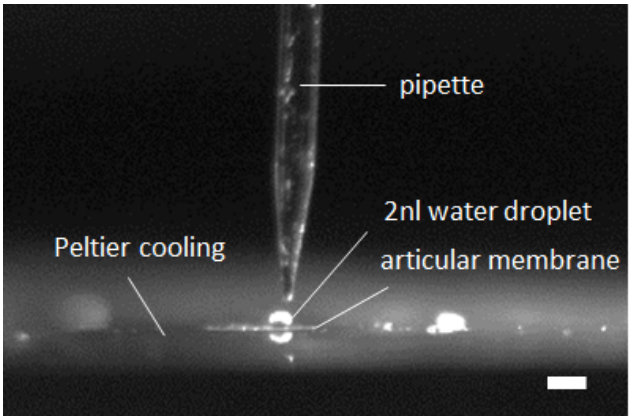

Figure 3.21: Contact angle measurement of water on articular membrane of jumping spider. Water droplet (2 nl) on femur-patella articular membrane of jumping spider. Glass slide with biological sample is placed on a peltier-element to cool the surrounding to avoid evaporation of the tiny water droplet. Scale bar: 0.5 mm

Finally, the first contact angle measurements of a water droplet on the microstructured surfaces (1 cm^2 size) could be measured (fig. 3.20). Preliminary results showed contact angles above 90°. However, the results were not satisfying as they highly depend on the successful microstructure imprinting and wax covering. With my moving to ETH, this project furthermore slowed down as fabrication process needed very long process times. Furthermore, it was questionable whether the results on the artificial membranes would give a new insight into the real functioning of spider membranes.

In the end of 2019 I found a method to directly measure the contact angle on the dissected spider membrane, using nano droplets of water which are cooled down with a Peltier-element to prevent evaporation of the droplet (fig. 3.21). This device is used by a group in Basel around Thomas Braun [8, 9, 102]. Unfortunately, due to high demand of this instrument and the necessity to readjust the experimental set-up for my purpose, we scheduled my experimental run to spring 2020, which has been shifted several times due to Corona lockdown.

Beside self-cleaning ability, I proposed that the microstructures might reduce friction and abrasive wear. While I was not able to measure these properties with the instruments given, a research group published friction studies of the jumping leg hinge joints (not the membrane!) of katydids (a type of grasshoppers) using nano-indentation [85] in 2017. Unfortunately, the method is not easily adaptable for the spider membrane analysis as the scales of the spider microstructures lie in the range of the used Berkovich tip for nanoindentation

(1μm). Furthermore, the studied katydid samples were 10-100 times greater than the spider membrane and the studied structures were at least 5-10 times larger. However, the findings might still be true for spiders. The researchers showed that in the hinge connection of the katydids, smooth-smooth contact which could cause high adhesion due to Van der Waals effects and rough-rough contact which could cause high friction and abrasive wear, could not be observed, but smooth-rough contact was observed at any time of motion, suggesting very well-adapted surfaces for fast jumping extension of the joint.

3.4 Hydraulics

Not even a hundred years ago, researchers still believed that spiders use only muscles for leg actuation. Studies in the early 1900s [7, 92] showed that although the spider's leg is packed with muscles, somehow the extensor muscles are lacking for the large joints of the legs. The erection of the leg hair (setae) and the absence of an extension when cutting the tip of the leg, led to the presumption that spiders use an increase in pressure for actuation forty years later [35]. Finally, in the 1960s , researchers were able to show experimentally that the pressure inside the body increases when the spider moves around [88].

3.4.1 Pump Source

Even though the increase in pressure was found to be the driving force behind the extension of spider legs, the pressure source was not fully identified. It quickly became clear, that the heart which is responsible for the general flow of the hemolymph, can only generate pressures of 1-2 kPa [37], and therefore could not be the main source behind this pressure increase, as the measured pressures inside the legs were higher (6 - 60 kPa [7]). Instead a volume reduction of the front body part (prosoma) by large muscles (*musculi laterales*) was postulated to cause an increase in pressure inside the legs [141]. Only in 2019, researchers 3D reconstructed the muscles inside different spiders and were able to track down several muscles which are presumably involved in this pressure generation. Their data suggest that the muscle involved for generation might have evolved over time and therefore highly differ among species [100].

3.4.2 Control, Valve and Resistance

3.4.2.1 Valves between the two body parts

The prosoma consists of two stiff shells (carapace, sternum) which are considered as ideal to create large forces and withstand the pressure. However,

the abdomen is described as a soft bag which can inflate during large food intake or after mating when the spider is pregnant. As the fluid inside the prosoma and the abdomen are connected, every volume increase of the abdomen counteracts the pressure increase. This would mean, that anytime the spider is increasing pressure inside, its abdomen expands to the maximum size at which the exoskeleton material can still withstand this pressure. The muscles in the prosoma generating the pressure have to therefore perform higher work compared to an only stiff system [139–141].

A solution might be a valve to separate the front and back part during pressure increase. This would however mean, that the flow between the two body parts is interrupted, which could cause a lack of oxygen in the front. Considering the large central nervous system in the prosoma of jumping spiders, a lack in oxygen could also be fatal, although thin trachae might support the oxygen transport during this time. Despite the flow problem, a valve between the two body parts has only been postulated [59] but not been described.

Early studies [141] observed muscle contraction inside the abdomen during the movement of the prosoma and postulated that these muscles might not prevent, but at least reduce hemolymph back flow. Nevertheless, the studies also observed a volume increase of the abdomen when the prosoma is compressed and they further showed that the volume displaced by the compressed prosoma would not be sufficient to extend all legs and the abdomen at the same time. They assumed that in long activity periods the loss of volume into the abdomen would result in a break down of the hydraulic system. Known as the *hydraulic insufficiency hypothesis* [141] there are still many studies today citing this issue and questioning the efficiency of this hydraulic actuation in comparison to only muscle based insects. Researchers assumed that this insufficiency is the reason why spiders seem to fatigue after 2 minutes of stimuli and need to recover for 5-10 minutes afterwards. Having said this, it has to always be kept in mind that behavioral studies have to be taken with caution. An observation of fatigue can have various reasons as sore muscles due to lack of oxygen or other biochemical causes or fatigue of the stimuli-neural response. Furthermore it could highly depend on the fitness, weight, size, sex and stage of development of the animal. Studies in the 1980s [7, 95, 123] showed that pressure levels are high throughout the complete activity of the spider, contradicting the insufficiency problem. Furthermore biochemical studies [95] on the lactate level, which are an important indicator for muscle activity, showed that the issue for fatigue would rather lie in the muscles than in the break down of the hydraulic pressure.

Despite all these studies, it would still be necessary to show the flow between the two body parts during resting and activity and compare it with pressure

measurements and muscle activity. High resolution images of the inside of the living animal will be key to get more information and answer how spiders are generating pressure and whether or not there are valves between the two body parts or not.

3.4.2.2 Valves inside the leg

Beside the question on where the pressure is generated inside the spider legs, the multi-legged locomotion and the multi-joint control of several segments at each leg is another problem to solve. Up to now, only descriptions and postulations were made of the complete spider locomotion mechanism. The "inverted marionette" model [59], describes the spider as an inflated body, where all legs are extended simultaneously when the pressure is increased. Muscles are counter-acting as the marionette's string to flex the legs into the desired position. However, this would mean, that the muscles are constantly acting against the high pressure inside the legs. Furthermore, the legs are provided with hydraulic fluid via defined arteries which flow back through spaces (lacuna) formed between the muscles. A system without valves would work in theory, but would mean that back flow from the hydraulic chamber into the arteries could happen. As arteries usually bring oxygen-rich blood, a back flow of used, oxygen-poor blood is avoided. In humans, there are defined veins, but also venous valves to support the upwards flow against gravity. While the heart of spiders does have heart valves to open and close during contraction, valves inside the arteries have only been postulated but never found [59]. Researchers therefore argued that the muscles which are filling up the leg change the diameter and therefore change fluid resistance [14, 69].

Authors comment on pump, control, valve and resistance At this point the reader might have realized that there are still many questions open and there will be many more experiments necessary to completely understand how spiders walk, generate pressure inside their body and prevent back flow without valves. Reading through the literature, I sometimes get the feeling that spiders should not even be able to walk considering the hypothesis created along this way, as the bumblebee was considered not be able to fly. As with the bumblebee, there are some key elements missing for a complete understanding how spiders do what they do. The literature provides many puzzle pieces and I would like to gather them together and try to fit them into a working principle about the possible mechanism of the spider locomotion. In this section, I would like to break ideas into smaller bits and define which experiments are necessary to finally prove how spiders are walking.

1. *Flow direction and pressure without valves*

Along the human circulatory system, the pressure drops continuously from the arteries to the veins down to zero. Assuming this type of pressure drop for spiders, it can be argued that valves would not be necessary for the general flow as the hemolymph would always follow the pressure gradient. Furthermore the heart is actively pumping the fluid in one direction. As veins are not existing in spiders and the flow does not fight against large height differences, valves might therefore not be necessary. When the pressure is increased by p_{add} in the prosoma without any change in volume or geometry, the absolute pressure drop Δp and flow direction would still remain, while the static pressure increases by p_{add}. This could explain why the measured pressure values inside the abdomen are smaller than in prosoma or legs, but still all body parts show a peak during activity [123].

2. *Pressure generation and leg extension*
   For leg extension, volume needs to flow inside the leg joint. When the prosoma is compressed, all legs thereby extend simultaneously, which is not the case when pushing the soft abdomen. The volume inside the leg segments is therefore considered to be provided by prosoma compression. When assuming that the complete prosoma is depressed, this could result in problematic back flow as the hemolymph could be displaced from the lacunae back into the leg joints or the sexual organ (pedipalps) as well as the abdomen could be unintentionally inflated, which means that the prosoma has to be compressed largely to fill up all relevant volumes and the muscles need to flex a lot to create enough volume flow and pressure. A large compression of the prosoma could further lead to lack of oxygen for nerves, stomach and muscles inside the prosoma and could cause the postulated hydraulic insufficiency.

   Assuming only the aorta being compressed by muscles, this would still increase pressure in all legs simultaneously. As the pressure value inside the abdomen is in total lower due to fluid resistance, the total pressure might be further low enough to not expand the abdomen cuticle. Then again, the volume could be shifted into the brain or pedipalp rather into the legs. This is why researchers have assumed that the hip segment (coxa) is compressed by muscles to create direct volume flow into each leg. However, this theory was dismissed as there are no muscles that could directly compress the coxa segment [100].

   An alternative hypothesis could be that the single leg arteries are di-

rectly compressed, providing the volume for the femur patella and tibia-metatarsus extension. This would match to the observation that a slight compression of the femur patella segment is enough to cause the leg to expand. The *musculi laterales* inside the prosoma is arranged in a star-shaped form right next to each leg segment and could, when flexed, provide the volume for each of the leg segments.

Although they were reported to be only a short muscles and therefore their ability to work as muscle pump was questioned, these muscles could be responsible for volume shifts during prosoma compression, while other muscles (e.g. sternum-coxa-articulation) can be added to provide extra pressure, if necessary. The flow direction would be sustained and only the necessary small amount of volume would be displaced towards the leg joints to extend the legs. To get a first hint whether this is possible or not, the complete volume filling up the joints and arteries needs to be measured and compared with the displaced volume to see whether they match or not. Live observations of muscle contraction, as well as hemolymph flow and leg extension could provide further information about the pump mechanism. Furthermore pressures inside the different body parts should be measured with modern techniques as the resolution of the older literature might be not high enough and could also contain artifacts due to indirect measurement methods.

It has to be mentioned, that the heart is also covered by a network of arteries, which take care of the digestive, reproductive and silk organs. This means that the pressure inside the abdomen depends highly on the place of measurement. Observed increase of pressure and muscle contraction of the abdomen can therefore also be totally independent of the hydraulic extension.

3. *Leg flexing and inverted marionette*
When the legs are flexed, the diameter in muscles increase and the diameter for channels decrease and therefore friction and pressure loss along the channels increase. This could result in a local pressure drop along the joints and therefore less pressure-induced forces acting on the joint, which might allow an easier flexing while still keeping the pressure high in all the other legs. This would support the "inverted marionette" theory as the muscles do not necessarily need to continuously work against high pressure, due to fluid resistance generated pressure loss. The larger pressure gradient might also help to guide the fluid into the right direction. Furthermore geometrical constructs e.g. by the arcuate sclerite and the

folding of the articular membrane and a pressure-dependence of the viscosity could also have an influence in flexing efficiency as well as back flow hindering.

3.4.3 Hemolymph Characterization

As already illustrated in a previous section (cf. section 2.5), spiders have an open circulatory system which pumps oxygen-enriched hemolymph from the heart to other organs through predetermined arteries. The oxygen-poor hemolymph gets back to the heart via spaces between the inner organs (lacunae) and pass the book lungs to gain oxygen. Similar to the blood of humans, hemolymph plays various roles beside the oxygen supply, including nutrient supply, immune system functions, wound healing and the hydraulic extension of the legs. Many of the functional roles of hemolymph are performed by a various number of proteins and cells whirling inside the hemolymph. The flow of hemolymph and inside cells and the physical properties of hemolymph are studied in the following.

3.4.3.1 Hemolymph flow inside the legs

First simulations of the fluid flow, pressure and velocity inside the tarantula leg showed that there is a large pressure drop along the joints. However, the simulation works with a lot of simplifications and assumptions [69]. The authors of that work also pointed out that the simulated pressure drops down to -30 kPa does not reflect the true values inside the leg. As they have only simulated the pressure drop along the tibia-metatarsus segment, the boundary values for pressure taken from the literature might not reflect the pressure at that position. They further did not include the direction of flow and hemolymph was considered as Newtonian with viscosity values from human blood.

In the study of Blickhan and Barth [14] the general arteries and lacunae were identified and drawn in a schematic figure (fig. 2.8). However, photography of histological sections have not been provided in literature as cutting through the articular membrane turned out difficult due to its thinness, transparency and softness. In this work several methods have been tested and adapted to present thin (4 μm) cross-sections of the legs (fig. 3.16). Using 3D reconstructions of the legs (fig. 3.22) the space between muscles and nerves could be presented, showing the area where hemolymph could traverse. As both of these methods needs dead spiders to achieve high resolution, question about hemolymph flow direction inside the legs could not be answered.

Optical coherent tomography (OCT), which has a maximal measurement

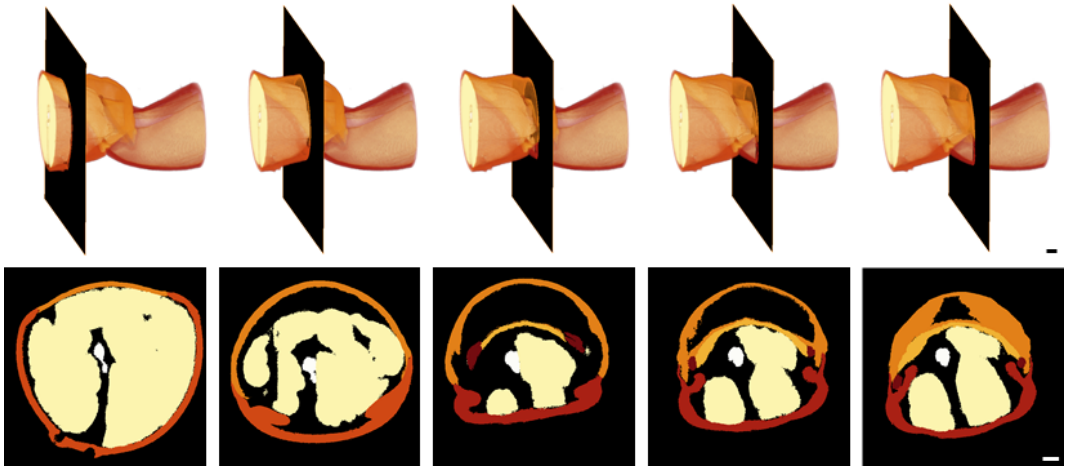

Figure 3.22: Cross section through 3D scan. 3D-reconstruction of femur segment (light red), patella segment (red) and the articular membrane (orange). The membrane (outer part: orange, inner part: light orange) and muscles (yellow) are attached to the arcuate sclerite (dark red) and form a chamber between the two leg segments. The empty spaces (black) form potential pathways of hemolymph flow between muscles and nerves (white). Top images, scale bar: 50 μm, bottom images, scale bar: 100 μm

depth of 3.5 mm, allowed the observation of particle flow inside the legs in living spiders (fig. 3.23), without feeding contrast agent or inject air into their blood stream [66]. The size (10-15 μm) of the observed particles correspond to the sizes of hemocytes [2, 60] floating inside the hemolymph. As the penetration depth is limited, juvenile spiders were used to scan the complete leg. Carbon dioxide was used to sedate the spider, to attach it upside down on a petri dish. High carbon dioxide concentration can have an influence on the hemolymph composition [80]. To avoid this, we did not directly expose the spider in a fully Carbon dioxide environment, but used a balloon filled with carbon dioxide to diffuse into the tube until the spider falls asleep. This method takes less than a minute, before the spider stops to move, but the spider also wakes up after 2-3 min. The cell flow were tracked, revealing cell speeds of 3.37 m/s (median: 2.67, std.: 2.29, n = 36) inside the artery, which would correspond to shear rates of 10^5 1/s considering an artery diameter of 100 μm. While previous calculations of shear rates inside locusts were limited by the video recording speed [66], resulting in shear rate estimations of 105 1/s [56] for insect hemolymph flow, the OCT recordings presented in this work was taken at 76 kHz and demonstrated much higher fluid speed and shear rates inside the legs.

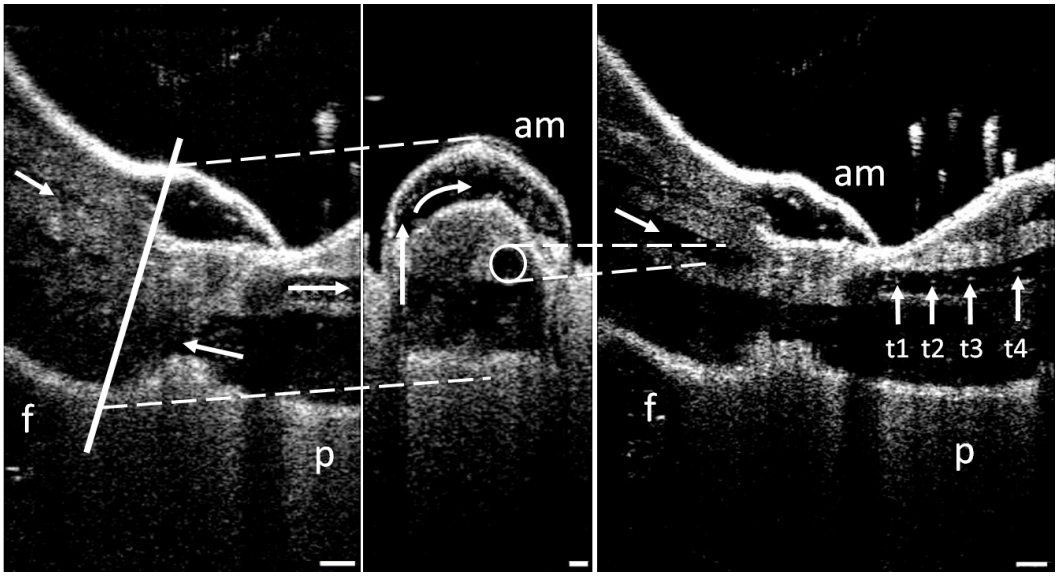

Figure 3.23: Optical coherent tomography (OCT) recordings of femur-patella joint. Left: Screen-shot of OCT recording of femur (f)- patella (p) joint showing the flow direction of hemolymph inside the leg. Cells floating inside a well defined artery between the muscles flow towards the leg tip, while cells inside the lacunae (empty space close to the joint connection) travel back to the body. The flow inside the pocket underneath the articular membrane can not be described from this view. Scale bar: 100 μm Middle: Cross-section through the leg shows the circular artery. Interestingly the cells travel clockwise inside the pocket below the articular membrane (am). In some recordings the cell flow seems to stop, accumulating inside this pocket until the muscles move. Scale bar: 50 μm. Right: longitudinal section overlay of the femur-patella joint showing cell movement at different time stamps (t1-t4). OCT videos were recorded at 76 kHz, revealing a cell speed of $\sim$3 m/s inside the artery. Scale bar: 100 μm.

3.4.3.2 Physical Analysis of Hemolymph

Another interesting aspect is the viscosity and physical behavior of hemolymph. Although it is not red as human blood, it does show similar biochemical compositions which is hinting to similar non-Newtonian behavior.

The viscosity has a great impact on hydraulic systems in performance and material wear. A detailed analysis of the importance of fluid characteristics in hydraulic systems for machines and robots can be found in the following chapter (cf. section 3.4.3.3).

So far, there is no study about the viscosity of spider hemolymph and kine-

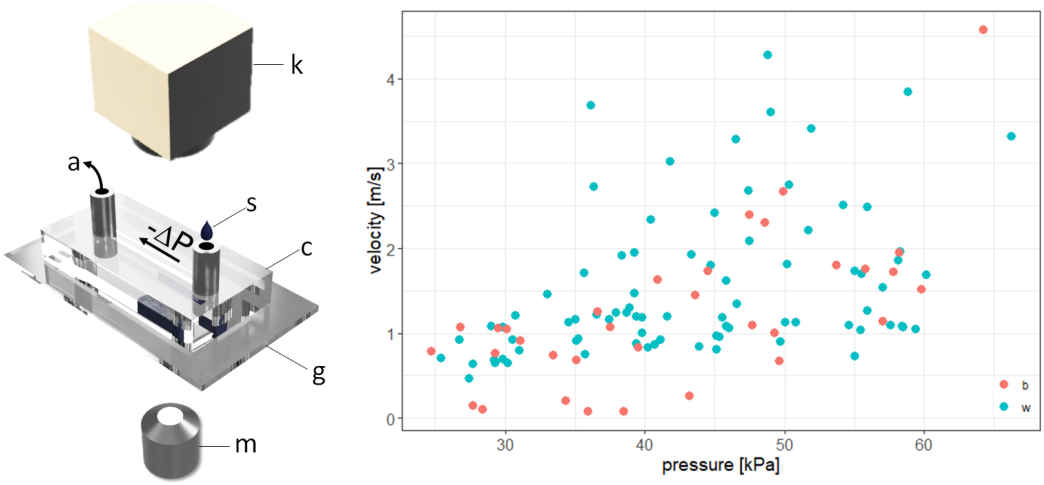

Figure 3.24: Pressure-velocity behavior of spider hemolymph. Left: The PDMS (polydimethylsiloxane) mold is attached to a glass slide (g) to form a micro-channel (c). This channel is connected to an aspirator (a) with a pressure sensor and a valve. By opening the valve, the aspirator creates a suction force and forms a pressure drop inside the micro-channel. A droplet of the sample (s) is pipetted into the opening of the micro-channel (c) and travels through the micro-channel following the pressure drop ΔP. The velocity of the fluid is tracked under a microscope (m) with a high speed camera (k). Right: The measured velocity at different pressures (ΔP) for water (w) and hemolymph (b) has been recorded. Interestingly, the velocities inside the micro-channel are ranging up to several m/s as it can be observed inside human arteries and as we also saw in the OCT recordings.

matic and dynamic studies assumed a Newtonian fluid and viscosity values close to water (1 cP) or human blood (5 cP). To get new insights into the physical fluid property, hemolymph was collected from adult jumping spiders and the fluid velocity through a slit-shaped, PDMS micro-channel at different pressures (ΔP) (fig. 3.24) was measured (experimental set-up modified according to [128]).

Given the Ostwald-de Waele relationship [118, 126] between shear stress τ_w and wall shear rate $\dot{\gamma}_w$ for Power-law fluids by

$$\tau_w = K \cdot (\dot{\gamma}_w)^n \tag{3.8}$$

(3.9)

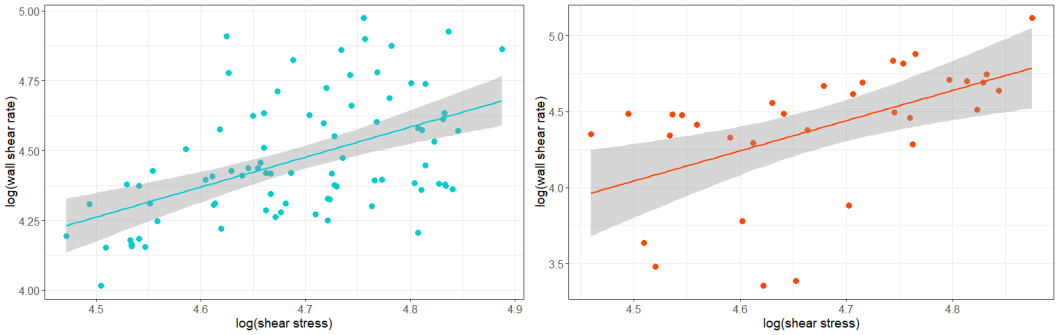

Figure 3.25: Log-Log-plot of shear rate and shear stress. The slope of the linear fit through the log-log relationship of shear rate and shear stress is needed to estimate the fluid flow behavior index (n). Left: Water shows a flow behavior index of 0.93 (close to 1) describing its Newtonian behavior and non-shear rate depending viscosity. Right: Hemolymph shows a flow behavior index of 0.5 corresponding to non-Newtonian, shear thinning behavior.

with

$$\begin{aligned} \dot{\gamma}_w &= \frac{2n+1}{3n} \cdot \dot{\gamma}_a; \\ \dot{\gamma}_a &= \frac{3v}{2H}; \end{aligned} \tag{3.10}$$

and

$$\tau_w = \frac{\Delta P \cdot H}{2L};$$

with $\dot{\gamma}_a$ describing the apparent shear rate, H the height (70 μm), L the length (30 mm) of the channel, v the measured fluid velocity and ΔP the set pressure difference.

Detailed derivation of these relations for slit shaped channels are elaborated in the Material and Method section (cf. section 6.6.4). The equations allow determination of the flow behavior index n and the flow consistency index K from the experimental measurements by plotting the log-log relationships of shear stress and shear rate. The dynamic viscosity μ can then be determined from

$$\mu = K \cdot (\dot{\gamma}_w)^{n-1} \tag{3.11}$$

For $n = 1$, the term of the shear rate disappears, showing that the fluid viscosity does not change with the shear rate, which is true for Newtonian

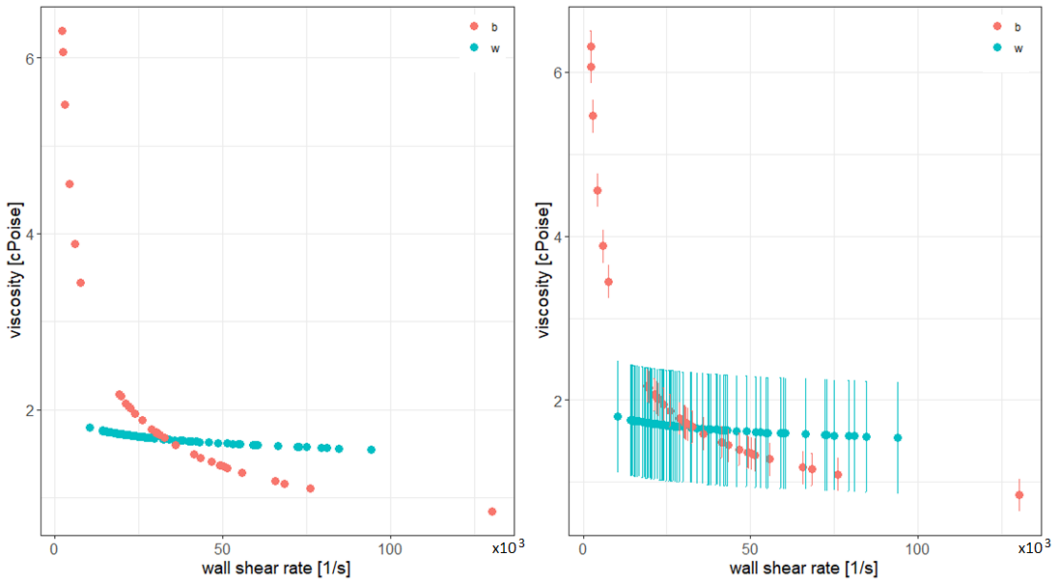

Figure 3.26: Viscosity at different shear rates. Left: The experimental data revealed wall shear rates up to 10^5 1/s corresponding to the speeds observed in the living spiders via OCT. While water (w) shows a shear-independent behavior, hemolymph (b) viscosity changes from 6 cP at low shear rates down to 1 cP during activity. Right: The measured viscosity value of water is 0.6 - 0.8 cP larger than literature values [12] (0.95-1.05 cP at 18-22°C). This error could be explained by small systematical errors in geometrical values (dimension of microchannel) or sensor sensitivity which propagate through the data evaluation.

fluids as water (fig. 3.26, blue).

For $n > 1$, the effective fluid viscosity increases rapidly with shear rate. This behavior is described as shear thickening of dilatant fluids as the corn starch-water mixture or silica-particles in polyglycerol for body armor.

For $n < 1$, the fluid shows shear thinning behavior and are called pseudo plastic fluids. Especially polymer solutions as paint, blood or ketchup show a decrease in viscosity with shear rate. The experimental results for hemolymph suggest a shear-thinning behavior with an estimated fluid behavior index of 0.5 (fig. 3.25, 3.26, red). The calculated viscosity ranges from 6 cPoise at pressures of 30 kPa down to 1 cPoise at 60 kPa (fig. 3.27). In comparision, water measurements revealed almost constant (dynamic) viscosities of 1.6 - 1.8 cP.

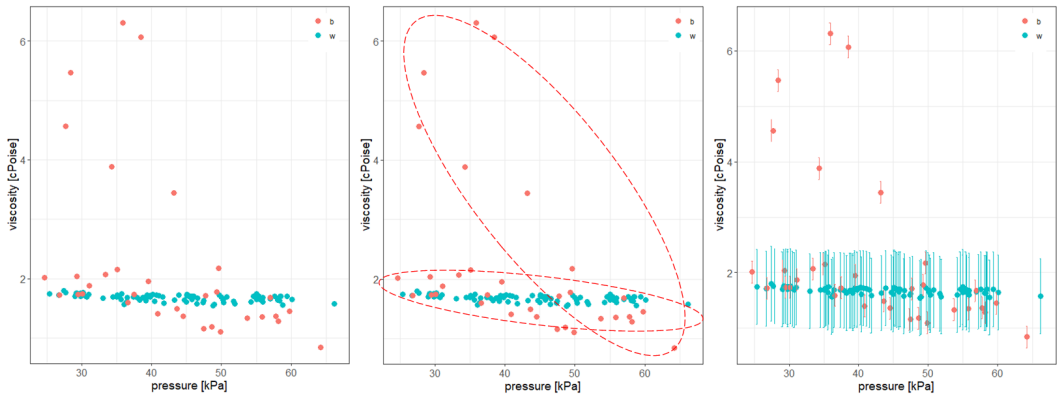

Figure 3.27: Pressure-viscosity behavior of hemolymph. Left: The plotted data show that many measured hemolymph data(b) show a similar pressure-viscosity behavior as water (w). Middle: However, it can be assumed that hemolymph shows two different behaviors with one group showing a linear decrease in viscosity with pressure increase and a second group with similar behavior to water. These two groups could be explained by the number of cells inside the sample volume [56]. Further experiments will be needed to exclude outlier effects. Right: A second behavior should therefore be discussed, as when assuming the same absolute error for all measured points, the upper values cannot be explained by the systematic errors.

This value is however larger than literature values[2] at 18-22°C [12]. The error propagation (fig. 3.26, right) describing effects of experimental errors (e.g. small errors in sensor values, microchannel dimensions) shows that the "real value" lies within the experimental variance (cf. section 6.3). Further explanations for this higher viscosity value could be material friction (PDMS), small sampling volume (2 μl), temperature and pressure effects, which were not included into the model. Additionally, a change of the height value by 10-15 µm would already result in analyzed viscosity values around 1.0 cP. This deformation corresponding to dimensions thinner than a human hair could happen during microchannel assembly errors (attaching PDMS mold on glass slide) or due to pulling effects on the inside of the microchannel by the high suction forces of the aspirator created pressure drop. While the same experimental errors have been used for hemolymph error propagation (cf. section 6.6.5), hemolymph could show a completely different range in unknown parameters as material friction or pressure effects and therefore an easy calibration of the hemolymph data to the water measurements cannot be done.

[2] https://wiki.anton-paar.com/en/water/ of 0.95 - 1.05 cP; last accessed on 19th Dec. 2020

When plotting the viscosity over pressure, hemolymph seems to show the same behavior as water (fig. 3.27). However, looking closely into the data, one can assume a second behavior of the measurements, showing a linear decrease of viscosity from 6.0 cP at low pressures to 1.0 cP at 60 kPa. This second behavior could be a result of a large amount of cells inside the hemolymph, while a lack of these cells could result to similar fluid behavior as water. Due to the small sample volume of max. 50 μl per spider and only 2 μl per experimental run different amount of cells inside the sample could occur. Although more measurement data will be needed to exclude outliers such a two type behavior of hemolymph has been reported for caterpillars [56]. The study showed that the plasma, so hemolymph with cells removed, shows viscosities of 2 cP, while full hemolymph viscosity ranges between 1-4 cP. Different to the caterpillar study, the measurements presented in this work simulate similar hydraulic diameters of 140 μm as observed for spider arteries (100 - 200 μm) and high in shear rates (10^5) corresponding to 100-1000 times higher than measured and estimated in previous research [56]. The estimated shear rate inside locusts of around 150 s^{-1} was based on the speed of artificial air bubbles inside tracked inside the circulatory system of locusts and reported pressure values generated inside the locust heart [66]. However, this research was limited in the speed they were able to track as they were not using high speed cameras, and when looking into their video recordings, one could see that there were many more air bubbles blurring out. While the non-hydraulic actuation of locusts and caterpillars could further show differences in shear rates, our fluid characterization fits to our flow studies with recorded speeds of cells inside the leg of $\sim$ 3 m/s.

Using our methods, we were therefore not only able to show shear-thinning behavior for spider hemolymph, but determine the flow behavior index n experimentally showed that the velocity speeds up and the viscosity lowers by 6 fold with higher pressure. These values and behavior have never been taken into account when estimating the kinematics and dynamics of spiders.

In the following section, I would like to theoretically discuss how the non-Newtonian behavior could have an impact on hydraulic actuation.

3.4.3.3 Hydraulic Motor

Considering the spider leg system as a hydraulic motor, the volumetric efficiency η_{vol} for rotational transmission is given by [1]

$$\eta_{vol} = \frac{1}{1 + G\frac{\Delta p}{n\mu}} \tag{3.12}$$

with

$$G = \frac{C_v}{|epsilon|}, \tag{3.13}$$

$$\tag{3.14}$$

and depends on the laminar leakage loss C_v, the displacement setting ϵ and the rotational speed n. With higher pressure difference Δp, the volume efficiency decreases, while it increases with higher dynamic viscosity μ. The hydromechanical efficiency on the other side is given by

$$\eta_{hm} = 1 - X - Y \cdot \frac{n\mu}{\Delta p}, \tag{3.15}$$

with

$$X = k_p \cdot e^{k_\epsilon(1-|\epsilon|)}, \tag{3.16}$$

$$\tag{3.17}$$

and

$$Y = k_v \cdot e^{k_\epsilon(1-|\epsilon|)} \tag{3.18}$$

$$\tag{3.19}$$

and depends further on the Coulomb friction k_p, viscous friction losses k_v and displacement coefficient k_ϵ. The mechanical efficiency increases with higher pressure difference, but decreases with viscosity.

The overall efficiency is given by the multiplication of the volumetric efficiency and the mechanical efficiency with

$$\begin{aligned}
\eta_{total} &= \frac{1 - X - Y \cdot \frac{n\mu}{\Delta p}}{1 + G\frac{\Delta p}{n\mu}}, \\
&= \frac{1 - X - Y \cdot \frac{n\mu}{\Delta p}}{\frac{\Delta p}{n\mu}(\frac{n\mu}{\Delta p} + G)}, \\
&= \frac{(1 - X) \cdot \frac{n\mu}{\Delta p} - Y \cdot (\frac{n\mu}{\Delta p})^2}{(\frac{n\mu}{\Delta p} + G)}, \\
&= \frac{X' \cdot a \cdot \mu - Y \cdot a^2 \cdot \mu^2}{(a \cdot \mu + G)}.
\end{aligned} \tag{3.20}$$

with

$$X' = 1 - X, \tag{3.21}$$

$$a = \frac{n}{\Delta p} \tag{3.22}$$

For a Newtonian system, where viscosity is not dependent on the pressure, the optimal viscosity is given by

$$\frac{\partial \eta_{total}}{\partial \mu} = -a \cdot \frac{X' \cdot a \cdot \mu - Y \cdot (a \cdot \mu)^2}{(a \cdot \mu + G)^2} + \frac{X' \cdot a - 2Y \cdot a^2 \cdot \mu}{(a \cdot \mu + G)}, \tag{3.23}$$

$$0 = a \cdot \mu^2 + 2G \cdot \mu - \frac{X' \cdot G}{Y \cdot a}. \tag{3.24}$$

The solution of this quadratic equation is

$$\mu_{1,2} = \frac{(-G \pm \sqrt{G^2 + G\frac{X'}{Y}}) \cdot \Delta p}{n}, \tag{3.25}$$

$$F = (-G + \sqrt{G^2 + G\frac{X'}{Y}}), \tag{3.26}$$

$$\mu_{opt} = \frac{(F \cdot \Delta p)}{n}. \tag{3.27}$$

The solution shows, that in case of Newtonian fluids, the higher the operating pressure, the higher the optimal viscosity needs to be, to work in the optimal window of the fluid.

The same solution can be observed when looking at the total efficiency in dependence of pressure.

By formulating the derivation depending on pressure instead of viscosity, the maximum pressure can be derived from

$$\frac{\partial \eta_{total}}{\partial \Delta p} = \frac{\frac{X'b}{\Delta p} - \frac{Yb^2}{\Delta p^2}}{\frac{b}{\Delta p} + G}, \tag{3.28}$$

with

$$b = n \cdot \mu, \tag{3.29}$$

which shows the solution of

$$0 = \frac{b}{\Delta p^2}\left(\frac{\frac{X'b}{\Delta p} - \frac{Yb^2}{\Delta p^2}}{(\frac{b}{\Delta p} + G)^2}\right) + \frac{\frac{-X'b}{\Delta p^2} + \frac{2Yb^2}{\Delta p^3}}{\frac{b}{\Delta p} + G},$$

$$0 = \frac{X'b^2}{\Delta p^3} - \frac{Yb^3}{\Delta p^4} - \frac{X'b^2}{\Delta p^3} + \frac{2Yb^3}{\Delta p^4} + G\left(\frac{-X'b}{\Delta p^2} + \frac{2Yb^2}{\Delta p^3}\right),$$

$$X'\Delta p^2 - 2Yb\Delta p - \frac{Yb^2}{G} = 0. \tag{3.30}$$

The quadratic equation can again be solved into

$$\Delta p_{1,2} = n\mu(\frac{Y \pm \sqrt{Y^2 + \frac{X'Y}{G}}}{X'}), \tag{3.31}$$

$$K = \frac{Y + \sqrt{Y^2 + \frac{X'Y}{G}}}{X'}, \tag{3.32}$$

$$\Delta p_{opt} = n\mu K \tag{3.33}$$

showing that the higher the fluid viscosity, the higher the optimal pressure, where the fluid works with highest efficiency. How does this change, when the fluid viscosity is dependent on the pressure?
For non-Newtonian fluids with, it is $\Delta p = f(\mu) = f$

$$\eta_{total} = \frac{X' \cdot n \cdot \mu \cdot \frac{1}{f(\mu)} - Y \cdot n^2 \cdot \mu^2 \cdot \frac{1}{f(\mu)^2}}{(n \cdot \mu \cdot \frac{1}{f(\mu)} + G)}. \tag{3.34}$$

To find the optimal viscosity, the first derivation

$$\frac{\delta \eta_{total}}{\delta \mu} = -(\frac{n}{f} - \frac{n\mu \cdot \dot{f}}{f^2}) \frac{\frac{X'n\mu}{f} - \frac{Yn^2\mu^2}{f^2}}{(n \cdot \mu \cdot \frac{1}{f} + G)^2} + \frac{(\frac{X'n}{f} - \frac{X'n\mu\dot{f}}{f^2}) - (\frac{2Yn^2\mu}{f^2} - \frac{2Yn^2\mu^2\dot{f}}{f^3})}{(n \cdot \mu \cdot \frac{1}{f} + G)} \tag{3.35}$$

is set to zero

$$0 = (\mu\dot{f} - f)(Yn^3\mu^2 - X'nGf^2 + 2fGYn^2\mu), \tag{3.36}$$

$$0 = n(\frac{\mu}{f})^2 + 2G\frac{\mu}{f} - \frac{X'G}{Yn}. \tag{3.37}$$

The maximum equation shows, that the derivative term $\dot{f}(\mu)$ disappears when searching for the optimum, unless $\mu\dot{f}(\mu) = f(\mu)$.

For $\Delta p = f(\mu) = \frac{\mu - c}{m}$; (observed/proposed behavior for spider hemolymph) (fig. 3.27); the derivative would be $\dot{f}(\mu) = \frac{1}{m}$. So only in case that $c = 0$, where the pressure can be directly described as $\Delta p = \frac{\mu}{m}$, the viscosity of the fluid, would correspond to the optimal viscosity at any pressure (as $\mu_{opt} = \frac{f(\mu)}{\dot{f}(\mu)} = \mu$).

If $c \neq 0$, the solution for the optimal viscosity can be described as

$$\begin{aligned}[\frac{\mu}{f(\mu)}]_{1,2} &= \frac{-G \pm \sqrt{G^2 + G\frac{X'}{Y}}}{n}, \\ &= \frac{-G \pm \sqrt{G^2 + G\frac{X'}{Y}}}{n}, \\ [\frac{\mu}{f(\mu)}]_1 &= \frac{F}{n}. \end{aligned} \tag{3.38}$$

For $\Delta p = \frac{\mu - c}{m}$; $m, c \neq 0$; it follows that

$$\mu = \frac{c}{1 - \frac{nm}{F}} \tag{3.39}$$

with c, describing the viscosity at $\Delta p = 0$. For slow rotational speed n, the highest efficiency is achieved at viscosities close to c. In Newtonian fluids, the optimal viscosity increases drastically the lower the rotational speed (fig. 3.28, 3.29).

Considering that the derivative term does not influence the maximum, the optimal values can be directly calculated from the solutions for Newtonian fluids: For $\mu = m\Delta p + c$

$$\mu = \frac{F \cdot \Delta p}{n} \tag{3.40}$$

$$m\Delta p + c = \frac{F \cdot \Delta p}{n}$$

$$\Delta p = \frac{c}{(\frac{F}{n} - m)} \tag{3.41}$$

or

$$\Delta p = n(m\Delta p + c)K$$

$$\Delta p = \frac{c}{(\frac{1}{nK} - m)} \tag{3.42}$$

$$\rightarrow F = \frac{1}{K} \qquad \text{(geometrical parameters)}$$

The optimal operating pressure increases with speed. The viscosity of Newtonian fluids affects the optimal operating pressure needed to achieve highest efficiency. Low viscous fluids perform best at low pressures in comparison to high viscous fluid (fig. 3.28). In non-Newtonian fluids, the optimal pressure approaches $\frac{-c}{m}$ with high speed.

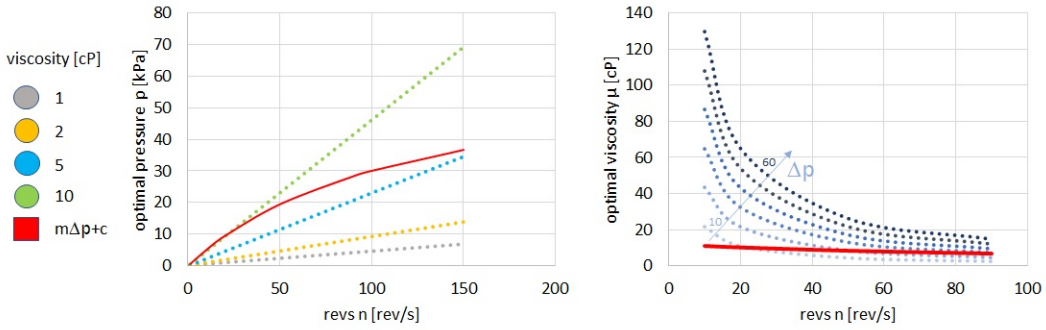

Figure 3.28: Optimal operating parameters depending on revolution speed. Left: Theoretical behavior of optimal operating pressure in Newtonian fluids with different viscosities (1-10 cP) compared to a fluid with linear pressure-viscosity behavior (red) as proposed for spiders. The results show that Newtonian fluids need high operating pressures for fast motions. Proposed behavior for spider hemolymph could create fast motions without a linear increase of pressure. As all parameters were estimated, the absolute pressure and speed values are only for demonstration. Low viscous fluids show in general less steep pressure increases with higher revolution speed. Right: Theoretical behavior of optimal viscosity for different operating pressures (10-60 kPa) and speeds. Systems with a wide range of revolution speed tend to need hydraulic fluids with drastically higher viscosities to perform efficient in low speed actuation. The theoretical behavior of the spider hemolymph would only increase linearly in viscosity to achieve optimal efficiency at lower speeds.

Comparing the optimal viscosity for maximum efficiency in Newtonian and non-Newtonian fluids it can be seen, that in case of Newtonian fluids, the optimal viscosity has to be chosen according to the operating pressure and rotational speed. In case of non-Newtonian fluids, the viscosity is almost independent from the rotational speed. Spiders perform at a various range of rotational speed for walking, running and jumping. Looking into the high speed recordings, a rotational speed of 80 - 140 rev/s could be estimated. As the generated pressure of the spider, depends on the moving of the prosoma shells and the volume that can be displaced, the operating pressure is limited. Choosing a non-Newtonian fluid $\mu = m\Delta p + c$, with $\frac{-c}{m}$ close to the maximum or highly used operating pressure, would allow the fluid to always work at its optimal efficiency. High total efficiency can normally be generated with high viscous fluids (fig. 3.29). However, torque can be reduced, when the viscosity is too high as the output torque M_{out} is given by

$$
\begin{aligned}
M_{out} &= \frac{\epsilon \cdot D}{2\pi} \cdot \Delta p \cdot (1 - (k_p + k_v \frac{n \cdot \mu}{\Delta p}) e^{k_\epsilon (1 - |\epsilon|)}), \\
M_{out} &= \Delta p R (1 - X) - nRY\mu, \\
M_{out} &= R(\Delta p X' - n\mu Y), \\
M_{out} &= R(\Delta p X' - n(m\Delta p + c)Y).
\end{aligned} \tag{3.43}
$$

Optimal torque values can therefore be achieved with low viscous fluids at high pressures. Low visocity furthermore allows fast volume flow at high pressure, which would reduce the risk of delayed volume shifts. The effective flow Q is thereby given as

$$
Q = \frac{\epsilon \cdot D \cdot n}{\eta_{vol}} \tag{3.44}
$$

with ϵ describing the displacement setting and D the displacement.

As spiders need to constantly provide the organs with oxygen and nutrients, a constant flow would be beneficial, high viscous fluids would provide a slow flow through the body giving the molecules enough time to exchange. However at high pressures with fast rotation and volume shift, a high viscous fluid could create a sudden break down in the oxygen supply when the fluid flow is interrupted by the inertia of the fluid. A rapid increase in effective flow as it can be observed for the non-Newtonian fluid (fig. 3.29) could therefore be beneficial for fast jumping motions. Non-Newtonian fluids bring another benefit. As the spider leg radius decreases towards the foot, higher shear rates can be assumed at the second hydraulic joint (tibia-metatarsus), which could cause heating and performance reduction. Considering the shear-thinning behavior of the hemolymph, heating at fast motion might be avoided.

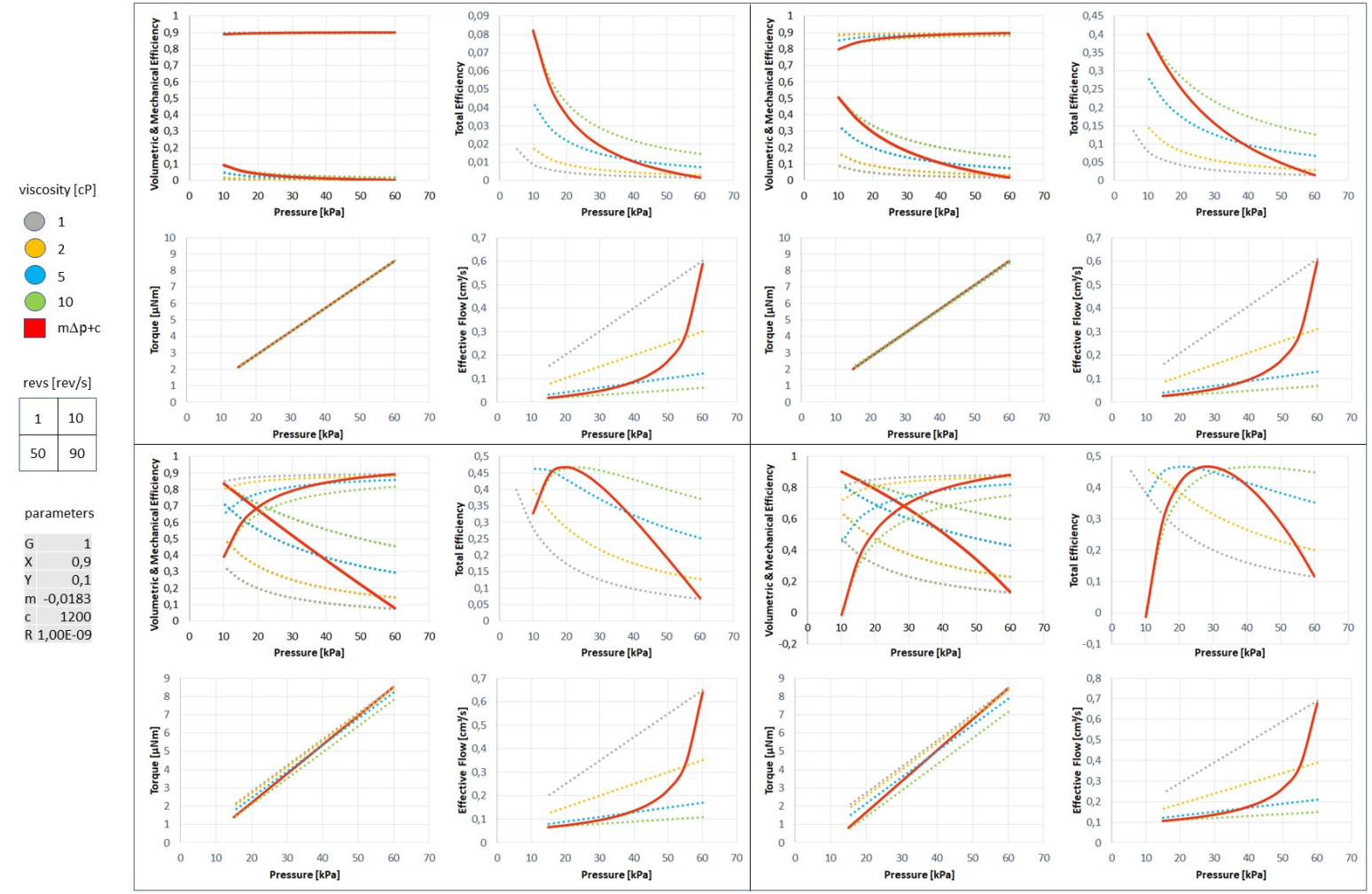

Figure 3.29: Theoretical calculation of volumetric and mechanical efficiency, torque and effective flow of fluids with different viscosities. The efficiencies and performances of Newtonian fluids with viscosity values between 1-10 cP and linear viscosity-pressure fluid for proposed spider hemolymph (red) at four different revolution speeds (1,10,50,90) were simulated. The used parameter values are listed on the left.

Chapter 4

Robotic Implementation

In this thesis, the fundamental folding principle of the spider joint was analyzed and adapted into a rotary actuation model. While the spider shows quite impressively what it is capable of, the question was whether the observed principles can be successfully implemented into a technical application and which advantages does it bring. Looking from the engineering aspect, a burning question arose, how spiders actually control so many different joints and legs and how the physical properties of their hydraulic fluid looks like and what difference it may mean for hydraulic devices. So on the one hand, a rotary fluidic actuator was designed, but on the other hand, new biological hypothesis arose and could also be tested, using the robotic platform and engineering methods.

Before diving into the world of spider-inspired implementations, I would like to give a short overview about terminologies used in the field of bio-inspiration. Afterwards, I will provide a short introduction into the principle of hydraulics, before specific spider-inspired approaches are covered, followed by the desgin and fabrication of my own prototype.

4.1 The Symbiosis of Biology and Technology

Driven by the idea that biology had plenty of time during their evolution to adapt and develop optimal solutions to given problems, bio-mimetics, bio-mimicry, bio-inspiration and bionics became popular fields over the last decades. All of these terms seem to be rather similar and standardized definitions do not existing, but vary highly over time and in different communities [51]. Bio-mimicry can either describe the detailed copying of the biological model even down to the molecular level, but is also used to describe a rather lose "mimicking" of the biological model for a greater accessibility to a general public.

Bionics describes the combination of biology and technology. Physical principles of biological models are abstracted to create new, "innovation" products. However, in the medical community bionics is used for the replacement of human organs or limbs with artificial or synthetic elements or their symbiosis. Bio-mimetics is used as another word for bionics or bio-mimicry. Bio-inspired is often used as the general term covering any work that has biological and technological elements. It is often used for applications and creations based on any type and level of inspiration from nature. Thereby the underlying biological principle does not necessarily need to be understood. Sometimes bio-inspiration is used when researchers developed a new technology which reminds them of the behavior or shape of an animal, although their design was not inspired by and often differ largely from that biological model. The term is therefore just used to attract a larger general public.

Growing up and studying in Germany, a slightly different term and approach has been shaped: Bionik. Made popular by Werner Nachtigall [78] in the 1980s, it describes the symbioses of biology (BIOlogie) and technology (TechNIK). It is sometimes translated into bionics, bio-mimetics or bio-inspiration. In contrast to the English terms, "Bionik" is defined very detailed. It describes the understanding of a biological principle, the abstraction of this principle and the implementation of this principle into a new, innovating approach, concept or product. Examples are optimization algorithms to reduce weak points in mechanical designs based on the growth of trees or bones. It also covers self-cleaning surfaces based on the cleaning principles of lotus leaves. It is important, that the principles do not need to be copied one-to-one. It is rather more of interest and importance to understand the underlying physical, chemical or design parameters behind the mechanism to adapt to or even enhance it for the desired application. Lotus leaves show rough, waxy surfaces, which lead to super-hydrophobicity and the self-cleaning ability. While the bumpy micro- and nano-structure of lotus leaves cannot always be replicated and might also not always be suitable, understanding the functioning behind super-hydrophobicity can lead to the production of textile fibers achieving this self-cleaning ability. It is thereby important to know which biological aspect to focus on and not to just simply copy the idea, but to understand what advantage this property can bring and to modify it when necessary. The detailed understanding of the underlying biological principle is required to solve the technological problem and allows the researchers to even abstract the mechanism and adapt it to robotic or mechanical systems rather different from the inspired biological purpose. Furthermore, chemical, physical or design principles can also be implemented without using the same scale or material of

the biological model.

Knowing the principle also allows to change parameters and to even enhance desired properties or to improve the technological adaption. In general two different approaches are distinguished: Bottom-Up and Top-Down. Bottom-Up describes the discovery and analysis of a biological phenomena, which shall be implemented into a technical application. An example is beside the lotus effect, the hairy feet of Geckos for reusable adhesives or structural coloration of beetles and butterflies for longer lasting colors. The Top-Down principle starts from a technical problem and searches for a solution in nature. Examples are the winglets of birds that were implemented into airplanes to reduce air resistance or a new design for wall anchors based on the mouth of ticks. In the process of development, both approaches often merge into a fruitful circle leading to new questions for technological implementations or biological functions.

Recently, technological implementations are even used to quantitatively analyze and understand biological behavior and structures and to proof hypothesis which cannot be easily tested on the biological model itself. However this approach is not established enough yet to have its own term. It often fails when too many aspects are tested at the same time as scale, material and complexity of the implementation differ highly from the biological model. It is therefore important to pick out a detailed (physical) parameter which should be tested. One simple example: Let's formulate the hypothesis that wing-lets of birds have to always look upwards to reduce air resistance. By building simple air planes with different wing-let orientation the design aspect can already be quantified. While trying to answer the question why birds always have the wing-lets upwards, which could be rather difficult to be answered, it might be easier to break this question down into material, design and structure questions. By changing these parameters, the importance of each for the functioning can be evaluated and one after another hypothesis can be rejected.

In this work, I will use spider-inspiration as a general term to describe research inspired by the working principle of spiders. I would classify my own work as mostly in the area of the bottom-up approach in understanding the underlying spider locomotion principles and adapting it into a new application. However, I would go a little further and say, true to Feynman's motto "learning comes with creating", that by creating a technological implementation, a deeper understanding of the biological system is given.

4.2 Hydraulics

Water powered mechanisms can be traced back long before ancient times, when heavy stone doors opened magically. The Greek engineer and mathematician, Heron of Alexandria (10 - 70 AD) even wrote a book (*Pneumatica*) describing early ideas for machines powered by air or water pressure, including a lovely chirping bird automata (fig. 4.1)[1,2].

Figure 4.1: Ancient Greek hydraulic automata. Left: Technical Drawing of chirping bird automata from the *Pneumatica* book by Heron of Alexandria. Photography taken from Wikimedia Commons. Right: Rebuild bird automata in museum of ancient greek technology[1] by Kostas Kotsanas. Screenshot from Youtube Video[2]

In the 17th century, the French physicist Blaise Pascal provided new insights on hydrodynamics and hydro-statics, which laid the pathway for the invention of the first hydraulic press by Joseph Braham in 1795. William George then developed the first piston engine, which led to the booming of hydraulic powered cranes and lifts during the industrial revolution in the late 19th century. Further developments as the introduction of oil as hydraulic fluid to additionally lubricate the metal parts and reduce friction, as well as radial piston pumps and the power steering for cars, lead to the versatility in applications for hydraulic pistons that can be found in today's everyday life.

Due to the incompressibility of water, hydraulics is known for fast, powerful and uniform motion. Traditional hydraulic actuators are however often made out of heavy metal to withstand high pressures and large forces that are

[1] http://kotsanas.com/gb/index.php; last accessed on 19th Dec. 2020
[2] https://www.youtube.com/watch?time_continue=20&v=SR4OqJqmbBE&feature=emb_logo; last accessed on 19th Dec. 2020

produced. Furthermore leakage and cavitation can be problems, which could make hydraulics either too expensive or not useful for certain applications.

Pneumatics (the use of air pressure) has become an alternative approach for lighter actuators and leakage would not induce environmental harm. The compliance of pneumatic actuators due to the compressibility of air, can on the one can lead to safer human-machine interactions, but can on the other hand come with the cost in precision and generated force. Nevertheless, the company Festo developed high-precision pneumatic actuators and matching control elements, sensors and valves for manufacturing and automation purposes. Their pneumatic flexible artificial muscle can further be found for medical applications. Such soft and flexible pneumatic or hydraulic actuators are nowadays rising in popularity to allow easy and safe human-robot interaction (HRI) enhancing flexibility and productivity in industry and everyday life [32].

Depending on materials and design, soft fluidic actuators fulfill many beneficial characteristics as lightweight design, compliance, adaptiveness, easy integration and environmental friendliness. The hydraulic principle in power transmission is further scalable, making it also attractive for small robotic applications. With the discovery of the semi-hydraulic actuation of spiders, researchers and engineers started to develop spider-inspired actuators [64]. In the following section, I will provide an overview about existing actuators, their approach ideas and their advantages and, more import, their problems. I would like to further introduce interesting actuators and techniques, that are important to evaluate and classify my work. The design and fabrication of this spider-inspired actuator was another main part of this work and will be covered in details afterwards.

4.3 Spider-inspired Research and Actuators

A detailed review on spider-inspired actuators was given by Landkammer in 2016 [64]. While I do not want to repeat this review, I would rather like to talk about ideas and approaches they have in common.

As illustrated in detail in the section before, bio-inspiration covers any type of inspirations. Therefore when searching for spider-inspired research there are many more actuators than covered in Landkammer's review [64]. One can distinguish between four different levels of inspiration. The first level would be research focusing on replicating locomotion behaviors as the jumping or the eight-legged gait to e.g. investigate the advantage of multi-legged systems (fig. 4.2). These researchers often do not replicate the mechanism of spider locomotion, but have either simple springs or rubber bands to simulate the

Figure 4.2: Level 1 Spider Inspiration. Top left: Jumping performance depending on the leg angle [36]. Top right: Omnidirectional, realistic spider robot (Robugtix, T8X)[4] using servomotor joints. Bottom left: ARAC ETH focus project[5,6] using tendon driven legs. Bottom right: Festo BionicWheelBot[3] uses spring-motor actuators to allow rolling and walking motion inspired by the desert spider *Cebrennus rechenbergi*.

jumping or use servomotor-based, piston-based joints to actuate. The second level describes spider-inspired actuators which use a balloon or a silicon-based chamber in the joint to achieve a fluidic based actuation (fig. 4.3). The third level covers spider-inspired actuators which use bellows in their joints to mimic the "bellow-like" folding mechanism [14] of the spider joint membrane (fig. 4.4). The last level covers the design of a mechanism with elements that slides into each other (fig. 4.5 [43, 72], corresponding to the mechanism described in the previous chapters (fig. 3.12).

The first level (fig. 4.2) is useful to compare new developed actuator principles with already established technologies. What are the advantages of a hydraulic actuated system to a spring, wire or complete servo-based actuators? How does a hydraulic piston differ from the spider system and which advantages or disadvantages does it have? Level 1 approaches are also important for studying biological aspects which seem to be not directly dependent on the exact joint design and mechanism, they could also help to better understand the real spider joint mechanism by e.g. excluding aspects and they help to give information

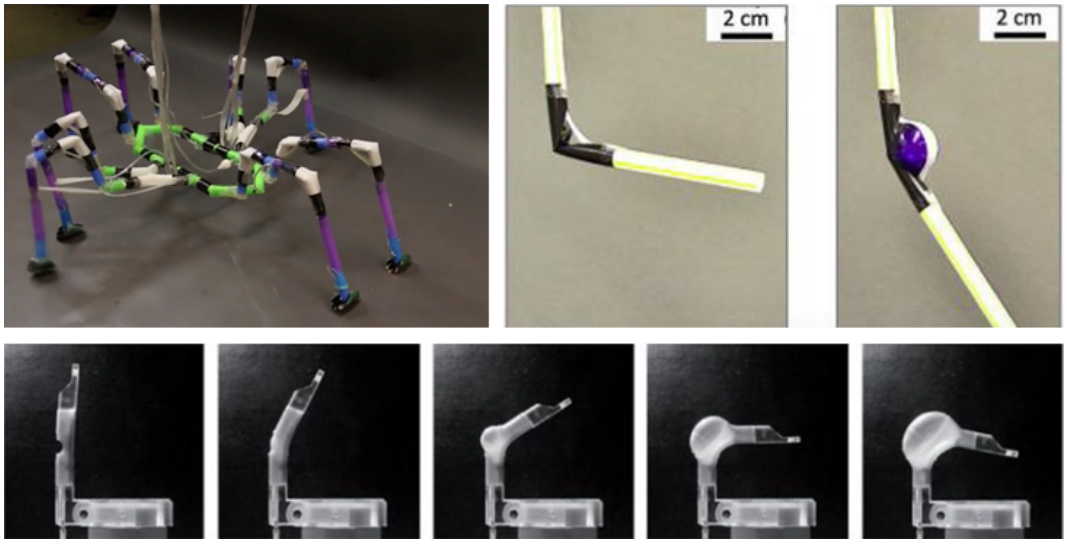

Figure 4.3: Level 2 Spider Inspiration. Top: Arthrobot[7] using balloon inflation for extension and a rubber band for flexing the joint [83]. Bottom: Pneumatic actuation based on inflating soft silicon rubber [144].

about implementation problems. Festo[3] built a rolling and walking spider robot based on the behavior of the desert spider which uses a wheel-like locomotion to traverse over hot sand. The most interesting and impressive realization is the T8X[4] spider robot which uses 26 servo motors to actuate several joints, giving the spider a very real appearance. The ARAC focus project at the ASL department [5,6] ETH Zurich built an impressive wire-based spider robot in 2012, which tried to reduce the weight of single legs, while still allow fast and versatile motion. A problem they faced in was that wire-based actuation has to be constantly re-adjusted after several runs as the tension might get lose over time.

The second level (fig. 4.3) is interesting as a comparison between reinforced anisotropic joint membranes (where e.g. stiffness varies along the membrane) and the simple balloon or soft membranes.[7] When describing the spider joint, Blickhan and Barth [14] have proposed that isotropic membranes would create parasitic volumes which would result in counter-acting forces restricting the

[3] https://www.festo.com/group/en/cms/13129.htm; last accessed on 19th Dec. 2020
[4] https://www.robugtix.com/t8x/; last accessed on 19th Dec. 2020
[5] https://asl.ethz.ch/education/focus-projects.html; last accessed on 19th Dec. 2020
[6] http://www.arac.ethz.ch/index.php?_1=gallery; last accessed on 19th Dec. 2020
[7] https://www.deviceplus.com/trending/insect-inspired-arthrobots-made-of-drinking-straws/; last accessed on 19th Dec. 2020

Figure 4.4: Level 3 Spider Inspiration. Top left: 3D printed Arachno-Bot[8] by Fraunhofer using pneumatic bellows for joint actuation [20]. Bottom Left: OHM-Krabbler Project[9,10] at TH Nürnberg mainly based on work by Landkammer [61] using TPU based flexible pneumatic bellows for extension and pneumatic muscles to flex the joint. Right: Robotic Arm using pneumatic bellow [42].

full movement of spiders and therefore proposed a reinforcement. The shown actuator examples show this kind of problem. With increase in pressure, the balloon or silicon blows up to a rather large chamber without giving much in rotational movement. Whiteside group's implementation tried to restrict this expanding by a sleeve and rubber band [83]. Early implementations also used the chamber on the outside of the joint instead of at the joint pit. While the fabrication of such types can be low cost, and down scaled easily and therefore even combined with micro-fluidic techniques, the reinforcement of this joint membrane seems to be necessary to create a serious application.

Over the last decades several presented spider-inspired actuators and applications have been published covering a bellow in the joint.[8,9,10] The actuators

[8] https://en.wikipedia.org/wiki/Arachno-Bot; last accessed on 19th Dec. 2020

[9] https://www.youtube.com/watch?v=JUB6c84rbbw&feature=emb_logo; last accessed on 19th Dec. 2020

[10] https://baybionik.de/wp-content/uploads/2019/06/P8_Eulenhalsgelenk_Poster.

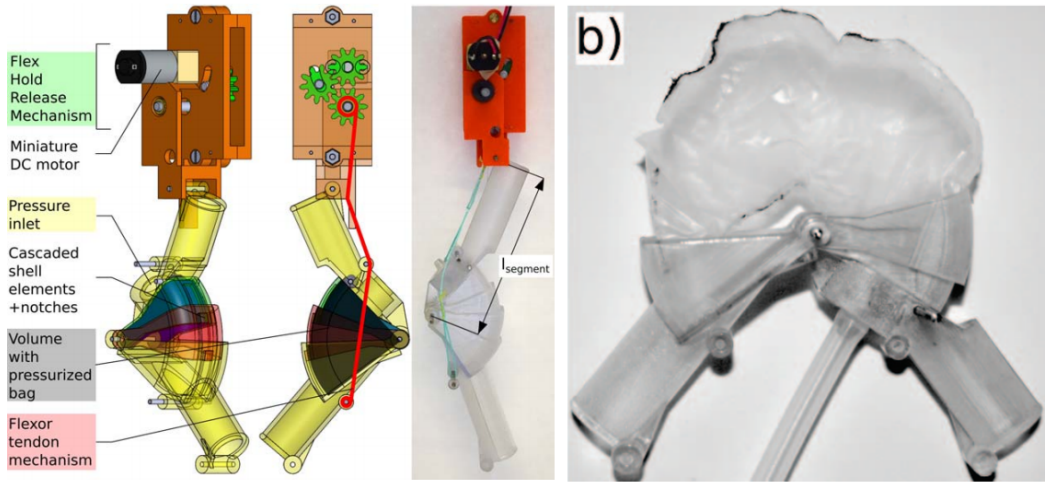

Figure 4.5: Level 4 Spider Inspiration. Left: CAD (computer-aided design) model of the spider inspired "Chinese Fan" prototype, with stiff shell elements and a flex-hold release mechanism. The prototype was fabricated via 3D printing and jumping abilities were experimentally tested. Right: Opened prototype showing the plastic bag, which inflates and causes extension when pressurized [120].

were pneumatically actuated and made out of either a soft material or a flexible material sometimes with integrated stiff elements. Bellows have been used in air and water pressure pumps for a long period. One and two sided bellow shaped actuators have further become a popular shape especially in soft robotics over the past twenty years (fig. 4.4 right). The fabrication of such a shape is therefore well established and can be easily integrated with tubes. Although Blickhan and Barth [14] described the folding as a bellow-like fold and the membrane is inter-folded in a zig-zag manner like a Chinese fan when cutting the flexed leg in half, the bellow used in robotic implementation does not represent the folding behaviour in general and does not reflect the drawings and descriptions of Blickan and Barth [14] or Manton [72]. As presented in the first part of this thesis, the membrane fold resembles more a stroller sun-shade in combination of the sliding mechanism of an ice-cream scooper, which both also reflect the rotary motion better than the bellow or accordion.

The level-four type (fig. 4.5) of inspiration covers actuators which use the slide mechanism. In the beginning of my PhD in 2016, I have developed such an actuator together with students and postdocs at the MPI-IS in Stuttgart which was then published at ICRA (International Conference on Robotics and

`pdf`; last accessed on 19th Dec. 2020

Automation) 2017 [120]. This actuator covers a thin plastic bag on the inside, which inflates with pressure and pushes the stiff "Chinese fan shell elements" open. The leg was flexed by a flex-hold release mechanism and, by sudden release, we showed that the leg could jump to 11.7 cm height within 100 ms. Although the underlying mechanism is scalable in theory, limitations come from fabrication and design. The stiff shell elements are connected by hooks, which have to be strong enough to withstand the sudden opening during jumps and can therefore not be 3D printed smaller. The shell elements need to be further printed with a 1-2 mm thickness as the cleaning of the elements could already destroy the material (Veroclear). The thickness restricts the overall working angle as the shells have to be folded into each other and the space inside is limited.

The shell elements are further hinged together along a metal pin. This hinge joint could break easily after landing. The inside plastic (polyethylen) bag is custom made by soldering two layers into the desired shape. This method allows easy fabrication and testing but brings many down sides. The bag can only withstand pressures up to 50 kPa before starting to rip or the the material starts to undesirably blow up and thin out. Another disadvantage of the inside bag is that it causes friction during the opening and closing process, limiting the performance of the system as well. Follow up studies by the postdocs[11] reveal that silicon or fabric material on the inside can help to withstand higher pressure, but also increase friction. Furthermore sleeves of latex or silicon can reduce the fabrication size, but leads to blowing up of the material as in can also observed in the level three inspiration models.

Along my biological research, I tried several approaches with the available 3D printable rubber material (tango black) and also combinations of both the stiff (veroclear) and the rubber material. However, the rubber material showed a high stickiness and often ripped during cleaning. All these observation in fabrication problems had a great impact on the final fabrication process and will be discussed in depth in section 6.7.2.

4.4 Other Studies of Interest

Besides spider-related research, there are a couple of different robotic research directions and robotic actuators which are closely related to the here presented work or show some similarities in problems and implementations. The most obvious related research are works on other arthropod-inspired robots. The tail and legs of lobsters has inspired researchers to design rotary actuators [25],

[11] https://cpb-us-w2.wpmucdn.com/sites.coecis.cornell.edu/dist/0/60/files/2017/12/arachnabot-spider-inspired-13dj8wg.pdf, last accessed on 19th Dec. 2020

where I have provided biological insights into the morphology and functioning of the lobster. However the legs of lobsters differ significantly from spiders, as although they have a membrane between their joints, this membrane does not show any micro-structures, nor stiffness difference nor any folding behavior. Considering that the lobsters are not the fastest animal and are not reported to using hydraulics for leg extension, this kind of adaption might therefore not be necessary. The arthrodial membrane of insects has been studied on the biological side, allowing joint movement, but also the expansion of insect abdomen after feeding (honeypot ants) or during pregnancy (locusts). Although the formfitting expansion of the termite queen abdomen of up to 15 times of the non-fertilized princess [19, 78], has given the idea (Werner Nachtigall [78]) to find flexible and growing material for e.g. packaging and the unfolding of the arthrodial membrane does again play an essential role in this expansion, the arthrodial membrane has not been further investigated for robotic research. The material (Chitin), the hierarchical structure, its properties and the folding behavior might play an important role in future soft robotics studies.

Soft actuators have been considered as the next step in robotics. Caterpillar-inspired rolling robots [68] and octopus-arm like water actuators [65] have been investigated and show that the adaptivity of soft robotics and actuators make them interesting approaches to store elastic energy, squeeze into small tubes, grip complex shapes and allow safe human-robotic interaction. Soft actuators can be driven by various techniques including tendons, magnetic field, light, heat and moisture. The most common approach is pneumatics and hydraulics. Soft fluidic actuators often use the hyper-elasticity of the silicon-based material, to cause extension or rotation due to expansion of the material under pressure. With pressure release, the material returns back to its original shape. The expansion, however, often comes with the cost of large balloon like volume creation. Therefore most soft actuators are supported with integrated stiff elements, to allow a better control and prediction of the system. Linear soft actuators as artificial muscles, e.g. the McKibben artificial muscle [5, 127], use a network of wires around an inflatable inside which restricts the expansion direction.

Silicon-rotary actuators have been designed for gripping purposes and also full soft robots [32, 101, 114, 137]. The casting method of silicon allows fabrication of fluidic actuators in various sizes. The soft material and compliance of the inside air allows the robot to withstand great impact (as the weight of a car driving over the robot legs). A downside of these type of soft robots is that it has to lift its own body weight, which often needs high pressure as the torque reduces when the material expands. In combination with the compressibiltiy of air, this results in a compliant but slow and wobbly walking robot. Alternative

materials as PET-based actuators, paper-based origami-inspired folding and 3D-printed fabric-like structures are further approaches to allow a combination of higher material stiffness, reduction of undesired expansion, but still keeping the flexibility of the actuator. Fabrication and scalability of these materials and methods can however be limited on the other hand. Beside air, small explosions inside soft actuators have been used to show jumping capabilities [11]. Biochemical reactions are further investigated to create air pressure for actuation for micro-scale approaches [132].

The oil-based Hasel-actuator and dielectric elastomer acutators (DEA) further allow electrical instead of fluidic actuation, but work at high voltage (5-10 kV) [55]. Approaches with liquid crystals have shown to reduce the required voltage down to (1-3 kV) [31]. It can be proposed that with smaller batteries, future tiny soft robotics can be fully on-board controlled and actuated without requiring large pumps, compressors, batteries or other devices to actuate.

4.5 Design and Fabrication of a Spider-Inspired Extension Mechanism

Before designing a new actuator, it has to be clear what kind of requirements need to be fulfilled. While design-wise, the spider mechanism shall be integrated in this work, there are several external aspects that have an impact on the material choice and fabrication method. On the fabrication side, low-cost and reproducibility are of importance. Especially in the prototyping phase, fast, on-site fabrication methods allow a high throughput of different designs. As the choice of actuation is hydraulics, sealing and pressure resistance have to be taken into account as well. Further requirements given by the (soft) robotics community are large deformation, fast motion and lightweight design [137]. As none of these requirements are directly contradicting with the spider-inspired mechanism, they will be implemented into the design and fabrication process. Scalability and environmentally friendly approaches were further criteria I set myself, although they were not first priority goals.

Along my PhD, I have tested a various number of fabrication methods and designs and would like to give a short summary and critical review of each of the methods in the following. An overview of all tested method are given in tab. 6.5.

4.5.1 Fabrication Methods Review

4.5.1.1 2D to 3D membrane fabrication

As the underlying spider-mechanism requires folding and unfolding motion similar to techniques used in origami and origami-based robots, the idea came up to start in 2D plane, to integrate stiff elements and folding lines, before creating the final tubular 3D shape (fig. 4.6). To create the stiffness variance, several techniques and materials were tried. While simple paper, cardboard and tape were ideal to create a quick version for testing the folding mechanism, they were not robust enough to withstand many cycles and water resistance as well as sealing were another issue. Alternatively, BoPET (biaxially-oriented polyethylene terephthalate) foil sealed with heat allow the forming of water repellent chambers. Stiffness variance as observed in the articular membrane of spiders was then created by integrating stiff elements as e.g. thin metal sheets or thicker rubber pieces glued on top. A similar technique was tried with self-sticky Nylon tape, where the metal sheets were glued inside, resembling the membrane of a stroller-umbrella. Another approach was integrating stiff elements on a fly-screen using FDM (fused deposition modeling) printing and sealing the grid with latex or silicon later on.

Figure 4.6: 2D to 3D membrane fabrication. Left: Cutting pattern for membrane with pockets to fill in stiffer elements. Middle: BoPET foil attached around stiff rings. Right: 3D printed PVA (polyvinyl alcohol) on fly net and subsequently cast in latex.

While all these methods allow to create flexible and light membranes with integrated stiff elements, the final forming of a functional 3D shape is challenging. As the whole membrane needs to be integrated into a tubular shape, attachment points for a hinge joint are necessary, which always result in weak points of the design. As the design is much smaller than the stroller-umbrella and needs to further have an integrated chamber and to be sealed, fabrication was

challenging. As this method would not allow fast prototyping and would also not be robust against fabrication and testing damages, it was put on ice.

4.5.1.2 Flexible ring cascade and casting

As the hinge joint connection in combination with a flexible membrane and stiff elements was one of the key weak points when assembling, an alternative approach was tested. By 3D printing three rubber rings, all connected on one point, a pin connection hole for the hinge joint could be avoided. By fanning out the three rings, a flexible material e.g. silicone or latex should then be casted in between the rings to form the thin membrane. However, the casting method turned out challenging and not successful. First of all, the liquid casting medium had to be prevented from flowing away from the gaps between the rings. Second, silicon did not fully cure on the used rubber material of the rings and latex did not form a proper bonding. Other casting materials as liquid plastic or chitosan turned out either too thick or too stiff. Glueing thin PET (polyethylenterephthalat) foil on the rubber rings was tested as an alternative, but the liquid super glue used to flow away from the rubber rings and formed stiff elements in between. Although this method might work with other casting materials, it was still discarded as the connection to the complete actuator would have created another weak point.

4.5.1.3 Molding

Molding is the current method to go to when working with silicon-based soft actuators. By casting the liquid components of silicone into the desired negative shape, 3D forms can be created. The negative shape can be 3D printed and using anti-molding spray, silicone can even be prevented from curing at specific areas to create chambers. This method is very useful to create very thin elements and to fabricate many samples of a specific design. Disadvantages are that some designs with layers of inner structures cannot be easily fabricated. Instead of casting the negative form, water-soluble 3D printed positive forms can be created and silicone or latex casted on top. In general this method takes a lot of time in the beginning, as the mold has to be created first before casting and the curing time can take from several hours to days. Therefore this method was not chosen for prototype designing, but might be the way in future for smaller versions of the final design.

4.5.1.4 3D printing

During my PhD, I had a various number of 3D printing methods and materials available, which are critically reviewed to give the reader a detailed insight into

why the final method was chosen. When starting with the first prototype, the Max-Planck-Institute had a 3D printer (Stratasys Objet 226), which allowed 3D printing of rubber (Tangoblack) and stiff (VeroClear) polymers. This 3D printer was used to design the first stiff prototype published at ICRA 2017. While the 3D printer allowed fast, precise and multi-material prototyping, it has a downside for the designs I was trying to achieve. When printing a hollow structure, this printing method uses support material on the inside, which needs to be washed out carefully. Thin and delicate membranes and pieces can get damaged or ripped during this process. Cleaning in Sodiumhydroxide helped to avoid this damage but resulted in long waiting and washing processes and a large waste production. Although water soluble support material was in development by the company, I never had the chance to test it. Furthermore, the available rubber material started to get sticky after washing, which would have created undesirable friction. I further tested the in house SLA (stereolithography apparatus) printing (Formlabs) service. However the available rubber material showed similar stickiness issues and prints tended to have an unpleasant smell.

With the switch to ETH Zurich, I was able to access a SLS (selective laser sintering) printer (HP Jet Fusion 3D 4200) at Wyss. This method allowed to 3D print lightweight structures, which were also water tight at the end, however the flexibility of the material was limited and the total time from ordering to receiving the 3D print took 4-5 days, which was too long to allow quick prototyping, beside the cost of 15-25 CHF per print.

Although FDM printing was considered not as precise as the other approaches, low price 3D printers with high precision and new available materials have come into the market during the period of my PhD. FDM printable silicone was freshly available, but unfortunately the material could not be printed very thin (below 0.5 mm) yet. Furthermore prices per print ranged from 60 - 100 Euros, which made silicone FDM printing not the method of choice for prototyping. Talking to several researchers at ETH, including to the Complex Material Group, who were working on silicone printing, they suggested to use thermoplastic polyurethane (TPU), a rising star in flexible FDM printing material. However, the suggestion came with a warning, that the printing conditions are highly depended on the brand and the used 3D printer.

The in house Ultimaker FDM 3D printer was tried at first. This 3D printer can print two different materials, using two different nozzles. While this 3D printer allowed precise 3D printing of the common PLA (Polylactic acid) material, TPU needed special adaptation in parameters. As the 3D printer was frequently used for other student projects, the second nozzle therefore needed to

be frequently calibrated and parameter adjustments were limited. A common problem was material clogging as PLA and TPU have a slightly different melting point and nozzle cleaning of the Ultimaker is very time consuming. In the end, I decided to use my own 3D printer (Creality Ender) in order to test different print settings and to use it only for the given TPU material. For TPU printing, I needed to find the right printing heat, so that the material melts, but hardens quick enough. This 3D printer allowed me to vary and control printing speed, cooling fan power, material flow, bed heat and nozzle heat on the fly, so that I was able to find the optimal printing parameters. Traditional bowden extrusion, where the material is pushed forward through a long tube, turned out not to provide consistent material flow when using flexible TPU filament. Therefore I changed the printing head of my 3D printer into direct extrusion, so that the material is directly pushed into the nozzle (fig. 6.11).

4.5.2 Sealing Methods Review

When working with hydraulic mechanisms, sealing is one of the great challenges to overcome, especially when handling dynamic objects and the material is constantly exposed to stress when used. While TPU is water-repellent itself and the 3D print can hold liquid without leakage, small irregularities can lead to water loss under pressure. As sealing methods for 3D printing are not well-established yet, several methods and materials were tried (tab. 6.6) and reviewed in the following sections.

4.5.2.1 Dipping

Dipping 3D prints into color or water resistant liquids is a common approach to give PLA prints a specific finish. Therefore, dipping the TPU print into liquid and flexible rubber material seemed to be the most promising way. Unfortunately silicone is not meant for curing on polyurethane surfaces. Latex and Plastidip worked easily. By letting the excess material drip off and curing at room temperature, very thin sheets were created. However, the viscosity of Latex and Plastidip can vary with temperature and batch, therefore the resulting thickness can vary a lot. Natural latex milk is normally mixed with ammonia to make it more liquid and lower viscosity. The ammonia level can also have an influence on the latex layer thickness. Thick cover layers have a great impact on the folding behavior and prevent the actuator from working properly and should therefore be avoided.

Another downside of Plastidip is its environmental harmfulness and the penetrating smell of petrol which makes it uncomfortable to work with. The ammonia in latex milk also causes an unpleasant smell and therefore only low

ammonia latex milk was used in a well-ventilated room to evaporate.

A disadvantage of the dipping method is that after using the actuator for a couple of times, the layer slowly detaches from the actual 3D print and water starts to accumulate inside the space between the 3D print and the cover layer. Furthermore, the holes used for flexing wire attachment are normally also sealed, when poking them open again with a needle, leakage can occur at these points. Moreover, scratches on the outside could already cause leakage and latex gets brittle when getting in contact with oil or left in the sun.

4.5.2.2 Spraying

PLA prints are also often sprayed with color or rough material, therefore spraying of anti-leakage spray and soft rubber was also tested. As listed in the table 6.6 some materials "attack" the TPU and stiffen or dissolve it slightly. Stop-leakage sprays form foamy structures, resulting in thick layers. Liquid rubber and spray-able Plastidip formed a thin cover layer on the outside of the 3D print. However, this layer is often too thin and rips easily and it does not fully seal the whole 3D print, especially on the inside.

While spraying might be an ideal method for color finish on larger objects, it was not very successful as sealing method.

4.5.2.3 Inside filling and baking

Although latex was not fully successful for outside dipping, it was finally used to fill the chamber. By baking, the latex directly in contact with the TPU cures, while excess latex stays liquid and can be pressed or washed out afterwards. To prevent thickness differences due to gravity, the 3D print was constantly rotated.

This method turned out successful and showed to withstand pressures over 200 kPa and did not influence the folding behavior nor the force needed to flex the prototype. An interesting aspect of latex is that in contrast to silicone, latex can cure on itself to provide thicker layers. When the inner bag is damaged, latex milk can be refilled into the chamber and the damage can be sealed again. Further testing is needed to see how often this kind of sealing can be carried out and whether the thickness of the latex inside increases over time.

4.5.3 Design of Spider-Rotary actuator

Along the decision on the fabrication method and biological studies, the design of the prototype changed continuously. In figure 4.8 the evolution of the prototypes is shown. In the following sections, I would like to provide the

conceptual ideas behind each of the evolution steps and the lessons learned from each step.

4.5.3.1 First trials

First drawings and prototypes have been designed with Solidworks. Although I have gained some experiences in drawing standard shapes and single elements with CAD (computer-aided design) programs, the challenge was here to design a complete functional actuator without any assembling elements. At this point, the 3D reconstruction of the jumping spider joint was not yet finished and directly transferring dimensions of the jumping spider joint seemed not to be useful anyway, as thickness will variate and muscles are not integrated. Furthermore it was not about drawing a spider leg model, but rather designing a functional prototype with features inspired by the spider. The only interesting geometrical number I tried to transfer was the angular distance between the different hoops. A finger-sized prototype was aimed for, as this is a reasonable dimension to work with, without getting into fabrication limitations especially when things still need to be manually fixed or changed. Four problems needed to be tackled. The first one is the design of a foldable membrane, the second is sealing of the leg for actuation by e.g. a chamber, the third focuses on the hinge joint itself, which needs to be able to follow the complete folding motion and the fourth problem comes with the idea to print the complete membrane without support.

The membrane needed to be thin enough to stay flexible for the folding, however the thinness of the membrane is limited by the 3D printer's resolution and also depends on the printing angle. In contrast to designs published by other researchers, the idea was to integrate the membrane directly into a chamber as it could be observed also in the spider joint itself. This would reduce the amount of fluid that is needed to be displaced during motion, reduces the overall weight of the prototype and the hinge joint can be designed separately. The reason why I wanted to avoid support is that the thin membrane element could get destroyed during cleaning and any support remnants would influence the folding behavior. Water-soluble support material was tested on the Ultimaker 3D printer, but normally doubled the printing time and the material had to be dissolved afterwards. Furthermore the change between TPU and the support material (PVA) was not always successful at very thin structures, which led to holes in the print. Printing without support with an integrated chamber only allowed one printing direction at the end (fig. 6.11).

The first printing tests showed several issues. First of all the bottom layer was loose and with the increase in Z-axis, the leg started to wobble due to the

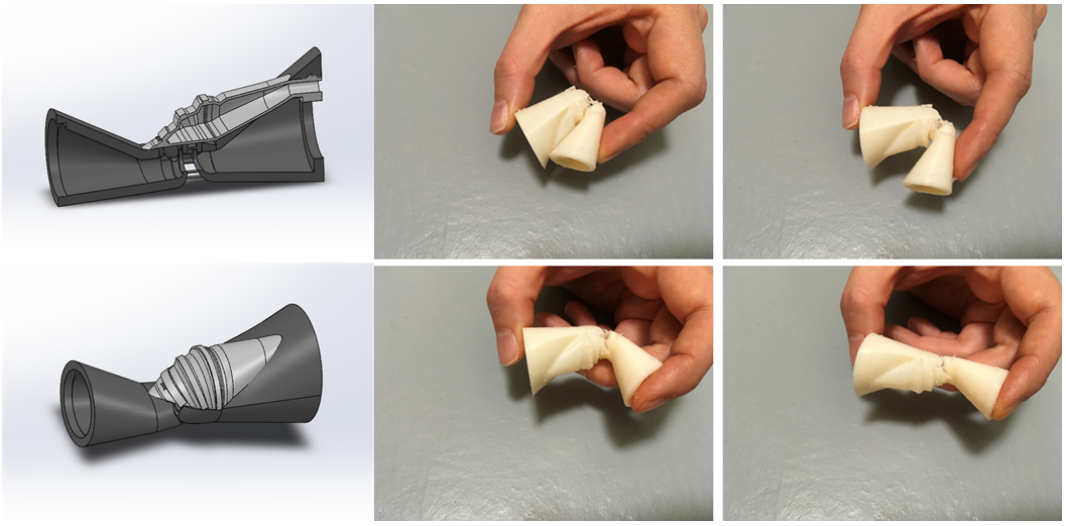

Figure 4.7: Intermediate status of spider inspired design. As it can be seen from the 3D drawings on the left side, the design consists of two "leg" segments (dark grey) and a small chamber with thick hoop elements (light grey). Although the chamber shows thicker hoops with decrease diameter, the folding does not occur as the pivot point is not defined in a right manner. In this design the joint was cut open after 3D printing to avoid ripping of the joint during flexing. This step revealed that the place and shape of the pivot point is critical to achieve the folding behavior to create a large working angle.

flexibility of the material. At this point, I was also still struggling to find the right printing parameters as, although printing a sheet or a small cylinder of TPU worked out fine, detailed prints caused clogging of the material when the flow and temperature were not right. This nozzle clogging was also the reason why after several runs, the prints started to have only a meshy structure instead of a solid print. To avoid this issue, I tried to print it in a slow mode to give the material enough time to flow, which ended up in printing times of over six hours and unfortunately the printing result was still not satisfying. Later, I found out, that this problem was not only a problem of the 3D printer and the material, but also on how Solidworks turns the 3D construct into a triangle mesh stl-file and how the slicer program, CURA changes that into machine gcode. The lessons to learn from this first attempt (fig.4.7) was to find the right printing parameters for high printing designs. The hinge joint was another issue, as it tends to rip when the joint is flexed. The membrane was attached to the patella segment through a single point. While folding could be observe at the first hoop, the larger hoops were just pressed down during flexing. The chamber however still appeared too angular and flat. Furthermore

the pivot point seemed to not lie at the right position. By manually drawing support lines at the hinge joint, which were cut open after print, the pivot point could be laid closer into the center of the 3D print, however the print result was still not satisfying.

4.5.3.2 Redesign

In a next step, the leg was completely redesigned using Fusion360. It allowed a better pipeline for 3D printing as the CURA slicer is directly integrated. Furthermore, drawing of non-linear lines and resulting shapes as well as generation of shell designs were generated easier and printing results were more consistent. In combination with the change into direct extrusion, the printing of thin membranes down to 0.4 mm was possible and printing time was reduced drastically down to 1 hour. The hinge joint still remains a thorn in the eye. By reinforcing the joint connecting, I hoped, this could prevent the ripping, unfortunately it just did the opposite as the increased thickness just resulted in a stiffer material. The hoops were now covering a larger area of the membrane. However the folding of the chamber was still not perfect. At this point, the hoops did not have the right dimensions and the distance between the hoops was not right, the membrane was not folding into each other yet.

4.5.3.3 Final approach

Findings from the previous design revealed, that the hinge joint needed to lie closer to the center axis of the model. Furthermore, it needs "enough material" to allow the complete bending of 125°. By designing a circular pivot point (fig. 4.9) this problem was solved. However, the printing of such a circular shape was only possible when keeping the gradient of the print in such a way, that overhang was still printable. Otherwise the print can start wobbling during the printing process and when the heating base is not perfectly calibrated, the print can peel off. Different to the previous design, the hoops needed to change orientation on the membrane. When drawing a 2D sketch, it reminded of the Pythagorean spiral, however this spiral needed to be stretched as the additional thickness of the hoops for the stiffness variance needed to be considered. While in 2D things were pretty clear, the elliptic cross section of the leg at each of the hoops needed to also allow the folding. Finally, the resulted design showed hoops, which were sliding into each other folding without ripping the hinge joint. Interestingly, the angular width of the thicker hoop (black part in fig. 4.9) is almost similar to the angular width of the thin foldable part in between two hoops (white part in fig. 4.9). When thinking about implementing a sliding or folding motion, one would intuitively think, that the thin foldable part has

Figure 4.8: Evolution of actuator design. Shown are a selection of the iterations made to achieve the final design. The first two designs were drawn with Solidworks. Bowden extrusion led to printing errors and the pivot point constantly ripped. The third design was a complete restart with new drawings using Fusion 360 and direct extrusion. Very thin membranes (0.4 mm) could be achieved. The next design had better working pivot point, but the sliding and dimensions of the hoops were not right yet and resulted in membrane ripping. The black print is the final design but sealed with PlastiDip. On the very right, the final design with a thin latex layer on the inside to seal any printing irregularities.

to be twice as large as the thicker hoops, however the spider membrane did not show this, nor does the final design.

4.5.3.4 Future extension

The prototype is designed in such a way, that it can be extended for multi-joint applications. Connection between several segments can either be directly 3D printed or supported by latex, creating a passive joint as observed for the patella-tibia joint in spiders. Currently the tube to prototype connection is made by purchasable stiff connectors, forming a weak and leakage point in a design which otherwise does not consist of any assembling parts. While leakage can be prevent by using latex, the stiffness of the connector can be bypassed by directly integrating the connection in the future model.

4.5.4 Design Ideas for a Flexing Mechanism

As spiders use muscles for flexing, the flexing mechanism was not of focus in this thesis. At current state, the flexing wire is layed outside, to allow quick exchange of the wire. Future approaches could directly 3D print a flexing wire on the inside to understand how the muscle position allows the large

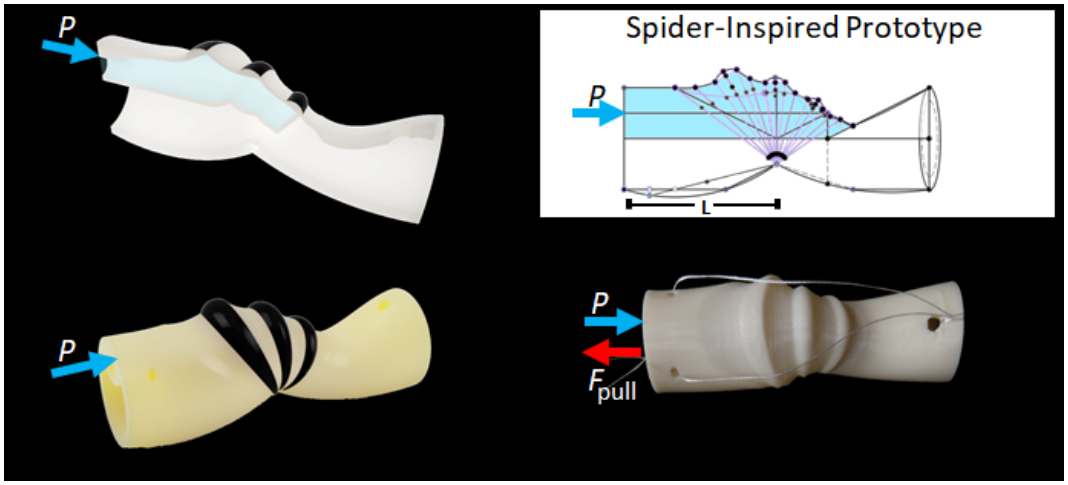

Figure 4.9: Spider inspired prototype. Published in [43]. Left: 3D rendering of spider-inspired design. The actuator consists of three thicker hoops with folding lines and form a chamber inside which extends when filled with water. The finger-sized prototype has a length of 6 cm and width of 2 cm. Top Right: Schematic drawing of spider-inspired design. The pivot point is designed in such a way that it enables a working angle of 125°. The chamber which is filled with water during extension is marked in blue. The femur leg has a length (L) of 3 cm. Bottom Right: The 3D printed TPU prototype has a 0.4 - 0.45 mm thick folding membrane. By increasing the pressure P, the leg is extended, flexing is induced by pulling on a flexing wire (F_{pull}).

working angle of up to 160°. Beside using wires as tendon for flexing, springs, artificial muscles and or a similar folding mechanism, as used for extension, could be implemented instead. Using wires antagonistically to the hydraulic mechanism brings the advantage that the joint angle can be controlled easily as it is proportional to the wire length. Furthermore, motion speed can be varied depending on how fast the wire is released or retracted. Furthermore it allows to hold the legs in flexed position, while increasing the pressure inside. The wire does not increase the weight at the joint, nor does it need a bulky construct which might reduce mobility. The downside of wires might be that after some time of usage, they can wear out, which would decrease precision of the mechanism, if the wire length is used to predict the joint angle. That is why braided fishing line was used as flexing wire as it is known to not be stretchable, but robust and abrasion resistant. Still, the attachment point of the wire is exposed to great stress, which could lead to stretching of the flexible material after several cycles of usage and therefore decrease in precision.

To allow multi-locomotion including walking and jumping, the control of

Figure 4.10: Working principle of ratchet release mechanism. Left: The ratchet (green) can be loaded be turning anti-clockwise. It is blocked by a pin (yellow) to avoid unwrapping. This pin is held in position by a spring (red). Right: By pulling on the pin through a motor (grey), the spring is compressed and the ratchet is released and turns clockwise.

wire flexing in combination with hydraulic extension need to work in tandem. Several design ideas will be introduced in the following.

4.5.4.1 Controlling semi-hydraulic actuators

While pulling a wire can be easily controlled by a linear actuator or by rotation around a cylinder, the displaced liquid needs to be pushed back into a reservoir. And this water needs to be again pushed back from the reservoir into the chamber for extension. By designing a rotational chamber (fig. 6.11) with an internal latex chamber for sealing, the liquid can be collected by increasing this volume while reducing the wire length when rotated around this chamber. By closing the reservoir shells, the volume inside decreases, while the wire gets released again and the water is pushed back into the leg. Not intentionally inspired, the reservoir shells somehow resemble the prosoma of spiders, which are assumed to decrease the volume inside by pushing the two prosoma shells towards each other and move the volume into the legs.

While in spiders, the muscles and prosoma reservoir are disconnected, the proposed mechanism has the disadvantage to not allow an increase in pressure inside while holding the muscle in position, an idea would be a hook mechanism, which holds the wire in position while the liquid is pushed back into the legs and which can unlock for jumping.

4.5.4.2 Ratchet mechanism

For demonstrating jumping motion, where high pressure needed to be build up while the legs are in flexed position, a ratchet was used for flexing several legs simultaneously (fig. 4.10, 4.19). The legs were locked in this flexed position,

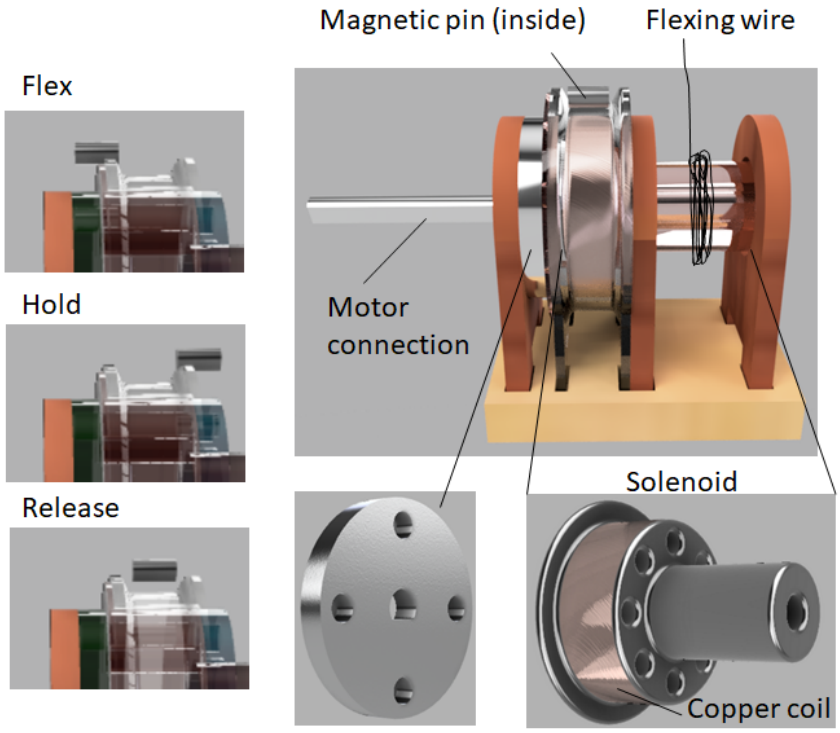

Figure 4.11: Conceptual design of magnetic release mechanism. The idea is create a switch between three stages (flex, hold, release), which can be used continuously to create different modes of (multi-legged) motion. In "flex" the wire is wrapped around a cylinder by a motor. By switching to "hold", the current state of wire shortening is fixed as the wire is now decoupled from the motor motion. By changing into "release" mode, the flexing wire can immediately unwrap, allowing a fast extension motion for e.g. jumps. The three different modes should be created by a solenoid switching small magnet pins into the different positions.

while pressure could be increased independently using a syringe or a pump. Afterwards a release mechanism pulling the ratchet stopper, allowed the legs to extend almost immediately, enabling the jumping motion. The ratchet did not allow slow motion as proposed in the previous system and the flexing motion was not coupled to the fluid flow and pump mechanism. This means that during flexing, the syringe or reservoir needed to open continuously, to collect the water.

4.5.4.3 Magnetic release

For future applications a system of solenoids allowing a walking and jumping mode could be a possible solution. Using a magnetic switch, the flexing wire can either be shortened, stayed locked or released. Using this mechanism, several legs could be integrated to a single motor, while still being decoupled. This kind of mechanism could further allow all three modes as the magnetic switch can be electronically switched into the desired position.

4.6 Characterization of the Prototype

The final design can be found in figure 4.9. It shows three thicker hoops which can be folded into each other. The advantage of this folding and the reinforced hooped is elaborated in the following. Afterwards flexing and extension of the prototype are characterized to give information about its performance. Finally several possible applications are demonstrated.

4.6.1 Comparison of folding behavior

The final design shows a large working angle of 125° and stiffness variations throughout the hydraulic chamber as inspired by the spider's articular membrane on the femur-patella joint. While in other soft fluidic actuators reinforcement is integrated to prevent the material from "overblowing" and for a better control, the joint movement of spiders and of this prototype is not based on expanding the membrane, but unfolding it.

At this point, one can ask, what are the advantages of such a "reinforced" membrane then? Similar working angles can also be achieved by designs without this reinforcement and thickness variation. To get a first insight of the advantage of this reinforcement, I designed three "control" prototypes which do not show the reinforcement. The first one consists of a bladder which covers up the same volume as the spider-inspired design, but does not show any folding lines nor thicker elements. The second control design has just a simple flat membrane. The third shows the same shape and folding lines as the final prototype but does not have the thick hoops as elements. Each of the four designs was run for 4 hours, in total 1000 cycles to test the robustness. All control designs showed damages afterwards (fig. 4.12). This can be explained due to sharp folding edges. During flexing, a lot of the membrane material needs to be displaced. The spider-inspired design supports this displacement by controlled folding, however the large bladder control design and the flat membrane design do not, which results in undesired wrinkles with sharp edges, where the damage occurs. In the case of the control design without the thick

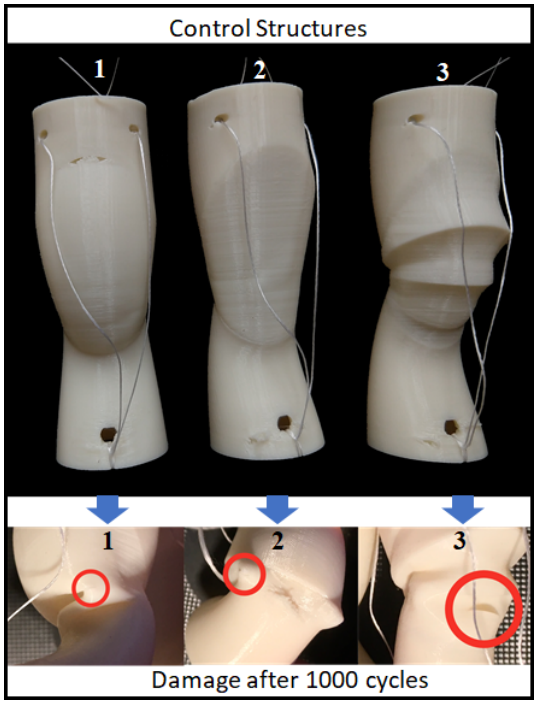

Figure 4.12: Cycling Testing of prototypes. Published in [43]. Beside the spider-inspired, reinforced structure, three control structures were used for testing the folding. While the spider-inspired design folds properly and does not show any damages after 1000 cycles, the control structures without reinforcements or folds show undesired wrinkles which finally lead to rupture.

hoops, but with the folding lines, the membrane does fold, but cracks occur at the folding lines as the 3D print itself creates sharp edges already. In the case of the flat membrane, not only is the chamber damaged but the hinge joint cracks. It can be proposed, that the reinforcement of the articular membrane of spiders is supporting the material to withstand high pressure, but more importantly it allows a proper folding of the membrane and therefore reduces damages which would be fatal for the hydraulic actuation. In spiders, damages directly at the hinge joint connection are normally avoided by a short and thin membrane extension connected between the arcuate sclerite and patella segment. However tiny damages at the hinge joint have been observed, when the joint is bent too strongly, which happens when the animal falls from large heights without securing its body with its usual safety wire. As the main membrane is not damaged and the tiny droplet of body fluid quickly coagulates at the hinge joint, the spiders were still able to walk without any fatal damage.

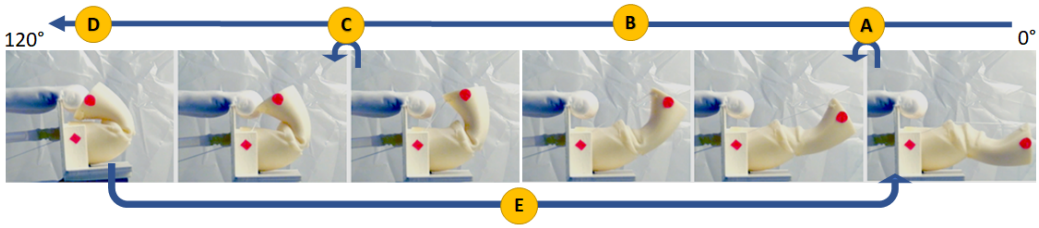

Figure 4.13: Flexing of spider inspired actuator. Published in [43]. To test the flexing and releasing behavior, the actuator was clamped inside a platform and manually flexed by a string. Red markers were used to track the angle in parallel to measurements of a pressure and force sensor. The flexing behavior can be divided into three parts (A, B, C). The initial pulling (A) does not influence the inner chamber. Pulling direction is almost orthogonal to the moving direction. (B) Pulling above 20° leads to the folding of the first and second ring. Pulling and moving direction are in parallel. (C) In a last step, the third ring is bend into the material, which creates large elastic energy. Pulling direction is furthermore almost orthogonal to moving direction again. While flexed, the actuator can be pressurized (D) before releasing (E).

4.6.2 Flexing

In a first step, the needed flexing behavior was characterized. Therefore, the leg was attached to a load sensor and flexed by rotating a water collection chamber to couple the flexing with the water collection. The experimental data shows that the flexing of the prototype can be divided into 3 phases (fig. 4.13, 4.14). When the leg is completely stretched out, the force needed to flex the leg increases up to 2 N. The next phase describes flexing angles of 20-100°. Here the measured flexing forces are staying around 1.5 N corresponding to torques of 0.05 Nm. The last phase describes the last infold where flexing forces increase drastically up to 5 N (0.15 Nm). This increase can be explained by the large area of material that needs to be bend and the thickness of the material. The measured flexing force further depends on the attachment points of the wire and the relative angle the wire is pulling at. When spanning the wire through the holes of the leg and pulling, the folding direction and the pulling direction are almost in parallel for angles between 20-100°. This is not the case for folding above 100°, as the second leg segment (patella) is now closer to the first (femur) and therefore the folding direction is almost orthogonal to the pulling direction. This effect can be seen more clearly when the wire is not threaded through the side holes of the femur segments. In this case, the forces needed increase linearly at each "hoop" for 3-4 N, so that for the final fold forces of up to 10 N are necessary. As spiders have their muscles on

the inside, an interesting question for future studies could be, how the muscle attachment points and the rotating arcuate sclerite reduce flexing forces. It can be assumed, that the rotation of the arcuate sclerite continuously reduces the distance between the two spanning points of the muscle and therefore support the overall shortening of the muscles. Interestingly this measurements also reveals that when holding the leg segments in flexed positions, then pressurizing up to 50 kPa and release the flexing wire in a sudden, the pressure drops into negative values for a short time.

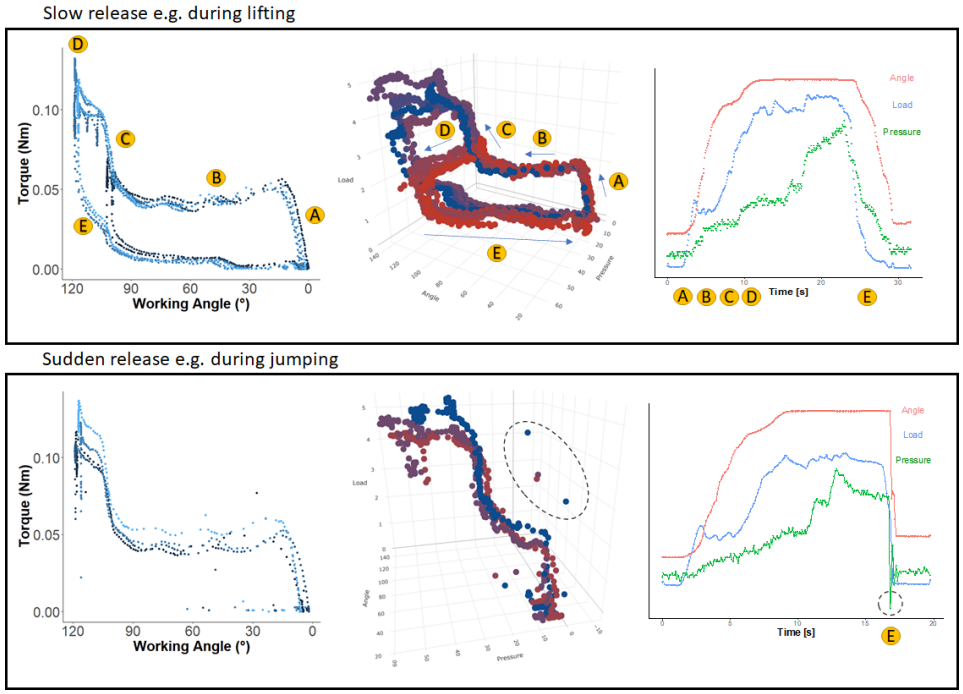

Figure 4.14: Angle-pressure-load characterization of spider inspired design. Published in [43]. Joint angle, load and pressure were recorded while flexing the joint using a a flexing mechanism, where the pushed-out water was collected into a latex bladder simultaneously. Two different release modes were tested. Top: Slow release (n = 6). A slow flexing and extension can be e.g. observed during lifting or grasping motion of spiders. Bottom: Sudden release (n = 4). The pressure is increased inside the chamber while keeping the leg flexed, before the flexing wire is released quickly. This results in fast extension needed for e.g. jumping. To characterize this behavior, the flexing wire was detached from the flexing mechanism to allow a sudden release. The flexing behavior can be divided into different phases (marked in yellow). In the first 20° working angle (phase A), the chamber is not flexed, so there is no pressure increase. When flexing further (phase B), the measured load shows dips for every stable position, but stays almost constant at 1.5 N ($\sim$ 0.05 Nm torque). The flexing forces increase rapidly to 4-5 N, when flexing the leg over 100° (phase C). The pressure constantly increases while flexing the leg, up to 30 kPa. When increasing the pressure manually with a syringe up to 50 kPa (phase D), the load shows almost no increase. Measured increase in load vary from 0.0-1.5N. When manually and slowly releasing the leg, the measured load drops down immediately, while pressure decreases constantly with the opening of the chamber. When carrying out a sudden release of the leg, the load and pressure drop immediately (dashed circle). Higher pressure values could not be tested as the collection latex bladder as well as the raw 3D printed actuator showed leakage issues.

4.6.3 Extension

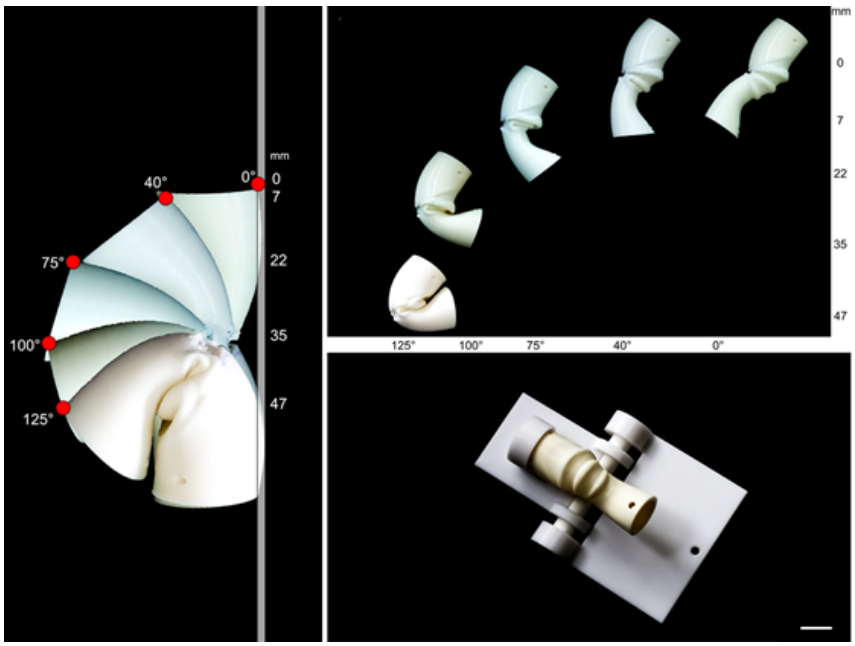

Figure 4.15: Experimental platform. Published in [43]. Similar to collapsible silicone bowls, the prototype shows five stable positions (0, 40, 75, 100, 125) created by the design and elastic material. The angles correspond to opening distances, for a ("patella")-segment length of 30 mm. Spiders show leg angles between the shown position 40 and 100 during walking and resting. Full closing (position 125) can be observed in dead spiders, when muscles are flexed, as well as in jump initialization. Spiders communicate with completely opened (position 0) front legs, showing their articular membrane to their fellow species. Fully extended femur-patella joints can also be observed during jumps. To measure the pressure-load-angle behavior at the stable positions, the prototype was clamped between the two plates to a given angle. The bigger plate is attached to a load sensor, the leg to a syringe and pressure sensor. Sensor data were recorded with an Arduino Uno, while pressure was increased with the syringe. Scale bar: 10 mm.

By using the measuring apparatus from the previous section, it could be seen that the torque is released almost immediately after the leg is released, slowly or suddenly. Interestingly, a sudden release could cause a negative pressure for a short moment, which can be explained by the fluid intertia and viscosity, as water needs to be shifted into the opening volume. This effect is known for hydraulic pistons, causing cavitation, where sudden air bubbles form, burst

and damage the surfaces. One can now be asked, whether spiders also have to struggle with such a dramatic change in pressure during a jump and whether the properties of the hemolymph prevent such behavior. Different to hydraulic pistons, spider have a continuous flow, which might support a volume shift already.

To test the highest forces that can be produced for extension, the experimental setup was changed (fig. 4.15) as the previous design could only allow pressures up to 50 kPa before the tube connection failed. Keeping the leg flexed in a specific degree and position, the water was now directly pushed into the leg by a syringe. Force and pressure were measured and jumping heights simulated (fig. 4.16, 4.17).

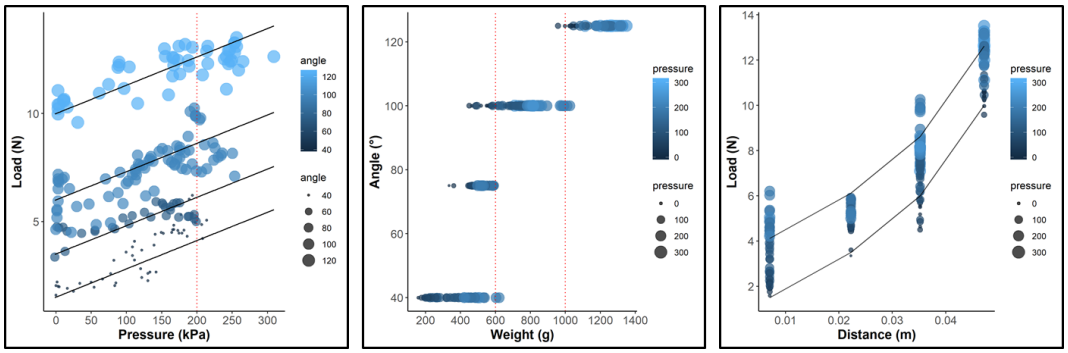

Figure 4.16: Angle-pressure-load characterization of latex sealed spider inspired design. Published in [43]. Left: The load and pressure at the stable positions (40°, 75°, 100°, 125°) have been measured. The value of angles was always defined as 0° in extended position and 125° in fully flexed position. Loads at zero pressure, reflecting the elastic forces of the material, were verified by the weight needed to flex the leg into a specific position (tab. 6.7). Linear fits show a factor of 0.013, which for $P = F/A$ would result in an effective area of $A = 13\text{mm}^2$. Middle: By transforming the measured load into its corresponding weight, the experimental data predict full lifting of 600 g at 200 kPa. Furthermore, up to 1 kg can be lifted for 20 degrees. Right: By transforming the angle into opening distances (fig. 4.15), the work generated by a single leg can be calculated.

The experimental data shows that weights up to 600 g can be fully lifted with pressures of 200 kPa. Furthermore lifting of weights over 1 kg from flexed position into 90°can still be achieved.
The generated work W of a single leg can be approximated by

$$W = 105.86 \cdot s^2 + 1.6731 \cdot s \tag{4.1}$$

$$s = l \cdot (1 - \cos(\alpha)) \tag{4.2}$$

with s giving the angular flexing distance, α the flexing angle and l the length of the patella segment of 30 mm. This generated work can be converted into jumping height (potential energy) by

$$h = \frac{W}{mg}, \tag{4.3}$$

This would mean that for a fully flexed (125°) leg, work of 0.3125 Nm can be generated. When neglecting the work needed to simply open the leg, the hydraulic generated work would correspond to an estimated jumping height of 3.19 m for a single leg with a weight of 10 g. The work created by the material only, thereby contributes to 0.096 Nm, corresponding to a jumping height of approximately 0.98 m. By simply flexing the leg and letting it catapult itself up in the air, jumps of 0.5 - 1 m height could be observed, whereby the launching angle could transfer some of the released work into lateral motion. The jumping height is drastically reduced when weight is added onto the system as simulated in figure 4.17 for a jumping platform (fig. 4.19).

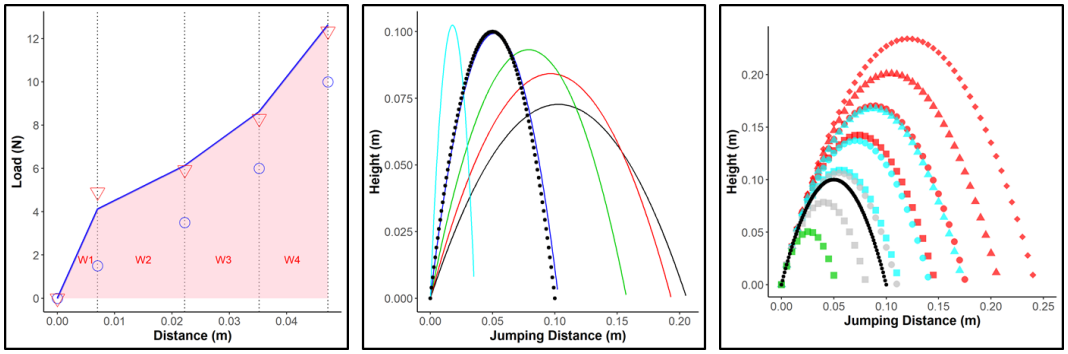

Figure 4.17: Jumping simulation. Published in [43]. Left: The work, W, can be approximated by the area (light red) below the load-distance curve and shows a quadratic characteristic (4.1). Blue circles show forces created by the elastic material; red triangles show mean of experimental data at pressures (200 kPa +/- 5kPa). Middle: The estimated work was used to simulate the jumping height and jumping distance at launching angles of 45 to 85° for the jumping platform (fig. 4.19) Right: The flexing angles of front and hind legs are evaluated separately and vary between 75 to 90° (shapes = flexing angle of front legs, color = flexing angle of hind legs). The best jumping performance of the jumping demonstration (fig. 4.19) shows a launching angle of 70-75° with front legs flexed in 80-90° and hind legs in 70-75°, with a jumping height and distance of approximately 10 cm (black curve), which fits to the estimated calculations based on the load-pressure experiments.

4.6.4 Demonstration

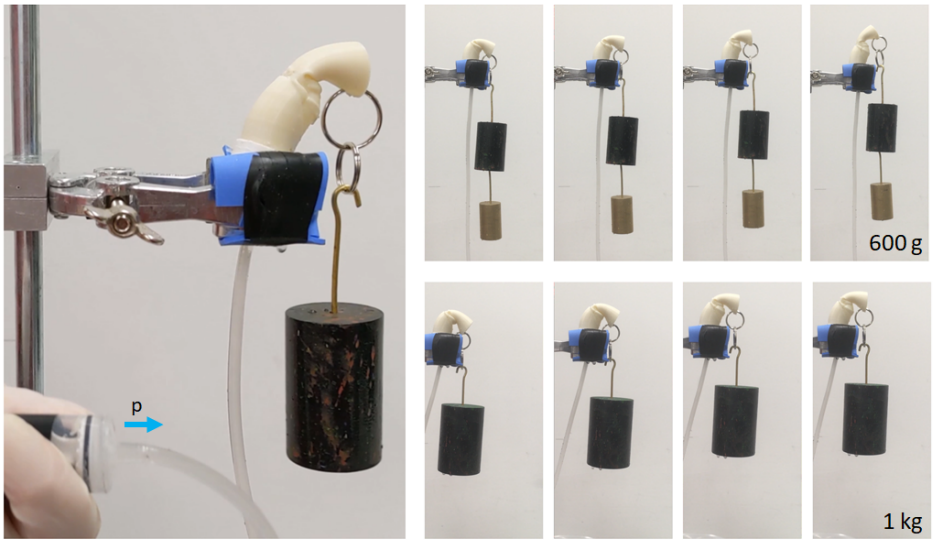

Figure 4.18: Weight lifting demonstration. Published in [43]. By pressing a syringe, the water is pushed inside the joint chamber, increasing the pressure p inside the chamber, allowing the leg to fully lift 600 g. Heavier weight can only be lifted up to 90°.

To verify the estimated numbers from the previous sections, two demonstration set-ups have been build up. The first one shows how much weight a single actuator could lift using hydraulic power. In a second attempt the jumping performance of the actuator shall be demonstrated.

The leg was mounted vertically and flexed by hanging different weights on the second (patella) segment. By pushing water into the leg via a syringe, the pressure is increased allowing to lift the iron weights. 500 to 600 g were completely lifted as predicted. Weights of 0.8 to 1.0 kg could only be lifted up the position of 90-100°. Impulsive pumping could increase the lifting height as the weight starts swinging. Weights over 1 kg can therefore still be lifted up to the 100°position. However, weights above 2 kg can lead to high internal pressures of 250 to 300 kPa, which could lead to leakage at connection points or the membrane. The lifting demonstration is fully reflected by the estimation of the previous section.

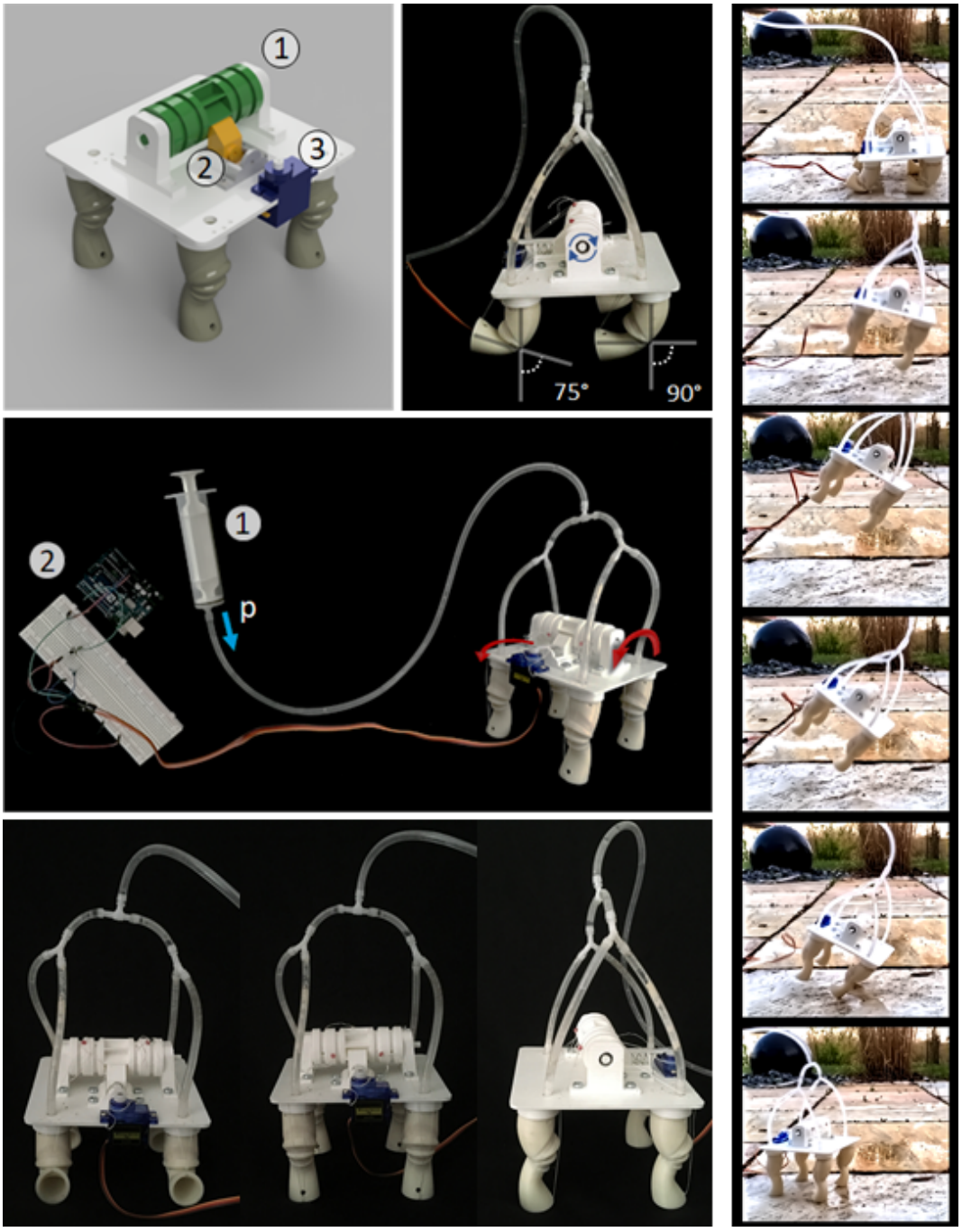

Figure 4.19: Jumping platform demonstration. Published in [43]. Top Left: 3D CAD model of the jumping platform. (1) Ratchet for flexing the legs, (2) Stopper which stays in position by a spring. (3) Servomotor, releases the stopper and ratchet. Top middle: 3D printed and assembled jumping platform. Ratchet is activated and legs are in flexed position. The front legs show flexing angles of 75°, the hind legs 90°. Middle: Activation of jumping platform. (1) Legs are connected to a water filled syringe via tubes. By pressing the syringe, the pressure is increased inside the legs. (2) The servo motor is connected to an Arduino Uno. By pushing a button, the servo motor pulls on the stopper to release the ratchet. Bottom: Jumping platform from different directions. Right: Jumping test outside. Platform achieved 10 cm high and wide jumps.

As the launching angle for a single leg, without an attached flexing mechanism and launching platform is difficult to control and the speed is very fast (20 rev/s angular speed), a jumping platform was designed to demonstrate the jumping ability. The jumping platform consists of 4 legs for a stable standing position, a flexing ratchet to hold the legs in flexed position while increasing the pressure and to allow a simultaneous release of all four legs via a servo motor. The total platform weighs roughly 120 g. As the legs are single jointed, the demonstration platform only allows a flexing between 70-90°as further flexed legs would not touch the ground and just hit the ground when released, rather than contribute to jumping. The elastic work generated by the material is not enough to make the platform jump, but allows the unfolding of all for legs and lift the platform from "squatting" into standing position. This means, that it can be assumed that the elastic work corresponds to the work needed to stand up the platform and therefore it needs to be subtracted from the overall work to estimate the jumping height. Given these parameters a maximum jumping height of 23 cm can be estimated for all four legs flexed into 70° angle. However during jumping demonstration it could be observed, that the front legs are flexed in position 70-75°, while the hind legs are opened a little more to position 80-90°. The maximum jumping performance at 75° launching angle was 10 cm height and 10 cm of jumping distance. Fitting the flexing positions into the simulation, it can be seen that the estimated jumping behavior is very well reflected by the calculated data.

4.6.5 Future Studies

4.6.5.1 Further robotic extension

Although first step demonstrations have been conducted in this work, it is still a long way to go to build a full robotic system. The integration of a functional pump system with fluid collection chamber, a flexing motor, battery and sensors would be on the electronic and hardware side. On the software side, the control of pressure and flexing for each of the legs would be necessary. Although valves have not been reported for spiders, it might still simplify the robotic implementation. Flexing mechanisms as proposed in previous sections need to be integrated in such a way that multi-locomotion behavior (gripping, walking, jumping) can be allowed by the system, which might result in higher complexity for the control of the interaction of pressure and flexing force. Considering the torques and pressures measured for the proposed prototype design, heavy pumps and flexing motors needed to be integrated along with a high energy source. While this is the reason why most of today's research on soft robotics have external power sources as they normally run on 10-100 times

higher pressures, the demonstrated prototype is shown to be able to lift large weight, so that a fully on-board multi-legged system might be possible to build. Another step which needs to be integrated would be a hip joint which would allow lateral motion. In spiders, the hip joint is realized by muscles pulling in one or the other direction, so it was not in focus of this study. A robotic implementation for a hip joint could be a simple servo or stepper motor, a wire - based joint similar to the mechanism used in low-cost prosthesis or again a hydraulic or semi-hydraulic joint.

Designed in a modular manner, the extension into a multi-joint leg would also be possible, but increase the complexity in control as more flexing wires are coming into play.

4.6.5.2 Fluid Flow

The experimental study on the influence of viscosity on the hydraulic performance is definitely another wide ranging research question to answer. As the presented sudden release shows a negative pressure peak, it might be interesting to see how fluids with higher viscosity as e.g. hydraulic oil or fluids with non-Newtonian behavior, as observed for spiders, influence the system. This could be done by combining standard fluid flow simulations with direct experiments on the here developed prototype with fluids varying from shear thinning behavior as ketch-up or blood, to shear thickening fluids as starch pulp. In general traditional hydraulic fluids for metal hydraulic pistons are chosen according to their specific purpose and the used viscosity depends highly on the desired working temperature, the dynamic range and the need of lubrication. Experimental studies on non-Newtonian fluid effects are however lacking and might not be only interesting to understand the spider locomotion better, but also to increase performances of (soft) fluidic actuators. Interestingly, a recent theoretical study [4] proposed shear-thickening fluids for hydraulic systems to prevent sudden loading or backflow, shear-thinning fluids however, were not covered in this work.

4.6.5.3 Finite element analysis (FEA)

Using finite element methods to study the material behavior during folding would be an interesting addition to the experimental results presented in this thesis. FEA could give information about weak points of the design and help to optimize the chamber shape. Furthermore it could be further studied how the difference in stiffness and thickness of the membrane would effect the folding behavior and performance of the joint. A particular difficulty for the FEA would be the hyperelastic behavior of the material and the 3D printed

layer orientation. To get a first insight into the material behavior, I have tensile testing of a defined shaped but different orientation of 3D printed layers. Unfortunately, this project was terminated due to Corona lock down and time limitations. Interesting observation to shear is that a printing with layers in parallel to the stretching direction allowed a stretching up to 5 times its original length, before material failure. However, the material did not return back into its original shape but falls apart into single, spaghetti-like strands. Further investigation and experiments will be needed to understand the influence of printing direction and material property on the final design.

4.6.5.4 Bio-material robot

Bio-materials as chitin (base material of arthropod exoskeleton) and silk show desirable features for future robotics. Deacetylized chitin (chitosan), which is used for many medical applications, has got risen popularity in making bio-plastic. In combination with silk, it allows creating of strong and compliant thin sheet structures (like e.g wings). While trying to refabricate the microstructures of the spiders, a thin sheet of silk fibroin layer was fabricated, with variation in stiffness by adding glycerol as a first proof of concept.

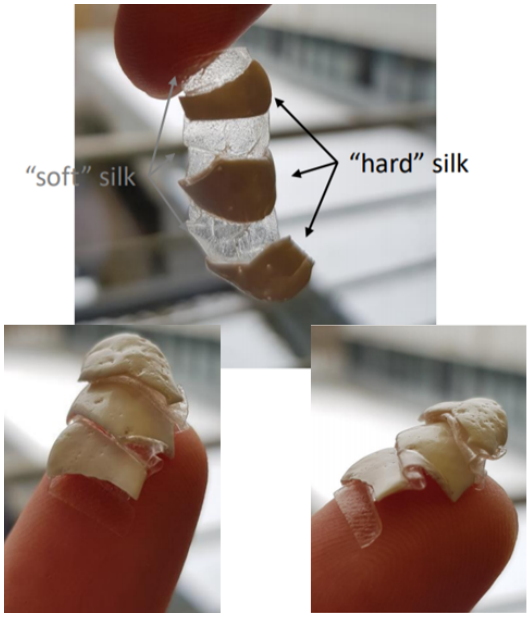

Figure 4.20: Fabrication of silk fibroin membrane with stiffness variance.. Stiffness of silk fibroin film could be variated by adding glycerol (0.35 ml to 14 ml of silk fibroin) into the liquid fibroin before casting and evaporating it into the silk sheet.

4.6.5.5 Future Applications

In the beginning of my PhD, I had the chance to join a interdisciplinary group working on different fields of agriculture (fig. 4.21). The vision was to use a heterogeneous group or swarm of robots which are adapted to specific tasks to allow agriculture in a non-structured terrain. While today's agricultural fields are shaped to fit to requirements of the farming robots, often leading to mono-cultured fields, the idea was to adapt robots to a more healthier multi-dimensional cultivation. In the proposed scenario, larger transport wheel robots, inspection and transport drones, worm-like suction robots and spider robots form a multi-agent system. The proposed work for the spider robots would have been delicate grasping tasks as for berries, wine grapes, but also removal of weeds or plant fitted fertilization. By splitting the tasks, the individual robot only needs to fulfill a limited number of tasks, which reduces the individual complexity. E.g. considering a lightweight spider robot, which is capable of grasping, drones could be used to transport them onto specific plants and back for harvesting or recharging.

The proposed project is not bound to the spider-inspired mechanism, but I personally still think it is an interesting idea to mention, considering that autonomous robots for agriculture become more and more importantly. And I would be more than happy to have a robot taking out the dandelions from my parents garden that I used to dig out for hours every spring. A personal vision I have and which would benefit from the flexibility and speed of the proposed spider-inspired fluidic actuator would be a hand prosthesis (fig. 4.21). Growing up playing piano and having a sister as a professional pianist, the biggest fear was always to injure or even lose a hand. Playing piano involves the interplay of finger, wrist, arm and shoulder movement. While hitting the keys in the right order can definitely performed much simpler by e.g. 88 little servo motors, it does not necessarily give back the music one would enjoy but rather mechanical sounds. It further does not achieve the "wow" moment when the hands and fingers are flying along the keys to fulfill the devil's composition. Beside all the musical aspect, it is the dynamic and delicacy of the hand, combined with the precise haptic feedback, which are still lacking in any of today's prosthesis or robotic arms. Although studies on brain-information recognition is increasing to allow patients to control more complex systems, and machine learning tools are pushing the agility of robotic hands, these studies would all benefit from an underlying platform which itself could already perform faster and stronger motion, but still being lightweight, compliant or soft.

The most obvious research application of the proposed prototype would be the study of spider locomotion. By varying material, surface coating, design and size, questions regarding friction, mechanical properties and dynamics can

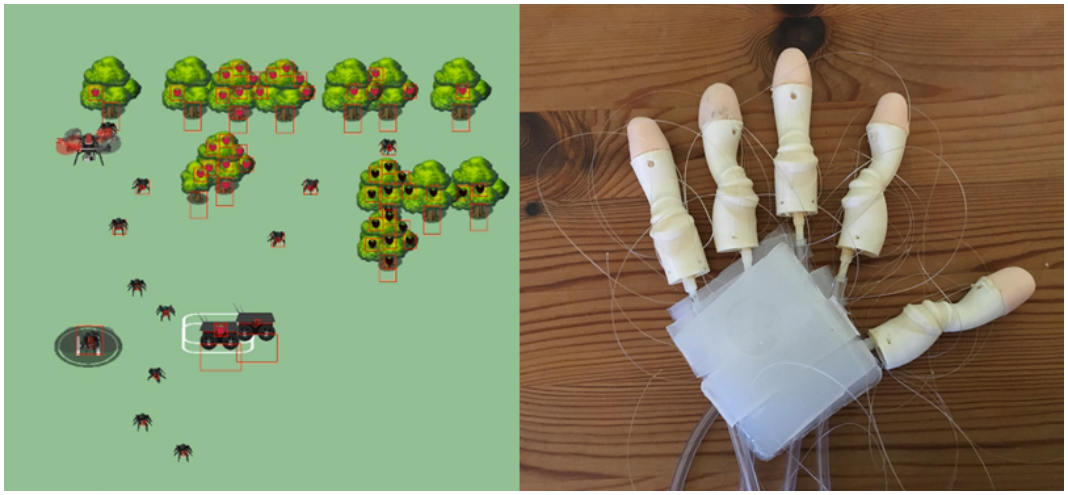

Figure 4.21: Future studies and applications. Left: Simulation of plantation with multi-agent system including UAVs transporting the spider robots and screening the field, autonomous wagons for ground transport and spider robots that collect fruits. Right: Concept prototype of soft fluidic hand using the spider inspired joint.

be answered. Depending on the question, the complete robot might not be of interest but rather a specific component or property can be isolated and tested and its purpose for the locomotion of spiders, but also for robotics can be evaluated.

Chapter 5

Discussion

In this work a variety of things have been tested and brought into context with the current state of research. To give the reader the quintessence of this work, I would like to discuss the main contributions, which I have summarized in the very beginning of this thesis and presented through out this work.

To get a clearer picture of the working principle behind the locomotion of spiders, I have used many different imaging techniques to get detailed information. While not all of them provided "quantitative" results, the development and optimization of preparation techniques to take these detailed images have been a large and time-consuming part of my thesis. I used close-up high-speed imaging recordings to get a qualitative view on the flexing and extending behavior of the spider legs as the data was not available in the beginning of my thesis. The videos revealed the fast extension of the femur-patella joint, emphasizing its importance for the jumps of jumping spiders. Furthermore, the recordings show the interplay of the four leg pairs, especially the third and forth pair and also the fixation process of the safety wire, which is essential for a targeted jump. The articular membrane, which unfolds rapidly during the jump, was the focus of this thesis and therefore characterized in detail. To get information about the three dimensional construct, I fully 3D reconstructed the femur-patella joint and its articular membrane using X ray scans. The articular membrane is usually missing in the published 3D scans due to its thinness, its wrinkling after death and special preparation requirements. Using stereo microscopy, I was able to observe the natural folding of the membrane on living spiders and took highly magnified images. In elder literature, photo images of the articular membrane are not very detailed due to the transparency of this membrane and the limited camera resolution. Therefore, the folding has only been described in schematic 2D drawings in previous literature, making it difficult to design a functional spider-inspired actuator. The frequently cited work of Blickhan and

Barth [14] describes the articular membrane as an anisotropic construct, which folds like a bellow. However, my video recordings revealed that the folding does not resemble bellows commonly used in today's technical applications.

The articular membrane appeared to be a thin fabric or cling film like sheet with stiffer elements (hoops) integrated. The folding mechanism reminds more of a stroller-umbrella, but with the difference that these hoops slide into each other like in an ice-cream scooper or a silicone salad bowl. These hoops were hypothesized to be stiff reinforcements [64] of the articular membrane. Therefore, I directly analyzed the mechanical properties of the articular membrane by nanoindentation and experimentally proved the anisotropic construct of the membrane. To get a better understanding of the cause of this stiffness variation, I conducted traditional thin histological cuts of the spider leg to characterize the membrane thickness and composition. Although exact matching of areas was not possible, the images suggested that the stiffer areas were thicker than the rest of the membrane, which would also coincide with the 3D reconstruction where the stiffer "hoops" appeared denser. As the elastic protein, resilin, is often incorporated into leg joints of jumping insects, I performed the indirect optical testing for resilin under UV light. The test revealed that the stiffer parts show a light blue autofluorescence response, which could be a hint for resilin. However, as resilin existence in spiders have not been reported so far, the light blue color might rather be a result of different cross-linked proteins embedded inside the outer most layer (epicuticula) of the membrane [138], giving another explanation for the anisotropy of the membrane. The integration of resilin inside the membrane would increase elastic energy stored during folding, supporting jumping and fast movement and could help to restore the shape of the membrane.

Additionally, I developed an SEM preparation method, which allowed me to get high detailed images of the articular membrane surface. Previous works failed to provide electron microscopy images of the native membrane, as the spiders flex their legs after death, deflating the membrane. With the SEM imaging, I discovered the microstructures, which changed with the stiffness variation. Deproteinization of the leg showed, that the microstructures are probably formed by proteins in the epicuticula of the exoskeleton, giving another explanation for the difference in membrane stiffness. I proposed that these microstructures could further be involved in communication due to their iridescent effect, as the jumping spiders have well-developed visual systems and extend and wave their front legs when meeting conspecifics. As the structures look similar to lotus-leaf surfaces [28], self-cleaning abilities might also be another function, given the constant and fast folding and unfolding during locomotion. The spiders furthermore do not seem to have any lubricants on

the surface of the articular membrane, so the microstructures might also be involved in friction reduction. Although, I was not able to conduct friction, adhesion and contact angle measurements in the scope of this work, I proposed methods and ideas to allow the measuring of these properties. Future studies of the microstructure on the articular membrane might reveal an evolutionary adaptation of these structures according to the behavior of the spider species as I showed that different species have different type of microstructures. Since surface-micro-patterning becomes more and more important for technological purposes [34, 44, 71] the study and understanding of the microstructures function could help to design new structures and surfaces.

The video recordings, live images and reconstructions provided detailed information for the design of a spider-inspired semi hydraulic actuator. The heart of this design was the "articular membrane" which showed thick and stiff hoops that slide into each other during folding. This folding allowed the hinge joint to cover a large working angle of 120°, performing in the same range as in the observed jumping spiders. I showed that a lack of these stiff hoops could lead to undesired wrinkles, causing damages and rupture of the membrane after frequent use, which would be fatal for the hydraulic locomotion. I furthermore characterized the folding and unfolding behavior of the prototype and showed that the flexing and extension can be controlled by simple linear equations as the generated torque is directly proportional to the input pressure (up to 300 kPa). In contrast to this, previous, soft silicon-based spider-inspired implementations, which extend by inflating and "blowing" up the material, normally work under pressures 10-100 times higher and tend to have unpredictable volume increase. Latter reduces the generated torque and increases the difficulty in control, which is why soft actuators tend to have wire-reinforcements to increase predictability of the motion, however that often comes with the cost in working angle and performance. The demonstrated lightweight actuator was able to lift 600 g against gravity and produced torques up to 0.4 Nm. For demonstration purposes, I built a jumping platform and showed that the resulting jumps were very well predicted by the jumping models. Although the jump of spiders has been studied several times and even new research work has been published during my PhD by other research groups, it is still not 100% clear, how spiders jump, which legs are actually involved and how much torque each of the joints contribute. Calculations and simulations for spider jumps are therefore still lacking many essential information about the leg behavior, angles and the fluid flow, resulting in the "doubt of hydraulics", as the estimated hydraulic performance seemed to be not efficient enough [133].

The demonstrated jumping platform might not fully resemble the actual spider, however it could help to test hypothesis and give a better understanding of the system. Estimating and demonstrating the jumping performance of the robotic actuator revealed, that by simply holding the legs, internally increasing the pressure and suddenly releasing the flexing wire, enough elastic energy is generated for jumping. Given that the legs are filled with flexor muscles, it can be assumed that spiders have enough flexing force to hold against the rising internal pressure. Comparing this hydraulic jumping to elastic protein or muscle-based jumping, it can be said, that the spring constant can be adjusted by the internal pressure. This means, a spring system with a given spring constant can only achieve a specific height when flexed to a specific angle. In contrast to this, the semi-hydraulic system allows to adjust the jumping performance by pressure while keeping the joint flexed at the same position. This might explain, why spiders have much better control over their jumping performance, essential for successful hunting, while insects normally just need a fast jump as far away as possible for escape, but not necessarily a good control. Resilin jumpers as leaf or grass hoppers, normally have their jumping leg already locked in flexed position and do not use them for walking so that they can catapult themselves away when needed. As the fourth leg pair of spiders is highly involved in the walking and running, a different jumping mechanism is necessary. For controlled jumps, spiders take the time to anchor the safety wire and flex their hind legs into position. For escape behavior, this preparation time might not be given, but as the legs can be immediately extended, by drastically increasing the pressure, fast (uncontrolled) jumps can still be conducted and even combined with high speed running.
The hydraulic performance might however be limited by the speed in volume shift. The sudden release characterization of the prototype showed, that the pressure drops even into negative values when the joint snaps open in high speed. This effect is known for hydraulic pistons, where it can cause cavition, leading to damage of the material and performance limitations.

However this might not be the case in spiders, as the physical properties of hemolymph could adjust in such a way, that a delay in volume shift is avoided.

To study this, I looked into the hemolymph flow of the spiders. The hemolymph flow constantly provides researchers with headaches, as it seems that spiders should not be able to do what they are doing. Although spiders are a two body parted, multi-legged, multi jointed system and one would assume that valves would be used for control, no valves have been reported so far. It is known that the heart pumps the hemolymph from the lungs to all the essential organs and that the prosoma increases the pressure inside the legs, but it still

remains unclear how the heart works against the high prosoma pressure. Also the fluid flow inside the leg is completely unknown. Researchers have assumed for a long time that the reduce in volume of the prosoma during pressure increase would lead to the loss of hemolymph to the abdomen. They further concluded that this would result in a lack of oxygen supply for the organs inside the prosoma, which would force the spider to recover after a short period of running or jumping. This problem is referred as the "hydraulic insufficiency hypothesis" [59]. Subsequent works have however provided evidence against this theory, by showing that spiders can perform high speed running for several minutes and that rather biochemical factors are limiting factors [80]. The hydraulic efficiency is however still questioned due to simulations showing that spiders over 3 g should not be able to jump when only using hydraulics [143]. However, all estimations were lacking essential information, which I tried to provide in this thesis.

Completing the schematic drawings given in elder literature, my 3D reconstruction and histological cuts revealed the inner composition and space inside the leg, especially in the joint region. However, I was not satisfied as this methods could only be conducted on dead animals and did not provide any information about the internal flow. I found that although the penetration depth is limited, optical coherence tomography (OCT) was able to show the fluid flow of the hemolymph cells inside the leg joint. The video recording revealed the different fluid path and speed inside the leg and joint for the first time. Furthermore an interesting spiral flow in the joint region was observed. Although, I was not able to find any of the proposed muscle ring-like valve structures [59], the observations might indicate that the arcuate sclerite plays a valve-like role. However, further investigations will be needed to fully prove this.

While for simulations, a large volume shift was assumed to be necessary for leg extension, the recordings show that only a small fraction of the leg joint forms the "extension chamber" under the articular membrane, necessary for extension and that not all space and channels inside the leg actually lead to the chamber.

Another important fluid property, the viscosity and its behavior under different pressure, was lacking in literature and the simulations. Viscosity is a key factor in traditional hydraulic systems as it helps to lubricate the system and therefore reduces wear and friction, cools the system during overheating and helps to avoid oxidation. Latter is the reason why water is usually not used in metal-based hydraulic systems since large amount of air is dissolved in water. Neglecting these effects, viscosity still directly influences the mechanical and

volumetric efficiency, making it necessary to choose the right hydraulic fluid for the working range of the system. High viscous fluids normally show a large volumetric efficiency, but low mechanical efficiency, while low viscous fluids behave the opposite way. Now considering the spider leg as an hydraulic motor, the optimal viscosity changes over the pressure range. When operating at low pressures during resting, the fluid is pumped through the body, providing oxygen and nutrients to all organs, therefore high volumetric efficiency is of importance, while the mechanical efficiency can be low. Highly viscous fluids are at this point of advantage. During normal walking, the pressure is now at normal working level, torque needs to be generated, therefore mechanical efficiency should be larger, while volumetric efficiency should stay as high as possible as most fluids are still only pumped through the body by the heart. When the spider rapidly increases pressure as for fast running or sudden jumps, the legs extend in a fast manner, resulting in the sudden opening of volume that needs to be filled. At this point, the effective flow needs to increase immediately to fill up this volume, furthermore, generated torque and mechanical efficiency should be as high as possible. This means at high operating pressure, during large motion, a low viscous fluid would be more beneficial. In conclusion, a fluid that shows decreasing viscosity with increasing pressure would be optimal for spiders.

Using microchannels, I was able to show non-Newtoninan, shear-thinning behavior of the hemolymph as it has been observed for human blood. The viscosity of hemolymph decreases, while the velocity increases with pressure, which would prevent a sudden pressure drop observed for the robotic prototype and commonly known to cause cavitation, resulting damages and inefficiencies. It would be interesting to test different viscous fluids with different shear behaviors on the robotic prototype in the future, to see how large the influence would be on its performance and whether non-Newtonian fluids have a benefit on hydraulic actuators.

A major difference between previous spider-inspired actuators to the mechanism proposed in this thesis and observed in spiders is the fluidic medium. Pneumatic actuation is often used instead of water or oil based hydraulics. Air brings the benefits of already being low-cost, lightweight, safe, compliant, environment-friendly and causes less leakage problems. For prototyping, pneumatics is therefore easier to implement as small leakage can be compensated by higher flow rate and fluid storage chambers are not necessary as air can be taken from the surrounding.

Since air is compressible, pneumatic systems are less susceptible to shock damage. This property however brings also the main disadvantage of pneumatic

actuation. To create high operating pressures, the air needs to be compressed by a compressor, which is often large and bulky. When moving or lifting heavy loads, pneumatic actuators furthermore show spongy movement caused by the compression. In combination with soft materials, this can cause undesired jerky, "wobble" motion, making a controlled positioning very difficult. To compare the performances of the existing actuators, I have listed their working angle, torques, operating pressures and effective area (fig. 5.1). As torque increases proportionally to area and pressure, larger actuators with high operating pressures would automatically have larger torque values. To give a rough value for comparison, I have introduced two performance values, which normalize the torque to the area (performance 1) and additionally to the pressue (performance 2). Although elastic energy, friction, the real effective area and leakage might also impact the measured torque, these factors are neglected as the data for these values are not given for the actuators. To give a fair comparison, I did not use the evaluated effective area (13 mm^2) but the cross-sectional area (100-140 mm^2) of the fluid chamber, as this was the only value available for the other actuators. It is no surprise to see, that those actuators, which are only based on the balloon-like inflation of rubber material (Schwörer [110], Zentner [16, 17, 143–145], Menon [73]), show a lower level in performance than those with a reinforcement. The actuation of the Arthrobots (Nemiroski [83]), build by researchers around G. Whiteside, are also based on the inflation of a balloon. However the highest torque values shown here were achieved when the inflation was restricted by a sleeve. As proposed by Blickhan and Barth [14] isotropic membranes would lead to bulging volumes and the creation of counteracting torque, reducing the performance. The standard-bellow shaped actuators (Schulz [40, 41, 54, 96], Becker [20], Landkammer [62, 63, 109, 142]) show a similar value in performance 1. Landkammer used a flexible material (TPU), which might explain the low operating pressure for material extension and the higher perfomance 2 value. The sliding-shell-model (Sprö witz [120]), which was developed in the beginning of my PhD, is based loosely on images I made of wolf spiders. The operating pressure was limited by the internal plastic bag, which is inflated during extension. While the performance 1 value is significantly lower in comparison to the prototype presented in this thesis (Göttler 2020), the performance 2 value is almost the same. An explanation could be that the flexible material, which brings the advantage of compliance and less damage after impact, need a higher operating pressure to withstand higher load. Alternatively, the cross-sectional area of the proposed actuator was estimated too large.

One significant difference between the proposed design to previous actuators

is the working angle. While only angles up to 90° where achieved before, the interfolding mechanism developed in this work allows a working angle up to 120 - 125°, which comes close to the working angle observed for the jumping spider (130-140°). Interestingly, the estimated performance range of the jumping spider *Phidippus regius* lies in the same range. As the pressure value inside the spider leg could be much higher during jumps than assumed, future detailed measurement of the inner pressure are required to get a better understanding of the locomotion principle.

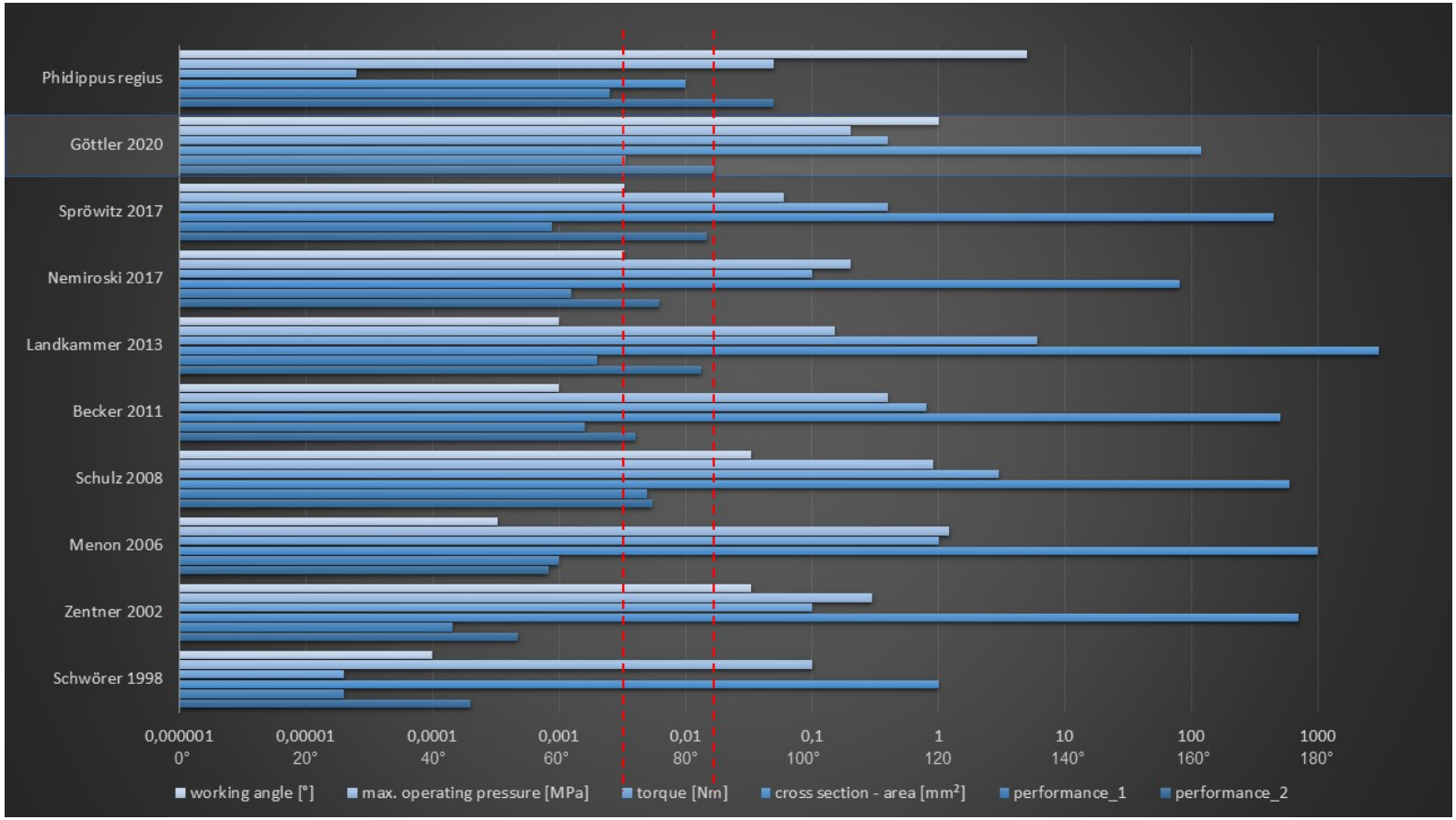

Figure 5.1: Comparison of spider inspired fluidic actuators. Red dotted lines mark the performance value of the prototype demonstrated in this thesis (Göttler 2020). Working angles are given in degrees, other values are following the logarithmic scale. Perfomance 1 is calculated from the torque normalized to the cross sectional area. Performance 2 is the max. torque normalized to the maximal operating pressure and the cross sectional area. Actuator values are taken from [63, 64, 83, 96]. Only Menon, Nemiroski and Göttler used hydraulics instead of pneumatics. Spider torque was roughly calculated with data from [77, 90], cross-sectional-area was estimated from OCT recordings and operating pressure was assumed to be around 50 kPa as measured in other spider species [90]. Area and pressure might differ highly from the real value.

Chapter 6

Material and Methods

6.1 Behavioural Observation

6.1.1 Spider Keeping and Breeding Condition

In biological studies, species, age, sex and fitness are important parameters to know, to avoid any side effects influencing the features of interest. That is why I decided to keep and breed my own spiders under controlled conditions instead of catching them from the outside forest as done in many studies. An interesting study species for actuation would be jumping spiders as they show a high versatility in locomotion behavior. The first generation of juvenile jumping spiders *Phidippus regius* were purchased from a local breeder. The second generation was bred in-house. After the spiders molded for two to three times (N2-N3 stage), they were separated from each other and kept in individual boxes to avoid interspecies attacking. As this species originally comes from Florida, the temperature was set between 25 to 35 °C with a nine-hours-daylight cycle and boxes were frequently sprayed with water. The spiders were fed with fruit flies (*Drosophila* sp.), meal worms and crickets matching their stage in development and size. The molding stage and any problems were documented. If not otherwise stated, adult spiders were used for experiments.

6.1.2 High Speed

To observe the jumping motion of the spiders, they were recorded at 1000 frames per second (Phantom Miro M140, 8032), with exposure time at 400 μs and resolution of 1024 x 768.

6.2 Outside Morphological Characterization of Spider Leg

6.2.1 Stereo Microscopy

To attach the spiders in position, they were first narcotized with carbon dioxide and carefully stuck on a petri dish using Dental polymer (Flexitime, Correct Flow), allowing detaching after experiments. The folding of the articular membrane was observed and recorded under the stereo microscope (Leica M205) while the leg segments were moved into different positions by a thin preparation needle.

6.2.2 Scanning-Electron-Microscopy SEM

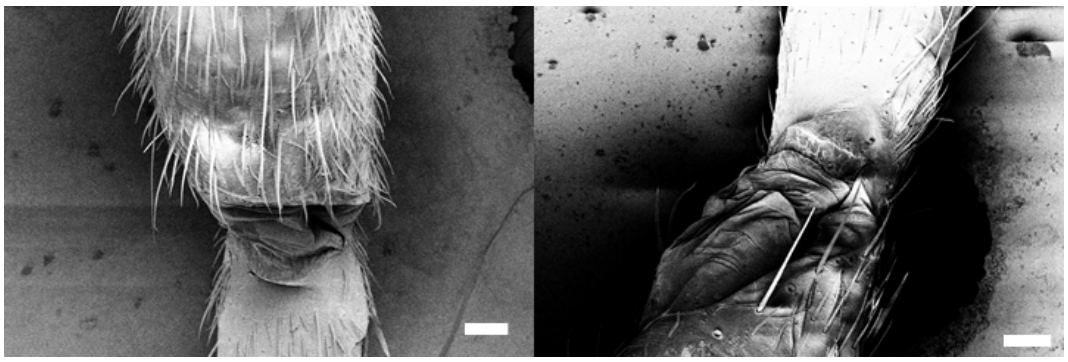

Figure 6.1: Deflated femur-patella joint. The initial scanning electron microscopy images reveal the deflated and deformed articular membrane when simply following standard preparation protocols. As spiders flex their legs after death, reopening the legs would result in such deformed images, which leads to sputtering problems and therefore charging effects (white areas) limiting the resolution. Images show the femur-patella joint of wolf spiders. Scale bars: 100 μm.

When spiders decease, they usually flex their legs into "mummy" position due to muscle contraction after death. Flexing moves the hemolymph back into the body and the articular membrane deflates. Reopening the legs leads to only partially deflated constructs (fig. 6.1) and even pre-attaching the whole spider also does not work, as the joints still curl and deflate. Furthermore, substances used in traditional fixation such Ethanol for dehydration, Acetone for washing or Glutaraldehyde for cross-linking, dissolve the tested adhesives for attachment. Therefore, I developed a preparation method (published in

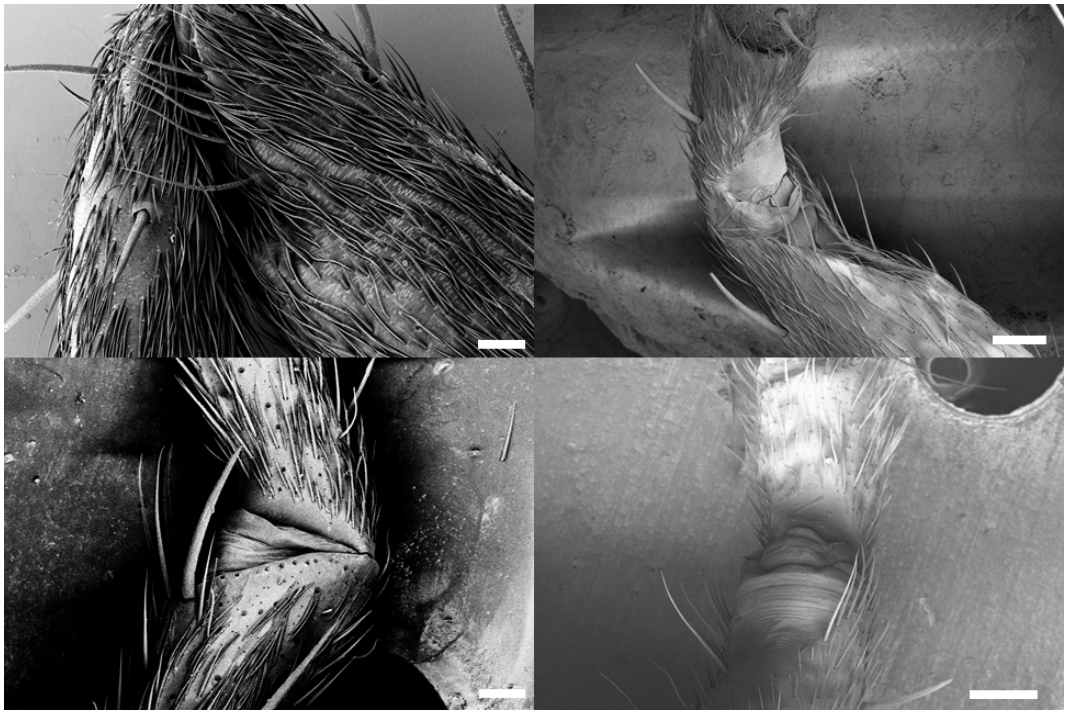

Figure 6.2: Scanning electron microscopy images of wolf spider femur-patella joint. The legs of wolf spiders (*Lycosidae* spec.) are covered with hair. Interestingly, in contrast to jumping spiders, they show long and thick, tapering spines surrounding the joint. The folding behavior of the membrane is corresponding to the observations made for jumping spiders. Right side images show slightly deflated joints. Scale bars, left side: 100 μm, right side: 200 μm.

[43]) to avoid deflation and keep the natural extended joint and membrane structure (fig. 6.2). First, the adult spider was narcotized with carbon dioxide for 10 min and transferred into a 70% water, 20% ethanol and 10% ethyl acetate solution for another 10 min. Ethyl acetate vapor is a common killing and insect preparation agent and known to re-soften joints of dead arthropods. The bathing inside the solution kills the spider immediately, while the whole body stays extended and completely soft and flexible. By transferring the body onto a water surface, the surface tension and hydrophobic characteristic of the solution separate the legs from each other symmetrically. Using a thin metal plate, the spider could be lifted out of the water. As the abdomen of the jumping spiders are large, the legs are lifted and attached into the same horizontal position by a hot glue base below. To avoid detachment, thin hot glue "handcuffs" have been formed by pulling hot glue strings around the foot (tarsus) to lock the legs mechanically as adhesives lose their stickiness in ethanol

during the critical point drying (1 h, slow speed, 28° on Leica EM CPD300 Automated Critical Point Dryer). To avoid charging effects, the spider was sputter-coated with 20 nm gold (Leica EM ACE200) and observed under the electron microscope (Zeiss Ultra Plus) with working distances of 10-15mm and electron high tension (EHT) of 3-5 kV.

6.2.3 Computer-tomography CT

A dead adult spider was carefully placed into an Eppendorf tube filled with 70% ethanol and two drops of iodide solution to enhance the contrast. Micro-CT scans were performed at the KIT, ANKA, IPS imaging laboratory for computed laminography and computed tomography with Marcus Zuber. An X-ray tube (XRay-WorX XWT-225), producing an cone beam, and a flat panel detector (PerkinElmer XRD 1621 CN14 ES) were used for the measurements. The X-ray tube was operated with an acceleration voltage of 50 kV and at a target power of 10 W. The sample was positioned and moved by a custom made sample manipulator. In total 2048 projections were acquired over an angular range of 360°. Each projection was exposed for 4s. The projection was reconstructed into slices with Octopus 8.6 (Inside Matters, Gent, Belgium). The geometrical magnification results in an effective pixel/voxel size of 7.07 μm.

6.3 Inside Morphological Characterization of Spider Leg

6.3.1 Histology

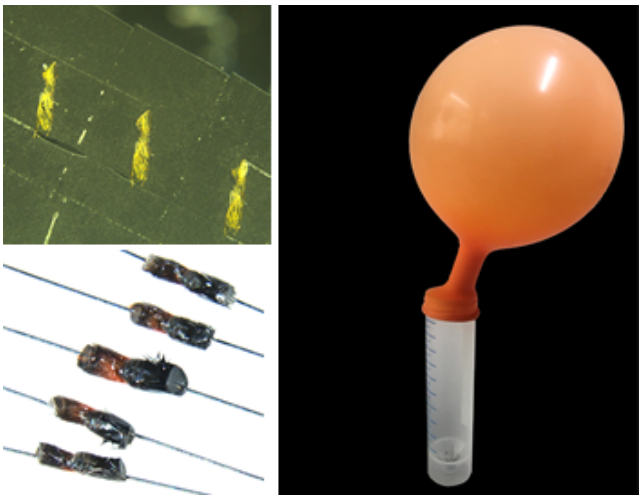

Figure 6.3: Histological dissection. CO_2 was filled into a balloon to let it slowly diffuse into a falcon tube to narcotize the spider. Legs were dissected and fixed with insect needles. The needles were removed when embedding inside paraffin wax and slicing it into thin sections (4 μm).

I have published this modified histological protocol to dissect spider joints in [43]. The following text will match largely with the published text, however, I have added some more details here.

Several fixation, embedding and staining techniques have been tested. Spiders were narcotized with carbon dioxide and attached to a petri dish with dental polymer. Legs were quickly cut off from the body and a targeted stitch through the abdomen (heart and digestive organs) killed the spider. Freeze killing or ethyl acetate as killing agent influenced the preparation results and could not be used. A petri dish with wet tissue (Ringer's solution) was prepared and the femur-patella joint was carefully stretched and held in position with insect needles inside. To keep this position during sample fixation and embedding, a thin insect needle was stitched through the leg segments near the hinge joint side (fig. 6.3).

Traditional dehydration with ethanol (30, 60, 70, 90, 96, 99%) was tried with variation in incubation time (5, 10, 30 min per step), but all fixation trials resulted in too brittle and stiff samples. Similar results were observed when

fixated with glutaraldehyde and osmium. A fixation with picric acid (Bouin solution [10]) resulted in bright yellow samples (fig. 6.3). Although this method was great for microscopic observations, the picric acid has to be washed out with ethanol after staining. Therefore, to spare the samples, Hartman's fixative (also Davidson's fixative, Sigma-Aldrich H0290) often used in vertebrate tissue fixation, was used. The fixative contains acetic acid, alcohol and formalin. Samples were fixated overnight. Embedding in epoxy (Technovit) and spurr was tested, but microtome cutting (with (sheet) glass, razor blades and (cryo) diamond knife, 4 mm, 45 °, Leica) resulted in rupture of the articular membrane due to too large cutting thickness ($\sim$2 μm), the thinness of the membrane and large differences between the stiffness of the sample and the embedding material. Paraffin embedding was therefore chosen and carried out in the standard way. Paraffin wax was heated in a beaker and filled into small clear lockable glass sample vials and left on the heating plate. Samples were incubated in a glass vial filled with xylene (also xylol, Sigma-Aldrich, isometric mixture, 1.08298) for 10 min. Longer incubation could lead to brittleness of the sample. Samples were transferred into a 1:1 xylol-paraffin wax mixture and incubated for 10 min.

Experiments were conducted under the fume hood with proper safety equipment (gloves, goggles, lab coat) and separate, close waste disposal to avoid health issues from xylene. Heating plate was set at the melting point of paraffin, so that the wax just stayed liquid. Samples were incubated for 30 mins and transferred to fresh paraffin twice. For cutting purposes, samples were transferred into stainless steel histology embedding molds, covered with the backside of a plastic histology cassette (fitting to microtome holder) and carefully filled with liquid paraffin. After cooling in air (1-2 min), molds were cooled in the fridge (-20°C) overnight. The embedding mold was carefully removed the day after. Samples were kept in fridge until microtome cutting. Wax molds were attached to the microtome (RM2245, Leica) and excess wax was cut away until biological sample appeared on the surface. Slices of 4-5 with 4 μm thickness were transferred with a brush to a heated water bath (35-40°C) and afterwards carefully lifted on a glass slide. After air drying and removal of excess water with a tissue, glass slides were baked at 45-50°C overnight. For staining, paraffin wax was removed by bathing the slides in xylene (10 min), hydrated with ethanol washing (96%, 70%, 60%, 5-10 mins per step) and rinsed with aqua dest. afterwards. Three different staining methods were tried out, Mallory (Morphisto, Mallory Kit, 10270), Masson-Goldner and Azan staining. Best staining results were obtained with a modified Masson-Goldner Trichrome staining.

Staining jars were used for all staining steps. Weigert's iron hematoxylin

solution from the traditional Masson-Goldner staining was not used as it is for nuclei staining. Samples were bathed in a 1:2 mixture of 1% acid fuchsine (Morphisto, Masson A, 10357) and 1% Ponceau de Xylidine (Morphisto, Masson B, 11518) for 5 min and carefully washed with 1% acetic acid and aqua dest. afterwards. Samples were then shortly (1-2min) dipped in a solution of Phosphormolybdic acid and Orange-G (Morphisto, 11195) and washed with acetic acid and aqua dest. again. After another staining step with anilin blue (Morphisto, Masson C, 10141) and washing, samples were quickly dehydrated with ethanol (96%, 5 min, twice) and xylene (2 min) and left under the fume hood for drying and total evaporation of xylene. Cover slides for microscopy were mounted with mounting medium (Morphisto, 12318) onto the glass slides. Coloration results show similarities to Azan staining after Heidenhain. The thin epicuticule, which is not stained in many staining protocols, is stained dark red with this method. The stiff exocuticule appears brown, while the endocuticle is stained blue. A mesocuticle, which does not show fiber orientation differences to the endocuticle but can be differently stained [10], was not distinguishable with this method.

6.3.2 Topology and Tomography Scans

In order to observe the 3D structure of the spider joints, detailed X-ray imaging was conducted at LAS (Laboratory of Applications of Synchrotron Radiation), synchrotron ANKA in Karlsruhe together with Thomas van de Kamp. The microtomography is performed using a parallel polychromatic X-ray beam produced by a 1.5 T bending magnet. The beam was spectrally filtered by 0.2 mm aluminum with a spectrum peak at about 15 keV and a full-width at half maximum bandwidth of about 10 keV. A fast indirect detector system consisting of an 18 µm LSO:Tb scintillator [24], diffraction limited optical microscope (Optique Peter) and a 12bit pco.dimax high speed camera with 2016 x 2016 pixels was employed. For the tomographic scan we took 3,000 projections at 200 frames per second and chose an optical magnification of 10X, resulting in an effective pixel size of 1.22 µm. We used the control system concert [130] for automated data acquisition. Tomographic reconstruction was done using the UFO framework [129]. Structures were presegmented with Amira (version 5.5) and refined with Biomedisa for 3D reconstruction.

6.3.3 Optical Coherent Tomography (OCT)

For observing the internal flow inside the spider joint, spiders were attached onto a petri dish using dental polymer (fig. 6.4). The spiders were only shortly (1-3 min) exposure to CO_2 to avoid any negative effects on the hemolymph flow. Short exposure time leads to fast wake up time, therefore the attachment of the spider has to be done quickly. The attachment is reversible, the spiders can be detached after the experiments.

As the penetration depth of the device (TEL320C1 - Spectral Domain OCT System) is limited to 3.5 mm, only smaller spiders were used. The coarse and fine focus were used to sharpen the image. A refractive index of 1 and an image speed with a medium sensitivity (76 kHz) was used for 2D and 3D images. For both image types the A-scan averaging was set to 3 and the B-scan averaging in 2D images was remained unchanged at 1 with a pixel size of 6.5 μm. The selection "Hann" was used for apodization window. The device has an axial resolution of 5.5 μm.

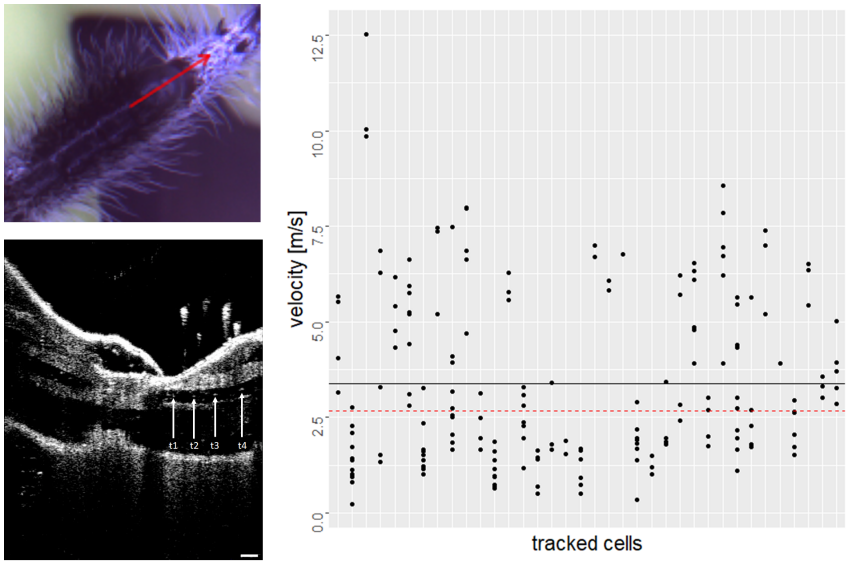

Figure 6.4: Measurement of cell flow using OCT. Juvenile jumping spiders were attached to a piece of paper using dental polymer, so that the femur-patella joint is lying in horizontal position. The inside flow is then recorded with the OCT (scale bar: 100 μm) and the cells were manually tracked with the Tracker tool (physlets.org/tracker/) and cell velocities were calculated. In total 36 cells were tracked (average: black line 3.37 m/s, median: red line 2.67 m/s).

6.4 Mechanical Property Analysis of Articular Membrane

6.4.1 Nanoindentation

I have published the results and protocol for nanoindentation of the articular membrane in [43]. The following text will match largely with the published text, however, I have added some more details here. Using carbon dioxide, spiders were narcotized and fixed with straight legs on a Petri dish using Dental polymer, Vinylpolysiloxan (Flexitime, Correct Flow). The legs were carefully cut off and the thin articular membrane between the femur-patella joint was dissected from the dead spider. This was done manually under the Stereomicroscope (Leica M205) using insect preparation needles, fine tweezers and bow spring micro scissors. The membrane was placed on a 3cm diameter aluminum block. As the membrane is very thin and deformable, a water droplet was used to adhere the membrane on the surface. Glass slides were used to carefully flatten the sample and water was removed by a small piece of tissue. Other adhesives were tested but the curing methods resulted in non-flat samples, or samples drowned in adhesives. The mechanical properties of the articular membrane were measured via nanoindentation (Nanoindenter XP, Keysight) with a pyramidal Berkovich tip (JDA, 1 μm) (fig. 3.13).

Table 6.1: Nanoindentation settings for Nanoindenter XP, Keysight with pyramide-shaped Berkovich tip

Parameter	**Value**	**Unit**
Surface approach velocity	2	nm/s
Surface approach distance	1	μm
Strain rate	0.05	1/s
Harmonic displacement	2	nm
Frequency	45	Hz
Depth limit	1	μm
Surface stiffness	220	°C
Poisson ratio	0.4 [119]	-
Max. Depth for Modulus Av.	100	nm
Min. Depth for Modulus Av.	150	nm
Max. Depth for Hardness Av.	500	nm
Max. Depth for Modulus Av.	600	nm

The hardness and Young's modulus of the two distinguishable parts (dot and line area) of the membrane were determined by the continuous stiffness measurement (CSM) method. As mentioned above, aluminum was used as a substrate and the sample was attached to the surface via the adhesion of a water droplet, which was removed afterwards. As the indenter had only a fixed 20x magnification, it was difficult to find the small and transparent membrane under the microscope. Therefore, a black marker arrow was drawn next to the sample on the aluminum block, before the aluminum block was tared inside the sample holder. Indentation points were chosen randomly among the surfaces but avoiding wrinkles. For noise balancing and calibration, 5 indents on a silicon wafer have been taken and for each area of the membrane 5-10 test indents have been performed to mark the x,y position of the different parts. An indentation depth of 1 μm was chosen, corresponding 2-10% of the membrane thickness avoiding substrate effects. Further parameters for the nanoindentation experiment are summarized in tab. 6.1.

Two experimental runs were performed. In the first run 50 and in the second 100 indentation runs for each area were done. Due to long surface approaching times, the last experimental run took 3 days and was performed over weekend, avoiding external vibrations due to e.g. elevators. Finally, only experiments in accordance with theory [67, 86, 93] have been chosen for calculation, to ensure successful contact finding and avoiding substrate effect. At the end, 57 measurements for the dot and 101 for black line area were analyzed. Statistical analyses (tab. 6.2) have been done using R internal statistic libraries.

Table 6.2: Statistical analysis of nanoindentation measurements. The distribution of Young's Modulus E and Hardness H experimental data were analyzed. Statistical testing was conducted with R. Normal distribution is tested with the Shapiro-Wilk-Test and the F-Test compares variances of two normal distributed groups. P-values above the significance level of 0.05 in these two tests are marked with an asterisk, indicating normal distribution or no difference in variance. Biological samples are often considered as normal distributed with similar variance, even when experimental data show different. As both, Shapiro- and F-Test are not clearly supporting normal distribution and similar variances, a standard t-test cannot be used to test similarity in means. Therefore, the Welch's t-Test is used, which considers differences in variances and the Wilcoxon-Test compares groups without assuming normal distribution. P-values, below the significance level 0.05 are marked with an asterisk, indicating a difference in means of the dot and line area.

Young's-Modulus E (GPa)	Mean(GPa)	Median (GPa)	Standard Deviation (GPa)	Shapiro-Wilk-Test p – value
dot area (D)	3.81	3.80	0.538	0.24 *
line area (L)	5.00	4.90	0.960	0.000114
F-Test	ratio of variance	0.31		
	p-Value	6.23e-06		
Welch's t-Test	95% confidence interval	[-1.42, -0.95]		
	p-Value	<2.20e-16 *		
Mann-Whitney Wilcoxon Test	p-Value	6.40e-15 *		
Hardness H (GPa)	Mean (GPa)	Median (GPa)	Standard Deviation (GPa)	Shapiro-Wilk-Test p – value
dot area (D)	0.12	0.11	0.041	0.000446
line area (L)	0.29	0.29	0.045	0.22 *
F-Test	ratio of variance	0.85		
	p-Value	0.509 *		
Welch's t-Test	95% confidence interval	[-0.18, -0.15]		
	p-Value	<2.20e-16 *		
Mann-Whitney Wilcoxon Test	p-Value	<2.20e-16 *		

6.4.2 Nanoindentation of Hydrated Samples

When I moved to ETH for the second part of my PhD, I found a tool called "FemtoTool" which is designed to measure the material properties of biological samples like cells. Out of interest, I wanted to give this method a try. FemtoTools is designed to measure the stiffness of rather soft material. As it turned out quickly during the experiments, dry samples of the articular membrane are to stiff and deflect the "hair" too much to measure any difference. However by rehydrating the samples, the membrane starts swelling and transforms into a much softer construct. I measured three different membranes and different positions from the line and dot area. The stiffness was calculated via the HERTZ model. Similar to the nanoindentation method, the hydrated samples show a stiffness difference between the line and the dot area. With the line area being the stiffer area.

6.4.3 Resilin Test

I have published the resilin analysis of the articular membrane in [43]. The following text could match with the published text. Using the autofluorescence property of resilin under UV light (385nm) [23, 138] the existence of resilin can be tested. Optical observation was done under a stereomicroscope (Leica, M205 FA) with fluorescent light source (EL600, mercury lamp) and filter (EX 395/25 nm, EM 435 LP). Higher magnified images were observed under an inverse microscope (Zeiss Axio Obser.A1) with UV light (385 nm) and filter (Ex 390/40, Em 450/40). Strong blue fluorescence indicates resilin existence, however the observed light blue color might be a result of nitrogen-rich cross-links in the epicuticle [138]. As the membrane is very small and still need to be used for further experiments, were not conducted, as the membrane tends to flush away inside larger droplets. However, pH-dependence of the autofluorescence could help to verify the existence of resilin [81].

6.5 Microstructure Analysis

6.5.1 Microstructure Fabrication

The microstructure of spiders are part of the outside layer (epicuticular) of the exoskeleton and consists of protein and a thin wax layer. To refabricate the microstructures, silk fibroin was used as a base protein and covered with parylene. Silk fibroin was gained from silk pupae of the silk worm *Bombyx mori* (fig. 6.5) according to standard protocols [99]. Silk pupae (VON DER PLANITZ product development, Bayreuth, Germany) were cut into small

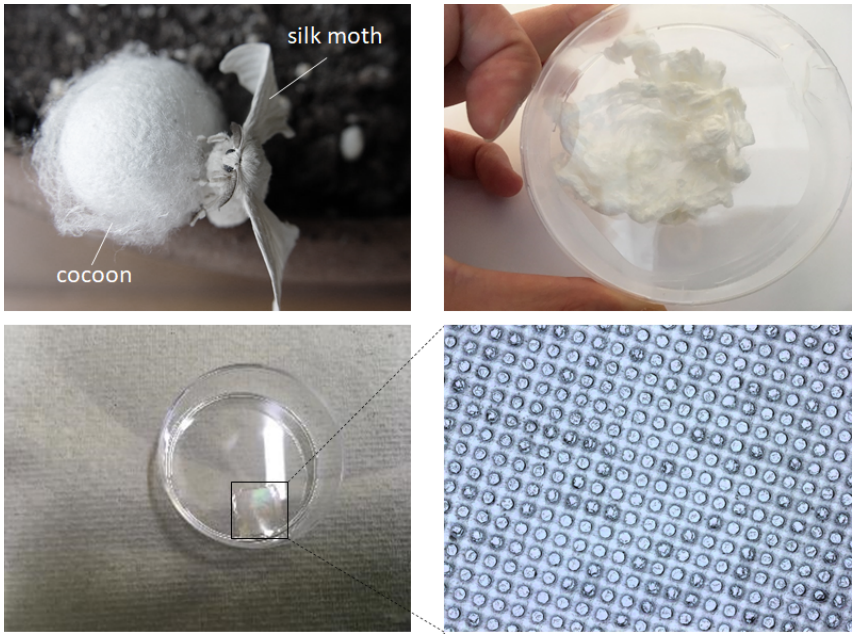

Figure 6.5: Microstructured silk fibroin film. Upper left: silk moth *Bombyx mori* hatched from its silk cocoon. Photography taken from wikimedia commons. Upper right: Degummed silk fibers after cooking the silk cocoons in Sodium carbonate. Bottom Left: Microstructured silk fibroin film. Bottom right: Cylindrical microstructures (5μm)

pieces and cooked in 0.02 M Sodium carbonate (Na_2CO_3) for 30 min. This removes the silk protein sericin, which adheres the fibroin together, resulting in degummed silk. Silk fibres were then rinsed with water (3 times, 20 min) and dried overnight. Silk fibroin was then dissolved in 9.3 M Lithium bromide (LiBr) for 4 h at 60°, whereby 4 ml of LiBr-solution was added to 1 g of silk.

In the beginning, the dissolving of the silk inside the LiBr was not successful. For trouble shooting we tested a higher solution-silk relation, higher LiBr concentration and longer incubation time. A solution was to rebath the degummed silk in water and directly slowly add the LiBr, which dissolves silk immediately. Resulting solution was golden (unsuccessful dissolving creates brownish solution). Silk fibroin was extracted via dialysis and therefore added into a dialysis cassette (Slide-A-Lyzer dialysis cassette 3500 MWCO, 3–12 ml capacity, Thermo Scientific) with a syringe and bathed in ultra pure water for 48 h. Water was exchanged after (30 min, 1h, and then three times after 2h and left for dialysis over the weekend). When higher LiBr concentration was used, longer dialysis and more water exchanges are needed. After dialysis, the liquid silk fibroin is centrifuged to remove any leftover particles and then stored in

the fridge (4°) until usage. To prepare the microstructure molds, silicon wafers with dot patterns (1-10 μm) were fabricated via photo lithography in the clean room (fig. 6.6). The patterns were cast with PDMS (10:1) and baked for 1h at 90°. The PDMS molds were treated with oxygen plasma (Diener Electronic Zepto, Ebhausen, Germany) and silanized with trichloro(perfluoroctyl)-silane (Sigma Aldrich, 448931) in the vacuum chamber under the fume hood for 1 h to create a anti-stick layer. The PDMS molds were then baked for another 1 h at 90°. Afterwards, walls are created with dental polymer, so that 1 ml of silk fibroin can be poured in, to create a thick layer of transparent silk sheet. Alternatively, the PDMS molds were fixed inside a well plate commonly used in cell culture and silk fibroin added on top. To allow the viscous solution of silk fibroin to better penetrate the micro structures, air trapped inside the microstructures was carefully removed via vacuum treatment in a desiccator, while the silk fibroin was still liquid. Afterwards, the silk was left for curing and a thin transparent sheet with impregnated microstructures resulted. To recreate the wax layer of the exoskeleton in spiders, chemical vapor deposition (CVD)[1] of parylene was used.

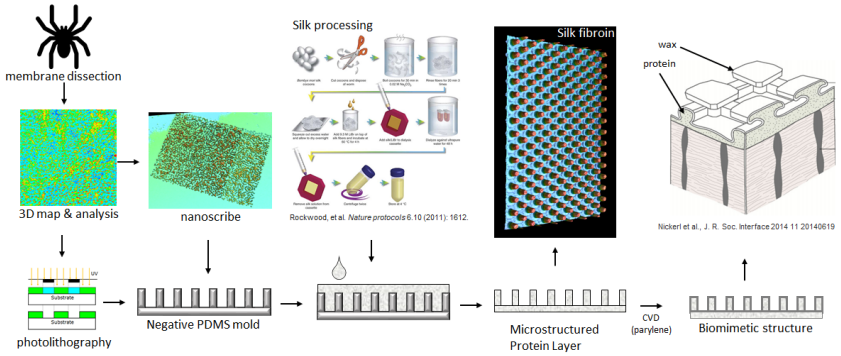

Figure 6.6: Fabrication protocol of silk fibroin sheet with parylene coating. Articular membrane was extracted from the femur-patella joint of the jumping spider. Microstructures were extracted from the flatten membrane using a Lasermicroscope. Artificial microstructures were fabricated by either nanoscribe 3D printing or photolithography to generate a negative PDMS mold. Silk fibroin was extracted from silkworm pupae [99] and poured over the mold. To completely penetrate all microstructures and remove air bubbles sample was carefully desiccated for less than 10 min to avoid too long evaporation. The fabricated microstructured silk fibroin sheet was then coated with parylene via CVD to mimick the layers of arthropod exoskeleton [84].

[1]For more information: https://vsiparylene.com/about-parylene/, last accessed on 19th Dec. 2020

6.5.2 Contact Angle Measurement

Sessile drop contact angle measurements[2] (Krüss DSA100S goniometer (Hamburg, Germany)) were conducted by adding a droplet of deionized water with defined volume of 3 μl onto the sample surface. The droplet was positioned by a flat end needle (Sterican, 0.40 × 25 mm, Blunt Gauge 27) and kept on the surface for 60 s. Videos were taken orthogonal to the surface at 10 fps using a side-mounted camera. For each sample (5, 10, 50, 100 μm dot and line microstructures), at least 3 different measurements were collected. Measurements were conducted at room temperature. The contact angles were then extracted from the video recordings and calculated by goniometer software.

6.5.3 Lasermicroscopy

To analyse microstructures of the spider and the self-fabricated membranes, laser microscopy (KEYENCE LASER PROFILOMETER VK-X200 series) was used. The device allows to give (optical) feedback about the surface structure and height and also distribution of micro structures.

6.5.4 Deproteinization

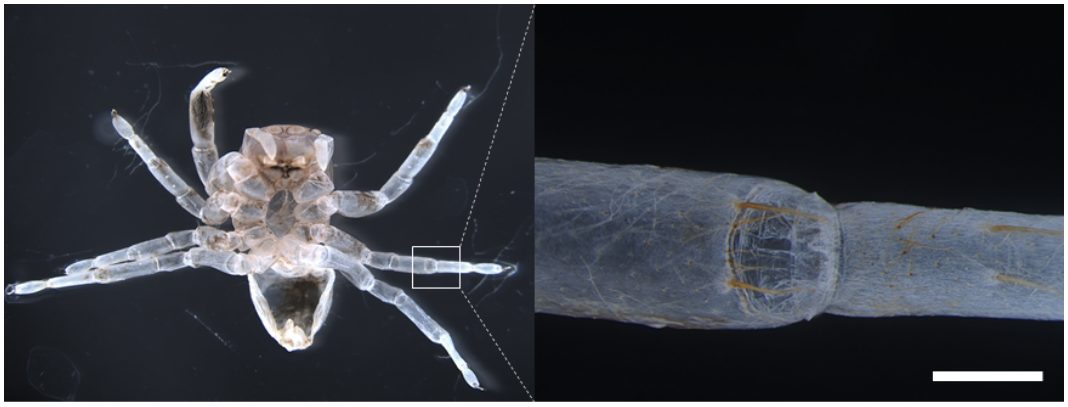

Figure 6.7: Deproteinized juvenile jumping spider. After boiling the dead spider inside 10% Potassium hydroxide solution, all proteins are removed, leaving a white-transparent chitin shell behind. Any kind of microstructures on the tibia-metatarsus joint disappeared. Scale bar: 350 μm

[2]For more information: https://www.kruss-scientific.com/en/know-how/glossary/contact-angle, last accessed on 19th Dec. 2020

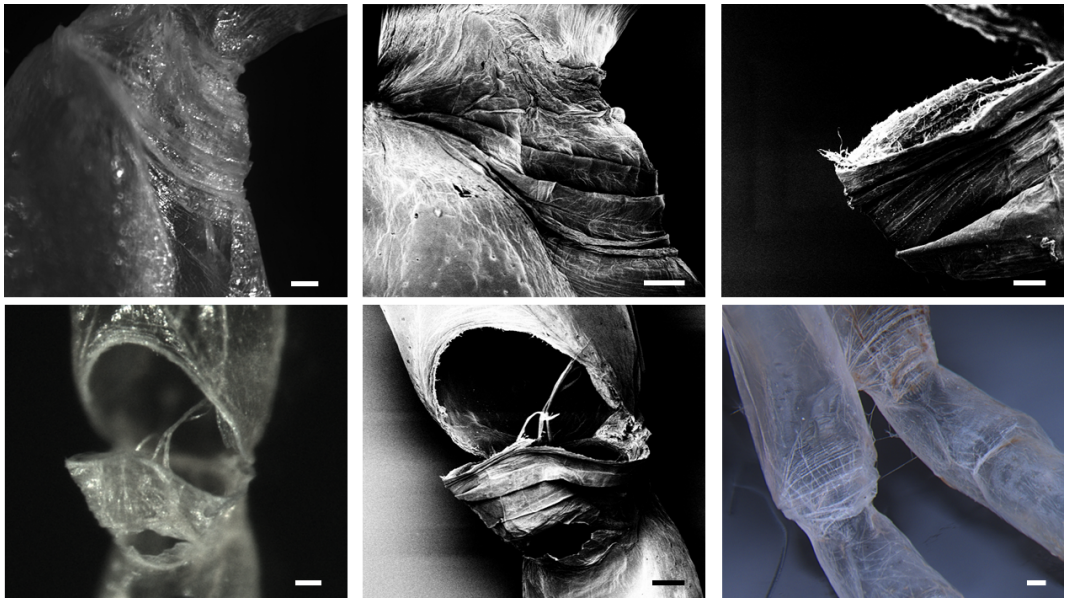

Figure 6.8: Deproteinized legs of juvenile jumping spider. Left: Leica Stereo microscopy image of deproteinized femur-patella joint. Scale bars: 100 μm. Middle: SEM image of the same samples showing no microstructures. Scale bars: 100 μm. Top Right: The articular membrane is formed by a fabric like chitin microfiber arrangement. Scale bar: 100 μm. Bottom Right: The leg segments are completely hollow, any muscles or nerves are "cooked away". Scale bar: 100 μm.

I have published the deproteinization of jumping spider joints in [43]. The following text will match largely with the published text. To analyze the base material of the articular membrane and its microstructures, proteins have been removed from the exoskeleton. Therefore, spiders were deproteinized by boiling in a 10% Potassium hydroxide (KOH) solution (modified according to [10]). Faster, microwave-assisted deproteinization methods have been proposed recently [70], but would have been too aggressive for articular membrane studies. To prepare the solution, ultra-purified water was boiled, and KOH drops were added under stirring. Boiling chips were added to avoid large bubble formation. A watch glass was used to minimize evaporation. Samples were boiled for 2 to 4 hours depending on sample size and rinsed with ethanol afterwards. When adding a whole spider into the solution, the spider inflates and air escapes out of the abdomen, propelling it along the water surface. After the boiling process, all hair and colors were removed, leaving a transparent, chitin fiber-like construct of the exoskeleton behind (fig. 6.7, 6.8).

6.6 Hemolymph Analysis

6.6.1 Hemolymph Collection Method

We started with the hemolymph of wolf spiders and crickets as I had only a small amount of jumping spiders at this point and they were not all adult yet. For the wolf spiders we used a method, which is commonly used to gain hemolymph from *Drosophila* flies, by poking a tiny hole into the exoskeleton and centrifuge the spider. The spider was shortly narcotized before. For crickets, the centrifuge method was not suitable as the gut content would also be collected. Therefore we collected hemolymph from the legs for testing. Later, for the adult jumping spiders, centrifuging was also not used due to the gut content, instead the ventral side of the spider prosoma is known to contain a large amount of hemolymph, where we collected it from (fig. 6.9). The amount of hemolymph was thereby always only in the 10th of μl maximum which was not enough for shear measurements under the viscosimeter. We started with analyzing the speed of micro beads inside the fluid. However, the fluid started to evaporate at the corners of the droplet influencing the observed speed, furthermore this method did not allow us to test the pressure-influence on the physical properties of hemolymph. In a next step we used thin glas capillaries attached to a suction pump commonly used in cell biology and analyzed the speed of the fluid through a defined section with high speed camera and microscopy. This method was improved, by adding a pressure sensor and using micro channels instead of the glass capillaries at the end. The first experimental results seemed promising, however at this point we were only able to use channels with grooves for our experiments and the control measurements had too many outliers. With the leave of my colleague to Netherlands in November 2017, the project was hold on ice until I was able to redesign and order a new mask for micro channels without the grooves, fabricate my own silicon wavers using photolitography and cast the final PDMS micro channels myself. Shortly before I left to ETH, in September 2018, I was able to collect hemolymph from adult jumping spiders and run the experiments. In the meanwhile another research group was analyzing the viscosity values of the hemolymph of finger-sized Tabacco Hornworm caterpillar *Manduca sexta*) in dependency of temperature. In contrast to our study, they were able to use the viscosimeter as the amount of hemolymph in the large caterpillar was much higher. They showed that with temperature increase, the viscosity of insect hemolymph viscosity decreases to 2-3 cP at room temperature. Although not in the focus of their study, the results further suggest a Non-Newtonian behavior of hemolymph, showing a slight decrease in viscosity with increase in shear rate. However, they did not further investigate or discuss this aspect and the value for spiders might be completely different.

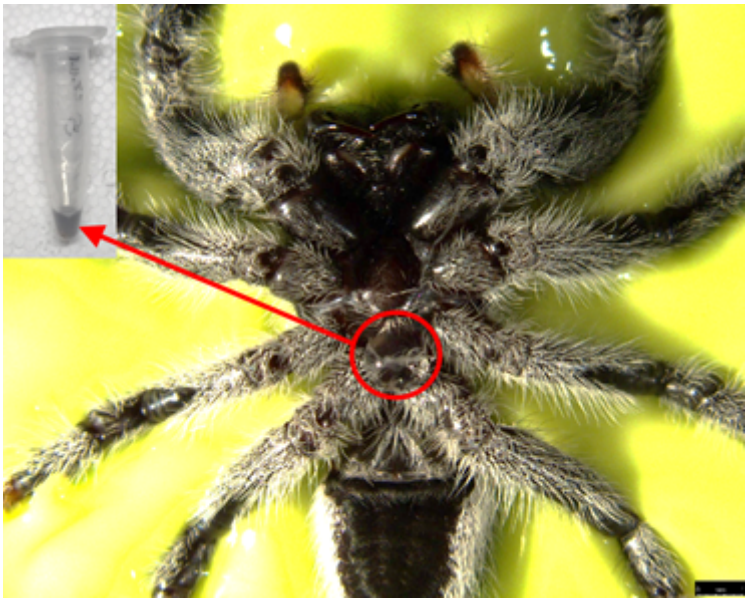

Figure 6.9: Hemolymph collection. Adult jumping spiders were narcotized with CO_2 and attached to a Petridish with dental polymer. A small hole is poked into the soft attachment membrane between the last leg pair, the sternum and the petiole and flowing out hemolymph was collected. Hemolymph collected from leg joints can show a darker color (as shown on the photography). Scale bar: 1 mm.

6.6.2 Microrheology

This method is only elaborated shortly, as it was not used as the final approach. The movement of spherical polystyrene microbeads (Polysciences, Inc., Washington, PA, USA; 0.99 ± 0.03 μm) inside the hemolymph sample was observed. For this purpose, microbeads were deposit onto a glasslide, a droplet of hemolymph sample was added and particle velocities tracked under the microscope. The microbead-glasslide was prepared according to standard protocols [6, 29]. The beads were washed to remove any surfactants and suspended in water. The glasslide was treated with oxygen plasma (Diener Electronic Zepto, Ebhausen, Germany) to increase hydrophilicity to allow an easier spreading of the water micro-particle drop (5 μl). The particles were flash frozen into position using liquid nitrogen and water was sublimated using a freeze dryer (Dieter Piatkowski Forschungsgeräte P4K Freeze Drier with JUMO IMAGO F3000 controller unit, Petershausen, Germany) to create a uniform particle monolayer. For testing purposes droplets (20 μl) of water or cricket hemolymph was used.

6.6.3 Aspiration

In a first attempt, thin glass capillaries (D = 0.3 mm) were used to mimic the circular channels of spiders. The capillaries were attached to an aspirator (Integra Bioscience 158300 Vacusafe Comfort Plus), commonly used for cellbiological purposes. As the fluid tends to stay inside the glass, the glass capillaries were silanized by bathing in water with three droplets of trichloro(perfluoroctyl)-silane (Sigma Aldrich, 448931) for 1h and baked in the 90°oven for 30 min to dry out water inside the glass capillary. Droplets of hemolymph were filled into the capillary and by opening the valve, the fluid was sucked through the glas capillary. After several trials, even with longer capillaries or by placing the droplet in front of the capillary, this method was discarded as it led to non-laminar flow inside the glass capillary.

Alternatively, micro channels were designed (length: 30mm, width: 1mm) for photolitography. And molds with 70 μm depth were produced on a silicon wafer (see next subsection). The silicon wafer molds were used to create PDMS micro channels. The ingredients for PDMS (Polydimethylsiloxan) were mixed (10:1, elastomer:hardener) with spatula for 1 min in a beaker. Trapped air was removed by vacuum pumping of the PDMS inside a dessicator for 15-20min. A plastic ring was fixed on a Petri dish with dental polymer to provide a border for the PDMS infill ($\sim$ 0.5 cm PDMS thickness) and PDMS was poured over the silicone waver. If air is trapped inside the mold, vacuum treatment could help. Otherwise, any air bubbles on the surface were removed with a thin needle and PDMS was cured by baking at 90° for 1h. Afterwards, PDMS was carefully removed from the silicone wafer and excess material cut off to receive a rectangular PDMS with the microchannel. Oxygen plasma treatment (1 min exposure) was used to enhance the stickiness of PDMS on the glass coverslide. Latter was used as the base of the microchannel. PDMS on the glasslide was baked inside the oven for 30 min. Circular endings of the microchannels were punctured with a needle and thin metal straws were inserted (1 mm) for connection purposes. One side is connected to the aspirator, with a pressure sensor and the other side is used to pipette a droplet of 2 μl of spider hemolymph which is sucked into the microchannel.

6.6.3.1 Photolithography Protocol

The SUSS MicroTec MJB4 Mask Aligner was used to fabricate molds with the Photoresist SU8-50 on Silicon wafers (Siegert Wafers and P-type and <100> orientation). The following protocol was developed at the Max Planck Institute for Intelligent Systems, Physical Intelligence Department to fabricate microstructures or microchannels inside the clean room.

Step 1: Cleaning and spin coating
Silicon wafers were cleaned in Acetone and then in Isopropanol alcohol for 5 minutes each and carefully rinsed with DI water afterwards. Then, the silicone wafer were placed on a hot plate(Precision hotplate Präzitherm) at 250°C for 10 min for dehydration baking (critical). After letting the wafer cooling down to room temperature, it was placed onto the spin coater (Laurell WS-650-23NPP Modular Spin processor). Photoresist was dispensed in the center of the wafer and span at 1500rpm (Step 1: 500rpm, 5 sec, Step 2: 2500 rpm 40 sec, acceleration 100 rpm, Step 3: 500 rpm, 5 sec). After carefully removing the silicon wafer and placed on the hot plate for pre-baking (first at 65°C for 10 min and slowly ramped up to 95°C and leave for 30 min) excess material on the inside of the spin coater was cleaned. The wafer was again cooled down to room temperature after pre-baking

Step 2: UV Expose
The desired photomask was load into the mask aligner. Using Vacuum contact as contact mode, the photoresist coated wafer was exposed for 15 sec (Wavelength of UV is 365 nm and Intensity is 13 mW/cm^2)

Step 3: Post bake and Develop
The silicon wafer was carefully removed and placed onto the hot plate (first at 65°C for 1 min and slowly ramped up to 95°C and leave it for 10 min). After it cooled down to room temperature, the wafer is immersed in the mr-600 developer with slight agitation (for 10 min) and afterwards carefully rinsed in Isopropanol for 2 min to remove any excess.

Step 4: Hard bake
In the final step, the patterns were hard baked by placing the wafer again on the hot plate for 30 min at 100°C.

The thickness of the patters was measured using a Laser microscope afterwards.

6.6.4 Calculation

Considering a flowing, incompressible fluid and neglecting friction, the total sum of energy along a streamline which keeps the fluid flowing remains constant. The sum of energy thereby consists of the following components: kinetic energy E_{kin}, the potential energy E_{pot} and the enthalpy H. Latter term can be split apart into the inner energy U, which is heat dependent and the work W needed to overcome the pressure when moving a specific volume V of matter. Therefore

$$\begin{aligned} \sum \text{energy} &= E_{kin} + E_{pot} + H \\ &= E_{kin} + E_{pot} + U + W \end{aligned}$$

$$= \frac{1}{2}mv^2 + mgh + U + PV \qquad (6.1)$$
$$= \text{const} .$$

By neglecting the inner energy U when neglecting thermal energy loss, the Bernoulli principle describing the energy along a pipe can be derived by dividing the term through mass m and the gravity constant g

$$\begin{aligned} \sum \text{energy}_{pipe} &= \frac{v^2}{2g} + h + \frac{P}{g}\frac{V}{m} \\ &= \frac{v^2}{2g} + h + \frac{P}{g\rho} \qquad \text{for } \rho = m/V \qquad (6.2) \\ &= \text{const} . \end{aligned}$$

Looking at two points along a pipe for an incompressible fluid with the density ρ, the Bernoulli equation says:

$$\frac{v_1^2}{2g} + h_1 + \frac{P_1}{g\rho} = \frac{v_2^2}{2g} + h_2 + \frac{P_2}{g\rho} . \qquad (6.3)$$

This term, however, does not include the influence on pipe friction, which can create head loss H_L between the two points, described by the Darcy-Weisbach equation:

$$H_L = f_D \cdot \frac{L}{D_h} \cdot \frac{v^2}{2g} . \qquad (6.4)$$

Thereby f_D describes the friction factor depending on the pipe material friction and the Reynolds number, L describes the distance between the two points, D_h the hydraulic diameter of the pipe, v the fluid velocity and g the gravity constant.

Considering this head loss H_L the fluid relationship (6.3) along the stream line changes to:

$$\begin{aligned} \frac{v_1^2}{2g} + h_1 + \frac{P_1}{g\rho} &= \frac{v_2^2}{2g} + h_2 + \frac{P_2}{g\rho} + H_L \\ \frac{v_1^2}{2g} + h_1 + \frac{P_1}{g\rho} &= \frac{v_2^2}{2g} + h_2 + \frac{P_2}{g\rho} + f_D \cdot \frac{L}{D_h} \cdot \frac{v_2^2}{2g} . \qquad (6.5) \end{aligned}$$

In a horizontal pipe the height and velocity does not change along the pipe ($h1 = h2$, $v1 = v2$). Therefore the equation can be further reduced to describe

the pressure gradient along the pipe.

$$\frac{P_1}{g\rho} = \frac{P_2}{g\rho} + f_D \cdot \frac{L}{D_h} \cdot \frac{v^2}{2g}$$
$$P_1 - P_2 = \Delta P = f_D \cdot \frac{L\rho v^2}{2D_h} \ . \tag{6.6}$$

In literature, this relation is often cited as the actual Darcy-Weisbach equation for pipes and becomes relevant for our experiments, written in a slightly different way:

$$\frac{\Delta P}{L} = f_D \cdot \frac{\rho}{2} \cdot \frac{v^2}{D_h} \ . \tag{6.7}$$

describing the pressure gradient along a pipe with length L and hydraulic diameter D_h for a fluid with density ρ and measured flow velocity v. The pressure gradient thereby depends on the the pipe friction and Reynolds number Re which is summarized in the Darcy friction coefficient f_D [118, 126] as

$$f_D = \frac{\beta}{Re} \tag{6.8}$$
$$Re = \frac{\rho}{\mu} \cdot v \cdot D_h. \tag{6.9}$$

The Reynolds number differs with the fluid velocity v, density ρ and viscosity μ as well as the the shape of the pipe. In a rectangular micro channel, β is not 64, as commonly used for laminar flow, but can be calculated from

$$\beta = 24 \cdot (1 - 1.3553\alpha + 1.9467\alpha^2 - \tag{6.10}$$
$$1.7012\alpha^3 + 0.9564\alpha^4 - 0.2537\alpha^5)$$
$$\alpha = \frac{H}{W} \ , \tag{6.11}$$

with α given as the ratio between height H and width W. For slit-shaped channels with a large width and a small height, β is close to 24. Furthermore, the hydraulic diameter D_h is defined as

$$D_h = \frac{4A}{U} \ , \tag{6.12}$$

with A describing the cross-sectional area of the flow and U the wetted perimeter of the cross-section. For a rectangular channel with height H and width W, the

hydraulic diameter is therefore

$$\begin{aligned} D_h &= \frac{4(W \cdot H)}{2(W+H)} \\ &= \frac{2(W \cdot H)}{(W+H)} \\ &\approx 2 \cdot H \qquad \text{for } W >> H \ . \end{aligned} \tag{6.13}$$

To analyze the experimental data based on velocity, measured at different pressure gradients, the Darcy-Weisbach equation needs to be reformulated into the terms of shear stress and shear rate. The relation of the pressure and wall shear stress τ_w is given by

$$\begin{aligned} \Delta P \cdot A_{cross} &= \tau_w \cdot A_{wall} \\ \Delta P \cdot W \cdot H &= \tau_w \cdot 2 \cdot (WL + HL) \\ &\approx \tau_w \cdot 2 \cdot (WL) \qquad \text{for } W >> H \\ \frac{\Delta P}{L} &= \tau_w \cdot \frac{2(W+H)}{W \cdot H} \\ \frac{\Delta P}{L} &= \tau_w \cdot \frac{4}{D_h} \\ \tau_w &\approx \frac{\Delta P \cdot H}{2 \cdot L} \qquad \text{for } W >> H \ . \end{aligned} \tag{6.14, 6.15}$$

Integrating this relationship into the Darcy-Weisbach equation (6.7), it follows

$$\begin{aligned} \frac{\Delta P}{L} &= f_D \cdot \frac{\rho}{2} \cdot \frac{v^2}{D_h} \\ \frac{\Delta P \cdot D_h}{4 \cdot L} = \tau_w &= f_D \cdot \frac{\rho \cdot v^2}{8} \\ &= \frac{\beta}{Re} \cdot \frac{\rho \cdot v^2}{8} \\ &= \frac{\beta \cdot \mu}{\rho \cdot v \cdot D_h} \cdot \frac{\rho \cdot v^2}{8} \\ &= \mu \cdot \frac{\beta \cdot v}{8 \cdot D_h} \\ \tau_w &= \mu \cdot \dot{\gamma}_a \ , \end{aligned} \tag{6.16}$$

where $\dot{\gamma}_a$ describes the apparent shear rate for Newtonian fluids, normally defined via the Hagen-Poiseuille relation. The more generic Ostwald-de Waele equation describes the relation between shear stress and shear rate, also includ-

ing power law fluids (non-Newtonian) fluids as

$$\tau_w = K \cdot \dot{\gamma_w}^n = K \cdot \dot{\gamma_w}^{(m+1)} \tag{6.17}$$

$$\mu_a = K \cdot \dot{\gamma_w}^{n-1} = K \cdot \dot{\gamma_w}^m \ , \tag{6.18}$$

with n, m the dimensionless flow behavior index, K the flow consistency index, $\dot{\gamma}_w$ the wall shear rate and μ_a the apparent, dynamic viscosity. It can be easily seen, that for $m = 0$, or the more commonly used index $n = 1$, the apparent viscosity does not depend on the wall shear rate, corresponding to a Newtonian fluid, while for n larger or smaller than 1, the fluid shows shear thickening or shear thinning behavior. The relation between the apparent and the wall shear rate is given by the Weissenberg-Rabinowitsch correction for slit shaped channels

$$\dot{\gamma}_w = \frac{2(m+1)+1}{3(m+1)} \cdot \dot{\gamma}_a = \frac{2n+1}{3n} \cdot \dot{\gamma}_a \ . \tag{6.19}$$

For rectangular channels with H/W ration not close to 0, this correction factor can be defined even finer as summarized in [126].
As in our case, H/W is 0.07 which is considered as close to 0, the needed equations can be reduced to the following:

$$\tau_w = \frac{\Delta P \cdot H}{2 \cdot L} \tag{6.20}$$

$$\dot{\gamma}_a = \frac{3v}{2H} \ . \tag{6.21}$$

To determine the viscosity from the measured fluid velocity at given pressure gradients, the wall shear stress τ_w and the apparent shear rate $\dot{\gamma}_a$ needs to be calculated in the first step. Given by the Rabinowitsch correction factor, the following relationship can then be established:

$$\tau_w = K \cdot \left[\left(\frac{2n+1}{3n} \right) \cdot \dot{\gamma}_a \right]^n \tag{6.22}$$

$$\log(\tau_w) = \log(K) + n \cdot \log\left(\frac{2n+1}{3n} \right) + n \cdot \log(\dot{\gamma}_a)$$

$$\log(\tau_w) = n \cdot \log(\dot{\gamma}_a) + C$$

$$\frac{1}{n} \cdot \log(\tau) - \frac{C}{n} = \log(\dot{\gamma}_a) \ . \tag{6.23}$$

Therefore n can be established by a linear fit through the log-log plot of the wall shear stress and the apparent shear rate. Important to notice is that as $\dot{\gamma}_a$ is proportional to the measured velocity v, which can have experimental

variance, while τ_w is only dependent on the set pressure gradient and shows only minimal error, it is important to conduct the linear fit for τ_w on the x-axis and $\dot{\gamma}_a$ on the y-axis, so that the standard fitting method (ordinary least square) works properly. As the variance between the shear stress and shear rate differ immense, the linear fit will not be the same when the x-y axis are swapped. In a next step, the wall shear rate $\dot{\gamma}_w$ can be calculated from the fitted n (be aware that the slope of the switched plot is 1/n) and the Rabinowitsch correction relation

$$\dot{\gamma}_w = \left(\frac{2n+1}{3n}\right) \cdot \dot{\gamma}_a \tag{6.24}$$

$$\tau_w = K \cdot \dot{\gamma}_w^n \tag{6.25}$$

$$\begin{aligned} \log(\tau_w) &= \log(K) + n \cdot \log(\dot{\gamma}_w) \\ \frac{1}{n} \cdot \log(\tau_w) - \frac{\log(K)}{n} &= \log(\dot{\gamma}_w) \\ -\frac{log(K)}{n} &= \text{intercept} \\ \log(K) &= \text{intercept} \cdot (-n) \\ K &= 10^{\text{intercept} \cdot (-n)} \ . \end{aligned} \tag{6.26}$$

By conducting a second linear fit through the log-log-plot of the wall shear stress and wall shear rate, the flow consistency index can be calculated from the intercept, which can then be used to calculate the apparent viscosity μ_a given in 6.18.

6.6.5 Error propagation

Table 6.3: Observational errors used for error propagation. The parameters were chosen according to ∼1% of the set parameter value. These values set the upper and lower margins of the given parameters.

parameter	estimated error	unit	
ΔP	0.1	kPa	pressure sensor
s	3	μm	tracked traveling distance
v	3000	μm/s	extracted velocity from video data
H	5	μm	height of the channel
W	5	μm	width of the channel
L	1000	μm	length of the channel
β	0	-	friction factor value

Due to systematic errors (tab. 6.3) , values of the experimental measurements could have uncertainties (fig. 6.10). These uncertainties propagate through the calculation of the analysis and are calculated by the sum of partial derivative multiplied with the error of the parameters.

$$\Delta y = \sum_{n=i}^{N} \left(\frac{\partial y}{\partial x_i} \cdot \Delta x_i\right) \tag{6.27}$$

(6.28)

$$\begin{aligned}\Delta\tau_w &= \left|\frac{\partial \tau_w}{\partial \Delta P}\right| \cdot \Delta(\Delta P) + \left|\frac{\partial \tau_w}{\partial H}\right| \cdot \Delta H + \left|\frac{\partial \tau_w}{\partial L}\right| \cdot \Delta L \\ &= \left|\frac{H}{2L}\right| \cdot \Delta(\Delta P) + \left|\frac{\Delta P}{2L}\right| \cdot \Delta H + \left|\frac{-\Delta P \cdot H}{2L^2}\right| \cdot \Delta L \end{aligned} \tag{6.29}$$

$$\begin{aligned}\Delta\dot{\gamma}_a &= \left|\frac{\partial \dot{\gamma}_a}{\partial \beta}\right| \cdot \Delta\beta + \left|\frac{\partial \dot{\gamma}_a}{\partial v}\right| \cdot \Delta v + \left|\frac{\partial \dot{\gamma}_a}{\partial H}\right| \cdot \Delta H \\ &= \left|\frac{v}{16H}\right| \cdot \Delta\beta + \left|\frac{3}{2H}\right| \cdot \Delta v + \left|\frac{-3v}{2H^2}\right| \cdot \Delta H \end{aligned} \tag{6.30}$$

$$\begin{aligned}\Delta n &= \left|\frac{\partial n}{\partial(\log(\tau_w))}\right| \cdot \Delta(\log(\tau_w)) + \left|\frac{\partial n}{\partial(\log(\dot{\gamma}_a))}\right| \cdot \Delta(\log(\dot{\gamma}_a)) \\ &= \left|\frac{1}{(\log(\dot{\gamma}_a) - \text{intercept})}\right| \cdot \frac{1}{\ln(10)} \cdot \frac{\Delta\tau_w}{\tau_w} + \\ &\quad \left|\frac{-\log(\tau_w)}{(\log(\dot{\gamma}_a) - \text{intercept})^2}\right| \cdot \frac{1}{\ln(10)} \cdot \frac{\Delta\dot{\gamma}_a}{\dot{\gamma}_a} \end{aligned} \tag{6.31}$$

$$\begin{aligned}
\Delta\dot{\gamma}_w &= \left|\frac{\partial\dot{\gamma}_w}{\partial n}\right| \cdot \Delta n + \left|\frac{\partial\dot{\gamma}_w}{\partial\dot{\gamma}_a}\right| \cdot \Delta\dot{\gamma}_a \\
&= \left|\left(\frac{-1}{3n^2}\right) \cdot \dot{\gamma}_a\right| \cdot \Delta n + \left|\frac{2n+1}{3n}\right| \cdot \Delta\dot{\gamma}_a \qquad (6.32) \\
\Delta(\log(K)) &= \frac{1}{(\ln(10))} \cdot \frac{\Delta K}{K} \\
\Delta(\log(K)) &= \left|\frac{\partial(\log(K))}{\partial(\log(\tau_w))}\right| \cdot \Delta(\log(\tau_w)) + \\
&\quad \left|\frac{\partial(\log(K))}{\partial(\log(\dot{\gamma}_w))}\right| \cdot \Delta(\log(\dot{\gamma}_w)) + \\
&\quad \left|\frac{\partial(\log(K))}{\partial n}\right| \cdot \Delta n \\
&= \frac{1}{\ln(10)} \cdot \frac{\Delta\tau_w}{\tau_w} + |-n| \cdot \frac{1}{\ln(10)} \cdot \frac{\Delta\dot{\gamma}_w}{\dot{\gamma}_w} + |-\log(\dot{\gamma}_w)| \cdot \Delta n \qquad (6.33) \\
\Delta\mu_a &= \left|\frac{\partial\mu}{\partial\dot{\gamma}_w}\right| \cdot \Delta\dot{\gamma}_w + \left|\frac{\partial\mu}{\partial n}\right| \cdot \Delta n + \left|\frac{\partial\mu}{\partial K}\right| \cdot \Delta K \\
&= \left|(n-1)K\dot{\gamma}_w^{n-2}\right| \cdot \Delta\dot{\gamma}_w + \left|K \cdot \ln(\dot{\gamma}_w) \cdot \dot{\gamma}_w^{(n-1)}\right| \cdot \Delta n + \\
&\quad \left|\dot{\gamma}_w^{(n-1)}\right| \cdot \Delta K \qquad (6.34)
\end{aligned}$$

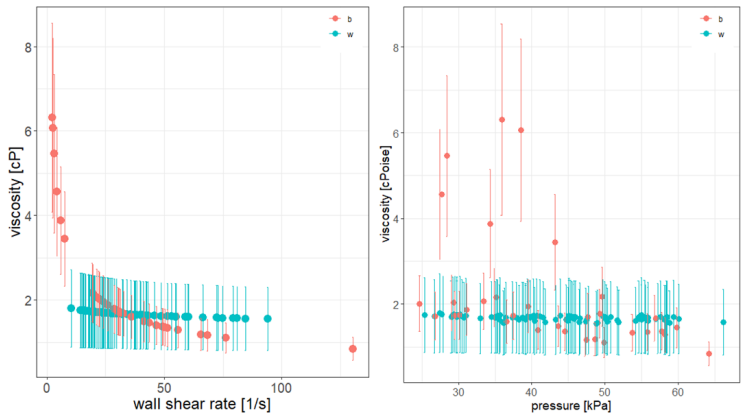

Figure 6.10: Error propagation with individual error values. When considering single error values per each measurement point, larger values would result in larger errors. For experimental discussions, it is assumed that the systematic error is the same throughout all measurement points (fig. 3.27, 3.26). The median of the here plotted single calculated errors was chosen as value to reflect the general systematic viscosity error.

6.7 Design and Fabrication of Actuator

6.7.1 Robotic Design and Fabrication

I have published the robotic design and fabrication of the spider-inspired joint design in [43]. The following text will match largely to the published text. 3D modeling was first performed with Solidworks, but to optimize fabrication and 3D printing results, Autodesk Fusion 360 was used in the final design. Construction was made according to 3D observations of the spider femur-patella joint. The models were sliced using the Ultimaker software CURA for the 3D FDM printer (Creality Ender-3 Pro) to generate the machine Gcode for 3D printing. Printing parameters can be found in tab. 6.4. The chosen TPU filament (EoFlex by EOLAS, Reference 1009600000) has a tensile strength of 40 MPa and a shore hardness of 94A. To improve performance for flexible material prints, the bowden extruder was moved directly on top of the printing head. For flexing the actuator, fishing yarn (0.12 mm, Spiderwire, Stealth Smooth 8) was used. To seal irregularities of the 3D print Latex milk (Laguna, natural liquid latex rubber, low ammonia (<0.3%), 60% solid content) was filled inside the chamber and cured for 30 min at 50° in the oven, to form a thin layer.

Table 6.4: 3D printing parameters. Published in [43]. Parameters used for fused deposition modeling (FDM) with Creality Ender-3 Pro. 3D model designed in Autodesk Fusion 360 and stl-file directly exported to CURA (Ultimaker). The software slices the model and generates G-codes for 3D printing.

Parameter	Value	Unit	R-value	p-value
Layer Height	0.2	mm	0.931	<2.2e-16
Wall Thickness	1.0	mm	0.890	<2.2e-16
Print Thin Walls	Enabled	-	0.795	<2.2e-16
Infill Density	100	%	0.905	<2.2e-16
Infill Pattern	Concentric	-		
Printing Temperature	205	°C		
Build Plate Temperature	25	°C	0.750	1.2e-15
Flow	100-150	%	0.576	2.9e-07
Print Speed	50.0	mm/s	0.520	6.0e-14
Retraction	Disabled	-	0.627	1.6e-12
Fan Speed	100-120	mm/s		
Build Plate Adhesion Type	Skirt			

6.7.2 Previous tested Fabrication Methods and Materials

Several materials and methods were tested for fabrication and sealing purposes as listed in tab. 6.5 and tab. 6.6.

6.7.3 Characterization

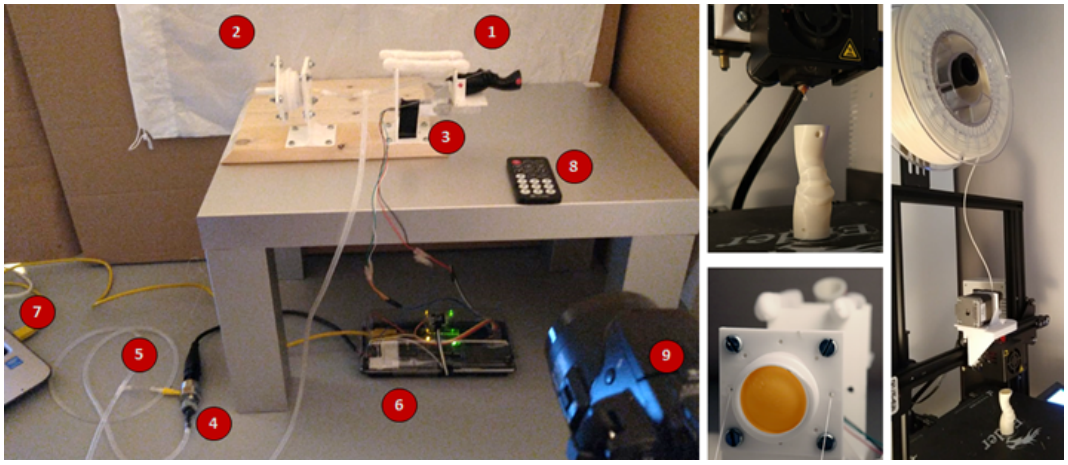

Figure 6.11: Experimental setup of characterization measurements. Published in [43]. Left: Experimental set-up for prototype characterization includes, the prototype with red tracking markers (1), a rotating flexing mechanism (2), a force sensor (3), a pressure sensor (4), a connection for a syringe to increase pressure (5), an Arduino Uno for sensor processing (6), a computer for recording (7), a remote control for changing into calibration mode (8) and a camera, recording folding angle (9). Top middle: 3D model of spider-joint-inspired actuator prototype is printed in vertical direction (femur to patella) to avoid support material inside the chamber. Bottom middle: The flexing mechanism consists of an inner latex bladder that inflates and collects the water, when the leg is flexed. Right: Bowden extruder head was rebuilt to direct extrusion, allowing better 3D printing of flexible material as rubber material show discontinued material pushing due to its elasticity properties.

I have published the experimental set-up for the characterization of the spider-inspired joint design in [43]. The following text will match largely to the published text. For the folding behavior and durability test, the flexing wire was attached to a 12 V-stepper motor (NEMA 17) and flexing runs (2 x 500 cycles) for each leg were performed (run time: 2 s/ cycle). For flexing characterization, an experimental set-up was 3D printed (PLA), including a load sensor platform and a rotational flexing chamber. A force sensor (5 kg

Table 6.5: Tested materials and fabrication methods. Several materials and fabrication methods were tested to investigate the most promising approach for a spider-inspired 3D prototype. The table summarizes observations and limitations of tested methods. Published in [43].

Material	Comment
Textile	· If not water repellent, sealing with different methods as wax or glue necessary · Limitation: thick material, stiffness variance by creating inlets with e.g. metal sticks as in stroller sunshades is time consuming and not scalable, high friction
PE foil	· Cheap · Bags can be formed using heat or glue · Good prototyping material · limitation in (air) pressure and sealing
Other foils	Nylon · Stitching, laser or glue processing · Limitations: sealing issues Foil balloons · Easy processing material with heat · Limitation: only one side can be heat treated
Silicon	· Not for fast prototyping due to time consuming molding/casting · Pressure resistance ("blowing up") and thinness might be limited · Good sealing quality · Useful as comparative material for future work for given design · 3D printing techniques are now evolving
Latex	· Not for fast prototyping due to time consuming molding/casting · Pressure resistance ("blowing up") and thinness might be limited · Good sealing quality, can be resealed · Useful as comparative material for future work for given design
Carbon fiber	· Time consuming in fabrication · Too thick or not flexible enough for desired purposes
Paper	· Complex 3D shapes by origami techniques · Easy processing for "quick and dirty" prototype testing · Limitation: Sealing, fractures forming after several usage · Might be useful in combination with a good sealing material
Tango Black	· Flexible, but sticky · High resolution and two material printing due to PolyJet technique possible · Not completely sealed · Limitation in thinness, rips easily during 3D print cleaning, non-water-soluble support material leads to time consuming washing · Useful as comparative material for future work for given design
TPU	· Available for FDM 3D printing, allowing fast prototyping and complex shapes · Comparatively cheap flexible material and fabrication method · Limitation: 3D printing set-up not fully evolved, can differ highly from 3D printer type, 3D prints need to be fully sealed as irregularities can occur

Table 6.6: Tested sealing materials and methods. Several materials and fabrication methods were tested for sealing purposes. Table summarizes observations and limitations of tested methods. Published in [43].

Material	**Comment**
Silicon	Smooth-On Ecoflex · Does not cure on the TPU surface
Plasti-Dip	Covering 3D print by dipping · Fast fabrication, but thickness varies with viscosity limiting folding · Changes TPU material, gets brittle · Material not environment friendly Spray · Thin layer, movements lead to peeling off
Leakage Spray	Stop Leakage Weicon, Universal Dicht-Spray (Allround Sealing Spray) · Gray, flexible sealing layer, good adhesion on TPU · Thickness varies · Small 3D irregularities cannot be fixed
Latex	Laguna, natural liquid latex rubber, low ammonia (<0.3%), 60% solid content Covering 3D print by dipping and drying at room temperature · Sticky layer, using baby powder to avoid self-sticking and peeling off, curing times vary · Difference in thickness when drying through draining · Small bubbles can form on the surface when dipping, leading to unsealed area · Peeling off can happen when pressurizing · Can influence "collapsibility" behavior due to thickness on the outside Filling chamber and baking at 50° for 30 min · Non-sticky inner layer, thin sheet of latex · Holes can be "healed", by repeating the process · No influence of the folding properties

load cell with HX711 AD amplifier) and pressure sensor (30 PSI, ∼ 200 kPa, stainless steel, GS01525, DC-5V) attached to an Arduino Uno (fig. 6.11) were used to measure load and pressure. Before every measurement, the force and pressure sensor were calibrated. The flexing mechanism consisted of a water reservoir with a Latex inner bladder, which fills up when the joins fold. During flexing, the wire rolls around the cylinder. By releasing the wire, the bladder is pushed by an inner cylinder, so that the water fills the joint. As flexing wire, a fishing yarn (Spiderwire, Stealth Smooth 8) was used to avoid curling. This rotational flexing mechanism has to be further tested in future, to allow higher pressure (failure in latex bladder connection at pressures above 50 kPa). Tracking markers were attached to the leg and the base (fixation) and the leg movement was recorded. The tracking angle was analyzed using the software Tracker (physlets.org/tracker/). The video and the sensor measurement were synchronized by hitting the force sensor with a pen to achieve a visual signal that could be correlated to a spike in the force sensors. Legs were flexed and released slowly (6 experimental runs) and suddenly (4 experimental runs) by detaching the wire from the flexing mechanism. For characterization of the extension property a hinge platform (fig. 4.15) was 3D printed (PLA). Legs were hold in the stable positions (40°, 75°, 100°, 125°) and pressure was increased with a syringe up to 200-300 kPa. The load was recorded. For each position, 3 experimental runs were conducted. At position 75°, tube leakage occurred during one experimental run and was therefore excluded from analyses. Position 100° was tested 5 times in total as it was considered as the critical position for jumping and lifting experiments. All sensors (pressure sensor: 100 PSI, ∼690 kPa; load cell: 5 kg, ∼50 N) were attached to an Arduino Uno. Leakages through tube connections were minimized by shorter PVC tubes and push-in tube connectors. As commonly done for hydraulic systems, pressure sensor attachment sealing was improved by roughening the tube connector thread and covering it with PTFE tape.

6.7.4 Jumping Performance Estimation

I have published the jumping performance estimation of the spider-inspired prototype in [43]. The following text will match largely to the published text. Pressure is defined as the force acting on a surface area. To estimate the load - pressure behavior of our system, a constant contact area at each stable position (fig. 4.15) was assumed, resulting in a proportional increase of load with pressure. Linear fits through the experimental data at each stable position have been carried out (tab. 6.7). Displayed linear functions show linear fits (fig. 4.16) with a mean slope of 0.013 N/kPa, corresponding to a contact surface of 13 mm^2. This surface would match to the surface at the entry of the chamber,

Table 6.7: Linear fit for load-pressure behavior estimation Published in [43]

position (°)	fixed intercept (N)	fitted slope (N/kPa)	R-value	p-value
40	1.5	0.017	0.931	<2.2e-16
75	3.5	0.012	0.890	<2.2e-16
100	6.0	0.012	0.795	<2.2e-16
125	10.0	0.012	0.905	<2.2e-16
	mean	0.01311004		
	fitted intercept			
40	1.47	0.017	0.750	1.2e-15
75	4.29	0.007	0.576	2.9e-07
100	5.89	0.012	0.520	6.0e-14
125	10.57	0.009	0.627	1.6e-12

were water supply is connected to. Further studies of this surface area have to be done in following works. The mean slope value was used to calculate the load at 200 kPa and the resulting work, mirrored by the sum of the area below the curve (W1, W2, W3, W4) (fig. 4.17). The resulting work shows a quadratic behavior with opening distance as

$$W = 105.86s^2 + 1.6731s \ . \tag{6.35}$$

As the work is the integral of force over distance, a linear force-distance behavior, would explain this quadratic function and shows that the initial flexing position s of the legs have a great impact on the jumping performance. This formula was used to estimate the jumping height, whereby the work created by the elastic material was subtracted as it is needed to just lift the platform. The elastic work for four legs lies between 0.17 Nm to 0.42 Nm for legs flexed between positions 75° and 100°. For calculation purposes, the mean-value (0.30 Nm) was used. The work left after deduction was treated as potential energy of the system, to estimate the jumping height as

$$h = \frac{\Delta W}{mg} \ . \tag{6.36}$$

6.7.5 Material Behavior Comparison

I have published the material behavior comparison of TPU und spider cutcile in [43]. The following text will match largely to the published text. The chosen

TPU filament shows a Shore Hardness of 94A, which corresponds to a Young's modulus E of approximately 0.005GPa (4.8 MPa) from

$$E = e^{(\text{ShoreA}\cdot 0.0235 - 0.6403)} \ . \tag{6.37}$$

For comparison, to achieve the same displacement s when bending two beams, one with the measured stiffness of spider membrane (5 GPa) and one with the stiffness of TPU (5 MPa), keeping length L, width b and applied force F of the beams the same, the thickness d of the TPU beam has to be 10 times higher than the spider membrane, computed from:

$$s = \frac{-4L^3}{Ed^3bF} \ . \tag{6.38}$$

Assuming the measured stiffness for the articular membrane could be 10 times lower under hydrated condition, it would still result in a ratio of 5. This means, to fabricate a membrane similar in the length scale of jumping spiders, a thickness of 250 μm of TPU membrane is needed to be comparable in its bending behavior to a 50 μm thick spider membrane.

Bibliography

[1] *Formula Book for Hydraulics and Pneumatics*. Fluid and Mechanical Engineering Systems Department of Management and Engineering, Linköping University, 2008. https://people.utm.my/shamsul/wp-content/blogs.dir/949/files/2015/11/FormulaBook_HydraulicsPneum.pdf.

[2] Functional differentiation of spider hemocytes by light and transmission electron microscopy, and {MALDI}-{MS}-imaging. *Developmental & Comparative Immunology*, 43(1):59–67, mar 2014. URL http://www.sciencedirect.com/science/article/pii/S0145305X13002991.

[3] B. Aberle, R. Jemmali, and J.-H. Dirks. Effect of sample treatment on biomechanical properties of insect cuticle. *Arthropod structure & development*, 46(1):138–146, 2017.

[4] M. F. Ahamed and S. Chauhan. Hydraulic actuator systems with non-newtonian working fluid. *Bonfring International Journal of Industrial Engineering and Management Science*, 6(4):135–139, 2016.

[5] J. Allen. *Design and application of external power and control of orthotic devices*. Rancho Los Amigos Hospital, 1962.

[6] G. J. Amador, T. Endlein, and M. Sitti. Soiled adhesive pads shear clean by slipping: a robust self-cleaning mechanism in climbing beetles. *Journal of The Royal Society Interface*, 14(131):20170134, 2017.

[7] J. Anderson and K. Prestwich. The fluid pressure pumps of spiders (chelicerata, araneae). *Zeitschrift für Morphologie der Tiere*, 81(4):257–277, 1975.

[8] S. A. Arnold, S. Albiez, A. Bieri, A. Syntychaki, R. Adaixo, R. A. McLeod, K. N. Goldie, H. Stahlberg, and T. Braun. Blotting-free and lossless cryo-electron microscopy grid preparation from nanoliter-sized protein samples and single-cell extracts. *Journal of Structural Biology*, 197(3):220–226, 2017.

[9] S. A. Arnold, S. A. Müller, C. Schmidli, A. Syntychaki, L. Rima, M. Chami, H. Stahlberg, K. N. Goldie, and T. Braun. Miniaturizing em sample preparation: Opportunities, challenges, and "visual proteomics". *Proteomics*, 18(5-6):1700176, 2018.

[10] F. G. Barth. Microfiber reinforcement of an arthropod cuticle. *Zeitschrift für Zellforschung und Mikroskopische Anatomie*, 144(3):409–433, 1973.

[11] N. W. Bartlett, M. T. Tolley, J. T. Overvelde, J. C. Weaver, B. Mosadegh, K. Bertoldi, G. M. Whitesides, and R. J. Wood. A 3d-printed, functionally graded soft robot powered by combustion. *Science*, 349(6244):161–165, 2015.

[12] K. Bett and J. Cappi. Effect of pressure on the viscosity of water. *Nature*, 207(4997):620–621, 1965.

[13] C. M. Biancardi, C. G. Fabrica, P. Polero, J. F. Loss, and A. E. Minetti. Biomechanics of octopedal locomotion: kinematic and kinetic analysis of the spider grammostola mollicoma. *Journal of Experimental Biology*, 214 (20):3433–3442, 2011.

[14] R. Blickhan and F. G. Barth. Strains in the exoskeleton of spiders. *Journal of Comparative Physiology A*, 157(1):115–147, 1985.

[15] R. Blickhan, S. Petkun, T. Weihmann, and M. Karner. Schnelle bewegungen bei arthropoden: Strategien und mechanismen. In *Autonomes Laufen*, pages 19–45. Springer, 2005.

[16] V. Böhm, L. Zentner, and N. Turkevi-Nagy. Stoffschlüssige gelenke nach biologischem vorbild. *Proceedings of the Wissenschaftliche Mitteilungen der*, 14:19–27, 2002.

[17] L. Bohmann and R. Blickhan. Der hydraulische mechanismus des sprunges einer spinne. *Forschung im Ingenieurwesen*, 63(7-8):224–230, 1997.

[18] N. Booster, F. Su, S. Adolph, and A. Ahn. Effect of temperature on leg kinematics in sprinting tarantulas (aphonopelma hentzi): high speed may limit hydraulic joint actuation. *Journal of Experimental Biology*, 218(7): 977–982, 2015.

[19] C. Bordereau. Ultrastructure and formation of the physogastric termite queen cuticle. *Tissue and cell*, 14(2):371–396, 1982.

[20] J. Breuninger, R. Becker, A. Wolf, S. Rommel, and A. Verl. *Generative Fertigung mit Kunststoffen: Konzeption und Konstruktion für Selektives Lasersintern*. Springer-Verlag, 2012.

[21] R. Briceño and W. Eberhard. Spiders avoid sticking to their webs: clever leg movements, branched drip-tip setae, and anti-adhesive surfaces. *Naturwissenschaften*, 99(4):337–341, 2012.

[22] M. Burrows and G. P. Sutton. Locusts use a composite of resilin and hard cuticle as an energy store for jumping and kicking. *Journal of Experimental Biology*, 215(19):3501–3512, 2012.

[23] M. Burrows, S. R. Shaw, and G. P. Sutton. Resilin and chitinous cuticle form a composite structure for energy storage in jumping by froghopper insects. *BMC biology*, 6(1):41, 2008.

[24] A. Cecilia, A. Rack, P.-A. Douissard, T. Martin, T. dos Santos Rolo, P. Vagovič, E. Hamann, T. van de Kamp, A. Riedel, M. Fiederle, et al. Lpe grown lso: Tb scintillator films for high-resolution x-ray imaging applications at synchrotron light sources. *Nuclear Instruments and Methods in Physics Research Section A: Accelerators, Spectrometers, Detectors and Associated Equipment*, 648:S321–S323, 2011.

[25] Y. Chen, H. Chung, B. Chen, B. Baoyinjiya, and Y. Sun. A lobster-inspired bending module for compliant robotic applications. *Bioinspiration & Biomimetics*, 2020.

[26] Y.-K. Chen, C.-P. Liao, F.-Y. Tsai, and K.-J. Chi. More than a safety line: jump-stabilizing silk of salticids. *Journal of The Royal Society Interface*, 10(87):20130572, 2013.

[27] Z. Chen, R. T. Corlett, X. Jiao, S.-J. Liu, T. Charles-Dominique, S. Zhang, H. Li, R. Lai, C. Long, and R.-C. Quan. Prolonged milk provisioning in a jumping spider. *Science*, 362(6418):1052–1055, 2018.

[28] Y. T. Cheng, D. Rodak, C. Wong, and C. Hayden. Effects of micro-and nano-structures on the self-cleaning behaviour of lotus leaves. *Nanotechnology*, 17(5):1359, 2006.

[29] C. J. Clemente, J. M. Bullock, A. Beale, and W. Federle. Evidence for self-cleaning in fluid-based smooth and hairy adhesive systems of insects. *Journal of Experimental Biology*, 213(4):635–642, 2010.

[30] J. Culin and M. L. Goodnight. Arachnid respiration, 2018. https://www.britannica.com/animal/arachnid/Respiration.

[31] Z. S. Davidson, H. Shahsavan, A. Aghakhani, Y. Guo, L. Hines, Y. Xia, S. Yang, and M. Sitti. Monolithic shape-programmable dielectric liquid crystal elastomer actuators. *Science advances*, 5(11):eaay0855, 2019.

[32] R. Deimel and O. Brock. A novel type of compliant and underactuated robotic hand for dexterous grasping. *The International Journal of Robotics Research*, 35(1-3):161–185, 2016.

[33] S. M. Doucet and M. G. Meadows. Iridescence: a functional perspective. *Journal of The Royal Society Interface*, 6, 2009.

[34] D.-M. Drotlef, M. Amjadi, M. Yunusa, and M. Sitti. Bioinspired composite microfibers for skin adhesion and signal amplification of wearable sensors. *Advanced materials*, 29(28):1701353, 2017.

[35] C. Ellis. The mechanism of extension in the legs of spiders. *The biological bulletin*, 86(1):41–50, 1944.

[36] H. Faraji, R. Tachella, and R. L. Hatton. Aiming and vaulting: Spider inspired leaping for jumping robots. In *2016 IEEE International Conference on Robotics and Automation (ICRA)*, pages 2082–2087. IEEE, 2016.

[37] R. Foelix. *Biology of spiders*. OUP USA, 2011.

[38] S. Franz-Guess, B.-J. Klußmann-Fricke, C. S. Wirkner, L. Prendini, and J. M. Starck. Morphology of the tracheal system of camel spiders (chelicerata: Solifugae) based on micro-ct and 3d-reconstruction in exemplar species from three families. *Arthropod structure & development*, 45(5): 440–451, 2016.

[39] D. D. Gaffin, L. A. Bumm, M. S. Taylor, N. V. Popokina, and S. Mann. Scorpion fluorescence and reaction to light. *Animal Behaviour*, 83(2): 429–436, 2012.

[40] I. Gaiser, S. Schulz, A. Kargov, H. Klosek, A. Bierbaum, C. Pylatiuk, R. Oberle, T. Werner, T. Asfour, G. Bretthauer, et al. A new anthropomorphic robotic hand. In *Humanoids 2008-8th IEEE-RAS International Conference on Humanoid Robots*, pages 418–422. IEEE, 2008.

[41] I. Gaiser, S. Schulz, H. Breitwieser, and G. Bretthauer. Enhanced flexible fluidic actuators for biologically inspired lightweight robots with inherent compliance. In *2010 IEEE International Conference on Robotics and Biomimetics*, pages 1423–1428. IEEE, 2010.

[42] I. Gaiser, R. Wiegand, O. Ivlev, A. Andres, H. Breitwieser, S. Schulz, and G. Bretthauer. Compliant robotics and automation with flexible fluidic actuators and inflatable structures. In *Smart Actuation and Sensing Systems-Recent Advances and Future Challenges*. IntechOpen, 2012.

[43] C. Göttler, K. Elflein, R. Siegwart, and M. Sitti. Spider origami: Folding principle of jumping spider leg joints for bioinspired fluidic actuators. *Advanced Science*, 8(5):2003890, 2021.

[44] M. J. Hancock, K. Sekeroglu, and M. C. Demirel. Bioinspired directional surfaces for adhesion, wetting, and transport. *Advanced functional materials*, 22(11):2223–2234, 2012.

[45] X. Hao, W. Ma, C. Liu, Y. Li, Z. Qian, L. Ren, and L. Ren. Analysis of spiders' joint kinematics and driving modes under different ground conditions. *Applied Bionics and Biomechanics*, 2019, 2019.

[46] D. P. Harland and R. R. Jackson. Eight-legged cats and how they see: A review of recent research on jumping spiders (araneae: Salticidae). *Cimbebasia*, 16:231–240, 2000.

[47] A. C. Hawthorn and B. D. Opell. van der waals and hygroscopic forces of adhesion generated by spider capture threads. *Journal of Experimental Biology*, 206(22):3905–3911, 2003.

[48] D. E. Hill. The behavior of eris militaris (araneae: Slaticidae). *Peckhamia*, 24:1–8, 1996.

[49] D. E. Hill. Jumping spiders in outer space (araneae: Salticidae). *Peckhamia*, 146:1–7, 2016.

[50] K. Huckstorf, G. Kosok, E.-A. Seyfarth, and C. S. Wirkner. The hemolymph vascular system in cupiennius salei (araneae: Ctenidae). *Zoologischer Anzeiger-A Journal of Comparative Zoology*, 252(1):76–87, 2013.

[51] A. Iouguina, J. Dawson, B. Hallgrimsson, and G. Smart. Biologically informed disciplines: a comparative analysis of bionics, biomimetics, biomimicry, and bio-inspiration among others. *International Journal of Design & Nature and Ecodynamics*, 9(3):197–205, 2014.

[52] A.-C. Joel, M. Meyer, J. Heitz, A. Heiss, D. Park, H. Adamova, and W. Baumgartner. Biomimetic combs as antiadhesive tools to manipulate nanofibers. *ACS Applied Nano Materials*, 3(4):3395–3401, 2020.

[53] K. Jürgens and G. Gros. Phylogeny of gas exchange systems. *Anasthesiologie, Intensivmedizin, Notfallmedizin, Schmerztherapie: AINS*, 37(4): 185, 2002.

[54] A. Kargov, T. Werner, C. Pylatiuk, and S. Schulz. Development of a miniaturised hydraulic actuation system for artificial hands. *Sensors and Actuators A: Physical*, 141(2):548–557, 2008.

[55] N. Kellaris, V. G. Venkata, G. M. Smith, S. K. Mitchell, and C. Keplinger. Peano-hasel actuators: Muscle-mimetic, electrohydraulic transducers that linearly contract on activation. *Science Robotics*, 3(14):eaar3276, 2018.

[56] M. C. Kenny, M. N. Giarra, E. Granata, and J. J. Socha. How temperature influences the viscosity of hornworm hemolymph. *Journal of Experimental Biology*, 221(21), 2018.

[57] D. Klocke and H. Schmitz. Water as a major modulator of the mechanical properties of insect cuticle. *Acta biomaterialia*, 7(7):2935–2942, 2011.

[58] K. Kronenberger and F. Vollrath. Spiders spinning electrically charged nano-fibres. *Biology letters*, 11(1):20140813, 2015.

[59] C. Kropf. Hydraulic system of locomotion. In *Spider ecophysiology*, pages 43–56. Springer, 2013.

[60] L. Kuhn-Nentwig and W. Nentwig. The immune system of spiders. In *Spider {Ecophysiology}*, pages 81–91. Springer, 2013.

[61] S. Landkammer. Grundsatzuntersuchungen, mathematische modellierung und ableitung einer auslegungsrichtlinie für gelenkantriebe nach dem spinnenbeinprinzip. 2019.

[62] S. Landkammer and R. Hornfeck. Drehantrieb, german patent application: 20.12. 2013, reference number: De 10, r.: 114 660 a1. *Technische Hochschule Nürnberg Georg Simon Ohm, Applicant*, 2013.

[63] S. Landkammer, D. Schneider, F. Winter, P. Hess, and R. Hornfeck. Static modeling of antagonistic pneumatic actuator for robotic applications. In *2015 IEEE International Workshop of Electronics, Control, Measurement, Signals and their Application to Mechatronics (ECMSM)*, pages 1–6. IEEE, 2015.

[64] S. Landkammer, F. Winter, D. Schneider, and R. Hornfeck. Biomimetic spider leg joints: a review from biomechanical research to compliant robotic actuators. *Robotics*, 5(3):15, 2016.

[65] C. Laschi, M. Cianchetti, B. Mazzolai, L. Margheri, M. Follador, and P. Dario. Soft robot arm inspired by the octopus. *Advanced Robotics*, 26 (7):709–727, 2012.

[66] W.-K. Lee and J. J. Socha. Direct visualization of hemolymph flow in the heart of a grasshopper (Schistocerca americana). *BMC physiology*, 9 (1):1–11, 2009.

[67] X. Li and B. Bhushan. A review of nanoindentation continuous stiffness measurement technique and its applications. *Materials characterization*, 48(1):11–36, 2002.

[68] H.-T. Lin, G. G. Leisk, and B. Trimmer. Goqbot: a caterpillar-inspired soft-bodied rolling robot. *Bioinspiration & biomimetics*, 6(2):026007, 2011.

[69] C. Liu, S. Chen, C. Sheng, P. Ding, Z. Qian, and L. Ren. The art of a hydraulic joint in a spider's leg: modelling, computational fluid dynamics (cfd) simulation, and bio-inspired design. *Journal of Comparative Physiology A*, 205(4):491–504, 2019.

[70] T. Machałowski, M. Wysokowski, M. V. Tsurkan, R. Galli, C. Schimpf, D. Rafaja, E. Brendler, C. Viehweger, S. Żółtowska-Aksamitowska, I. Petrenko, et al. Spider chitin: an ultrafast microwave-assisted method for chitin isolation from caribena versicolor spider molt cuticle. *Molecules*, 24(20):3736, 2019.

[71] N. A. Malvadkar, M. J. Hancock, K. Sekeroglu, W. J. Dressick, and M. C. Demirel. An engineered anisotropic nanofilm with unidirectional wetting properties. *Nature materials*, 9(12):1023–1028, 2010.

[72] S. Manton and J. Harding. Hydrostatic pressure and leg extension in arthropods, with special reference to arachnids. *Annals and Magazine of Natural History*, 1(3):161–182, 1958.

[73] C. Menon and C. Lira. Active articulation for future space applications inspired by the hydraulic system of spiders. *Bioinspiration & biomimetics*, 1(2):52, 2006.

[74] J. Michels and S. Gorb. Detailed three-dimensional visualization of resilin in the exoskeleton of arthropods using confocal laser scanning microscopy. *Journal of microscopy*, 245(1):1–16, 2012.

[75] J. Michels, E. Appel, and S. N. Gorb. Functional diversity of resilin in arthropoda. *Beilstein journal of nanotechnology*, 7(1):1241–1259, 2016.

[76] J. Moya-Laraño, D. Vinković, E. De Mas, G. Corcobado, and E. Moreno. Morphological evolution of spiders predicted by pendulum mechanics. *PLoS One*, 3(3):e1841, 2008.

[77] M. R. Nabawy, G. Sivalingam, R. J. Garwood, W. J. Crowther, and W. I. Sellers. Energy and time optimal trajectories in exploratory jumps of the spider phidippus regius. *Scientific reports*, 8(1):1–15, 2018.

[78] W. Nachtigall. Bionik-grundlagen und beispiele für ingenieure und naturwissenschaftler (1998), 2002.

[79] T. Nagata, M. Koyanagi, H. Tsukamoto, S. Saeki, K. Isono, Y. Shichida, F. Tokunaga, M. Kinoshita, K. Arikawa, and A. Terakita. Depth perception from image defocus in a jumping spider. *Science*, 335(6067):469–471, 2012.

[80] S. Navarro and A. Friedlander. The effect of carbon dioxide anesthesia on the lactate and pyruvate levels in the hemolymph of ephestia cautella (wlk.) pupae. *Comparative Biochemistry and Physiology Part B: Comparative Biochemistry*, 50(1):187–190, 1975.

[81] D. Neff, S. F. Frazier, L. Quimby, R.-T. Wang, and S. Zill. Identification of resilin in the leg of cockroach, periplaneta americana: confirmation by a simple method using ph dependence of uv fluorescence. *Arthropod Structure & Development*, 29(1):75–83, 2000.

[82] X. J. Nelson and A. Card. Locomotory mimicry in ant-like spiders. *Behavioral Ecology*, 27(3):700–707, 2016.

[83] A. Nemiroski, Y. Y. Shevchenko, A. A. Stokes, B. Unal, A. Ainla, S. Albert, G. Compton, E. MacDonald, Y. Schwab, C. Zellhofer, et al. Arthrobots. *Soft robotics*, 4(3):183–190, 2017.

[84] J. Nickerl, M. Tsurkan, R. Hensel, C. Neinhuis, and C. Werner. The multilayered protective cuticle of collembola: a chemical analysis. *Journal of The Royal Society Interface*, 11(99):20140619, 2014.

[85] J. K. Oh, S. T. Behmer, R. Marquess, C. Yegin, E. A. Scholar, and M. Akbulut. Structural, tribological, and mechanical properties of the hind leg joint of a jumping insect: Using katydids to inform bioinspired lubrication systems. *Acta Biomaterialia*, 62:284–292, 2017.

[86] W. C. Oliver and G. M. Pharr. An improved technique for determining hardness and elastic modulus using load and displacement sensing indentation experiments. *Journal of materials research*, 7(6):1564–1583, 1992.

[87] B. C. Palmquist. The itsy-bitsy spider: An analysis of spider locomotion. *National Center for Case Study Teaching in Science. University at Buffalo, State University of New York. Buffalo, New York, USA. http://sciencecases. lib. buffalo. edu/cs/collection/detail. asp*, 2015.

[88] D. Parry. Spider leg-muscles and the autotomy mechanism. *Journal of Cell Science*, 3(43):331–340, 1957.

[89] D. Parry and R. Brown. The hydraulic mechanism of the spider leg. *Journal of Experimental Biology*, 36(2):423–433, 1959.

[90] D. Parry and R. Brown. The jumping mechanism of salticid spiders. *Journal of Experimental Biology*, 36(4):654–664, 1959.

[91] R. Paul, K. Tiling, P. Focke, and B. Linzen. Heart and circulatory functions in a spider (eurypelma californicum): the effects of hydraulic force generation. *Journal of Comparative Physiology B*, 158(6):673–687, 1989.

[92] A. Petrunkevitch. Contributions to our knowledge of the anatomy and relationships of spiders. *Annals of the Entomological Society of America*, 2(1):11–21, 1909.

[93] G. Pharr and W. Oliver. Measurement of thin film mechanical properties using nanoindentation. *Mrs Bulletin*, 17(7):28–33, 1992.

[94] Y. Politi, M. Priewasser, E. Pippel, P. Zaslansky, J. Hartmann, S. Siegel, C. Li, F. G. Barth, and P. Fratzl. A spider's fang: how to design an injection needle using chitin-based composite material. *Advanced Functional Materials*, 22(12):2519–2528, 2012.

[95] K. N. Prestwich. The constraints on maximal activity in spiders. *Journal of Comparative Physiology B*, 158(4):437–447, 1988.

[96] C. Pylatiuk, A. Kargov, I. Gaiser, T. Werner, S. Schulz, and G. Bretthauer. Design of a flexible fluidic actuation system for a hybrid elbow orthosis. In *2009 IEEE International Conference on Rehabilitation Robotics*, pages 167–171. IEEE, 2009.

[97] P. Ramdya, R. Thandiackal, R. Cherney, T. Asselborn, R. Benton, A. J. Ijspeert, and D. Floreano. Climbing favours the tripod gait over alternative faster insect gaits. *Nature communications*, 8(1):1–11, 2017.

[98] A. Rising, H. Nimmervoll, S. Grip, A. Fernandez-Arias, E. Storckenfeldt, D. P. Knight, F. Vollrath, and W. Engström. Spider silk proteins–mechanical property and gene sequence. *Zoological science*, 22(3):273–281, 2005.

[99] D. N. Rockwood, R. C. Preda, T. Yücel, X. Wang, M. L. Lovett, and D. L. Kaplan. Materials fabrication from bombyx mori silk fibroin. *Nature protocols*, 6(10):1612, 2011.

[100] J. Runge and C. S. Wirkner. A unified morphological scenario for the evolution of haemolymph pressure generation in spiders (araneae: Arachnida). *Zoological Journal of the Linnean Society*, 186(2):353–384, 2019.

[101] D. Rus and M. T. Tolley. Design, fabrication and control of soft robots. *Nature*, 521(7553):467–475, 2015.

[102] C. Schmidli, S. Albiez, L. Rima, R. Righetto, I. Mohammed, P. Oliva, L. Kovacik, H. Stahlberg, and T. Braun. Microfluidic protein isolation and sample preparation for high-resolution cryo-em. *Proceedings of the National Academy of Sciences*, 116(30):15007–15012, 2019.

[103] A. Schmitz. Metabolic rates during rest and activity in differently tracheated spiders (arachnida, araneae): Pardosa lugubris (lycosidae) and marpissa muscosa (salticidae). *Journal of Comparative Physiology B*, 174 (7):519–526, 2004.

[104] A. Schmitz. Spiders on a treadmill: influence of running activity on metabolic rates in pardosa lugubris (araneae, lycosidae) and marpissa muscosa (araneae, salticidae). *Journal of Experimental Biology*, 208(7): 1401–1411, 2005.

[105] A. Schmitz. Respiration in spiders (araneae). *Journal of Comparative Physiology B*, 186(4):403–415, 2016.

[106] A. Schmitz and S. Perry. Respiratory system of arachnids i: morphology of the respiratory system of salticus scenicus and euophrys lanigera (arachnida, araneae, salticidae). *Arthropod structure & development*, 29 (1):3–12, 2000.

[107] A. Schmitz and S. F. Perry. Bimodal breathing in jumping spiders: morphometric partitioning of the lungs and tracheae in salticus scenicus (arachnida, araneae, salticidae). *Journal of Experimental Biology*, 204 (24):4321–4334, 2001.

[108] A. Schmitz and S. F. Perry. Respiratory organs in wolf spiders: morphometric analysis of lungs and tracheae in pardosa lugubris (l.)(arachnida, araneae, lycosidae). *Arthropod Structure & Development*, 31(3):217–230, 2002.

[109] D. Schneider, S. Landkammer, R. Valek, and R. Hornfeck. Integrated angle measurement for bio-inspired joints with fluidic actuation. In *Proceedings of the Applied Research Conference 2014*, volume 4, pages 350–353, 2014.

[110] M. Schwörer, M. Kohl, and W. Menz. Fluidic microjoints based on spider legs. In *Conf. on New Actuators (Bremen)*, 1998.

[111] J. Sens. *Funktionelle Anatomie und Biomechanik der Laufbeine einer Vogelspinne (Grammostola spatulata FO Pickard-Cambridge)*. PhD thesis, Verlag nicht ermittelbar, 1996.

[112] A. T. Sensenig and J. W. Shultz. Mechanics of cuticular elastic energy storage in leg joints lacking extensor muscles in arachnids. *Journal of Experimental Biology*, 206(4):771–784, 2003.

[113] P. S. Shamble, R. R. Hoy, I. Cohen, and T. Beatus. Walking like an ant: a quantitative and experimental approach to understanding locomotor mimicry in the jumping spider myrmarachne formicaria. *Proceedings of the Royal Society B: Biological Sciences*, 284(1858):20170308, 2017.

[114] J. Shintake, V. Cacucciolo, D. Floreano, and H. Shea. Soft robotic grippers. *Advanced Materials*, 30(29):1707035, 2018.

[115] J. W. Shultz. Walking and surface film locomotion in terrestrial and semi-aquatic spiders. *Journal of Experimental Biology*, 128(1):427–444, 1987.

[116] J. W. Shultz. Evolutionary morphology and phylogeny of araghnida. *Cladistics*, 6(1):1–38, 1990.

[117] J. W. Shultz. Evolution of locomotion in arachnida: the hydraulic pressure pump of the giant whipscorpion, mastigoproctus giganteus (uropygi). *Journal of Morphology*, 210(1):13–31, 1991.

[118] Y. Son. Determination of shear viscosity and shear rate from pressure drop and flow rate relationship in a rectangular channel. *Polymer*, 48(2): 632–637, 2007.

[119] F. Song, K. Xiao, K. Bai, and Y. Bai. Microstructure and nanomechanical properties of the wing membrane of dragonfly. *Materials Science and Engineering: A*, 457(1-2):254–260, 2007.

[120] A. Spröwitz, C. Göttler, A. Sinha, C. Caer, M. U. Öoztekin, K. Petersen, and M. Sitti. Scalable pneumatic and tendon driven robotic joint inspired by jumping spiders. In *2017 IEEE International Conference on Robotics and Automation (ICRA)*, pages 64–70. IEEE, 2017.

[121] S. D. Stellwagen, B. D. Opell, and K. G. Short. Temperature mediates the effect of humidity on the viscoelasticity of glycoprotein glue within the droplets of an orb-weaving spider's prey capture threads. *Journal of Experimental Biology*, 217(9):1563–1569, 2014.

[122] D. M. Stewart and A. W. Martin. Blood and fluid balance of the common tarantula, dugesiella hentzi. *Zeitschrift für vergleichende Physiologie*, 70 (3):223–246, 1970.

[123] D. M. Stewart and A. W. Martin. Blood pressure in the tarantula, dugesiella hentzi. *Journal of comparative physiology*, 88(2):141–172, 1974.

[124] J. Sun, B. Bhushan, and J. Tong. Structural coloration in nature. *Rsc Advances*, 3(35):14862–14889, 2013.

[125] N. Tan, R. E. Mohan, and K. Elangovan. Scorpio: A biomimetic reconfigurable rolling–crawling robot. *International Journal of Advanced Robotic Systems*, 13(5):1729881416658180, 2016.

[126] S. K. Tiwari, S. Bhat, and K. K. Mahato. Design and Fabrication of Low-cost Microfluidic Channel for Biomedical Application. *Scientific Reports*, 10(1):1–14, 2020.

[127] B. Tondu. Modelling of the mckibben artificial muscle: A review. *Journal of Intelligent Material Systems and Structures*, 23(3):225–253, 2012.

[128] C. Trejo-Soto, E. Costa-Miracle, I. Rodriguez-Villarreal, J. Cid, M. Castro, T. Alarcon, and A. Hernandez-Machado. Front microrheology of the non-Newtonian behaviour of blood: scaling theory of erythrocyte aggregation by aging. *Soft Matter*, 13(16):3042–3047, 2017.

[129] M. Vogelgesang, S. Chilingaryan, T. dos_Santos Rolo, and A. Kopmann. Ufo: A scalable gpu-based image processing framework for on-line monitoring. In *2012 IEEE 14th International Conference on High Performance Computing and Communication & 2012 IEEE 9th International Conference on Embedded Software and Systems*, pages 824–829. IEEE, 2012.

[130] M. Vogelgesang, T. Farago, T. F. Morgeneyer, L. Helfen, T. dos Santos Rolo, A. Myagotin, and T. Baumbach. Real-time image-content-based beamline control for smart 4d x-ray imaging. *Journal of synchrotron radiation*, 23(5):1254–1263, 2016.

[131] L. Wang, U. Culha, and F. Iida. A dragline-forming mobile robot inspired by spiders. *Bioinspiration & biomimetics*, 9(1):016006, 2014.

[132] M. Wehner, R. L. Truby, D. J. Fitzgerald, B. Mosadegh, G. M. Whitesides, J. A. Lewis, and R. J. Wood. An integrated design and fabrication strategy for entirely soft, autonomous robots. *Nature*, 536(7617):451–455, 2016.

[133] T. Weihmann. Crawling at high speeds: steady level locomotion in the spider cupiennius salei—global kinematics and implications for centre of mass dynamics. *PLoS One*, 8(6):e65788, 2013.

[134] T. Weihmann, M. Karner, R. J. Full, and R. Blickhan. Jumping kinematics in the wandering spider cupienniussalei. *Journal of Comparative Physiology A*, 196(6):421–438, 2010.

[135] T. Weihmann, M. Günther, and R. Blickhan. Hydraulic leg extension is not necessarily the main drive in large spiders. *Journal of Experimental Biology*, 215(4):578–583, 2012.

[136] T. Weihmann, P.-G. Brun, and E. Pycroft. Speed dependent phase shifts and gait changes in cockroaches running on substrates of different slipperiness. *Frontiers in zoology*, 14(1):1–15, 2017.

[137] G. M. Whitesides. Soft robotics. *Angewandte Chemie International Edition*, 57(16):4258–4273, 2018.

[138] W. D. Wiesenborn. Uv-excited fluorescence on riparian insects except hymenoptera is associated with nitrogen content. *Psyche*, 2011, 2011.

[139] R. Wilson. The heart-beat of the spider, heteropoda venatoria. *Journal of Insect Physiology*, 13(9):1309–1326, 1967.

[140] R. Wilson. Some comments on the hydrostatic system of spiders (chelicerata, araneae). *Zeitschrift für Morphologie der Tiere*, 68(4):308–322, 1970.

[141] R. Wilson and J. Bullock. The hydraulic interaction between prosoma and opisthosoma in amaurobius ferox (chelicerata, araneae). *Zeitschrift für Morphologie der Tiere*, 74(3):221–230, 1973.

[142] F. Winter, S. Landkammer, R. Hornfeck, P. Heß, and K. Paetzold. Optimized leg proportion to enhance rough terrain mobility of a biomimetic walking robot. In *International Conference on Robotics in Alpe-Adria Danube Region*, pages 320–327. Springer, 2016.

[143] L. Zentner. Modelling and application of the hydraulic spider leg mechanism. In *Spider Ecophysiology*, pages 451–462. Springer, 2013.

[144] L. Zentner and V. Böhm. On the mechanical compliance of technical systems. *Mechanical Engineering; Gokcek, M., Ed.; INTECH Open Science: Morn Hill, UK*, pages 341–352, 2012.

[145] L. Zentner, V. Böhm, and N. Turkevi-Nagy. Fluidisch angetriebenes stoffschlüssiges gelenkelement. *Offenlegungsschrift, Deutsches Patent-und Markenamt, DE*, 103(16):959, 2004.